Investigating dichotomous projections from ventral hippocampus to prefrontal cortex

Candela Sánchez Bellot

A dissertation submitted in partial fulfillment

of the requirements for the degree of

Doctor of Philosophy in Neuroscience

of

University College London.

Department of Neuroscience, Physiology and Pharmacology

University College London

28 August, 2020

I, Candela Sánchez Bellot, confirm that the work presented in this thesis is my own. Where information has been derived from other sources, I confirm that this has been indicated in the work.

Abstract

The ventral hippocampus is thought to be key in the production of exploratory, goal-directed and anxiety-like behaviour as well as in the expression and extinction of contextual fear. These roles are thought to be carried out via strong projections to structures such as the prefrontal cortex (PFC), where the hippocampus exerts tight excitatory and inhibitory control over downstream circuitry. The ventral hippocampal-prefrontal (vH-PFC) pathway is involved in the production of a range of behaviours including working memory, aversive learning and anxiety and its dysfunction is linked to key aspects of several psychiatric disorders. How this pathway supports these functions is not fully understood and a mechanism for hippocampus-driven excitatory and inhibitory control of PFC, dependent on task demands, remains elusive. Moreover, how this hippocampal control over PFC and activity in the vH-PFC pathway is altered in disease is poorly understood. In this thesis, I found that the vH-PFC projection is composed of two distinct populations of neurons. These neurons form two layers, at the deep and superficial poles of the radial axis of the hippocampus. In line with previously established property gradients along the hippocampal radial axis, cells in the deep layer are more excitable and burst-firing, while cells in the superficial layer are regular-spiking. Additionally, cells in the two layers of the projection are differentially controlled by upstream structures. Superficial cells receive biased cortical input while deep cells preferentially receive input from subcortical structures. These two subpopulations have unique connectivity within downstream PFC, where differential recruitment of pyramidal cells and

interneuron subclasses provide a mechanism for bidirectional control of PFC activity. Superficial layer cells preferentially recruit feedforward inhibition, while cells in the deep layer promote excitation. This long-range push-pull circuit provides a mechanism for regulation of exploratory behaviour in an approach-avoidance conflict through tight hippocampal control of PFC, where activation of deep layer cells promotes avoidance and activation of superficial layer cells promotes exploration of the elevated plus maze.

Impact statement

A central goal of circuit and hippocampal neuroscience is to understand the extent of sequential or concomitant flow of information through circuit subpopulations. In other words, answering how for instance, the hippocampus can carry out more than one function at once, or how multiple functions can be associated with the same neural pathway. What are the mechanisms behind this? The data shown in this thesis offers an example of circuit motifs and ways in which cellular heterogeneity serves as an efficient way for bidirectional modulation of one brain area by another. In recent years, understanding the precise wiring of specific neural circuits has become of increasing interest. Even widespread illnesses such as anxiety and depression, which have been diagnosed in the same manner for decades, are starting to be seen as possible results of complex circuitopathies (Ressler and Mayberg, 2007; Spellman and Liston, 2020). In fact, the DSM is moving towards a more holistic, circuit-based approach to investigating mental illness rather than focusing on a single biological factor or list of symptoms. This approach may prove to encompass all consequences of circuit dysfunction along a spectrum, rather than boxing separate disorders up into unique definitions, which ignore the commonalities between different disorders. Disorders that share symptoms may be caused by slightly different forms of circuit dysfunction and thus respond differently to treatment. Truly understanding the mechanisms involved in information transfer between brain areas is crucial for interpreting the consequences of dysfunctional communication. Specifically, in this thesis I focus on elucidating the

circuitry that allows for hippocampal-prefrontal communication - a pathway heavily associated with multiple neuropsychiatric illnesses. Combining electrophysiological and behavioural experiments with viral constructs to selectively target the hippocampal-prefrontal pathway, we elucidate the role of ventral hippocampal (vH) cells in the decision to explore a novel, potentially threatening environment. Adaptive exploratory behaviour is essential for survival - too little exploration reduces the likelihood of finding novel sources of reward, while excessive exploration increases risk such as injury. The methodology implemented throughout this thesis allowed us to investigate the circuit mechanisms behind the controlling role that vH cells exert over PFC circuitry to modulate anxiety-like behaviour during exploration. I believe that circuit investigation protocols such as the one described here could be implemented in the study of a variety of neural circuits that are crucial for adaptive and appropriate emotional and decision-making behaviour.

In the academic sphere, examples of how certain methodology may change how we ask questions or try to answer them are key and go on to inform decisions on funding and strategy. I hope with this thesis to shed light on the multifaceted and thorough nature of neural circuit investigation, which may in the future get us closer to understanding the many shared as well as exclusive symptoms of affective and behavioural disorders. In addition, the work presented in this thesis offers novel insight into the circuit motifs utilised by the hippocampal-prefrontal pathway and may aid in clarifying current discrepancies in the field regarding its associated roles.

Acknowledgements

First and foremost I would like to extend a massive thank you to Andrew for being such a supportive supervisor and mentor in the lab and throughout my entire PhD. It has been a great journey since I joined the lab, from building it up with the few members at the start to where it is now. Thanks for being so encouraging with all of my ideas and projects and helping me with everything from endless hours in surgery to writing and practicing presentations. I am very grateful to you for taking the time to teach me so many new techniques and always being available for scientific rants and to endlessly discuss my project. Your enthusiasm for the scientific process and discovery is inspiring and I hope to follow in your footsteps with that.

To Rawan, I would like to reiterate once again that I could not have done this without you and I am extremely happy that we ended up in the same lab. We have been in it together since the very beginning and you have always been there to cheer me up after a bad patching session and to have a dance-off when the patching was going our way. Countless are the things you have made easier for me in the lab - I am very grateful to you. Thanks for introducing me to Wine Fridays, Drake, good books and your amazing hugs. And thanks for always listening. Good luck for your final stretch, you can do it!

To Ryan, ever since you brought Honey & Co. cookies on your first lab visit I was sold. Thanks for introducing me to great food and coffee at reasonable distances from the lab... A million thank yous for being so patient with all of my Python conundrums and actually making my life a lot easier by teaching me proper coding.

Thank you also for the endless chats and pep talks, especially during my final year. To Karyna, thank you for making me laugh a lot with your sense of humour. Also thank you for helping me recycle and always supporting my eco-rants. Your help with the little things in the lab was always greatly appreciated and I've always enjoyed our many conversations where we try to solve the world. Thank you for introducing me to babkas too, and encouraging the consumption of proper coffee. I am routing for all your great science to come!

To Svenja, thanks for the great company during dance-offs and providing so many essential pep-talks this past year. It has been truly great to have you join the lab during my final stretch and I look forward to accompanying you in yours!

To Anushka, Danny, Anne, Quentin and everyone who has been through the MacAskill lab during these past 4 years, thanks for creating such a great atmosphere. You have made it very easy to love coming to work.

To Carlota, Leonor and everyone at the Dickenson lab, thank you for constantly offering moral support and great lunchtime chit chat. Your lab has been a safe haven throughout all these years.

To David Attwell and Francesca Cacucci, thank you for your mentorship, guidance and support. You have been extremely helpful at many stages throughout my PhD and always offered good advice and understanding.

To my friends and family beyond the lab, you have made the process all the more enjoyable. Thank you to my sister Elena for always being there and celebrating the little things. Thank you for building a home away from home for me. To Alex, thanks for being an amazing friend, getting me into running and teaching me a lot about birds. To Irena, thanks for keeping me sane and being such a vital support. To my parents, thank you for all the effort and love you put in so that I could pursue my interests and end up where I am today.

Lastly, thank you to the Wellcome Trust who generously funded my research and time at UCL.

I dedicate this thesis to Conchita Cantó Pellín, my grandmother, who taught herself how to read and write at age 10, and through her effort and determination may see her granddaughter graduate with a PhD. Gràcies valenta.

Contents

List of Figures

List of Tables

Chapter 1

Introduction

The hippocampus is a complex structure that has been associated with a large variety of distinct behaviours and functions. For example, it has been proposed to support learning and memory formation, social memory, spatial navigation, emotional, goal-oriented and motivated behaviour (O'Keefe, 1979; Moser and Moser, 1998; Adhikari et al., 2010; Ruediger et al., 2012; Okuyama et al., 2016; Wikenheiser et al., 2017; Strange et al., 2014; Bannerman et al., 2002; Aronov et al., 2017; Andersen et al., 2006). Its structure and function have been extensively studied and techniques for its investigation are well established, lending itself to multiple levels of enquiry. However, despite large volumes of research into hippocampal function and its associated behaviours, there is still much debate surrounding how this relatively well-understood circuitry can support such a diverse array of behaviours. Throughout this thesis, I carry out *in vitro* experiments on acute transverse hippocampal slices from adult mice and *in vivo* experiments manipulating activity from the intact hippocampus in freely behaving mice. These experiments focus on studying the characteristics of projection neurons in the hippocampus. In particular, they investigate the characteristics and functional consequences of activity in prefrontal cortex (PFC)-projecting hippocampal pyramidal cells, which are predominantly located in the ventral hippocampus (vH) (Hoover and Vertes, 2007; Cenquizca and

Swanson, 2007; Tannenholz et al., 2014). The ventral hippocampus is thought to be involved in emotional processing (Henke, 1990; Kjelstrup et al., 2002; Fanselow and Dong, 2010; Strange et al., 2014; O'Mara, 2006) and as will be discussed below in more detail, the ventral hippocampus to prefrontal cortex (vH-PFC) pathway is involved in fear and threat-related behaviours, and its activity is compromised in a variety of psychiatric disorders (Adhikari et al., 2010; Padilla-Coreano et al., 2019; Harrison, 2004; Marek et al., 2018a; Meyer et al., 2019; Godsil et al., 2013; Sigurdsson and Duvarci, 2016). Despite being an extensively studied pathway with potential therapeutic target value, the circuit mechanisms supporting its many proposed functions have not been fully clarified. Specifically, it is currently not well understood what cellular and circuit mechanisms ventral hippocampal cells implement to exert control over PFC circuitry and how these circuit motifs may be adapted dependent on task demands. In this introduction I will firstly discuss the functions associated with the hippocampus and the prefrontal cortex and the current understanding of the ventral hippocampal to prefrontal pathway in affective behaviour. To aid in the understanding of the role of the hippocampus in this pathway I will give an in-depth description of hippocampal structure, function and its connectivity with brain structures relevant to the production of affective and motivated behaviour. I will expand on the differences along the hippocampal longitudinal (dorso-ventral), transverse (proximo-distal) and radial (superficial-deep) axes and other important structural sub-classifications. Lastly, I will focus on how the hippocampus may control PFC function via implementation of canonical circuit motifs.

1.1 The ventral hippocampal-prefrontal pathway

The vH-PFC pathway is crucially involved in cognitive processes such as executive function and emotional regulation (Godsil et al., 2013). It has been shown that this pathway transmits information serving working memory, learning and contextual processing, which may support its role in emotional regulation (Place et al., 2016; Spellman et al., 2015; Wikenheiser et al., 2017; Marek et al., 2018a; Godsil et al.,

2013). Anatomical evidence for ventral hippocampal input to prefrontal cortex has been obtained by axonal tracing methods (Rosene and Van Hoesen, 1977; Swanson, 1981; Jay and Witter, 1991; Barbas and Blatt, 1995; Ongür and Price, 2000). Despite the relatively long time that has passed since the first anatomical observations characterising ventral hippocampal terminals in PFC, there are still discrepancies in hypotheses as to what circuit functions and behaviours the vH-PFC pathway supports. In the following section I will firstly discuss background information on hippocampal and prefrontal cortex function. This will aid in understanding their characteristics and the implications of providing input onto these structures. Building on this discussion, I will then describe the data that is available on the ventral hippocampal-prefrontal pathway and its associated functions.

1.1.1 The hippocampus

The hippocampus is located at the posterior end of the mammalian brain, in the medial temporal lobe, adjacent to the entorhinal cortex. It is placed to receive dense cortical input from entorhinal cortex and routes information to a variety of both cortical and subcortical brain structures (Tannenholz et al., 2014; Naber and Witter, 1998; Witter, 1993; Cenquizca and Swanson, 2007; Aggleton and Christiansen, 2015). Its dense connectivity allows for the hippocampus to process multimodal information and to be involved in a range of different functions. For example, it is critically involved in memory, spatial navigation and emotional processing (O'Keefe, 1979; Moser and Moser, 1998; Adhikari et al., 2010; Strange et al., 2014; Bannerman et al., 2002; Aronov et al., 2017; Tannenholz et al., 2014). It is thought that its dense connections to higher cortical areas support its role in memory formation and encoding. Its projections to retrosplenial cortex and thalamus support its involvement in spatial navigation and its projections to prefrontal cortex, nucleus accumbens and connectivity with the amygdala are consistent with its role in affect and emotion (Cenquizca and Swanson, 2007; Tannenholz et al., 2014; Fanselow and Dong, 2010). Thus, hippocampal associated functions are reinforced by its afferent

and efferent connectivity with areas involved in bringing them about. Although being one the most widely studied structures in the brain, there is still debate regarding how many associated functions it is involved in, which are the most predominant, and the mechanisms that support them. Here, I will briefly outline the evidence for its implication in memory, spatial navigation and emotional processing, before focusing in more detail on its projection to PFC. Understanding the current models of hippocampal function is important when investigating its communication with other brain areas like the PFC, as it provides a framework of possible roles for these pathways.

1.1.1.1 Memory

The hippocampus is classically implicated in episodic and contextual memory formation. Reports as early as the late 19th century in primates and early 20th century in humans (by neurologist Vladimir Bekhterev) mention patients with memory deficiencies that were posthumously found to have bilateral hippocampal tissue abnormalities as well as compromised structural integrity of neighbouring cortical areas. Early studies on human patients by Scoville and Milner (1957) most convincingly pointed at the hippocampus as the localisation of or central player in memory formation within the temporal lobe. Famously, the epileptic and later amnesic patient H.M. showed impairments in episodic memory formation following a bilateral medial temporal lobectomy intended as a remedy for his non-remittent epilepsy. However, he did not suffer from impairments in procedural memory i.e. learning a new set of motor skills, or in recall of memories acquired long before the operation. This surgical procedure removed both his hippocampi and rendered him incapable of forming any new memories and of retaining information for longer than a few minutes (Scoville and Milner, 1957, 2000). These consequences of damage to the hippocampus have been observed repeatedly in otherwise previously healthy patients (Squire, 1992). Hippocampal lesion studies in rodents have since replicated this data, confirming the crucial role of the hippocampus in episodic-like and

contextual memory formation (Eichenbaum and Fortin, 2005; DeVito and Eichenbaum, 2010). Episodic memory is described as a long-term memory for events or episodes, accessible to conscious recollection. As with patient H.M., rodents with hippocampal lesions fail to remember associations acquired directly prior to the lesioning while associations learned a few days or weeks prior are spared (Kim and Fanselow, 1992). For example, rodents with partial hippocampal lesions fail to recall odour-context associations learned prior to lesioning in non-match to sample tasks (Eichenbaum and Robitsek, 2009). Furthermore, rats with hippocampal lesions are impaired in forming new associations between events and in utilising past events to guide behaviour during tasks such as avoiding locations previously paired with punishment (Isaacson and Kimble, 1972; Morris et al., 1982; Phillips and LeDoux, 1992). This suggests that the hippocampus is involved both in retrieving past associations and in forming new ones, enabling learning of task structures and goal-directed behaviour.

1.1.1.2 Spatial navigation

The discovery of hippocampal place cells (O'Keefe and Dostrovsky, 1971; O'Keefe, 1979) prompted the unfolding of a new field of enquiry into hippocampal function. Namely, to investigate the hippocampus as a cognitive map representing location in space. Place cells are neurons that increase their firing at a particular location in space while the animal is actively exploring, encoding what can be thought of as spatial memories. The animal will map out familiar environments with an array of place cells, uniquely active at their preferred location in space. Place cells can be found throughout the hippocampal formation and a different type of spatially tuned cells called grid cells (which segment an environment into a hexagonal lattice grid-like map) can be found in the entorhinal cortex (Hafting et al., 2005). This field has also identified various other spatially tuned neurons that encode different aspects of spatial location (Barry and Burgess, 2014). These findings explain deficits in spatial navigation following hippocampal lesions and have

been built on very extensively to understand how the hippocampus encodes spatial information (Best et al., 2001; Hartley et al., 2014). For example, bilateral dorsal hippocampal lesions encompassing a minimum of 20% total hippocampal volume or ventral hippocampal lesions where above 50% of total hippocampal volume is affected have been shown to impair spatial memory during a water maze task in which animals have to remember the location of a hidden platform to escape the maze (Moser et al., 1993; Broadbent et al., 2004; Morris et al., 1982). Spatial navigation requires working, short-term and long-term memory and it is thought that the processes involved in mapping the environment are also involved in ordering language and non-spatial memories (Squire, 1992; Ramos, 2000; Liu and Bilkey, 2001). Thus, it has been suggested that memory deficits and learning difficulties may be explained by impaired spatial processing (Passolunghi and Mammarella, 2010; Mammarella et al., 2009).

1.1.1.3 Emotional and motivated behaviour

In addition to having a role in cognitive tasks such as memory formation and spatial representation, of specific interest for this thesis is the involvement of the hippocampus in emotional and motivated behaviour. Early lesion studies of ventral, but not dorsal, hippocampus result in altered emotional behaviour such as anxiety-driven susceptibility to fear and responses to stress (Bannerman et al., 2003). Animals with ventral hippocampal lesions present reduced anxiety-like behaviour in response to stressful environments such as brightly lit arenas or exploration of the open arms in an elevated plus maze (Kjelstrup et al., 2002). Rodent lesion studies have also highlighted the role of the ventral hippocampus in Pavlovian fear conditioning (Maren, 1999). Along similar lines, prolonged and fatal stress in primates as well as in rodents is specifically neurotoxic for hippocampal tissue (Uno et al., 1989; Sapolsky et al., 1990). The hippocampus is a prime target for the stress hormones glucocorticoids while surrounding cortical areas are spared (Sapolsky et al., 1990), suggesting a key role for the hippocampus in mediating the glucocorticoid

response. The hippocampus contains a very high density of glucocorticoid receptors and is thus highly vulnerable to even mild levels of stress, which can alter hippocampal function (Kim et al., 2015). The ventral hippocampus specifically has been shown to exert inhibitory regulatory control over the hypothalamic-pituitary-adrenal (HPA) axis (Dedovic et al., 2009), thus providing a key node of influence over the hormonal stress response to actual or perceived threat. However, despite the evidence supporting the involvement of the hippocampus in mediating emotionally valent stimuli to guide the animals' behaviour (Kjelstrup et al., 2002; Okuyama et al., 2016; Meira et al., 2018; Trouche et al., 2019), it is not entirely clear how the hippocampus processes this type of information and how it communicates with the relevant downstream brain areas to coordinate an adaptive interaction of the animal with its environment.

Overall, from the data described above, it is clear that the hippocampus supports many different functional roles. The question thus arises of how one single structure can be associated with such a vast number of functions. In describing the distinct roles of the hippocampus it becomes apparent that complex, perhaps parallel circuit mechanisms must be at play in order to fulfil all of these roles, as they do not exclusively happen in a temporally independent fashion, but can occur simultaneously. For example, during a hippocampal-prefrontal pathway dependent task, mice learn to use spatial working memory to navigate a t-maze, avoiding the previously entered arm (Spellman et al., 2015). However, during this task mice also have to utilise goal-directed behaviour - associated with a different hippocampal projection to NAc (LeGates et al., 2018; Floresco et al., 1997) - as entering the correct arm will result in a sugar pellet food reward and an error will lead to no reward. These observations suggest that parallel hippocampal projections may be one way in which concurrent, hippocampally-dependent processes may be supported. It is also possible that different, specific subregions along the hippocampal axes are responsible for bringing about these separate functions. Furthermore, distinct sets of neurons that respond to different afferent inputs, hormones and neurotransmit-

ters may be recruited in a task-dependent manner along the hippocampal axes and within functional domains. The specialisation of the hippocampus in such varied functions, from cognitive maps to mood regulation and involvement in neuropsychiatric disorders arises in part due to the heterogeneity along its dorsoventral axis (Strange et al., 2014; Cembrowski and Spruston, 2019). For example, functional heterogeneity is proposed to allow for the dorsal hippocampus to be involved in spatial navigation and spatial contextual memory formation, while the ventral hippocampus is involved in emotional, affect-related behaviours (Fanselow and Dong, 2010; Bannerman et al., 2002). In this thesis, I suggest that hippocampal heterogeneity might be important to understand how this structure carries out the functions described here, and will be discussed in depth below.

1.1.2 Prefrontal cortex

The prefrontal cortex in rodents is located at the most anterior part of the cerebral cortex, immediately adjacent and posterior to the olfactory bulbs (see Figure 1.4). It has been classically associated with a vast array of functions, including cognitive flexibility, goal-oriented behaviour, attention, social and emotional behaviour, working memory and motivation (Miller and Cohen, 2001; Ridderinkhof et al., 2004; Euston et al., 2012; Starkweather et al., 2018; Shrestha et al., 2015). Human cases of prefrontal lesions provide support for the role of prefrontal cortex in action inhibition, rational decision making and emotional processing (Damasio et al., 1994).

Anatomically, PFC can be divided into three main areas, the medial, lateral and orbital prefrontal cortex, although there is great discrepancy in the nomenclature of this brain structure across species and even within the rodent literature (Laubach et al., 2018). For the purpose of this thesis, we will refer to the structure as prefrontal cortex, focusing mainly on the medial and (to a lesser extent) the orbitofrontal prefrontal cortex, which for all of our experiments in adult mice are

located 2.3 mm anterior to reference skull landmark bregma. The medial prefrontal cortex region can be further divided into prelimbic (PL) and infralimbic (IL) PFC, in descending order from the dorsal pial surface with the more ventral infralimbic PFC being homologous to ventromedial PFC in humans (Quirk and Beer, 2006; Myers-Schulz and Koenigs, 2012).

All cortical areas are composed of cell layers. Most contain five layers (I-VI; layer IV is absent in prefrontal areas), which are characterised by different cell types and which fulfil specific roles within the prefrontal microcircuitry (Fuster and Barbas, 2009). Most subcortical input (including limbic inputs from hippocampus and amygdala) arrives at layers II/III and to a lesser extent, layer V. Layer VI serves as an output layer to other brain areas, while layer III serves as an internal relay centre between cortical columns. Layer I is closest to the pia, which in a coronal rodent brain slice of medial prefrontal cortex is nearest the midline.

Amongst cortical areas, PFC is considered highest in the hierarchy of action execution, representation and planning, while areas lower in the hierarchy are involved in the processing of motor and sensory information (Fuster, 2001; Fuster and Barbas, 2009). The PFC is involved in complex behaviours requiring the integration of aspects such as social cognition and action inhibition, both in humans and in rodents (Bicks et al., 2015; Kupferschmidt and Gordon, 2018; Sigurdsson and Duvarci, 2016; Warden et al., 2012; Mayberg et al., 1999; Covington et al., 2010; Ramanathan et al., 2018). Action inhibition or inhibitory control is a key role associated with the PFC. It refers to the ability to cease learned responses to a given situation or stimulus when the continuation of the response becomes no longer pertinent to the task at hand (Ramanathan et al., 2018) as well as to the non-selection of innate (not learned) responses (Warden et al., 2012). Importantly, the inhibition of one action allows the uptake of another behaviour. This process allows for execution of task-appropriate behaviour and is deficient in many psychiatric disorders. Action inhibition is especially important for exploratory behaviour

where decisions to approach potentially threatening areas have to be made (Ridderinkhof et al., 2004; McGuire and Botvinick, 2010; Warden et al., 2012; Adhikari et al., 2011; Amat et al., 2005). In primates and rodents with medial prefrontal lesions this function is lost, leading to impulsive and repetitive behaviour and loss of control over autonomic and motor processes (Vertes, 2006). In line with its regulatory role on emotional processes, the prefrontal cortex serves an orchestrating role in conditioned fear behaviours and responses to stressors (Davidson, 2002). PFC dysfunction leads to loss of control over the HPA axis, altering responses to stress. More specifically, prefrontal lesioning or silencing has been shown to impair extinction of fear memories, due to lack of fear response inhibition to no longer dangerous stimuli (Milad and Quirk, 2002).

Overall, the data discussed here places the PFC as a key player in integrating different streams of input to inform decision-making and both the selection and inhibition of actions. These functions are essential for survival and are impaired in many different disorders. Thus, in the interest of studying how animals make decisions based on their spatial or emotional state, or based on previous episodic memories, it is important to study how afferent inputs from structures like the vH, carrying the relevant contextual and emotional information, influence PFC circuitry. Mechanistic understanding of this afferent circuitry will aid in clarifying the role of PFC in health and disease.

1.1.3 The vH-PFC pathway

Direct input from the ventral hippocampus to the prefrontal cortex has been observed both in rodents and in monkeys (Jay and Witter, 1991; Thierry et al., 2000; Vertes, 2004; Barbas and Blatt, 1995). Also in humans, fimbria and fornix fibres originating from the hippocampal formation terminate in the medial orbital PFC (Croxson et al., 2005). From the ventral hippocampus, efferent PFC-projecting fibres ipsilaterally reach the PFC via the fornix, terminating in the infralimbic, pre-

limbic, and anterior cingulate PFC areas (Hoover and Vertes, 2007; Jay and Witter, 1991; Varela et al., 2014). Within these prefrontal areas, ventral hippocampal terminals target excitatory pyramidal neurons as well as GABAergic inhibitory interneurons, suggesting that bidirectional control of prefrontal activity by hippocampal cells is possible (Jay et al., 1992; Carr and Sesack, 1996; Tierney et al., 2004; Parent et al., 2010). Additionally, there are indirect poly-synaptic projections between these two structures for example via the thalamic nucleus reuniens and the amydgala (Vertes, 2006; Hoover and Vertes, 2007; Sotres-Bayon et al., 2012; Cenquizca and Swanson, 2007).

These anatomical investigations have led to a relatively general understanding of the areas innervated and cellular targets that can be recruited by hippocampal terminals in PFC. However, significantly less emphasis has been placed on studying the functional and cellular properties of this projection, particularly its hippocampal component i.e. the hippocampal pyramidal cells sending axons to PFC. In addition, although the PFC and the vH both have well established roles in cognitive flexibility, memory processes and emotional control, it is less clear how these two structures communicate to orchestrate these functions.

Input from the vH to the PFC plays an important role in the regulation of short-term working memory, goal-directed behaviour, the encoding and extinction of fear memories, updating action plans and in emotional behaviour (Spellman et al., 2015; Sotres-Bayon et al., 2012; Marek et al., 2018a; Sigurdsson and Duvarci, 2016; Numan, 2015; Parfitt et al., 2017; Phillips et al., 2019; Wang and Cai, 2006; Wang et al., 2016). These functions will be discussed in more detail below. Given the role of the PFC in goal-oriented behaviour and the role of hippocampus in memory formation and in providing emotional context, a framework of potential function arises for the vH-PFC pathway. Namely, hippocampal-prefrontal communication may integrate memory-based, spatial or emotional context with possible outcomes of behaviour to inform decisions regarding the selection or inhibition of upcoming

actions.

It lies within this framework that a disruption in vH-PFC communication would be present in many disorders characterised by cognitive impairment and emotional dysregulation. In fact, disruptions in this pathway feature in many psychiatric disorders including schizophrenia, anxiety, chronic stress and depression (Mukherjee et al., 2019; Sigurdsson et al., 2010; Adhikari et al., 2010; Padilla-Coreano et al., 2016; Godsil et al., 2013; Li et al., 2015; Brady et al., 2010). The involvement of this pathway in psychiatric disorders warrants an in-depth investigation of its circuitry, both from the prefrontal and hippocampal perspectives. Such investigations may lead to finding potential therapeutic nodes within the affected circuitry (Spellman and Liston, 2020).

1.1.3.1 Memory, context and goal-oriented behaviour

The vH-PFC pathway is implicated both in long and short-term memory as well as in the encoding of contextual cues. These features are all important for carrying out goal-directed behaviour. vH-PFC interaction in long-term memory has been studied during retrieval, showing that hippocampal-prefrontal communication allows for the specification of retrieval cues, which can be used to retrieve stored memories (Jin and Maren, 2015b). The hippocampus in this context is thought to provide the PFC with the relevant memories to carry out actions and once retrieved, hippocampal-prefrontal communication ensures the disambiguation of the retrieved memories. If these are found to be the wrong information for the task at hand, the retrieval cue may be amended or updated for future searches (Simons and Spiers, 2003). During encoding of the memories, the retrieval cues are encoded by the hippocampus in a way that benefits goal-directed behaviour. In line with this role, aberrant, hyperactive vH-PFC connectivity has been shown to impair retrieval of social memories (Phillips et al., 2019).

Simultaneous recordings of hippocampus and PFC during working memory tasks show synchronisation of their activity (Benchenane et al., 2010; Spellman et al., 2015). Transient inactivation of the ventral CA1 / subiculum area disrupts performance of spatial memory in delayed radial-arm maze tasks where animals have to remember previous location of food items during a delay period in the task to inform subsequent choices (Floresco et al., 1997). The impairment of performance in the delayed task after transient vH-PFC disconnection (via lidocaine injections into ventral CA1 / subiculum and PFC or via optogenetic silencing of vH terminals in PFC) suggests that communication between these two brain areas is required for goal-directed behaviour that relies on short-term working memory (Floresco et al., 1997; Spellman et al., 2015). During goal-searching tasks that require hippocampal activity, goal cells that encode goal location have been recorded in PFC while place cells in the hippocampus encode all locations, suggesting that different aspects of goal-oriented behaviour may be processed along distinct parts of this pathway (Hok et al., 2005). In general, it seems that hippocampal-prefrontal directed communication is necessary for the implementation of memory in guiding goal-directed strategies and in the encoding and updating of task-relevant cues (Goto and Grace, 2008; Spellman et al., 2015; Brady et al., 2010).

Contextual processing during memory encoding and retrieval is highly important, allowing for adaptive behaviour and resolving ambiguity. Contextualising a cue ensures that the appropriate meaning is given to it e.g. seeing a dangerous animal in your house versus at the zoo, behind bars, or even in a movie scene do not warrant the same reaction. Interestingly, both the ventral hippocampus and the prefrontal cortex are crucial players in contextual retrieval (Kennedy and Shapiro, 2004; Maren et al., 2013; Komorowski et al., 2013). Learning of task-specific goal-context relationships as well as aversive learning is impaired in animals with vH lesions (Ruediger et al., 2012; Kjelstrup et al., 2002), supporting the notion that vH is important for relating reinforcers to context during learning. Together, this suggests that the role of memory may be at least in some cases to use contextual

information to help disambiguate between two conflicting actions. In fact, when context retrieval strategies fail and inappropriate behaviours are not inhibited, psychological disorders such as post-traumatic stress disorder (PTSD) may emerge, highlighting the importance of this process (Maren, 2011).

1.1.3.2 Anxiety and threat behaviour

In line with its role in using memory and context to guide decision making under uncertainty, the hippocampal-prefrontal pathway also plays a critical role in anxiety and threat behaviour. In particular, this function is characterised by its involvement in the encoding of fear memories, forming representations of anxiogenic environments and adapting behavioural strategies, all of which are impaired after disconnection of the vH-PFC pathway via pharmacological inhibition and optogenetic silencing (Jin and Maren, 2015a; Hobin et al., 2006; Marek et al., 2018a; Wikenheiser et al., 2017; Adhikari et al., 2011; Padilla-Coreano et al., 2019). An important distinction for understanding the role of this circuit is that anxiety is considered a different behavioural state to fear: where anxiety results from a more distant and uncertain threat, fear occurs as a response to near or imminent, more certain threat (McNaughton, 2011; Graeff, 1994; Blanchard and Blanchard, 1990). Thus, while fear is an acute response to threat, anxiety is a prediction of the likelihood of threat in the future. The hippocampal-prefrontal pathway function in context and prospective memory described above may extend into and be crucial for guiding appropriate avoidance behaviour to potential upcoming, uncertain threats. By using past memories and contextual information, anxiety behaviour can emerge if the projected outcome of a particular action is deemed threatening.

To study anxiety behaviour in the laboratory, distant and potential threats must be recreated. For this purpose, approach-avoidance tasks like the elevated plus maze (EPM) are commonly used (Pellow et al., 1985; Pellow and File, 1986; Walf and Frye, 2007; Calhoon, Gwendolyn G and Tye, Kay M, 2015; Belzung and

Griebel, 2001). Rodents exhibit robust avoidance behaviour of environments in which the likelihood of future threat is increased such as open, exposed and bright areas where they are more visible to predators. The open arms of the EPM represent such an anxiety-inducing environment, in contrast to the safer, closed (walled) arms. In this task, avoidance of the open arms is taken as a proxy for anxiety-like behaviour. Higher anxiety-like behavioural states will exert a pull towards the innate drive to avoid danger, while lower anxiety-like behavioural states will be more permissive of the animal's instinctive exploratory drive (McNaughton, 2011).

Activity in the vH-PFC pathway during conflict-based approach-avoidance tasks has been studied closely in recent years. It has been shown that theta rhythm synchrony increases between the vH and the PFC in anxiogenic environments and drives avoidance behaviour on the EPM (Adhikari et al., 2010; Ciocchi et al., 2015; Padilla-Coreano et al., 2019). In line with this role, anxiety behaviour can be disrupted by vH terminal inhibition in PFC and disruption of theta coupling along the vH-PFC pathway has been shown to reduce anxiety-like avoidance behaviour during EPM exploration (Padilla-Coreano et al., 2016; Kjaerby et al., 2016; Schoenfeld et al., 2014). Furthermore, only a subset of cells in PFC robustly respond to vH input *in vivo*, and these cells harbour spatial representations of aversive and anxiogenic environments (Adhikari et al., 2011; Padilla-Coreano et al., 2016). Importantly, while activation of the vH-PFC pathway increases avoidance, similar manipulations selectively targeting lateral septum-projecting hippocampal cells have the opposite effect (Parfitt et al., 2017; Padilla-Coreano et al., 2019), suggesting that the vH-PFC may have a unique role in initiating avoidance behaviour.

Importantly, ventral hippocampal terminals targeting distinct regions within PFC can regulate both the inhibition and expression of threat responses. Via the learning of safety signals, vH terminals targeting prelimbic PFC promote an anxiolytic effect (Sotres-Bayon et al., 2012; Meyer et al., 2019). However, vH terminals targeting the same prefrontal area have also been shown to regulate the expression

of threat responses like avoidance (Padilla-Coreano et al., 2019), thus promoting an anxiogenic effect. Furthermore, inhibitory vH drive onto infralimbic PFC has been shown to promote the relapse of fear expression (Marek et al., 2018a). Thus, it seems not only that different parts of PFC mediate fear responses differently (Vidal-Gonzalez et al., 2006), but rather that even within a prefrontal area, differences in inhibitory versus excitatory input and cell targeting by vH terminals may underlie opposing roles in behaviour. Hence, it may be the case that distinct sub-circuits within the vH-PFC pathway could mediate opposing responses to uncertain threat. However, this has never been investigated.

Overall, the role of hippocampal-prefrontal communication in anxiety-like behaviour echoes the description given above, which highlights the use of memory and contextualisation in guiding behaviour. For appropriate approach-avoidance behaviour, the emotional context i.e. the perceived future threat producing anxiety must be taken into account. Thus, utilising short and long-term memory and contextualising those memories are key for representing mental and emotional states, shifting between representations and guiding adaptive behaviour (Salzman and Fusi, 2010). Importantly, ventral hippocampal input to PFC seems to inform goal-directed behaviour by supporting both early learning of context associations and emotional processing during anxiety behaviour. This begs the question of how the pathway is involved in relating internal states to task-related goals during emotionally complex tasks. How are context and relevant memories integrated to inform decision making under anxiety-inducing or uncertain paradigms? Crucially, it is important to understand the circuit mechanisms supporting such complex roles in healthy animals and how these may differ in models of psychiatric disorders. Further study into the involvement of the vH-PFC pathway in behaviours such as anxiety-driven avoidance may elucidate anxiogenic and anxiolytic neural mechanisms and pave the way to circuit-based interventions of anxiety-related disorders.

1.1.3.3 Conflicting reports - possible subcircuits?

Studies looking at the role of the vH-PFC pathway during behaviour have consistently brought up conflicting reports on the controlling role of vH over PFC. From neuroanatomical and electrophysiological studies, it has been shown that ventral hippocampal neurons are capable of both inhibiting and activating PFC via recruitment of feed-forward inhibition and direct targeting of excitatory pyramidal cells, respectively (Jay et al., 1992; Carr and Sesack, 1996; Tierney et al., 2004; Parent et al., 2010).

Interestingly, different behavioural studies suggest that the role of vH in controlling PFC circuitry may depend on task demands. Hippocampal activity during memory representation can drive both excitation of PFC cells involved in representation-relevant activity and inhibition of those with unrelated representations to the ongoing experience (Jadhav et al., 2016; Tang et al., 2017). In further examples, during avoidance behaviour, high excitatory drive in PFC anxiety-related neurons correlates with vH input activity (Adhikari et al., 2011) and as discussed above, activation of PFC circuitry drives avoidance, while inactivation promotes exploration. Conversely, inhibition of vH terminals in PFC has also been shown to increase excitatory drive due to a reduced input onto interneurons leading to increased avoidant behaviour (Sotres-Bayon et al., 2012), suggesting that vH input may also mediate approach behaviour via feed-forward inhibition. Importantly, recruitment of specific PFC inhibitory neurons by vH terminals can gate representations of threatening environments such as the EPM open arms and thus inhibit or disinhibit avoidance behaviour (Lee et al., 2019a). Although there is evidence that the vH can flexibly recruit both excitatory and local inhibitory circuitry, little is known about the synaptic and circuit mechanisms that might underlie this dual role.

As described above, in addition to vH-PFC pathway-specific functions, the hippocampus is also involved in memory, spatial navigation and a variety of emo-

tional behaviours. Although involvement of the vH-PFC pathway in these processes has been observed (Spellman et al., 2015; Phillips et al., 2019; Place et al., 2016), the extent of and mechanisms behind the role of ventral hippocampal-prefrontal communication in these processes is still poorly understood. What is clear is that the hippocampus and in particular, the vH-PFC projection participates in multiple distinct behaviours.

With the aim to clarify the mechanisms allowing for such disparate functions to be associated with one pathway, my key questions are i) given that the hippocampus seems to send more than one type of information to PFC, are there multiple routes in this pathway that send distinct types of information? ii) how are hippocampal neurons that project to PFC controlled by upstream circuitry and iii) how does the hippocampus control PFC at a circuit and synaptic level? I will investigate these questions by gaining a better understanding of the cellular makeup of this circuit.

In the next section, I will describe the detailed hippocampal anatomy that underlies the projection to PFC, and the evidence suggesting that it might be far more heterogeneous than previously thought. I will also describe the afferent and efferent connectivity of the hippocampus. In line with the reasoning of Fuster (2001), I propose that it is the connectivity and thus the information available for processing in a given brain area that will confer its given functions. Therefore, key to understanding the role of the vH-PFC pathway is to understand the connectivity and functional properties of the neurons that make up this projection. In particular, my hypothesis is that there are subpopulations in ventral hippocampus that send different information to PFC by receiving unique afferent input.

1.2 Hippocampal structure and function

1.2.1 Hippocampal structure and its circuitry

The mammalian hippocampus is formed by an infolding of the cortex and consists of a group of well-characterised areas (Figure 1.1). In rodents, the hippocampus forms a curved tube-like structure spanning the dorsoventral (or septotemporal) axis of the brain. It is comprised of the dentate gyrus (DG) and the three cornu ammonis (CA) regions CA1, CA2 and CA3 (Figure 1.1 b and c). Although there are differences in opinion as to whether the subiculum should be classified as part of the hippocampus proper or whether it is better classified as part of the subicular complex (which includes the pre- and parasubiculum), here I suggest that it be classified as part of the hippocampal formation (O'Mara, 2006). Thus, throughout this thesis, the hippocampal formation or hippocampus will refer to the DG, the CA areas and subiculum.

Together, these areas form the excitatory hippocampal circuit known as the trisynaptic loop, first described by neuroscientist Santiago Ramón y Cajal (Ramón y Cajal, 1909). In this simplified scheme, information received from entorhinal cortex is routed via the perforant pathway through from the dentate gyrus to subiculum (see Figure 1.2). In addition to the perforant pathway, entorhinal cortex input to hippocampus also reaches the CA1 / subiculum areas via the direct temporoammonic (TA) projection (Figure 1.2). More specifically, in the trisynaptic loop, mossy fibres arising from DG granule cells project to CA3 pyramidal cells; Schaffer collateral fibres originating from CA3 synapse onto pyramidal cells in CA2, CA1 and also extend terminals onto subiculum (Anderson et al., 2000; Valero and de la Prida, 2018). CA1 sends its primary projection to the neighbouring subiculum, alongside projections to extra-hippocampal targets (Amaral et al., 1991; Cenquizca and Swanson, 2007). The subiculum in turn is the main output region of the hippocampus.

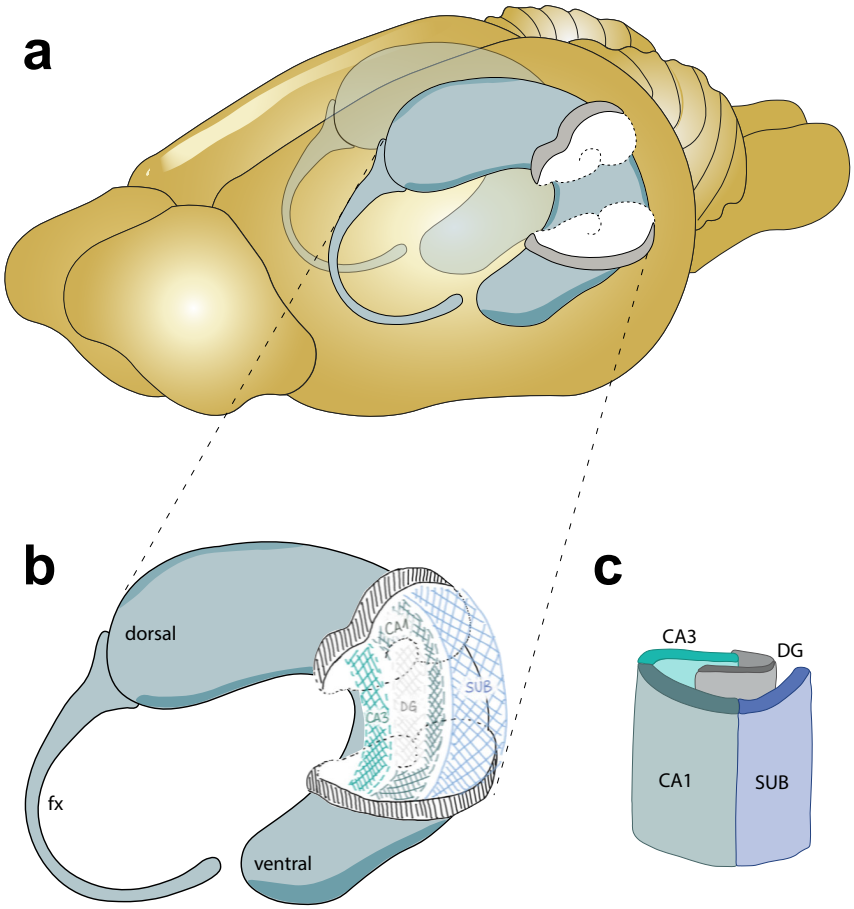

Figure 1.1: Hippocampal structure
(**a**) Schematic of the hippocampal structure (blue; in both hemispheres) in the mouse brain. The cross-sections (white) show a typical transverse hippocampal slice at different points along the longitudinal hippocampal axis. (**b**) Schematic showing a closer view of the hippocampal structure with the hippocampal areas DG, CA1, CA3 and SUB drawn over the slices as they appear in the intact structure. The fornix is a C-shaped fibre bundle that acts as the main output tract of the hippocampus (fx: fornix). (**c**) Schematic of the cortical infolding that gives the hippocampus its characteristic internal structure, as would be seen in a cross-section.

Although there is general consensus on this simplified model, there is still much argument about what actually constitutes CA1 and / or subiculum and where the exact anatomical border between both areas lies (Lee et al., 2014c; Dong et al., 2009; Ding et al., 2020; Wee and MacAskill, 2020; Kim and Spruston, 2012; Bienkowski et al., 2018; Soltesz and Losonczy, 2018). Therefore, for the purpose of consistency throughout this thesis, I will consider them jointly as hippocampal

output areas, focusing on the anatomy of the projection under study.

The stereotyped trisynaptic circuit is maintained throughout the length of the hippocampus. This simple description is referred to as the 'classic' hippocampal circuit and serves as a baseline for understanding hippocampal function and information processing through this structure. Here, information processing refers to how a given input from e.g. entorhinal cortex will be passed on through the hippocampal circuit alongside many other inputs, be altered at every stage along the circuit and ultimately be combined with other inputs to affect local circuitry and produce an output. In a transverse hippocampal slice (cut perpendicular to the hippocampal dorsoventral axis, as depicted in Figure 1.2), the trisynaptic excitatory circuit is spared and mostly intact, allowing for *in vitro* recordings with preserved within-slice connectivity. This experimental setup has allowed for the hippocampus and its circuitry to be studied extensively in the laboratory.

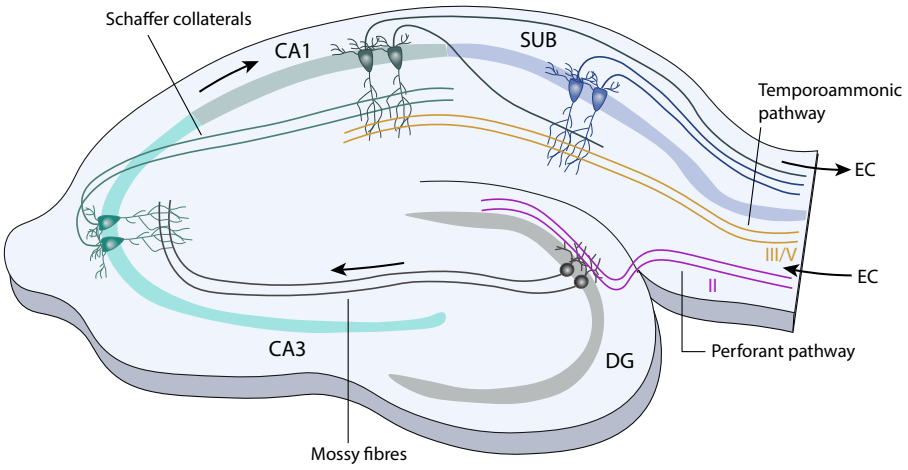

Figure 1.2: The hippocampal trisynaptic circuit
Information flows into the hippocampus via the perforant path input from entorhinal cortex (EC). Perforant path axons synapse onto dentate gyrus (DG) granule cells which then extend mossy fibres to synapse onto CA3 pyramidal cells. CA3 pyramidal neurons send axons known as Schaffer collaterals to synapse onto CA1 neurons, which in turn synapse onto pyramidal cells in subiculum (SUB) and also send axons directly back to EC. EC layers III and V also send synaptic contacts directly onto CA1 and SUB pyramidal cells, bypassing the trisynaptic loop, via the temporoammonic (TA) pathway.

However, despite being one of the most studied brain structures, there are increasing amounts of evidence pointing at a vast, previously overlooked level of heterogeneity amongst hippocampal pyramidal cells along the different anatomical axes (Hunsaker et al., 2008; Leonardo et al., 2006; Strange et al., 2014; Cembrowski et al., 2016a; Cembrowski and Spruston, 2019; Soltesz and Losonczy, 2018). This heterogeneity uncovers many questions regarding its functional consequences for circuit wiring within the hippocampus and behavioural output. The potential of pyramidal cell heterogeneity warrants further investigation to understand how the classical hippocampal circuitry discussed above is parsed out amongst different populations of neurons.

1.2.2 Heterogeneity in hippocampal circuitry

1.2.2.1 A dorsoventral gradient in the hippocampus

One of the most prominent examples of hippocampal heterogeneity is along the dorsal (septal and anterior in humans) to ventral (temporal and posterior in humans) axis of the hippocampus. The ventral and dorsal poles of the hippocampus have been associated with different functions in behaviour as well as presenting gradients in gene expression, physiological properties and connectivity (Cembrowski et al., 2016b,a; Dong et al., 2009; Hunsaker et al., 2008). The dorsal pole is associated with learning and spatial navigation, while the ventral pole is associated with emotional and motivated behaviour (Fanselow and Dong, 2010). However, the demarcation of functional areas seems not to be as strict as a dorso-ventral split, but rather a gradient-like organisation of features superimposed on smaller functional domains along the longitudinal (dorsoventral) axis of the hippocampus (Strange et al., 2014).

Although the trisynaptic pattern of connectivity repeats itself along the lon-

gitudinal axis of the hippocampus, spanning the full length of the structure, the afferent and efferent connectivity along this axis is not consistent. As will be described below, inputs onto and outputs from the hippocampus change as one moves from the dorsal to the ventral pole. The ventral hippocampus is preferentially connected with areas associated with affective and emotional behaviour such as the amygdala, prefrontal cortex and nucleus accumbens, while the dorsal hippocampus is connected with spatial and memory systems such as the retrosplenial cortex.

Consistent with this differing connectivity and as briefly discussed above, lesion studies where dorsal (but not ventral) hippocampus is damaged show deficits in spatial navigation tasks and ventral hippocampal cytotoxic lesions produce anxiolytic effects, but do not affect spatial learning (Bannerman et al., 2002, 2003). Dorsal and ventral hippocampal regions also show differences in their contributions to goal-oriented searching behaviour such as during the Morris water maze task, or foraging behaviour. Ventral hippocampal lesions impair early goal-oriented searching in complex trial-and-error learning tasks whereas dorsal hippocampal lesions impair only late phases of spatial learning (Ruediger et al., 2012). Lesions to the ventral hippocampus also impair the conditioned expression of fear (Maren and Fanselow, 1995). Thus, it seems that heterogeneity brings with it the possibility of multiple parallel streams of information processing within the same structure.

In support of the differential functional outcomes of dorsal versus ventral lesions, the presence of the cells thought to represent space, place cells, varies along the dorsoventral axis (Ciocchi et al., 2015; Strange et al., 2014; Fanselow and Dong, 2010). Dorsally, place cells are more abundant, stable and spatially tuned, whereas ventrally they are more sparse and show larger, diffuse place fields (areas they represent) (Moser et al., 1993; Maurer et al., 2005; Ciocchi et al., 2015; Kjelstrup et al., 2008) - much like a visual cortex cell can be more or less tuned to a specific visual stimulus. Partial lesion studies, sparing either the dorsal or the ventral portions of the structure, show that rats with ventral hippocampal lesions perform at near-

normal rates in a water maze task requiring spatial learning as long as 20 to 40 % of the dorsal hippocampus remains intact, suggesting that the function of spatial navigation may not be represented along the entire longitudinal axis of the hippocampus, but specifically in the dorsal region (Moser et al., 1995). This specialisation of the dorsal hippocampus is likely to be a result of a combination of its upstream and downstream connectivity, genetic markers and many other characteristics.

Consistent with anatomy and function, marked gradients in gene expression exist along the dorsoventral axis as well, where many genes have limited expression to either dorsal or ventral areas (Cembrowski et al., 2016a; Dong et al., 2009; Thompson et al., 2008; Lein et al., 2007). For instance, in line with its involvement in emotional processing, the ventral hippocampus has a much higher expression of serotonin (5-HT) and gastrin-releasing peptide receptors than the dorsal hippocampus (Tanaka et al., 2012; Roesler et al., 2006) and distortions in the expression of both of these receptors have been found in models of psychiatric disease that present deficits in emotional processing (Garcia-Garcia et al., 2017; Lowry, 2002; Dong et al., 2009). Strikingly, more extensive heterogeneity can be found within hippocampal cell-types along the dorsoventral axis i.e. CA1 neurons at dorsal and ventral hippocampal poles than across cell types e.g. CA3 and CA1 pyramidal cells at the same dorsoventral position (Cembrowski et al., 2016a). In combination with pyramidal cell position along the dorsoventral axis, projection-specificity also determines heterogeneity, with cell populations in the hippocampus with different downstream targets presenting varying degrees of transcriptomic heterogeneity (Cembrowski et al., 2018b). Elucidating the molecular architecture of different hippocampal regions provides a key framework for predicting functional differentiation along a given axis. The anatomical differentiation between dorsal and ventral hippocampus helped reconcile its function in spatial navigation versus affect, and perhaps similar disconnects can be revealed by teasing apart hippocampal heterogeneity at many additional levels.

Interestingly, intrahippocampal projections from dorsal onto ventral pyramidal cells are also present (Tannenholz et al., 2014; Meira et al., 2018). This suggests that dorsal hippocampal inputs may be integrated into affective and emotional behaviour via these internal projections. In turn, this internal communication points at a more diffuse separation of functions along the dorsoventral axis, where function may be more accurately described by projection identity and connectivity of a given population of cells within the hippocampus rather than purely by anatomical position along a given axis.

1.2.2.2 Multiple topographic gradients in hippocampus

In the CA1 / subiculum area, distinct cell types based on their projection targets and positioning along the hippocampal axes show different electrophysiological, morphological and connectivity characteristics (Igarashi et al., 2014a; Lee et al., 2014c; Graves et al., 2012; Kim and Spruston, 2012). The three main hippocampal axes along which these features are compared are the longitudinal or dosoventral axis, described above, the radial (superficial-deep) and the transverse (proximal-distal) axis (see Figure 1.3).

Pyramidal cells can be classified into two overarching groups on the basis of their electrophysiological firing properties, regular-spiking cells and burst-firing cells (Jarsky et al., 2008; Menendez de la Prida et al., 2003). These cell groups are organised along the hippocampal axis from CA1 to subiculum, with bursting cells occupying deeper layers in subiculum (closer to stratum oriens) further from CA1 (more distally) and regular spiking cells more proximal to CA1 and in more superficial layers (closer to stratum lacunosum moleculare). This suggests that in addition to a marked dorsoventral heterogeneity, the properties of hippocampal cells are dramatically altered along both the superficial-deep axis, and the proximal-distal axis (from CA1 to subiculum; see Figure1.3).

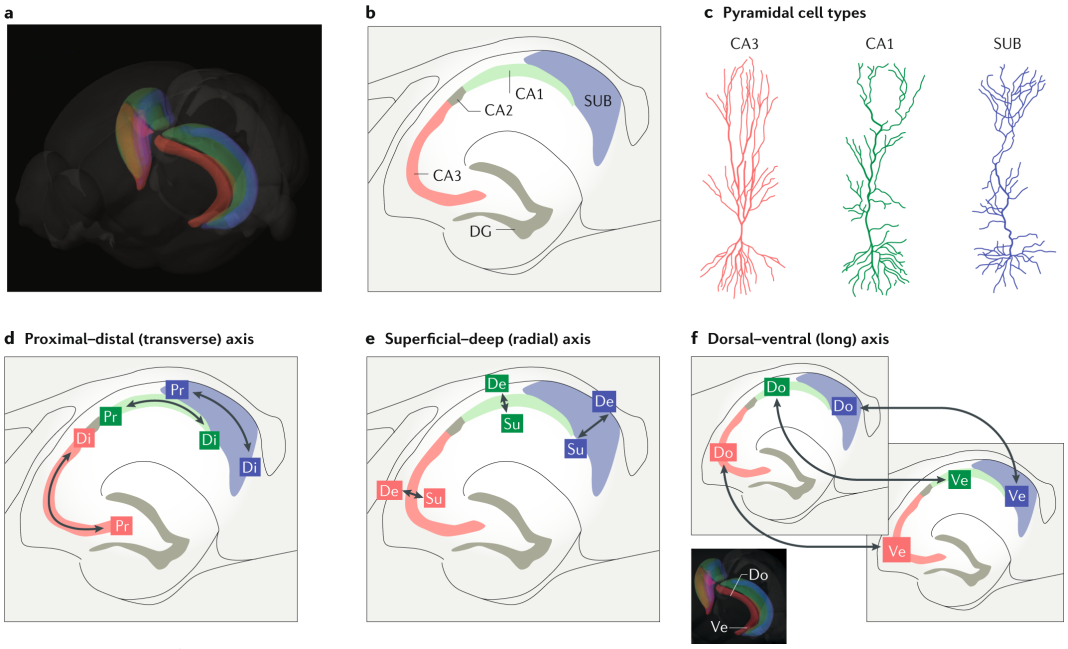

Figure 1.3: Overview of axes and cell types of the hippocampus ((a) A 3D overview of the structure of the hippocampus in the mouse brain. The CA3, CA1 and subiculum (SUB) regions are respectively coloured red, green and blue. The image was prepared using the Allen Brain Explorer 2. **(b)** A 2D illustration of the hippocampal circuit, as seen in a cross section of the hippocampal long axis. **(c)** Morphological illustrations of pyramidal cells in CA3, CA1 and the SUB. **(d-f)** Schematic illustrations of the three spatial axes of the hippocampus: the proximaldistal (PrDi) axis (also known as the transverse axis (d)), the superficial-deep (SuDe) axis (also known as the radial axis (e)) and the dorsal-ventral (DoVe) axis (also known as the long axis (f)). Figure taken from Cembrowski and Spruston (2019).

Reinforcing the importance of distinctions across these axes, recent experiments have aimed to probe the functional contribution of distinct areas along CA1 and subiculum. These data show that across both the transverse and radial axes, the function and wiring of CA1 / subiculum neurons is dramatically different. Cells in the superficial layers have been shown to encode stable representations of the environment and engage in sharp wave ripples, while deep cell layers flexibly encode representations of the environment, allowing for learning via salient stimuli (Valero et al., 2015; Lee et al., 2014c; Soltesz and Losonczy, 2018; Cembrowski et al., 2018a; Danielson et al., 2016). Along the transverse axis, time and space are thought to be separately represented distally and proximally, both in CA1 and in CA3 (Beer et al., 2018; Nakamura et al., 2013; Knierim et al., 2014). Memory

retrieval has also been shown to require activity in proximal, but not distal CA1 (Nakazawa et al., 2016). Hence, the processing of distinct streams of information along these axes may provide a mechanism for integrating spatial, memory and emotional components to guide decision making and goal-directed behaviour.

Overall this suggests that in order to understand the circuit function of the hippocampus, these anatomical gradients must be taken into account. By doing so, gradients in connectivity, gene expression, electrophysiology and morphology segregated along these axes will likely uncover many yet unknown functional differences. Ultimately, understanding any underlying principles of hippocampal heterogeneity will aid in predicting the organization of synaptic connectivity within hippocampal circuits, a key determinant of circuit function. This in turn will aid in mechanistically understanding the ability of the hippocampus to carry out so many seemingly varied functions.

1.3 Efferent and afferent connectivity of the vH

1.3.1 Efferent outputs from vH are organised in parallel and have unique functions

In addition to the marked heterogeneity along spatial gradients of the hippocampal CA1 and subiculum, it is becoming increasingly apparent that the output from the classical trisynaptic loop circuit is also markedly heterogenous. In particular, ventral areas of CA1 and subiculum send projections to a vast array of limbic structures, including the nucleus accumbens, medial prefrontal cortex, amygdala, bed nucleus of the stria terminalis, the ventral portion of lateral septum and hypothalamus (Figure 1.4) (Tannenholz et al., 2014; Naber and Witter, 1998; Cenquizca and Swanson, 2007; Gaykema et al., 1991).

Interestingly, the collateralisation of pyramidal cell axons arising from the hippocampus is very low. In particular those originating from the subiculum, where the most dense extra-hippocampal projections arise, range from 0 to 12 %, while in CA1, which provides lower density projections, it ranges between 17 and 39 % (Naber and Witter, 1998; Ciocchi et al., 2015; Wee and MacAskill, 2020). This suggests that the vast majority of projection neurons in ventral hippocampus send information to one area only. Thus, each of these populations of projection neurons is proposed to have unique functions during behaviour. As follows, this suggests that the projection to PFC from ventral hippocampus arises from a unique population of neurons, distinct from those projecting to other areas. In the following paragraphs I will provide a summary of specific ventral hippocampal projections to areas other than PFC and their associated functions.

Within the limbic system, the ventral hippocampus projects to the nucleus accumbens (NAc). The NAc is part of the striatum and its structure is composed of a core and a shell. It is important for reward-seeking behaviour and its circuitry is heavily affected in addiction (Russo et al., 2010; Stuber et al., 2011; MacAskill et al., 2014). Ventral hippocampal axons preferentially project to D1 receptor expressing medium spiny neurons (MSNs), which are part of the direct striatal pathway (Goto and Grace, 2005; MacAskill et al., 2012) and in turn send projections to the ventral tegmental area (VTA) to regulate motivated behaviour (Yang et al., 2018a). This projection has been associated with regulating susceptibility to depression and storing social memory (Bagot et al., 2015; Okuyama et al., 2016; LeGates et al., 2018).

The ventral hippocampus also sends strong projections to various amygdala nuclei (Cenquizca and Swanson, 2007; McDonald and Mott, 2017; Kishi et al., 2006). The amygdala is classically associated with innate fear responses, anxiety-like behaviour, fear conditioning and extinction of fear memories (Davidson, 2002; Namburi et al., 2015; Tye et al., 2011; Duval et al., 2015) and its connectivity onto

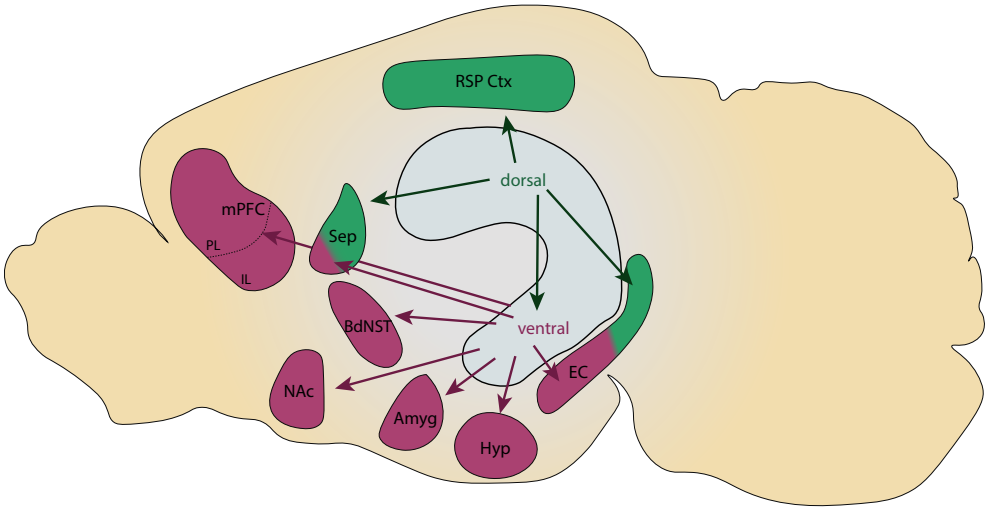

Figure 1.4: Hippocampal efferents along the dorsoventral axis
The hippocampus sends projections to a vast array of brain structures along its dorsoventral axis. These projections mostly arise from CA1 and subicular pyramidal neurons. The dorsal hippocampus sends projections to the ventral hippocampus and the extrahippocampal retrosplenial cortex (RSP Ctx) and septum (Sep). The ventral hippocampus projects more densely to a variety of limbic structures such as the medial prefrontal cortex (mPFC), bed nucleus of the stria terminalis (BdNST), nucleus accumbens (NAc), amygdala (Amyg) and hypothalamus (Hyp). Both dorsal and ventral hippocampus send projections to the entorhinal cortex (EC). Figure layout taken from (Tannenholz et al., 2014).

the ventral hippocampus mediates anxiety-related behaviours (Felix-Ortiz et al., 2013; Maren and Fanselow, 1995). In accordance with the functional gradient along the dorsoventral axis of the hippocampus, ventral CA1 and subiculum project much more strongly to the amygdala than their dorsal counterparts (Canteras and Swanson, 1992; van Groen and Wyss, 1990). Although amydgala inputs onto hippocampus have been extensively studied, less has been investigated on the function of the hippocapo-amygdalar side of the reciprocal circuit (Pitkänen et al., 2000). Recently, it has been shown that the ventral hippocampal-amygdala projection is involved in mediating the retrieval of contextual fear memories (Xu et al., 2016). In line with these findings, inhibition of hippocampal terminals in the basal amygdala impairs contextual fear memory formation (Jimenez et al., 2018). Characteristic of the limbic system, its constituent structures are highly interconnected. The amygdala also modulates anxiety-like behaviours via reciprocal connectivity with the PFC (Felix-Ortiz et al., 2016).

In line with its role in mediating anxiety-like behaviours and stress responses, the ventral subiculum also sends direct projections to the bed nucleus of the stria terminalis (BdNST) and the lateral hypothalamus (Cullinan et al., 1993; Jimenez et al., 2018). The BdNST regulates anxiety-related behaviours within anxiogenic environments and interestingly, different output streams from BdNST to downstream structures modulate anxiety behaviour in opposite directions (Kim et al., 2013). Via its projections to the lateral hypothalamus, which is involved in fear and stress responses (Tovote et al., 2015), the ventral hippocampus can exert a direct influence over the hypothalamic-pituitary-adrenal (HPA) axis. The HPA axis mediates stress responses to systemic and psychological stressors. Psychological stress responses can be activated and inhibited by limbic structures like the hippocampus (Ulrich-Lai and Herman, 2009). Thus, via this pathway, the ventral hippocampus can exert control over innate anxiety, where activation of hippocampo-hypothalamic terminals increases avoidance behaviour (Jimenez et al., 2018). Ventral hippocampal lesions can lead to exaggerated HPA axis responses to stressors, suggesting that perhaps different cells to those identified by Jimenez et al. (2018) may mediate inhibition of hypothalamic cells (Herman et al., 2005; Smith and Vale, 2006). Pyramidal cells in the vH express corticosteroid receptors making them sensitive to HPA-driven release of corticosteroids during stress responses. This in turn creates a negative-feedback loop of HPA activity allowing the hippocampus to inhibit hypothalamic activity and thus prevent further stress-induced corticosteroid release when corticosteroid levels are high (Jacobson and Sapolsky, 1991).

Overall, the ventral hippocampal circuit is organised such that each distinct projection to a downstream region is arranged as a parallel circuit. In summary, the parallel projections from vH described here seem to support varied functions. Projections to the NAc are involved in motivation and reward in line with its roles in social and drug-seeking behaviour. Hippocampo-amygdalar communication is implicated in learned threat responses and anxiety-like behaviour and connectivity with the lateral hypothalamus and the BdNST mediates responses to acute stress.

As discussed previously, the vH projection to PFC is involved in the integration of memory and emotional context to guide decision making and goal-oriented behaviour and its activity is associated with avoidance behaviour.

This projection-target driven functional heterogeneity has profound consequences for our understanding of how the hippocampus receives and utilises information. In particular with respect to the projection of vH to PFC, it suggests that the neurons that make up this projection form a unique subpopulation of hippocampal projection neurons that may be wired very differently to other subpopulations within the classic trisynaptic loop. Genetic heterogeneity amongst hippocampal projection neurons supports the idea of parallel streams of information (Cembrowski et al., 2016a, 2018b). Interestingly, amongst these unique hippocampal projection populations, PFC-projecting pyramidal cells show the highest level of within-population genetic heterogeneity (Cembrowski et al., 2018b). Overall, the ventral hippocampus is composed of multiple unique populations of neurons, each projecting to distinct downstream regions, and mediating unique behavioural functions. Of these projections, the projection to PFC seems to have a particularly high level of heterogeneity, perhaps underscoring the complexity of information required for its associated functions.

1.3.2 Afferent input to vH is poised to relay unique information to different projection neurons

The heterogeneity of both structure and function of the ventral hippocampal circuit suggests there are multiple parallel streams of projection neurons, each involved in different functions. A key question is how these different populations may be uniquely controlled. A crucial point of control is the afferent input each population receives. However, how individual populations of neurons in vH are innervated by afferent input is only beginning to be understood (Wee and MacAskill, 2020).

The densest afferent input to vH arises from entorhinal cortex (Aggleton and Christiansen, 2015). It is the main source of cortical input and provides most of the sensory information that is then processed by the hippocampus (Witter, 1993). However, there are also numerous other brain regions that provide input to the ventral hippocampus, both directly and indirectly, including medial septum, certain thalamic regions and the amygdala (Fanselow and Dong, 2010). Here, I will discuss the main afferent projections targeting ventral CA1 and subiculum cells, some of which will be studied in more detail throughout this thesis.

Entorhinal cortex layers II and III project to CA1 pyramidal cells via the indirect perforant path as well as directly from layer III onto CA1 via the temporoammonic (TA) pathway (see Figure 1.2), forming connections that are a crucial part of the hippocampo-neocortical dialogue. The entorhinal cortex is a key node in the encoding of spatial as well as time representations, both crucial functions for survival and for the correct formation of episodic memories (Tsao et al., 2018). Its two main subdivisions, medial and lateral entorhinal cortex, relay spatial and non-spatial information to the hippocampus, respectively, and target different regions along the proximo-distal and superficial-deep axes of the hippocampus (Tsao et al., 2013; Hargreaves et al., 2005; Masurkar et al., 2017; Valero and de la Prida, 2018; Aronov et al., 2017). Entorhinal cortex provides high-order, contextual and processed multimodal sensory information to the hippocampus which has been associated with consolidation of long-term memories, memory-guided behaviour and forming contextual and cue associations (Squire, 1992; Remondes and Schuman, 2004; Li et al., 2017; Igarashi et al., 2014b).

In line with the topographical connectivity between entorhinal cortex and hippocampus (more ventral parts of the former targeting ventral regions of the latter) only ventral entorhinal spatially tuned cells, which have a much lower spatial resolution than their dorsal counterparts, contact the more ventral hippocampal regions (Hafting et al., 2005). Although there is evidence for entorhinal cortex sub-

regions relaying spatial and non-spatial representations to the hippocampus, recent emerging theories suggest that the role of this circuitry may not be exclusive to one or the other. Rather, entorhinal input is hypothesised to compute a more general and abstract cognitive map which encompasses task-relevant features across time (Tavares et al., 2015; Schiller et al., 2015; Aronov et al., 2017). Such computations are thought to be crucial for adaptive emotional behaviour and may inform activity in the vH-PFC pathway.

Beyond cortical inputs, the CA1 and subicular areas of vH receive weaker, although varied afferents from a wide range of subcortical areas providing sensory and contextual information (Strange et al., 2014). Afferent regions include the amygdala, anterior thalamic nuclei, the nucleus of the diagonal band of Broca (DBB), medial septum and hypothalamus (Wyss et al., 1979; DeVito, 1980; Amaral and Cowan, 1980; Aggleton, 1986; Pikkarainen et al., 1999; Müller and Remy, 2018; Shibata, 1993; Pi et al., 2020; Wee and MacAskill, 2020).

Inputs from basolateral amygdala to ventral hippocampus are engaged during sociability and mood-related behaviours such as responses to chronic stress and they provide bidirectional control of anxiety-related behaviours (Kim and Han, 2016; Felix-Ortiz et al., 2013). Amygdala neurons projecting to vH have been found to respond to both positive and negative valence cues (Beyeler et al., 2016), suggesting that the amygdala may relay general information about task-relevant stimuli as well as anxiety-related information. With regards to anxiety-related information, amygdala activity increases during exploration of an anxiogenic environment (Adhikari et al., 2015). Recently, it has been shown that different amygdala nuclei project to the ventral hippocampus in a lamina-specific pattern along the radial axis, and promote both avoidance and approach behaviour within an anxiogenic environment by engaging deep or superficial layer CA1 cells, respectively (Pi et al., 2020). Together, these findings suggest that the amygdala-hippocampal input pathway carries information regarding anxiogenic environments, allowing the hippocampus to

form a representation of its surroundings to inform behaviour. Notably, it mediates this in a bidirectional manner.

The basal forebrain areas of the medial septum and diagonal band of Broca send cholinergic, glutamatergic and GABAergic input to the hippocampal CA3 as well as CA1 / subiculum areas (Krnjević and Ropert, 1982; Amaral and Cowan, 1980; Witter and Amaral, 2004; Okada and Okaichi, 2010; Wee and MacAskill, 2020; Huh et al., 2010). These projections play a role in learning and memory and importantly, exert control over excitability levels in CA1 depending on behavioural state (Smythe et al., 1991; Müller and Remy, 2018). Furthermore, the medial septum and diagonal band of Broca strongly synchronise with hippocampal theta rhythm activity and are hypothesised to be the driving force initiating these oscillations (Vertes and Kocsis, 1997; Vertes et al., 2004; Buzsáki, 2002). As described above, the vH synchronises at theta with the PFC, prominently within anxiogenic environments (Adhikari et al., 2010; Padilla-Coreano et al., 2019). Together, these findings suggest that basal forebrain input to vH may have a crucial role in supporting theta-dependent anxiety-like behaviour.

Thalamic input to ventral hippocampus has also been studied due to its implication in memory and generation of theta oscillations, with midline and anterior thalamic nuclei such as the nucleus reuniens providing excitatory drive onto hippocampal output regions CA1 and subiculum (Herkenham, 1978; Varela et al., 2014; Witter, 2006; Wouterlood et al., 1990; Bertram and Zhang, 1999; Dolleman-Van Der Weel and Witter, 1996). These inputs have been shown to be subthreshold onto pyramidal cells and suprathreshold onto interneurons (Dolleman-Van der Weel et al., 1997). They are thought to amplify signals from other sources, such as entorhinal cortex and CA3, and play a role in episodic memory formation (Aggleton and Brown, 1999; Zhang and Bertram, 2002; Mitchell and Dalrymple-Alford, 2005). The nucleus reuniens also serves as a relay for prefrontal cortex feedback onto ventral hippocampus and targets different projection-specific cells in CA1 to

different extents (Varela et al., 2014; Wee and MacAskill, 2020). While the anterior thalamus projects preferentially to subiculum, nucleus reuniens afferent terminals contact more cells in CA1 (Shibata, 1993; Prasad and Chudasama, 2013). Tracing and thalamic stimulation studies suggest that anterior thalamic input is weaker onto ventral than onto dorsal subiculum, in line with the proposed role for the anterior thalamus in spatial memory (Bertram and Zhang, 1999; Van Groen and Wyss, 1995; van Groen et al., 2002; Zugaro et al., 2001). Similar to septal neurons, cells in anterior thalamus are also theta-modulated and aid in the generation of hippocampal theta-oscillations (Buzsáki, 2002; Child and Benarroch, 2013). The hippocampus projects back to the anterior thalamus via subicular projection neurons, suggesting that thalamic nuclei may modulate CA1 and subicular excitability dependent on hippocampal output (Dolleman-Van der Weel et al., 1997; Herkenham, 1978; Witter et al., 1990).

As with efferent output, gradients have been observed in hippocampal afferents, so that cells at different positions along the dorsoventral axis receive distinct combinations of input (Amaral and Witter, 1989; Strange et al., 2014; Fanselow and Dong, 2010; Amaral and Cowan, 1980; Agster and Burwell, 2013). Inputs are usually topographically conserved, so that cells along the e.g. dorsoventral axis of the entorhinal cortex project in a parallel fashion to cells along the hippocampal dorsoventral axis. Most differences in connectivity are present in a gradient-like manner. However, some inputs are segregated in a more binary fashion. For example, retrosplenial cortex (which receives dorsal hippocampal input), projects exclusively back to dorsal hippocampus and conversely, prefrontal cortex (which receives input mostly from ventral hippocampus) provides input back onto ventral CA1 cells via nucleus reuniens (Prasad and Chudasama, 2013; Aggleton and Christiansen, 2015). This differential afferent connectivity provides a blueprint for dissociation of functions along different hippocampal axes and amongst different projection populations, which are largely non-overlapping and occupy distinct areas within the hippocampus (Bannerman et al., 2004; Strange et al., 1999; Wee and

MacAskill, 2020; Kim and Spruston, 2012).

Overall, afferent connectivity is key to determining the functional role of a given brain area or subregion within a brain structure, as it will determine the information that is processed there. Gradients of afferent input into different hippocampal regions or onto different projection populations may thus underlie the functional segregation along the hippocampal axes (Wee and MacAskill, 2020). Therefore, in order to more fully understand the functional role and supporting circuitry of the vH-PFC pathway, it is important to investigate its afferent connectivity and any possible patterns or heterogeneity within it.

Synthesis

In the two sections above I have discussed the heterogeneity across multiple axes of the hippocampus, both spatially, genetically and in terms of downstream projection target and afferent connectivity. As discussed in section 1.1, understanding of the role of the vH-PFC projection is confounded by the fact that it seems to fulfil many different functions. Therefore, the main theme running through this thesis is that there may be two or more populations of PFC-projecting neurons in vH, varying across the genetic or spatial axes, each conveying unique information to PFC, and with a distinct role during behaviour.

1.4 Hippocampal control of PFC circuitry: use of canonical circuit motifs

Despite a large body of work aiming to understand the role of hippocampal input into PFC, it is still unclear exactly how the vH exerts its control over PFC circuitry. In order to address this question, it is important to understand the existing circuit

motifs within PFC and those utilised across different long-range projections that may facilitate this control. Additionally, the type of cells recruited during specific tasks by vH terminals in PFC may support the distinct roles of this pathway and is an important point of investigation. In this section I will discuss circuit motifs and cell types present in the PFC and ventral hippocampus as well as what is known so far regarding the synaptic mechanisms of vH-PFC communication. The aim is to provide an overview of the possible ways in which ventral hippocampal projection neurons may be exerting control over PFC circuitry to affect behaviour.

The connectivity of the PFC with other brain areas is crucial for granting it its associated functions. For example, PFC receives sensory information from external stimuli via thalamic afferents. Information regarding internal and emotional states is relayed mostly to the pre- and infralimbic PFC via structures such as the hippocampus, the hypothalamus and the amygdala (Adhikari et al., 2010; Felix-Ortiz et al., 2016; Hoover and Vertes, 2007). From the ventral hippocampus, efferent PFC-projecting fibres ipsilaterally reach the PFC via the fornix, terminating in the infralimbic, prelimbic, and anterior cingulate prefrontal regions (Hoover and Vertes, 2007; Jay and Witter, 1991; Varela et al., 2014). In these areas, they target excitatory pyramidal neurons as well as GABAergic inhibitory interneurons in a monosynaptic manner (Jay et al., 1992; Carr and Sesack, 1996; Tierney et al., 2004; Parent et al., 2010). Single-pulse stimulation of the hippocampus *in vivo* induces both excitatory (EPSP) and inhibitory (IPSP) post-synaptic potentials in prefrontal pyramidal cells (Dégenètais et al., 2003), confirming that the hippocampus is capable of both stimulating and inhibiting prefrontal circuitry. The vH-PFC pathway also displays activity-dependent plasticity, providing an additional mechanism by which the hippocampus can alter PFC network activity (Jay et al., 1995).

The prefrontal cortex, like the hippocampus, is marked by a vast heterogeneity of interneurons that can be found across its structure (Harris et al., 2018; Huang and Paul, 2019; Donato et al., 2015; Isaacson and Scanziani, 2011). The presence

of various classes of interneurons aids in the production of combinations of connectivity motifs within neuronal circuits, which will be described in detail below. The array of connectivity motifs in turn allows for efficient coordination of parallel streams of information and plays a key role in learning, memory and cognitive flexibility (Garcia-Junco-Clemente et al., 2017; Lee et al., 2019a; Artinian and Lacaille, 2018; Abbas et al., 2018; Gruber et al., 2010; Khan et al., 2018; Xia et al., 2017). The vast diversity of inhibitory neuron populations in PFC also plays a crucial role in maintaining an appropriate excitation/inhibition (E/I) balance amongst cortical circuits. Dysfunctions in cortical E/I balance are a common feature of psychiatric disorders involving cognitive and social impairments (Belforte et al., 2010; Ohta et al., 2020) and are exacerbated by adverse early life experiences, which are ubiquitous amongst psychiatric disorders (Liang et al., 2015; Holland et al., 2014; Gruber et al., 2010). Thus, it is overwhelmingly clear that the correct functioning and innervation of inhibitory interneurons in PFC is a crucial element to maintaining the correct E/I balance and allowing for normal cognitive and emotional function (Sohal and Rubenstein, 2019).

In line with their role in coordinating prefrontal activity, inputs onto different classes of prefrontal interneurons can act as gating mechanisms for specific afferent information and affect behavioural output during social, anxiety-like, exploration and decision making behaviour (Lu et al., 2017; Lee et al., 2019a; Abbas et al., 2018; Lagler et al., 2016; Serrano and Caroni, 2019; Sun et al., 2020). The involvement of various classes of interneurons in cortical circuit motifs increases the computational power of PFC and may aid in channeling afferent inputs differently dependent on task demands (Tremblay et al., 2016). These gating or channeling effects are brought about by inhibiting or allowing parallel inputs onto PFC. Interneurons can regulate the segregation of intermingled pyramidal cells involved in separate cortical circuits by selectively silencing projection-specific neurons. For example, amygdala inputs onto PFC have been shown to recruit soma- and dendrite-targeting inhibitory interneurons that silence prefrontal-amygdalar but not cortico-

cortical communication (McGarry and Carter, 2016). To reinforce this segregation, axon-targeting interneurons in PFC selectively target amygdala-projecting but not cortico-cortical pyramidal cells (Lu et al., 2017). The recruitment of prefrontal interneurons into distinct neuronal ensembles by different afferents may thus support distinct computations and behavioural roles attributed to the PFC. Overall, input to different prefrontal cortex interneurons varies in a task-dependent manner and is an important mechanism to affect behavioural output of any prefrontal targeting projection.

With regards to ventral hippocampal input, recent experiments have shown that vH terminals also target different types of interneurons in PFC, which in turn mediate different behaviours. Soma-targeting vasointestinal polypeptide (VIP)-positive interneurons are recruited by vH during the exploration of anxiogenic environments to allow for increased vH-PFC synchronisation via disinhibition of prefrontal pyramidal cells (Lee et al., 2019a). Interestingly, VIP+ interneurons can both inhibit and excite prefrontal pyramidal cells through direct inhibitory contacts (Garcia-Junco-Clemente et al., 2017) or indirect disinhibition mediated by the silencing of neighbouring interneurons (Pi et al., 2013). Soma-targeting parvalbumin (PV) positive interneurons have been shown to be recruited by vH for a variety of functions such as social behaviour (Sun et al., 2020) and fear relapse (Marek et al., 2018a) and have also been shown to be important for hippocampal-prefrontal synchronisation (Korotkova et al., 2010). Dendrite-targeting somatostatin (SOM) positive interneurons are also recruited by vH terminals in PFC and have been shown to regulate the flow of information between these two structures during spatial working memory encoding (Abbas et al., 2018) and have more recently also been implicated in the expression of fear (Koppensteiner et al., 2019; Cummings and Clem, 2020). Overall, ventral hippocampal input onto distinct prefrontal interneuron classes and pyramidal cell populations allows for the engagement of many canonical circuit motifs, from feed-forward inhibition to disinhibition and at a larger scale, push-pull circuits allowing for bidirectional control of prefrontal activity.

Thus, hippocampal-prefrontal communication may exploit not only different circuit motifs but also the cellular heterogeneity available across the pathway in order to support multiple functions. Different subsets of pyramidal cells in PFC also receive distinct forms of excitation and inhibition that allow for different computations (Lee et al., 2014a). In line with this, vH terminals in PFC have been shown to preferentially target pyramidal neurons based on their projection targets (Liu and Carter, 2018). Thus, a more in-depth understanding of both the cellular and synaptic targets of vH terminals in PFC and the circuit motifs that may facilitate multiple streams of communication between the two structures is crucial to clarify how the vH-PFC projection can support multiple functions.

Overview

In the following chapters, I explore a step-by-step approach to understanding and mapping the ventral hippocampal-prefrontal circuit genetically, physiologically and behaviourally. I firstly introduce the methodology implemented to carry out these experiments in Chapter 2. In Chapter 3 I show that hippocampal-prefrontal projection neurons form two different populations, segregated along the deep and superficial poles of the radial axis of the hippocampus. In Chapter 4, I discuss results characterising afferent inputs to PFC-projecting cells in ventral hippocampus as well as local connectivity of PFC-projecting cells with neighbouring interneurons. In Chapter 5, ventral hippocampal influence on PFC is examined, comparing the effects of superficial and deep layer hippocampal efferent axons on prefrontal pyramidal cells and interneurons. Furthermore, the behavioural relevance of these projections during the exploration of an anxiogenic environment is tested using *in vivo* optogenetics. Finally, in Chapter 6 I discuss my findings and how they fit into the current working hypothesis of the ventral hippocampal-prefrontal circuit and what they may add to the existing hypotheses on general superficial and deep layer hippocampal function. I also focus on the caveats of the presented data as well as future directions in which to take this piece of work.

Chapter 2

Materials and Methods

2.1 Animals

All experiments were performed on adult mice ranging from 6 to 13 weeks of age. For eletrophysiological experiments, the age was kept between 7 and 10 weeks. For breeding of transgenic animals, breeding pairs were kept for a maximum of 6 months or 8 litters, whichever came first.

Four animal groups were used for the experiments presented throughout this thesis: (1) All electrophysiological experiments studying intrinsic properties of the two PFC-projecting cell layers and NAc-projecting cells in ventral hippocampus were carried out on 6 - 10 week old (adult) male C57BL / 6 (wild-type) mice provided by Charles River. Mice were ordered at 5 - 6 weeks of age. For anatomical characterisation of the different projection populations, adult female mice were used as well as male mice. Lastly, wild-type C57BL / 6 mice (or wild-type littermates from our transgenic colony (see group 2) were used for hippocampal to PFC long-range input experiments (see Chapter 5). (2) The *Calb1-IRES2-Cre-D* (Jackson Laboratories #028532) knock-in line was used for experi-

ments targeting superficial layer (*Calbindin1*-expressing; see Chapter 3, Figure 3.3) PFC-projecting cells. *Calb1-IRES2-Cre-D* knock-in mice have Cre-recombinase expression directed to *Calbindin1*-expressing cells. Both the endogenous *Calbindin1* and Cre-recombinase expression are under transcriptional control of the endogenous promoter and enhancer elements of the *Calbindin1* locus. (3) The *Slc32a1(VGAT)-IRES-Cre* (Jackson Laboratories #016962) knock-in line was used to target interneurons (see Chapter 4). In these mice, Cre-recombinase expression is targeted to inhibitory GABAergic cells expressing vesicular GABA (γ-aminobutyric acid) transporter (*VGAT*), under transcriptional control of endogenous *VGAT* locus enhancers and promoters. The publication documenting the generation of this transgenic line does not show extensive Cre-recombinase expression in cortex in contrast to sub-cortical structures, which may explain the low cell count of interneuron-contacting cells observed in ventral hippocampus when tracing with G-deleted rabies via cortical interneurons (see Figure 5.3, Chapter 5; (Vong et al., 2011)). (4) The *B6.129P2-Pvalb*$^{tm1(cre)Arbr}$*/J* (Jackson Laboratories #017320) knock-in line was used to target parvalbumin (PV) expressing interneurons (see Chapter 4, Figures 4.8 and 4.9). *B6.129P2-Pvalb*$^{tm1(cre)Arbr}$*/J* knock-in mice have Cre-recombinase expression directed to parvalbumin-expressing interneurons under transcriptional control of endogenous parvalbumin locus enhancers and promoters. Both the endogenous PV and Cre-recombinase expression are under transcriptional control of the endogenous promoter and enhancer elements of the *Pvalb* locus.

Mice were housed in cages of 2 - 4 and kept in a humidity and temperature controlled environment under a 12 h light/dark cycle (lights on 7 am to 7 pm) with ad-libitum access to food and water. All experiments were approved by the U.K. Home Office as defined by the Animals (Scientific Procedures) Act 1986 and University College London ethical guidelines.

2.2 Stereotaxic surgery

2.2.1 Retrograde tracers

Red and Green fluorescent retrobeads (Lumafluor, Inc.) were injected into PFC and NAc to label neuronal cell bodies sending afferent input to these structures. Retrobead-labelled cells allowed for visually guided electrophysiological recordings. A second retrograde tracer cholera toxin subunit B (CTXβ) tagged with Alexa 555 or 647 (Molecular Probes) was used to visualise PFC- and NAc-projecting cell bodies in vH for histology experiments. CTXβ provides efficient cell membrane labelling and thus easier identification of cells in comparison to fluorescent beads, which sparsely label cell bodies (Lencer and Tsai, 2003; Conte et al., 2009).

2.2.2 Viruses

Virus	Source	Figure
AAV2/1-CaMKII-GFP	Addgene plasmid 64545	5.11
AAV1.CAG.FLEX.Ruby2sm-Flag.WPRE	Addgene plasmid 98925	5.1, 5.2
AAV2/1-Ef1a-DO-DIO-TdTomato-EGFP	Addgene plasmid 37120	3.4
AAV2retro-CAG-Cre	UNC vector core	4.1, 4.2
AAV2/1-CaMKii-Cre	UNC vector core	5.1 - 5.4
AAV2/1-synP-FLEX-split-TVA-EGFP-B19G	Addgene plasmid 52473	4.1, 4.2, 5.3, 5.4
EnvA-ΔG-RABV-H2B-mCherry-2A-CLIP	Marco Tripodi, LMB Cambridge	4.1, 4.2, 5.3, 5.4
pAAV-EF1a-FLEX-hChR2(H134R)-EYFP	Addgene viral prep 20298-AAV1	4.8, 4.9, 5.5 - 5.7, 5.9, 5.11
pAAV-hSyn-hChR2(H134R)-EYFP	Addgene viral prep 26973-AAV1	4.3 - 4.7
pAAV-CaMKIIa-hChR2(H134R)-EYFP	Addgene viral prep 26969-AAV1	5.5 - 5.7, 5.9, 5.11
AAV2/9-mDlx-NLS-mRuby2	Addgene viral prep 99130-AAV1	4.10, 5.9
pAAV2/9-hSyn-FLEX-soCoChR-GFP	Addgene viral prep 107712-AAV	4.10

Table 2.1: Viral constructs used

2.2.3 Surgery

Stereotaxic injections were performed on 7 - 12 week old mice anaesthetised with isofluorane (Isofluorane 100%; Piramal Critical Care). For induction, mice were placed in a red perspex chamber (AN010ASR; VetTech) with 1 L / min flow of 4 % vaporised isofluorane (in medical oxygen, 99.5 % minimum purity). For the duration of the surgery anaesthesia was maintained at the same flow rate, but the concentration was brought down to 1 - 2 %. At all times, the mouth-piece delivering anaesthesia was connected to an activated carbon scavenging filter (Cardiff Aldasorber; Shirley Aldred & Co) and an active scavenging unit (Model AN005; VetTech). Mice were placed on a homeothermic blanket control unit which was maintained between 35 and 37°C throughout the surgery (50-7001; Harvard Apparatus). Injections were carried out following protocols established by previous publications (Cetin et al., 2007; MacAskill et al., 2012). Firstly, fur on the scalp was shaved off using a small trimmer (ChroMini Pro; MOSER) followed by secure mounting of the animal's head on a stereotaxic frame (Model 902 Dual Small Animal Stereotaxic Instrument; KOPF). The scalp was washed and sterilised with HiBiSCRUB® and the skull exposed with a single incision. A few drops of the local anaesthetic Marcain (0.025% in sterile saline) were applied to the exposed skull before removing the connective tissue with sterile cotton buds. After ensuring the horizontal alignment of bregma and lambda skull landmarks, small holes were drilled in the skull directly above the injection site using a steel bur (007 tip - 310 104 001 001; Meisinger) attached to a miniature drill (PRO 398D PCB Drill; RS). All surgical instruments were purchased from Fine Science Tools.

Injections were carried out using long-shaft borosilicate glass pipettes with a tip diameter of $\sim$ 10 - 50 μm. Pipettes were back-filled with mineral oil and front-filled with $\sim$ 0.8 μL of the substance to be injected. A total volume of 250 - 500 nL of each virus was injected at each location in 14 or 28 nL increments every 30 s at a flow rate of 23 nL / s using a micro-injection pipette (NanoJect II; Drummond

Scientific Company). If two or more substances were injected in the same region, they were mixed prior to injection. The pipette was left in place after injections were done for an additional 5 - 10 min before slow removal of the pipette to minimise upward diffusion whilst retracting the pipette and maximising absorption by the tissue. Injection coordinates used are shown in Table 2.2 (mm relative to bregma). During this process, mice were subcutaneously injected with carprofen (0.5 mg / kg) to aid with reducing inflammation.

After injection, the wound was sutured (6-0 Coated VICRYL polyglactin 910 suture; ETHICON) and sealed (Medbond skin glue; Animus), and mice recovered for a minimum of 30 minutes on a heat pad before they were returned to their home cage. Animals received carprofen in their drinking water (0.05 mg / ml) for 48 hrs post-surgery. Expression occurred in the injected brain region for $\sim$ 2 weeks until preparation of acute slices for physiology experiments, or fixation for histology. The locations of injection sites were verified for each experiment histologically or, for some electrophysiological experiments, visually if the acute slices recorded from also contained the injection site.

Brain region	**RC**	**ML**	**DV**
infralimbic PFC	2.3	$\pm$ 0.4	-2.4
Nucleus accumbens	1.1	$\pm$ 0.9	-4.6
DBB	0.7	$\pm$ 0.2	-4.0
Anterior thalamus	-0.4	$\pm$ 0.2	-3.2
CA3	-3.0	$\pm$ 2.8	-4
Entorhinal cortex	-5.2 (@ 10°)	$\pm$ 2.7	-4.5
Ventral hippocampus	-3.7	$\pm$ 3.4	-4.3

Table 2.2: Stereotaxic injection coordinates.
Injection coordinates taken from the Franklin & Paxinos, Waxholm and Allen Brain Atlas. Coordinates were calculated as averages of those given by these three atlases, and further adapted through observation. All coordinates given were calculated relative to bregma. RC : rostrocaudal, ML, mediolateral, DV: dorsoventral, DBB: Diagonal band of Broca

2.2.4 Pseudotyped rabies labelling from PFC

For pseudotyped rabies experiments, two injections were necessary. We followed the protocol published by Osakada and Callaway (2013). First, *AAV2/1-synP-FLEX-split-TVA-EGFP-B19G* was injected into the PFC of either *VGAT-Cre* mice, to express TVA and G-protein in inhibitory neurons, or was co-injected in a 1:1 mixture with *AAV2/1-CaMKii-Cre* into Cre negative littermates to express TVA and G-protein in excitatory neurons. In addition, CTXβ was co-injected into PFC to achieve non-specific retrograde labelling of PFC-projecting neuronal cell bodies in vH for comparison across mice. 2 weeks later, 200 nL of *EnvA-ΔG-RABV-H2B-mCherry* was injected into the PFC of the same mice to infect and induce transynaptic spread only from neurons expressing TVA and G-protein (and thus also Cre; either inhibitory interneurons or excitatory pyramidal cells). Animals were prepared for histology after 7 days of rabies-mediated expression.

2.2.5 TRIO labelling from PFC-projecting vH neurons

The TRIO or 'tracing the relationship between input and output' method was used to map inputs onto PFC-projecting ventral hippocampal neurons. This labelling technique required two surgeries. First, *AAVretro-CAG-Cre* was injected into the PFC to be retrogradely transported by terminals to express Cre-recombinase in neurons projecting to PFC (here, focussing on those in ventral hippocampus; vH^{PFC}). In the same surgery, a virus expressing Cre-dependent TVA and G-protein, *AAV2/1-synP-FLEX-split-TVA-EGFP-B19G*, was injected into the vH to express TVA and G-protein only in vH neurons that express Cre (i.e. only those that project to PFC). Hence, vH neurons projecting to PFC and thus expressing Cre-recombinase are capable of expressing the TVA receptor (necessary for infection with pseudotyped EnvA-rabies) as well G-protein necessary for trans-synaptic spread of rabies. 2 weeks later, 200 nL of *EnvA-ΔG-RABV-H2B-mCherry* was injected into vH to in-

fect and induce trans-synaptic spread only from PFC-projecting vH neurons. Cells positive both EGFP (hence expressing TVA and G-protein) and mCherry (hence expressing EnvA-ΔG-RABV) are referred to as vH^{PFC} 'starter cells', from which input onto vH^{PFC} cells is traced. Cells positive only for mCherry have been infected via transsynaptic spread from these starter cells and are thus classified as cells that send afferents onto vH^{PFC} cells (identified via TRIO). Animals were prepared for histology after 7 days of rabies-mediated expression.

2.3 Anatomy

2.3.1 Histology

Mice were anaesthetised with 0.5 - 1 mL of a mixture of ketamine (100 mg / kg) and xylazine (10 mg / kg) in sterile saline (KetaVet; Zoetis and Rompun; BAYER, respectively). Deep anaesthesia was confirmed by waiting until the animals had no reflex response to firm paw pinching. Following confirmation, mice were perfused intracardially with cold 4 % PFA (wt / vol) in PBS (pH 7.2) and the brains dissected and post-fixed overnight in 4 % PFA at 4 °C. Brain samples were transferred to PBS (pH 7.2) after overnight fixation. For visualisation of tissue, 70 μm thick slices were cut in PBS using a vibratome (Campden Instruments) in either the transverse, coronal or sagittal planes, as necessary. Slices were mounted on Superfrost glass slides (BRAND) with ProLong Gold® or ProLong Glass® (for visualisation of GFP) antifade mounting medium (Molecular Probes). ProLong Gold® and Glass® both contain NucBlue, which labels cell nuclei and aids in visualising gross anatomy. Slides were imaged with an Axio Scan Z1 (Zeiss) microscope equipped with standard filter sets for excitation / emission at 365-445/50 nm, 470/40-525/50 nm, 545/25-605/70 nm and 640/30-690/50 nm. Raw images were visualised using the Zen (lite edition) software from Zeiss and analysed with FIJI.

2.3.2 2-photon imaging

For reconstruction of pyramidal cells, neurons were filled with 30 μM Alexa 594 dye (mixed in with K^+ Gluconate internal) via the patch pipette for $\sim$ 10 minutes while electrophysiological recordings were being taken and then imaged using a customised Slicescope (Scientifica), based on a design described in Carter and Sabatini (2004). The waiting time before imaging allowed for the dye to diffuse throughout the entire cell, and also for dye that had been blown out of the pipette during the experiment to be washed away by the perfusion system. 780 nm light from a femtosecond pulsed Erbium fibre laser (Menlo Systems) was used to excite Alexa Fluor 594 during 2-photon imaging. Images were acquired using a water-immersion Plan FL N 40X/0.8 NA objective. A few high-resolution (512 x 512 pixels, each pixel corresponding to 0.43 μm) stacks were taken to capture the entire neuron, and then stitched using the Volume Integration and Alignment System software package (VIAS: v 2.4; CNIC, Mount Sinai). The stitched reconstructions were loaded into Neuron Studio (v 0.9.92; CNIC, Mount Sinai) where dendrites were manually reconstructed.

2.3.3 Immunohistochemistry

For staining (see Chapter 5, Figure 5.2), brain slices were prepared as described in the section above. Firstly, brain slices (70 μm thick) were incubated in blocking solution (3 % BSA and 0.5 % triton in PBS) for 3 hours at room temperature on a rocker, to ensure uniform contact of all brain tissue with the blocking solution. Blocking solution was used to block non-specific binding of the antibody to the tissue. This enhanced signal to noise ratio, improving the image quality obtained. Following incubation in blocking solution, slices were incubated overnight at 4 °C in a 1:5000 dilution of anti-DDDDK Tag (anti-Flag Tag) primary antibody (ab1257, Abcam) in blocking solution. After primary antibody incubation, slices

were washed 3 times (30 minutes per wash) in PBS and then incubated in a 1:500 dilution of secondary antibody (Alexa 555 donkey anti-goat; A21432, Invitrogen) in blocking solution for 4 hours at room temperature. Following this final incubation, slices were washed again in PBS as before and mounted for imaging (as in the section above).

2.3.4 Analysis of spatial distribution of PFC-projecting vH neurons

The spatial distribution of retrogradely labelled PFC-projecting hippocampal neurons was analysed in transverse slices from mice injected with the retrograde tracer cholera toxin β in PFC, and imaged as described in subsection 2.3.1. 3 - 6 slices spanning 300 μm between $\sim$ -3.5 and -5.0 mm DV were analysed per injection. The hippocampal cell body layer was straightened using the *Straighten* macro in FIJI to produce a single field spanning from proximal CA3 to distal subiculum (see Figure 2.1). Labelled cells within the straightened hippocampal sections were manually counted, and the coordinates saved for later analysis. The width of the section to be straightened was kept constant throughout all slices at 700 pixels, which was roughly the width of the subiculum cell layer. The length of the straightened section (i.e. the distance from CA3 to subiculum) was normalised to 1, and I defined the CA1 / subiculum border as the point where the hippocampal cell layer widens into a thicker, more subicular-like structure, which was consistently observed at 0.7 of the distance of the straightened field. Custom scripts written in Python based around the scikit.learn package were used to cluster the coordinates using a probabilistic Gaussian Mixture Model (GMM). When implementing a GMM, it is assumed that the data points fed into the model stem from a finite number of Gaussian distributions or components. Models containing between 1 and 6 components were fit to the cell coordinate data, and Bayesian Information Criterion (BIC) was used to select the best fit. The model with the lowest BIC score, which indicates the lowest number of outliers to the selected fit, was selected. Full covariance (as opposed to

spherical, tied or diagonal) was allowed when selecting the number of components with the lowest BIC score in order to make no assumptions about the distribution of the data. With full covariance, each component may have its own general covariance matrix, and so it is not assumed that each cluster i.e. layer of cells must have an equal variance in its distribution.

2.3.5 Analysis of rabies tracing from *VGAT* and *CaMKii*-expressing neurons in PFC

In order to quantify the rabies-positive cell bodies in the ventral hippocampus traced from either interneurons (*VGAT*-expressing) or pyramidal cells (*CaMKii*-expressing) in PFC (experiment described in subsection 2.2.4), a method similar to the above described (subsection 2.3.4) was used. Transverse hippocampal slices containing cholera toxin β labelling all PFC-projecting cells and rabies labelling (only in cells specifically contacting *VGAT* or *CaMKii* positive neurons in PFC) were used for cell counting. All cells in the straightened hippocampal formation (as above) were counted, and different markers were used for CTXβ and rabies-positive cells, for later analysis. Again, the coordinates were clustered using a GMM, and all analysed fields were best fit by two components, consistent with previous experiments. Following the GMM clustering, rabies-positive cell coordinates were plotted onto the clustered data and assigned to one of the two components i.e. superficial and deep layers. To quantify the proportion of cells contacting *VGAT* or *CaMKii*-positive cells in each layer, 5 slices were analysed per injection. The proportion of rabies-positive cells per component was calculated as a proportion of all rabies-positive cells present in that slice. The same method was used to calculate the proportion of CTXβ-positive cells in each of the two layers, as a control. This helped to show that there was no difference in the overall PFC-projecting cell layer structure between *VGAT* and *CaMKii* conditions.

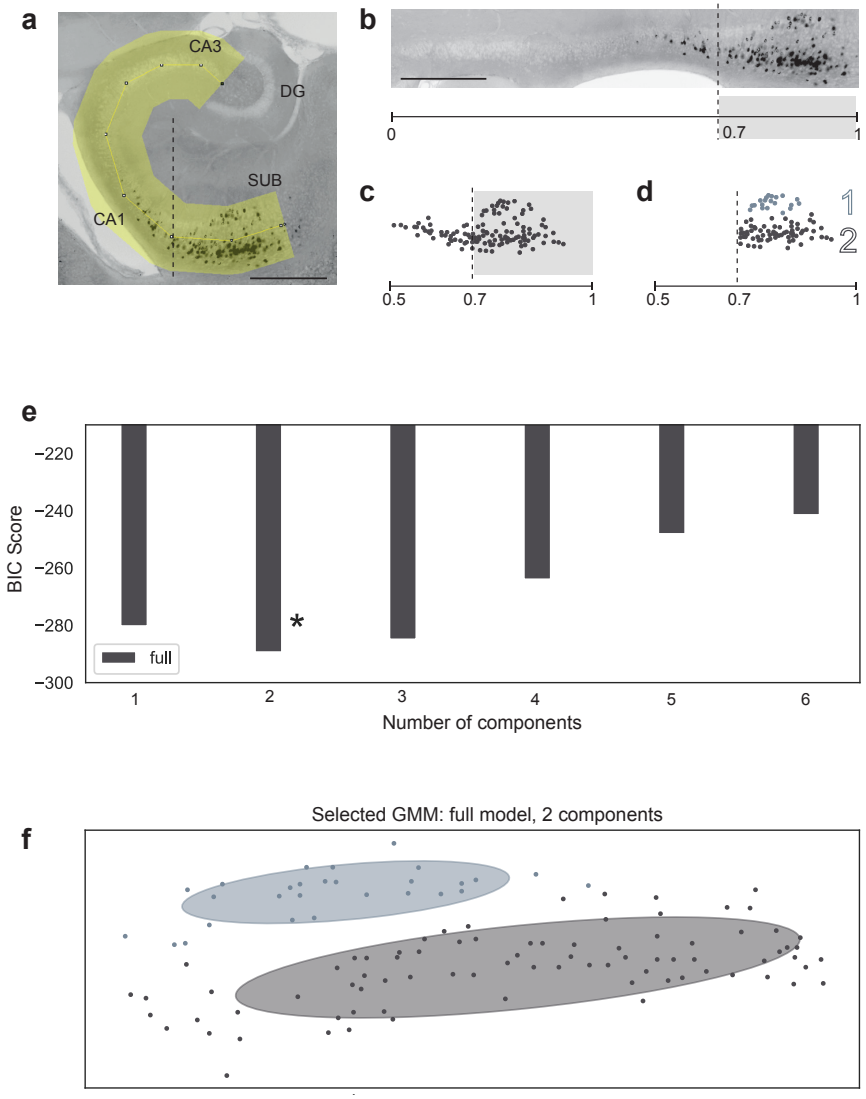

Figure 2.1: GMM Model

Working example of the Gaussian Mixture Model used to cluster cells. (**a**) Representative transverse hippocampal slice showing PFC-projecting cells labelled with cholera toxin β conjugated with Alexa Fluor 647 (black dots). The yellow selection represents the outlined hippocampal section then straightened in (**b**). The vertical dotted line represents the 0.7 of total distance cut-off mark separating CA1 proper from subiculum. Scale bars = 1000 μm. (**c**) Dark grey dots represent the manually traced cells found in the straightened hippocampal section. The grey box highlights the cells past the 0.7 cut-off mark that are used as data for clustering using the GMM model in (**d**), that divides the cells into superficial (light grey) and deep (dark grey) components. (**e**) Bayesian Information Criterion (BIC) scores given by the GMM model with full variance for a range of possible components. Note that the lowest score (*) and thus most accurate representation of the data is given at 2 components, shown in (**f**).

2.4 Electrophysiology

2.4.1 Slice preparation

Hippocampal recordings were studied in acute transverse slices to maintain within-slice connectivity (also referred to as 'magic slice preparation'; Bischofberger et al. (2006)), while PFC recordings were studied in acute coronal slices. All slices were prepared using a Leica 1200S vibratome. Firstly, mice were anaesthetized with a lethal dose of ketamine (100 mg / kg) and xylazine (10 mg / kg), and perfused intracardially with ice-cold sucrose cutting solution (see Table 2.3) bubbled with 95% O_2 and 5% CO_2. All slices were cut in this solution, which was bubbled throughout the entire process. Transverse 'magic' slices were used to preserve the natural hippocampal axis and thus the connectivity between cells in a given slice. To achieve transverse hippocampal slices, the brain was cut into its two hemispheres at the midline and placed onto a glass dish (the midline cut surface facing the glass) and the cortical surface was trimmed at a 10° angle away from the midline (moving the base of the blade away from the cortex by 10°) both in the horizontal and vertical axes (slanting the top of the blade from a vertical position to 10° closer to the brain surface). The brain hemispheres were then mounted on the cut cortical surface, up side down, and sliced at a 300 μm thickness starting ventrally. After slicing, all slices were immediately transferred into chambers containing a muslin mesh on which to rest them, filled with artificial cerebrospinal fluid (aCSF; see Table 2.3) kept at 35 °C and bubbled with 95% O_2 and 5% CO_2. After a 30 minute incubation at 35 °C, slices were kept in the same chamber for 30 minutes at controlled room temperature (24 °C). All recording experiments were conducted at room temperature (22 - 24 °C) and all chemical compounds for cutting and recording solutions were purchased from Sigma.

aCSF recording solution		Sucrose cutting solution	
Compound	**Concentration (mM)**	**Compound**	**Concentration (mM)**
NaCl	125	Sucrose	190
Glucose	22.5	NaCl	10
$NaHCO_3$	25	Glucose	25
$NaH_2\ PO_4$	1.25	$NaHCO_3$	25
KCl	2.5	$NaH_2\ PO_4$	1.2
Na^+ ascorbate	1	Na^+ ascorbate	1
Na^+ pyruvate	3	Na^+ pyruvate	2
$MgCl_2$	1	$MgCl_2$	7
$CaCl_2$	2	$CaCl_2$	0.5

Table 2.3: Recording and cutting solution components

2.4.2 Whole-cell electrophysiology

2.4.2.1 Voltage clamp recordings

The voltage clamp or *current following* configuration is used to measure current flowing through the cell membrane in response to voltage steps (e.g. depolarising the cell membrane) or in response to stimulation of physiological inputs that will affect the membrane potential. For example, to isolate excitatory postsynaptic currents (EPSCs), we clamped cells at the reversal potential for chloride, -70 mV (making the command voltage (V_{comm}) -70 mV; see Figure 2.2). If current arrives from the cell (e.g. in response to presynaptic input) at the electrode (I_e), its flow via the electrode resistance will create a change in voltage (V_{pip}), which will arrive at the inverting input of the operational amplifier (OPA) and V_{pip} and V_{comm} will not be equal (Figure 2.2). If the OPA notes a difference between V_{comm} and V_{pip}, it produces a voltage proportional to this difference but much larger (i.e. it amplifies the difference). The detected difference in turn, causes a current to flow through

R_f (the feedback resistor) back into the pipette, to ensure $V_{comm} = V_{pip}$. Current will flow into the pipette until there is no more difference in potential between the two entry ports on the OPA, effectively clamping the cell at the desired potential. Thus, the amount of current fed back into the cell (I_f) to maintain $V_{comm} = V_{pip}$ is a read-out of the current flowing through the cell membrane in response to a given presynaptic input or voltage step ($V_{clamp\ current}$).

Two different internal solutions were used for recording in voltage clamp (see Table 2.5). Caesium gluconate internal was used to record EPSCs while holding at -70 mV (the reversal potential for chloride, Cl^-, thus isolating excitatory currents) and inhibitory postsynaptic potentials (IPSCs) at 0mV (the reversal potential for several cation channels; to isolate inhibitory inputs). An NMDA (*N*-methyl-D-aspartate) receptor antagonist APV ((2R)-amino-5-phosphonovaleric acid) was added to the bath at a 10 μM concentration for recordings during which the cells were held at 0mV, to block any NMDA currents active at this potential. High Cl^- internal was used in order to record IPSCs as inward currents when holding the cells at -70 mV. By elevating the internal concentration of Cl^-, the driving force is reversed such that the opening of Cl^- channels leads to an outward flow of Cl^- ions at -70 mV, which can be recorded as inward currents (EPSCs). This experimental setup allows for recordings of Cl^- flux at -70 mV thus avoiding clamping the cell at 0 mV, which is both unhealthy for cells over prolonged periods of time as well as experimentally difficult and more unreliable due to space clamp issues. These experiments were conducted in NBQX (2,3-dioxo-6-nitro-7-sulfamoyl-benzo[f]quinoxaline) to block excitatory currents through glutamatergic AMPA (α-amino-3-hydroxy-5-methyl-4-isoxazolepropionic acid) receptors active at this potential. Having caesium in the internal solution reduces potassium currents in the cell and thus facilitates more efficient space clamp. The internal solutions also contained TEA and QX-314 (K^+ and Na^+ voltage-gated channel blockers, respectively) to block action potentials in the patched cells only.

Hardware and software used for electrophysiology		
Component	**Specifications**	**Source**
Amplifier	MultiClamp^{TM} 700B Amplifier	Molecular Devices
Digitiser	NI USB 6221	National Instruments
Acquisition Software	WinWCP V 5.1.8	University of Strathclyde
Headstage	CV-7B CC and VC headstage	Molecuar Devices
Microscope	Custom design	Scientifica and THOR Labs
Micromanipulators	PatchStar PS-7500	Scientifica
Anti-vibration table	CleanTop	TMC Vibration Control

Table 2.4: Electrophysiology setup

	Cs^+ gluconate internal	**High Cl^- internal**	
Compound	**Concentration (mM)**	**Concentration (mM)**	**Source**
Cs^+ gluconate	135	-	Sigma
CsCl	-	135	Sigma
HEPES	10	10	Sigma
Na-Phosphocreatine	10	10	Sigma
Mg-ATP	4	4	Sigma
Na-GTP	0.4	0.4	Sigma
EGTA	10	10	Sigma
TEA	-	10	Hello Bio
QX-314	-	2	Hello Bio
pH to 7.2 using CsOH and osmolarity to 290-300 mOsm			

Table 2.5: Voltage-clamp internals

2.4.2.2 Current clamp recordings

In current clamp or *voltage following* configuration, voltage is continuously recorded (V_{out}) and a command current ($I_{clamp\ comm}$) can be injected through a resistor (R_f) into the cell for stimulation (see Figure 2.2). The negative feedback loop from the amplifier allows for faithful following of the observed voltage at the electrode tip, as $V_{out} = V_{pip}$. All current clamp recordings were carried out while holding cells at either -70 mV or at rest. Potassium gluconate internal containing the calcium chelator EGTA (to stabilise the intracellular levels of free calcium) was used to measure postsynaptic potentials (PSPs). All voltage- and current-clamp recordings were made using a Multiclamp 700B amplifier, filtered at 2 kHz and sampled at 10 kHz and at 100 kHz for a subset of cells. All recordings sampled at 100 kHz were compared to equivalent recordings sampled at 10 kHz, downsampled and pooled, as no differences were found in the properties measured.

K^+ gluconate internal		
Compound	**Concentration (mM)**	**Source**
K^+ gluconate	135	Sigma
HEPES	10	Sigma
KCl (1M)	7	Sigma
Na-Phosphocreatine	10	Sigma
Mg-ATP	4	Sigma
Na-GTP	0.3	Sigma
EGTA	10	Sigma
pH to 7.2 using KOH and osmolarity to 290-300 mOsm		

Table 2.6: Current-clamp internal

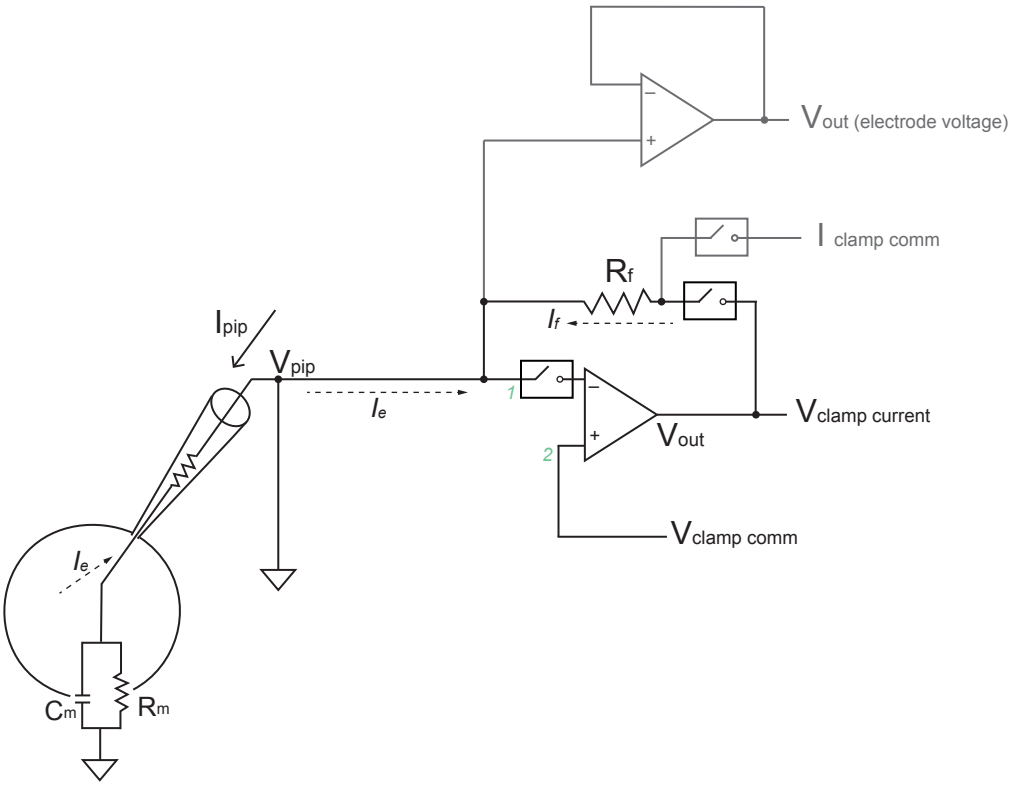

Figure 2.2: Equivalent circuit of whole-cell voltage and current clamp recordings
In black, spanning the cell membrane (circle) is the equivalent RC cicuit of the cell, where the capacitor is the membrane capacitance, C_m, and the resistor is the membrane resistance, R_m. Current flowing across the cell membrane and into the patch pipette electrode (I_e) creates a change in the potential across the electrode inside the pipette (V_{pip}). Also in black, outside the cell, the voltage clamp mode equivalent circuit. Upon current flow through the electrode in response to cellular activity (I_e), (V_{pip}) is compared at the amplifier entry (1) with the command voltage (2; $V_{clamp\ comm}$), and any mismatch is translated into a current injection (I_f) to clamp the electrode at ($V_{clamp\ comm}$). Using Ohm's law, V_{pip} - V_{out} = IR_f. In grey is the schematic circuit engaged in the amplifier in current clamp mode. The change in voltage in response to current injections ($I_{clamp\ comm}$) is constantly monitored, as V_{out} is updated to equal the potential change recorded at the electrode tip (V_{pip}).

2.5 RNA sequencing

Four 6 - 8 week old mice were injected with red retrobeads in PFC (see subsection 2.2.3). After 2 weeks, acute 400 μm thick transverse hippocampal slices were prepared and incubated for 30 minutes at 35 °C in oxygenated aCSF as above (see section 2.4) containing TTX (tetrodotoxin; 100 nM) to block sodium channels, NBQX (20 μM) and APV (50 μM) to block AMPA and NMDA receptor transmission, respectively, and Pronase (1 mg / ml) to disrupt the extracellular matrix. This incubation was followed by a further 30 minute wash in aCSF without Pronase. Following the incubation and wash, slices were placed in a sylgard-filled chamber under a dissection stereomicroscope (Leica MZ16FA) equipped with fluorescence and transmitted light. The ventral CA1 / subiculum was separated from the rest of the slice, and a single cut was made to separate superficial and deep cell layers, guided by the red fluorescence of retrobead-labelled PFC-projecting cells. Superficial and deep excised sections from each animal were then pooled (4 samples of superficial and deep sections per animal), and tissue was manually triturated for dissociation using three glass Pasteur pipettes of decreasing tip diameter. The resulting suspension was mixed with DAPI (Molecular Probes) to monitor cell health, and then separated using FACS (carried out by staff at the UCL FACS facility) to isolate red fluorescent (PFC-projecting), and viable (DAPI negative) cells in superficial and deep layers. Cells were sorted directly into buffer for SMART-Seq v4 Ultra Low Input RNA Kit (Clontech Laboratories, Inc.). Subsequent processing was carried out by the UCL Genomics sequencing facility.

Briefly, SMART (Switching Mechanism at 5' End of RNA Template) technology produces full-length PCR amplified cDNA starting from low input (as low as a single cell). 12 cycles of PCR were used to generate cDNA from lysed cells. The amplified cDNA was checked for integrity and quantity on the Agilent Bioanalyser using the High Sensitivity DNA kit. 200 pg of cDNA was then converted to a sequencing library using the Nextera XT DNA protocol (Illumina, San Diego,

US). This uses a transposon able to fragment and tag double-stranded cDNA (tagmentation), followed by a limited PCR reaction (12 cycles) adding sample specific indexes to allow for multiplex sequencing. For sequencing, libraries to be multiplexed in the same run are pooled in equimolar quantities, calculated from Qubit and Tapestation fragment analysis. Samples were sequenced on the NextSeq 500 instrument (Illumina, San Diego, US) using a 43bp paired end run, generating approximately 200M read pairs in total. Fragments Per Kilobase Million (FPKM) scores were calculated from the raw data using TopHat and Cufflinks via Illumina Basespace software. Only raw FPKM scores over 10 were included. Due to the manual nature of the dissection, for identification of robust markers for the two layers only hits where the standard deviation across samples in the two conditions was under 1 were included in final analysis. Statistical significance was compared across superficial and deep samples using false discovery rate correction and hits were defined as those where $q < 0.1$. The distribution along the radial axis of the hippocampus of a selection of hits was verified using *in situ* hybridization data from the Allen Brain Atlas.

2.6 Behaviour

2.6.1 Elevated plus maze

To investigate anxiety-like and exploratory behaviour, animals were tested on the elevated plus maze (EPM) - a 4-armed plus-sign shaped maze, in which two opposing arms have walls (closed arms; 30 x 5 cm x 16 cm, L x W x H) and the other two opposing arms have no walls, resembling a platform (open arms; 30 x 5 cm, L x W). Avoiding the open arms and reduced exploratory activity is classically associated with higher anxiety-like behaviour (Walf and Frye, 2007; Pellow and File, 1986). In order to carry out this test while stimulating axon terminals in PFC (see Chapter 5, Figure 5.11), all mice were first habituated to the experimenter, the

experimental room and the optic fibre attachment. Two weeks post-surgery were allowed for recovery, followed by an 8 day habituation protocol. For habituation, mice were familiarised firstly with the experimenter's hands, placing them in the cage for a few minutes on day 1, followed by two days of picking them up onto the hands. During habituation days 4 and 5, the mice were acclimatised to the experimental room whilst also being handled by the experimenter. On days 6, 7 and 8, the optic fibre cables were connected to the implanted ferrules and mice were allowed to freely explore their home cages for 2 to 3 minutes to become familiarised with tethered exploration. During the task, mice were placed in the centre of the elevated plus maze using a home-cage tube for handling. One end of the tube was covered when placed in the EPM so that the mice always faced the same wall and an open arm upon entry to the maze for testing. Mice were allowed to freely explore the maze for 9 minutes and were filmed with an overhead camera (High Definition Handycam® Camcorder HDR-CX130; SONY). During 'light on' epochs, 470 nm light was activated at 20 Hz with a power of 10 mW at the end of the fibre for axonal stimulation whenever the animal entered or was in the open arms. Testing was carried out with red lighting (100 lux) only, to minimise any aversive influence or differences due to reaction to bright overhead lighting. The apparatus was wiped clean with 70 % ethanol and deionised water between subjects and left to dry completely, to minimise potential odor-related confounds.

2.7 Data Analysis

All final analysis of data presented here was carried out using custom scripts in Python 2 and 3, with implementation of appropriate packages. Imaging data was pre-processed as detailed in subsections 2.3.1 and 2.3.2. Electrophysiological data was analysed by implementing the eFEL (electrophys Feature Extract Library; version 2.12.6; BlueBrain software) package on Python. Below, I have given more detailed information regarding the analysis of voltage-clamp data and the eFEL package used for electrophysiological feature extraction and analysis for current-clamp

data. All spike-related measures (recorded in current clamp mode) were averaged across all current steps (from 20 pA to 160 pA) that yielded spikes, unless otherwise stated. For behavioural experiments, the raw data i.e. tracking of movement in videos, was first analysed with EthoVision (XT 10.1.856; Noldus Information Technology) before being analysed further on Python.

2.7.1 Electrophysiological voltage-clamp data analysis

For every stimulation power (light duration or pA pulses), 3 recordings were made in order to obtain an average response of the particular cell to the stimulation. The average trace per stimulation was calculated for every cell before carrying out any pooled analysis. For analysis of EPSCs and IPSCs, a custom Python script was used to extract the maxima and minima of the traces respectively, relative to baseline. The baseline was taken to be the average voltage value across the 10 ms preceding optogenetic or electrical stimulation. Stimulation was delivered 100 ms into the recording. For normalisation to baseline, the baseline value was subtracted from the entire trace. The time at which the maximum (or minimum for IPSCs) value occurred was taken as the time of the peak between 105 and 140 ms into the recording. A 5 ms gap after the stimulation was allowed to avoid picking up the stimulus artefact as the peak value, especially important for small physiological responses. The average voltage value 1 ms around the peak time point (i.e. 0.5 ms either side of the maximum or minimum value) was taken as the absolute peak voltage value. For ratio response data between superficial and deep vH^{PFC} neuron pairs, the data for each pair is divided by the deep response (i.e. normalised to deep response).

2.7.2 Electrophysiological current-clamp data analysis

The eFEL package is a feature extraction tool for analysis of voltage electrophysiology traces. Implementing it alongside custom scripts, the following trace features

shown in Chapter 3 were extracted:

- Input resistance (R_i; MΩ) – the sum of the series resistance (R_s) and the membrane resistance (R_m), was calculated as the ratio of the average voltage deflection value during the last 10 % of the stimulus and the stimulus current injection.

- Threshold (mV) – the voltage trace value at which the depolarisation becomes a spike. The eFEL package yields the spike onset where the derivative of the voltage trace is greater than 12 V / s for at least five points.

- Rheobase (pA) – the first current step that yielded spikes was calculated using a custom script. Rheobase was taken as the first current step during which the voltage trace crossed the 0 mV value at least once.

- Sag amplitude (mV) – which is indicative of the Ih current component in the cell, was calculated as the difference between the minimum voltage in the voltage trace in response to a -160 pA current injection and the average steady state voltage during the last 10 % of the stimulus duration.

- ISI ratio – the interspike interval (ISI) ratio (ratio between the first and the last ISI in a train of spikes) was measured as the distance between the first and second peak times divided by the distance between the last two peak time points in any trace containing three or more action potentials.

- Fast AHP (ms) – the fast hyperpolarising undershoot or AHP (afterhyperpolarisation) following spikes, in which the membrane voltage briefly falls below the normal resting potential, was measured as the voltage value of spike threshold relative to the subsequent AHP at its minimum value. The minimum value of the AHP was taken as the minimum voltage value between the

spike peaks preceding and following it.

- AP width (ms) − the action potential (AP) or spike width was measured as the time between peak onset (where the voltage trace crosses the threshold value) and the peak offset (the downward crossing of the voltage trace and threshold).

- Peak voltage (mV) − was measured as the voltage trace value at the maximum peak of each spike.

- AP amplitude (mV) − the spike amplitude was calculated as the difference between peak voltage and spike threshold.

- Mean frequency (Hz) − the mean frequency of the firing rate was measured by dividing the number of peaks in a voltage trace by the time from stimulus start to the last spike. This was potted for the +160 pA step only.

2.8 Statistics

Summary data are reported as mean ± s.e.m. (standard error of the mean) or median ± s.e.median (standard error of the median) for ratio data where indicated. For comparisons between two normally distributed, unpaired datasets, two-sample t-tests were implemented. For paired, non-normally distributed data, samples were compared by carrying out a Wilcoxon paired test. In the case of two samples of non-normally distributed, unpaired data a Mann-Whitney U test was implemented. Comparisons of repeated variables between two normally distributed datasets were performed using a Repeated measures within and between subjects ANOVA (analysis of variance; with Greenhouse-Geisser correction for sphericity where variance was not equal throughout). For very small samples, where the data can be sorted

into contingency tables, the Fisher's Exact test was used. Statistical significance was considered as $p < 0.05$ for all tests. Statistical tests were performed using the statistics package in Python 2 and Python 3 (scipy.stats), as well as statistics modules imported from R onto Python. Repeated measures ANOVAs were carried out on SPSS (version 25; IBM®).

Chapter 3

Hippocampal neurons projecting to PFC form two distinct populations

3.1 Introduction

As described above in the main introduction, the vH to PFC projection is remarkably complex and carries out dramatically different roles at different times. The vH-PFC pathway is involved in bringing about motivated, goal-directed, threat and emotional behaviour and activity in this pathway is compromised in a vast array of emotional disorders. Functionally, the heterogeneity inherent to pyramidal projection neurons in the CA1 / subiculum area of the ventral hippocampus (Cembrowski and Spruston, 2019; Ding et al., 2020) may serve as a substrate for separate streams of processing and information routing between the vH and PFC. This functional and behavioural complexity led me to hypothesise that there might be more than one circuit between vH and PFC, each carrying out unique roles. Specifically, that hippocampal heterogeneity might provide the basis for separate vH-PFC pathways that support its many associated roles.

Neurons in CA1 and predominantly in subiculum are the main output neurons of the ventral hippocampus and send axons to a variety of brain areas. Despite targeting multiple downstream regions, its efferents (axons projecting from hippocampus to target areas) are thought to be organised as parallel projections (Naber and Witter, 1998; Wee and MacAskill, 2020). Subicular projection neurons can be classified on the basis of their projection targets. Although there is some degree of collateralisation within the subiculum, it is very low overall (0-12 %, with the highest collateralisation found in ventral vs distal and proximal vs distal subiculum), suggesting that hippocampally processed information is distributed in a parallel fashion, with any one neuron targeting only one downstream region (Naber and Witter, 1998; Böhm et al., 2015). This means that neurons that project to PFC are a distinct subpopulation of vH neurons, and may explain why their function can be so different from projections to e.g. the NAc or amygdala (Bagot et al., 2015; Xu et al., 2016; Jimenez et al., 2020; Padilla-Coreano et al., 2016). It is worth noting that the degree of collateralisation within subiculum has been studied using double-labelling and paired recording approaches (Naber and Witter, 1998; Böhm et al., 2015), while far more specific genetic 'barcoding' techniques have been used in CA1 to map axonal projections (Gergues et al., 2020). Implementing more specific and high-throughput techniques in subiculum may yield a more representative and nuanced overview of its degree of collateralisation.

However, even within a specific projection population such as PFC projecting neurons, there is much additional heterogeneity. It is known that cells distributed along the dorso-ventral, proximo-distal and superficial-deep axes have distinct properties (Ishizuka, 2001; Dougherty et al., 2012; Jarsky et al., 2008; Slomianka et al., 2011; Graves et al., 2012; Kim and Spruston, 2012; Soltesz and Losonczy, 2018; Malik et al., 2016; Fanselow and Dong, 2010; Strange et al., 2014). It is clear, that even within projection populations there is a tight relationship between neuronal function, connectivity, and spatial location along these axes (Kim and Spruston, 2012; Wee and MacAskill, 2020).

Pyramidal cells in the hippocampus can also be segregated on the basis of gene expression. Recently, it has been shown that in dorsal subiculum up to eight distinct subcategories can be classified on the basis of differential gene expression (Cembrowski et al., 2018b). It is also known that some genes are specifically expressed in subregions of the hippocampal formation (Ishihara and Fukuda, 2016) as well as in specific parts of the hippocampal cell layer in a lamina specific manner rather than in a graded fashion (Cembrowski et al., 2018b; Pi et al., 2020). When this genetic heterogeneity is mapped onto different projection populations it becomes clear that there is remarkable variability in gene expression even within a particular projection population. This is particularly striking for PFC projecting neurons (Cembrowski et al., 2018b), reinforcing the idea that there may be multiple unique populations of neurons projecting to PFC from hippocampus.

Hippocampal projection neurons can also be classified by their electrophysiological and morphological properties, and such properties are thought to have profound consequences for their functioning within a circuit (Losonczy et al., 2008; Schmidt-Hieber et al., 2017; Hunt et al., 2018). Electrophysiologically, cells can be broadly separated into two categories, regular-spiking neurons with a high Ih current, and bursting neurons with a low Ih current (Staff et al., 2000; Greene and Totterdell, 1997; Kim and Spruston, 2012; O'Mara et al., 2001; Menendez de la Prida et al., 2003). Interestingly, the incidence of burst-firing cells varies dramatically along the deep to superficial and along the proximal to distal axes from CA1 to subiculum, with bursting neurons preferentially occupying the deep cell layer and more distal locations, while regular-spiking neurons are distributed more abundantly in CA1 and proximal subiculum, along the superficial cell layer (Greene and Mason, 1996; Jarsky et al., 2008; Harris et al., 2001). These electrophysiological properties also vary greatly across projection populations, where - allowing for much intra-population variability - different projection populations show distinct combinations of neurons with specific electrophysiology (Kim and Spruston, 2012). Thus, the electrophysiological properties of neurons covary with spatial lo-

cation and projection population in vH (Naber and Witter, 1998; Kim and Spruston, 2012; Harris et al., 2001; Soltesz and Losonczy, 2018; Cembrowski et al., 2018a).

Heterogeneity in electrophysiological properties is accompanied by specific morphological features in CA1 and subiculum. For example, burst-firing cells have been shown to have longer apical dendrites that bifurcate further from the soma than their regular-spiking counterparts (Menendez de la Prida et al., 2003; Graves et al., 2012; Hunt et al., 2018). Furthermore, morphology varies in a gradient-like manner along the different axes of the hippocampus. Deep layer (closer to stratum oriens) and superficial layer (closer to stratum radiatum) cells in the CA1 / subiculum area cover different hippocampal strata to varying degrees with their dendritic trees. While superficial layer cells extend more processes into the stratum radiatum, dendrites from deep layer cells cover more area in stratum oriens, and cells with somas in deeper positions along the radial axis also have longer, less branching apical dendrites (Bannister and Larkman, 1995).

Overall, given the remarkable heterogeneity in vH neurons, in particular those projecting to PFC, coupled with the multiple distinct behavioural roles of the vH to PFC projection, I hypothesised that this projection may be composed of multiple populations of neurons that differ in i) their spatial location within the axes of the hippocampus, ii) their gene expression and iii) their electrophysiological properties.

3.2 Results

PFC-projecting neurons segregate across the vH radial axis

The anatomical distribution of neurons in CA1 and subiculum based on their projection target has been investigated by injecting fluorescent retrograde tracers into various target areas and visualising labelled cell bodies in the hippocampus (Kim and Spruston, 2012; Wee and MacAskill, 2020). Neurons projecting to lateral entorhinal cortex (LEC), amygdala, nucleus accumbens (NAc) and lateral hypothalamus (LH), among others, occupy largely non-overlapping regions within the CA1 / subiculum area. However, the precise location and distribution of PFC-projecting neurons in vH has only recently begun to be explicitly investigated (Wee and MacAskill, 2020). In order to better understand this projection and determine its distribution within the ventral hippocampus, we set out to trace and map PFC-projecting neurons. In particular, we were interested in the idea that the projection may form multiple groups across the different gradients of the hippocampus (Cembrowski and Spruston, 2019).

To label PFC-projecting cell bodies, the retrograde tracer choleratoxin subunit B (CTXβ) conjugated with Alexa 555 or 647 dye was injected into infralimbic prefrontal cortex (Figure 3.1 a). CTXβ was taken up by presynaptic terminals in PFC and transported back to the cell bodies along axonal processes. After allowing for two weeks of retrograde transport, transverse slices of ventral hippocampus (vH) were imaged using fluorescence microscopy to visualise labelled cell bodies sending axons to PFC. In Figure 3.1 b, the black dots mark cell bodies of PFC-projecting neurons. Qualitatively, we observed that the cells were distributed in two separate bands or layers along the radial axis of the CA1 / subiculum border area of vH (note the gap between cells superficially and deep within the dotted box in Figure 3.1 b, zoomed in on right).

To summarise this finding, we plotted fluorescence profiles of CTXβ labelling in the CA1 / subiculum border area. Three to four hippocampal slices were taken per injection to obtain fluorescence profiles and equally sized regions were taken per slice. The fluorescence profiles consistently showed two peaks in fluorescence, as shown in the example in Figure 3.1 b, *right*. These superficial and deep peaks correspond to layers II and IV of subiculum, respectively (Bienkowski et al., 2018). Overall, these data suggest that PFC-projecting cells in vH form two layers at the CA1 / subiculum border, at opposite (superficial and deep) poles of the radial axis. A recent publication studying heterogeneity in this hippocampal area in rodents has defined it prosubiculum (Ding et al., 2020). However, for the purpose of this thesis, it will be referred to as the CA1 / subiculum border or area.

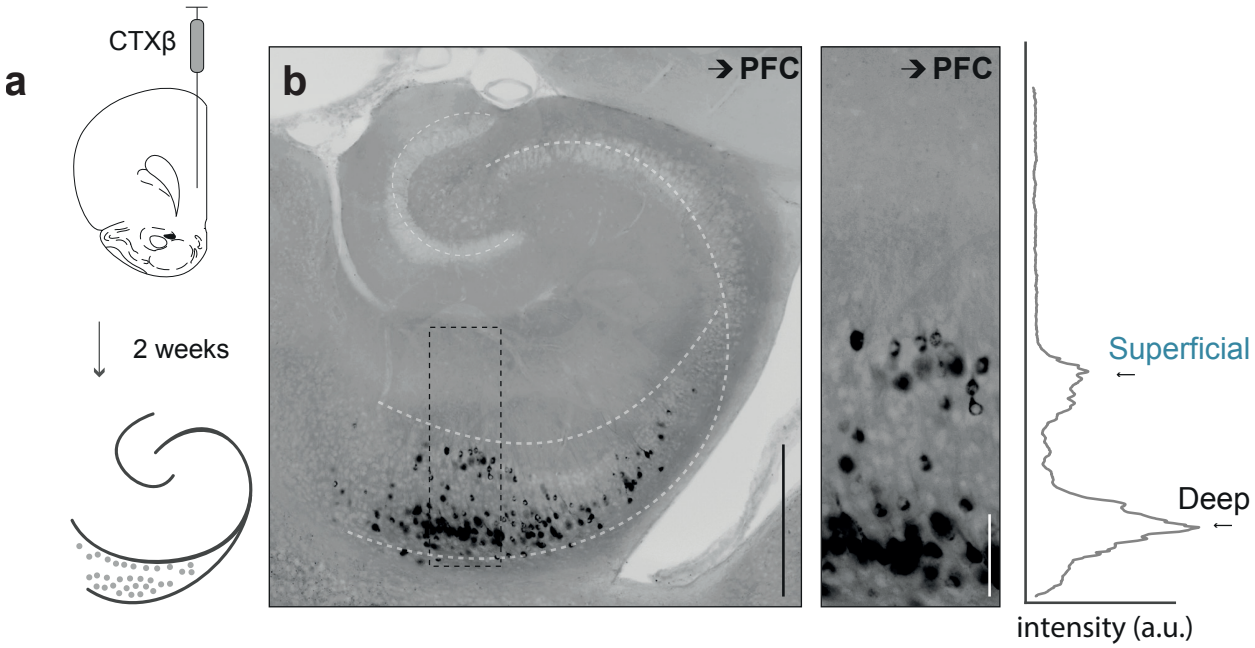

Figure 3.1: PFC-projecting vH cells are segregated across the radial axis
(**a**) Schematic of cholera toxin (CTXβ) injection into PFC and retrograde labelling in hippocampus. 2 weeks of retrograde transport were allowed. (**b**) *Left*, Transverse hippocampal slice containing PFC-projecting cells labelled with CTXβ. Black boxed region marks the CA1/subiculum area enlarged on right. *Right*, zoom of retrogradely labelled neurons in boxed region, with fluorescence intensity profile. Arrows highlight the two distinct peaks of fluorescence at the two extremes of the radial axis. Scale bars = 500 μm (*Left*) 100 μm (*Right*).

To understand the relevance of this observation, it was important to know whether this striking feature was unique to the PFC-projecting population or whether other projection populations are distributed in similar ways. I chose the projection to the nucleus accumbens (NAc) as a comparison because of the extensive literature available on this population of cells and their presence in the same CA1 / subiculum border area as PFC-projecting neurons (Wee and MacAskill, 2020). CTXβ conjugated to different Alexa dyes, Alexa 555 and Alexa 488, was injected into the PFC and NAc of the same animal in a counterbalanced manner. As before, two weeks were allowed for retrograde transport. By injecting CTXβ conjugated to two different coloured dyes in the same animal, it was possible to visualise cell bodies from both projection populations in vH simultaneously. Counterbalancing colour placement across animals ensured that any observed spatial patterning was not due to the nature of the tracer construct itself. Labelled cell bodies in the two different Alexa dyes, corresponding to PFC- and NAc-projectors were visualised in transverse sections of vH (Figure 3.2).

As in the example in Figure 3.1, two layers of cells were observed at either pole of the radial axis for PFC-projectors in contrast to NAc-projectors, which were found positioned in one wider, more central layer (Figure 3.2 c and d). Different members of the MacAskill lab also analysed the distribution of vH neurons projecting to lateral hypothalamus (LH) and basomedial amygdala (BMA) and did not see any layered distributions. Overall, this suggests that the layered distribution at the CA1 / subiculum border area of vH may be unique to the PFC-projecting population.

Following this qualitative observation, we wanted to see if it would hold up quantitatively. In order to quantify the layered distribution in an unbiased fashion, I clustered the locations of manually mapped neuron coordinates (Figure 3.2 e: *traced*) using a Gaussian Mixture Model (GMM). GMMs containing between 1 and 6 components were fit to the data and compared, and Bayesian Information

Criterion (BIC) was used to select the best fit i.e. the number of components that best fit the given cell coordinates and account for the variance (see Methods section 2.3.4). PFC-projecting neuron coordinates were consistently best fit when they were clustered into two groups (2.0 ± 0.0) and NAc-projecting neurons were best fit by a single cluster (1.2 ± 1.33) in the centre of the cell body layer (Figure 3.2 f and g; Fisher's exact test, odds ratio = 0.0, p = 2.063e-07). Thus, the layered organisation appears to be unique to the PFC-projecting population.

We next wondered if each layer was similarly occupied, or whether the layers had different proportions of cells. To quantify this, we took the proportion of coordinates in each of the two clusters fit to the data in Figure 3.2 f and g. The clusters (or layers) of vH^{PFC} cells (PFC-projecting vH cells) were differentially populated, with $30.97\% \pm 2.20$ of cells in the superficial and $69.03\% \pm 2.20$ in the more numerous deep layer (Figure 3.2 h; Mann Whitney, U = 0.0, p = 3.658e-05). Overall, these findings suggest that the PFC-projecting population in vH is segregated along the radial axis of the hippocampus, with two separate layers occupying the opposite superficial and deep poles. The superficial layer accounts for roughly a third of the population and the deep vH^{PFC} cell layer represents the remaining, larger component of the population.

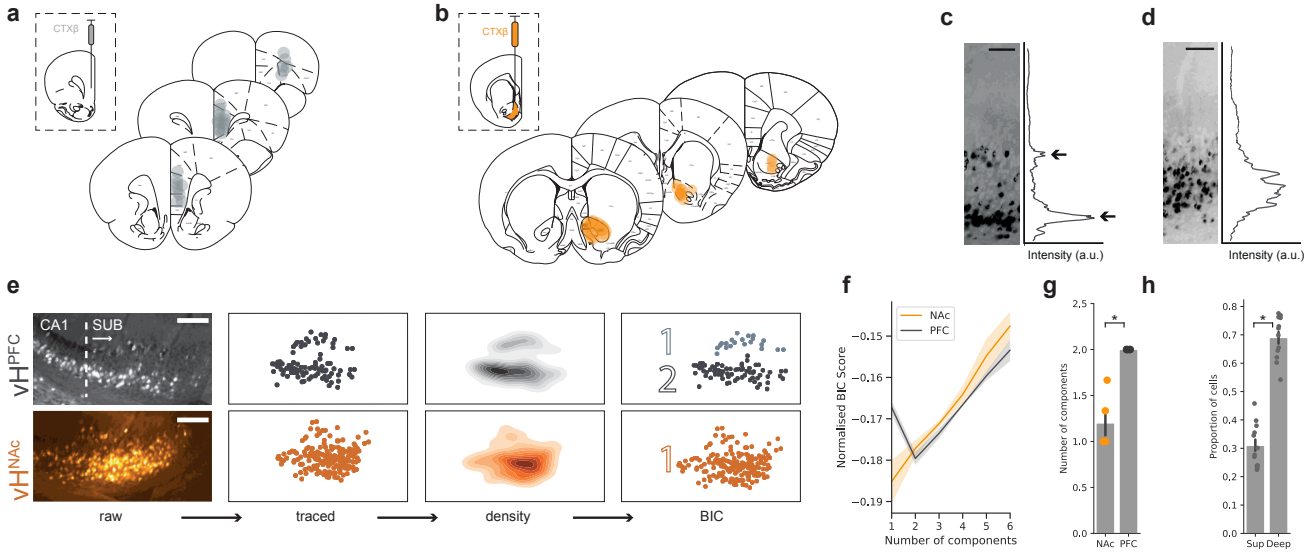

Figure 3.2: Clustering reveals two distinct populations for PFC- but not NAc-projectors (**a**) Schematic of CTXβ injection into PFC and location of injections (n = 16). Each injection is represented as a translucent fill. Thus, higher intensity reflects consistent labelling across injections. (**b**) As in (**a**) but for injections into the NAc (n = 12). (**c,d**) Example fields of retrogradely labelled neurons in transverse slices of vH after CTXβ injection into PFC (**c**) and NAc (**d**). Profile on right indicates fluorescence intensity profile along the radial axis. Note PFC-projecting neurons have two peaks, while NAc has one. Scale bars = 100μm. (**e**) Locations of neuron coordinates were clustered using a Gaussian Mixture Model (GMM). Figure shows example of clustering of spatial location of both PFC-projecting neurons (which consistently form two layers) and NAc projecting neurons (which consistently form a single cluster in the centre of the cell body layer). Images from left to right show raw images (raw), coordinates of neuronal cell bodies (traced), a kernel density estimate plot showing the density of cell bodies (density) and the neuronal cell bodies colour coded according to the groups that gave the best BIC score (BIC; 2 components for PFC in grey and black, one component for NAc in orange). Scale bars = 100 μm. (**f**) BIC scores for positions of PFC (grey) and NAc (orange) projecting neurons for $1-6$ components. (**g**) Summary of component number that gave the lowest BIC score across all experiments. Note PFC projectors are consistently best fit by two components, while NAc projectors are best fit by one component. (**h**) Summary of proportion of PFC-projecting neurons in each component (superficial and deep layers), quantified from CTXβ-labelled neurons. Note that roughly 70% of the projection population is composed of deep-layer neurons. Grey dots represent brain slices quantified from 4 injections.

Calbindin1 is enriched in the superficial PFC-projecting layer

Following from the observation that the vH^{PFC} projection population is spatially segregated, I hypothesised that the two layers may consist of different types of cells, perhaps representative of two distinct circuits. Subicular projection populations have been shown to have unique gene expression patterns (Cembrowski et al., 2018b,a). In particular, as mentioned in the introduction above, the projection to PFC can be clustered into multiple unique genetic populations (Cembrowski et al., 2018b). Thus, we next wondered if the layered distribution of the PFC projection reflected known variation in gene expression across the radial axis and heterogeneity within the PFC-projecting population (Cembrowski et al., 2016a,b; Cembrowski and Spruston, 2019; Soltesz and Losonczy, 2018).

To address this question, we set out to perform RNA sequencing of superficial and deep layer vH^{PFC} cells (Figure 3.3). For visualisation of PFC-projecting cell bodies in vH, fluorescent retrobeads were injected into PFC, where they were taken up by presynaptic axon terminals and retrogradely transported to label cell bodies in vH (see Figure 3.3 a). Following a 2 week period to allow for retrograde transport, acute hippocampal slices were prepared to isolate PFC-projecting cells from both layers. In collaboration with Dr. Andrew MacAskill and the UCL Genomics sequencing facility, the two cell layers were manually dissected, guided by retrobead fluorescence. Cells were subsequently dissociated, sorted by fluorescence and RNA was extracted (see Methods section 2.5 for a more detailed description). RNA samples were sent to the UCL Genomics facility, who acquired and provided the RNA sequencing data. We observed a variety of differentially expressed genes across the two layers, which are presented in Figure 3.3b as a heatmap, where violet represents enrichment in expression (shown by a higher z-score). By taking the FPKM (Fragments Per Kilobase of transcript per Million mapped reads - normalised unit of transcript expression that accounts for differences in transcript length and sequencing depth) value for each sample and calculating the z-score for

each gene, we plotted a heatmap of the z-scores. We observed differential expression for 27 genes (Figure 3.3 b). The fifth gene shown on the heatmap is *Calbindin1*, which was enriched in the superficial layer samples and has previously been shown to be a hippocampal marker for superficial layer neurons (Li et al., 2017; Pi et al., 2020; Soltesz and Losonczy, 2018). Thus, with regards to the expression of *Calbindin1*, the PFC-projecting population in vH is consistent with previously identified radial axis gene expression gradients.

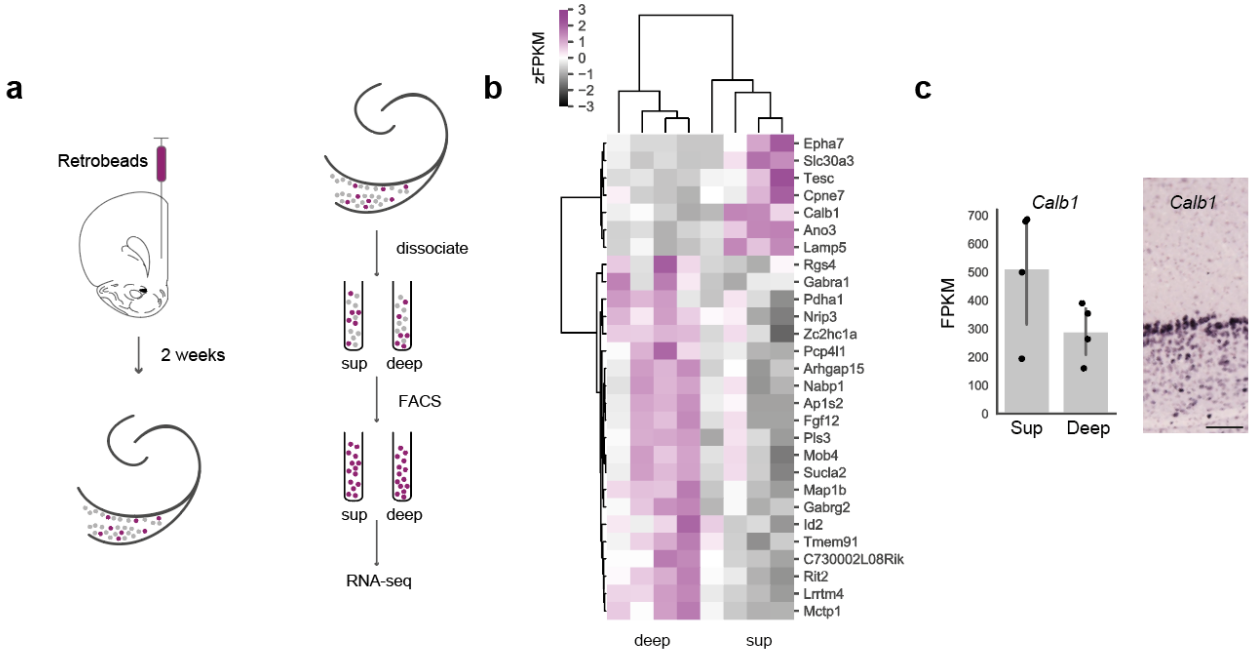

Figure 3.3: RNA sequencing of superficial and deep PFC-projectors
(**a**) Schematic of strategy to isolate retrogradely labelled neurons from each layer. Transverse slices were manually dissected down the middle of the cell body field and labelled cells were isolated using FACS before undergoing RNA sequencing. (**b**) Hierarchical clustering of genes with differential expression across the two groups, showing enrichment of genes in both superficial and deep populations across 4 biological replicates (n = 4 dissected hippocampi). Colour is scaled based on a row-wise Z score of the FPKM value. Analysis was carried out by Andrew MacAskill. (**c**) Validation of example gene *Calbindin1*. The raw FPKM scores are plotted for superficial and deep layers on the left, and *in situ* hybridisation (ISH) data of vH from the Allen brain atlas is presented on the right. Note that the ISH data recapitulates superficial enrichment of *Calb1* gene expression. Scale bar = 100 μm.

Further, hierarchical clustering analysis of the RNA sequencing z-score data unbiasedly clustered our hits into superficial and deep groups (Figure 3.3 b). In Figure 3.3 c, the raw values for the 4 biological replicates used for sequencing show the superficial enrichment of *Calbindin1*. Figure 3.3 c (*right*) shows *in situ* hybridisation data from the Allen Brain Atlas with enriched (darker purple) expression of *Calbindin1* in the superficial hippocampal layers, corroborating our finding. Overall, these data show that the PFC-projecting population is genetically heterogeneous and reflects known gradients in gene expression along the radial axis.

To confirm selective *Calbindin1* expression in the superficial PFC-projecting layer and thus exploit this specificity for circuit investigation, a *Calbindin1*-Cre mouse line was used, which expresses Cre under the control of the *Calbindin1* gene. *Calbindin1*-expressing neurons in this mouse line are therefore Cre-positive. To test the differential expression of *Calbindin1* across the two PFC-projecting cell layers in vH, a Cre-dependent retrograde 'switch' virus was injected into the PFC of *Calbindin1*-Cre mice, resulting in fluorescently labelled cell bodies in vH sending axons to PFC (Figure 3.4 a and c). The transgenes in the open reading frame (ORF) of the 'switch' virus are flanked by mutually exclusive lox sites, which are used by Cre to invert the ORF. Once the ORF is inverted, it is locked in place. Under Cre-negative conditions, tdTomato is expressed (and followed in the ORF by an inverted EGFP sequence that is not expressed). In Cre-positive cells, the ORF is inverted and EGFP is expressed in place of tdTomato (Figure 3.4 b). In Figure 3.4 c an example of this dual expression is shown. As described above, the identity of the fluorescent reporter expressed in each cell was dependent on the presence of Cre, such that tdTomato was expressed in Cre negative cells and EGFP in Cre positive (i.e. *Calbindin1*-expressing) cells. Cells in the superficial layer, where the RNA sequencing results showed an enrichment in *Calbindin1* expression, were almost exclusively labelled with the marker EGFP whereas cells in the deep layer were predominantly labelled with tdTomato, due to the absence of Cre (Figure 3.4 c and d). The proportion of *Calbindin1*-expressing (i.e. EGFP positive) and *Calbindin1*-

negative (i.e. tdTomato positive) cells in each layer was calculated from 4 injections (3 slices quantified per injection) to show that 67.32% $\pm$ 3.93 and 10.25% $\pm$ 6.90 of *Calbindin1*-positive (Cb+) and *Calbindin1*-negative (Cb$-$) fluorescently labelled cells were found in the superficial layer, respectively (Mann Whitney, U = 0.0, p = 0.03, n = 4 injections). The inverse proportion of EGFP (Cb+) and tdTomato (Cb$-$) fluorescently labelled cells was present in the deep cell layer, with 32.68 % $\pm$ 3.93 EGFP-labelled and 89.75 % $\pm$ 6.90 tdTomato-labelled cells found in deep layer. Overall, these results show that *Calbindin1* can be used successfully as a marker for superficial layer vH^{PFC} cells and conversely, the absence of *Calbindin1* as a marker of deep layer vH^{PFC} cells. Furthermore, they confirm the observed RNA sequencing result and highlight the value of this mouse line for further circuit investigation.

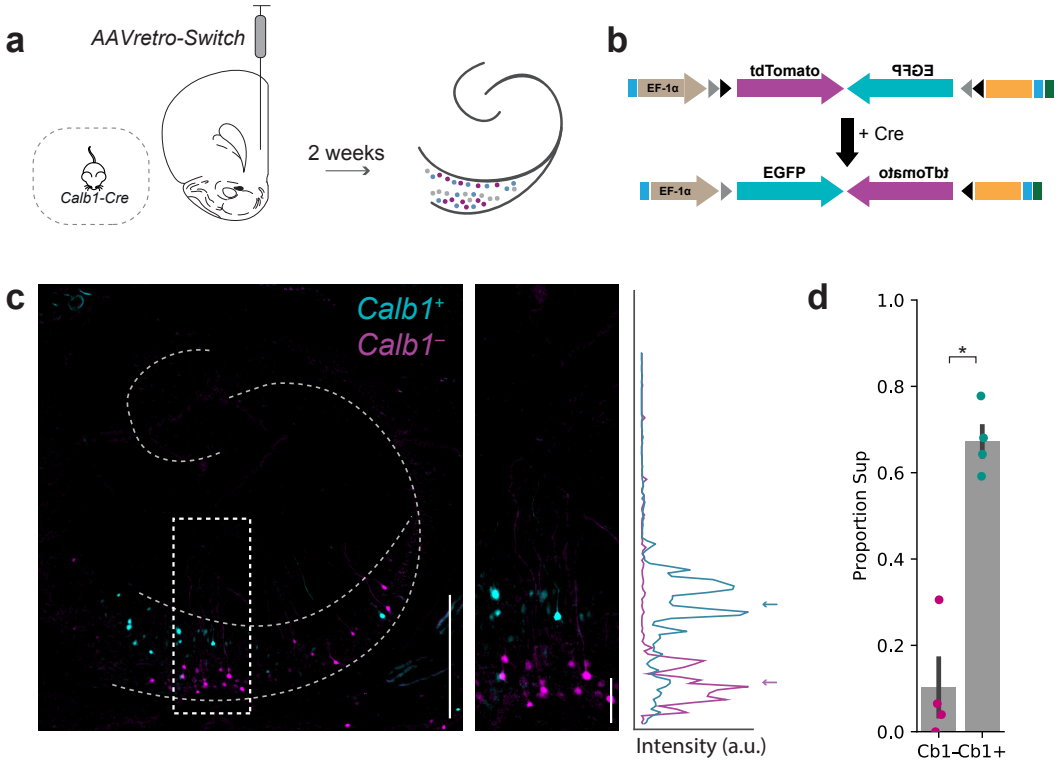

Figure 3.4: Switch virus consistently separates two vH^{PFC} layers in *Calb1*-Cre mouse (**a**) AAVretro-Switch injection into the PFC of *Calb1*-Cre mice and subsequent Cre-dependent retrograde labelling in hippocampus. (**b**) Schematic of Cre-dependent color-flipping reporter construct used. The viral construct expresses tdTomato in the absence of Cre and EGFP in its presence. (**c**) Transverse slice of hippocampus labelled with AAVretro-Switch. Cyan labels *Calb1*+ PFC-projecting neurons and magenta labels *Calb1*- neurons. *Right*: zoom of retrogradely labelled neurons in boxed region, with fluorescence intensity profile for *Calb1*+ (cyan) and *Calb1*- (magenta) neurons. Arrows highlight the two genetically distinct peaks of fluorescence at the two extremes of the radial axis. Scale bar = 500 μm (*Left*) and 100 μm (*Right*). (**d**) tdTomato- (Cb1-) and EGFP-positive (Cb1+) cells in the superficial layer were quantified as a proportion of all tdTomato- and EGFP-positive cells in the slice, respectively. Note that *Calbindin1* positive cells are mostly present in the superficial layer while *Calbindin1* negative cells are found almost exclusively in the deep layer, confirming specific superficial *Calbindin1* enrichment.

Superficial and deep PFC-projectors have different electrophysiological and morphological features

Gradients in electrophysiological and morphological properties across multiple hippocampal axes, including the radial axis, have previously been identified and superficial and deep cells in the CA1 / subiculum region are known to have distinct properties (Kim and Spruston, 2012; Li et al., 2017; Geiller et al., 2017b; Soltesz and Losonczy, 2018; Slomianka et al., 2011). I therefore wondered whether the two PFC-projecting layers were also segregated in their properties, in line with previously identified radial axis gradients amongst non-projection specified cells. It was unclear whether PFC-projectors would present homogeneous properties dictated by their common target (ignoring existing gradients) or whether their properties would be different across layers, staying true to the radial axis gradients. In order to address this question, I characterised superficial and deep PFC-projecting cells in their electrophysiological and morphological properties. As previously for anatomical distribution, NAc-projectors were used as a comparison.

To visualise cell bodies of neurons in vH projecting to PFC and NAc, fluorescent retrobeads were injected into the target area of interest. These were taken up by axon terminals and transported to the vH and other afferent areas. Approximately 7 - 10 days after the injection, acute hippocampal slices were prepared. Visually guided by the fluorescent retrobeads, PFC- and NAc-projecting cell bodies were recorded from using patch-clamping and current steps were injected to study their electrophysiological properties (Figures 3.5 and 3.8). I will firstly describe data comparing the electrophysiology and morphology properties of superficial and deep vH^{PFC} cells and secondly the comparison of the vH^{PFC} as a whole to the vH^{NAc} population.

When comparing superficial and deep PFC-projectors, many differences be-

came apparent (see Figure 3.5). Voltage traces were recorded during the injection of a progression of current steps (from -160 pA to 160 pA) and later analysed to extract subthreshold and spike features. Concurrently, a subset of cells was filled with fluorescent dye for subsequent morphological analysis (see Figure 3.6). Deep vH^{PFC} cells consistently displayed more excitability, firing on average more action potentials in response to current injections than their superficial counterparts (Figure 3.5 c; between and within subject repeated measures ANOVA, interaction of current steps and cell type: $F_{(9,297)} = 4.3$, $p = 0.00$). This deep layer characteristic has been previously observed *in vivo* in a non-projection specific manner (Mizuseki et al., 2011). Deep cells also showed a higher input resistance than superficial cells (Deep: 229.95 MΩ ± 21.47 and superficial: 166.61 MΩ ± 11.48. Mann Whitney: U = 393, $p = 0.028$; Figure 3.5 e), a likely contributor to their increased excitability.

Interestingly, no differences were seen in spiking threshold, rheobase or action potential width (threshold - deep: -38.85 mV ± 1.27, superficial: -41.76 mV ± 0.64, Mann Whitney: U = 348, $p = 0.122$; rheobase - deep: 56.8 pA ± 7.18, superficial: 65.4 pA ± 6.32, Mann Whitney: U = 317.5, $p = 0.355$; AP width - deep: 3.17 ms ± 0.19, superficial: 2.62 ms ± 0.10, Mann Whitney: U = 192, $p = 0.08$). As a consequence of the higher input resistance observed amongst vH^{PFC} deep layer cells, it would have followed that these cells on average require less current to reach the AP firing threshold (i.e. have a lower rheobase) than their superficial layer counterparts. However, this was not the case (Figure 2.4 f). A possible explanation for this unexpected result may be that deep cells have a lower resting membrane potential, as has been observed for non-projection specific cells in CA1 ((Soltesz and Losonczy, 2018), data not obtained from the current dataset). This would require more current to reach the AP threshold (which is equivalent for cells in both layers, Figure 3.5 e) than would otherwise be expected from cells with higher input resistance. Alternatively, the 20 pA sized current step protocol implemented to gather electrophysiological data may be too coarse (i.e. the steps too large) to pick up more subtle differences in rheobase, which may be lower than 20 pA.

Characteristic of burst-firing and deep-layer cells (Brumberg et al., 2000; Soltesz and Losonczy, 2018), neurons in the deep layer of the projection had a smaller sag amplitude (Ih current component) than their superficial counterparts in response to hyperpolarising current steps (deep: 6.88 mV ± 0.58, superficial: 9.22 mV ± 0.46, Mann Whitney: U = 200, p = 0.002) and a lower ISI (interspike interval) ratio, comparing the ISIs between the first two and the last two APs in the recorded trace (where a ratio of 1 is regular firing and below 1 represents a shorter first ISI or burst; deep: 0.68 ± 0.065, superficial: 0.86 ± 0.04, Mann Whitney: U = 175, p = 0.03). The proportion of burst-firing cells in the deep layer was over 7-fold larger than that in the superficial layer (Figure 3.5 g; deep: 45 % ± 11.41, superficial: 6.25% ± 6.25, Fisher's exact test: Odds ratio = 12.5, p = 0.009). Although these findings support previous observations showing that deep layer hippocampal cells are burst-firing and have low levels of Ih current (sag) (Soltesz and Losonczy, 2018), some publications focusing on subiculum proper interestingly show opposite correlations between burst firing and Ih current (van Welie et al., 2006; Greene and Mason, 1996), suggesting that low Ih in deep layer burst-firing cells may be specific to the CA1 / subiculum border area. Despite their lower excitability, spikes in superficial vH^{PFC} cells reached higher peak voltages (Figure 3.5 j; deep: 38.12 mV ± 1.39, superficial: 44.41 mV ± 1.26, Mann Whitney: U = 130, p = 0.002) and had overall larger amplitudes (Figure 3.5 k; deep: 77.09 mV ± 2.24, superficial: 86.21 mV ± 1.69, Mann Whitney: U = 139, p = 0.004) and faster AHPs than their deep counterparts (Figure 3.5 m; deep: 5.63 ms ± 0.71, superficial: 7.90 ms ± 0.52, Mann Whitney: U = p = 0.02).

Interestingly, it has been shown that a small percentage of Ih current channels (HCN channels) are active at rest (Lüthi and McCormick, 1998), and that this conductance consequently contributes to the determination of the resting membrane potential. Blocking Ih currents in many cell types results in slight hyperpolarisation of the membrane potential (Lüthi and McCormick, 1998), suggesting that the higher Ih current component in superficial layer vH^{PFC} (Figure 2.4 n) may be a determi-

nant in elevating its resting membrane potential and thus reducing its rheobase, making it equivalent to that of the deep layer population, despite having a lower input resistance (Figure 2.4 i).

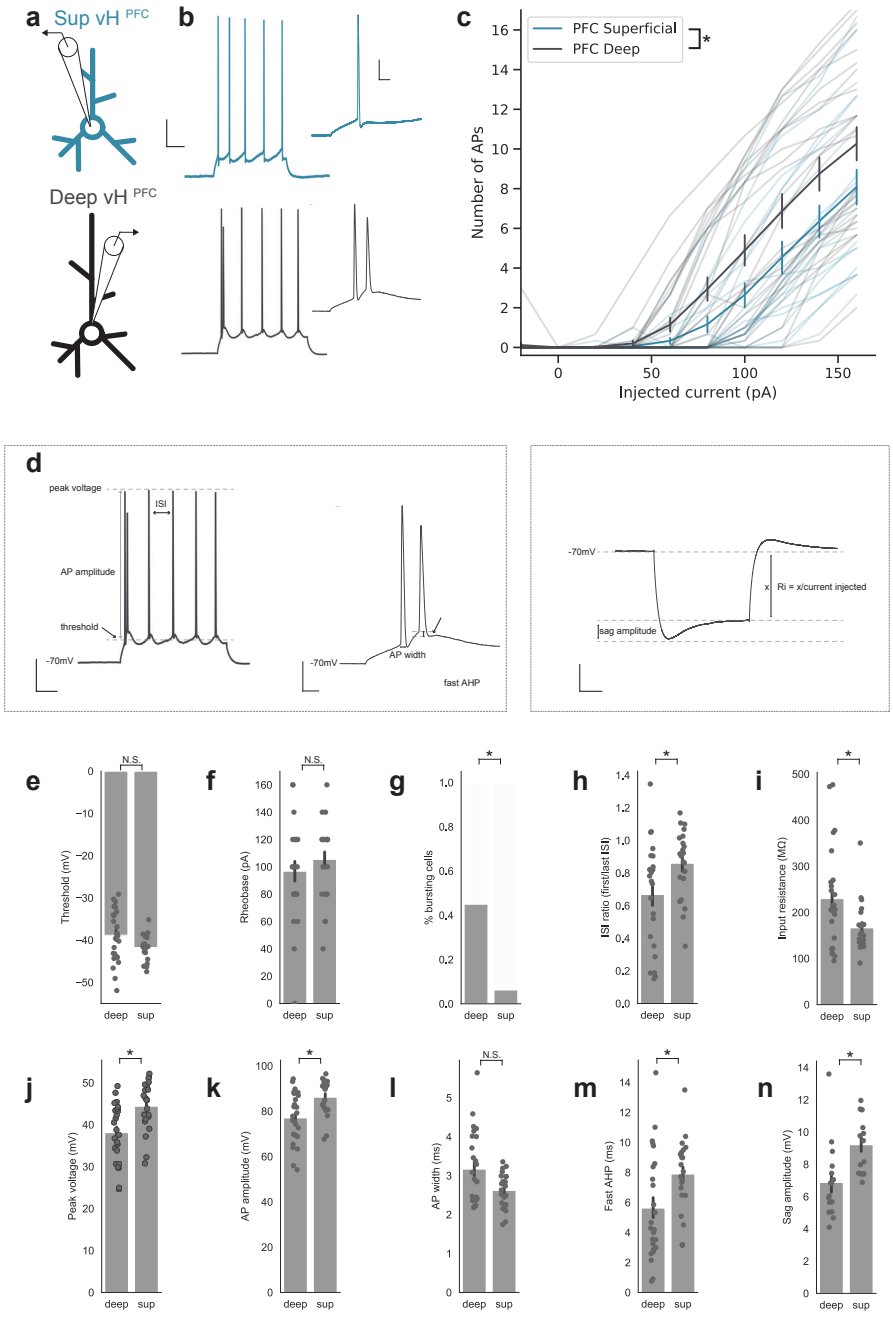

Figure 3.5: Electrophysiological characterisation of deep and superficial PFC-projectors (**a**) Schematic of experimental setup. Retrobead labelling allowed for visually guided patching from superficial and deep vH^{PFC} cells. (**b**) Sample traces from superficial and deep neurons in response to 140 pA current injection. Note burst in zoom (*right*) of deep cell response. (**c**) Average number of action potentials in response to increasing current injections. (**d**) Example voltage traces from a deep vH^{PFC} cell in response to current injections (140 pA for first two traces, -160 pA for last trace). *Middle*: zoom of first two events. Arrows point at different aspects of the traces analysed below. Scale bars = 100 ms, 20 mV; 10 ms, 20 mV; 200 ms, 10 mV. (**e-n**) Electrophysiological properties of n = 22 (sup) and 26 cells (deep) from 12 and 16 animals respectively, for all measures.

A subset of the cells recorded from (n = 7 superficial vH^{PFC} and 6 deep vH^{PFC}) were filled with Alexa 594 dye for visualisation and subsequent tracing for morphological analysis. As with electrophysiological properties, differences in morphology were apparent between the two layers of PFC-projecting cells. Superficial vH^{PFC} cells were generally smaller, more highly branched and stellate-like than deep vH^{PFC} cells, which resembled layer 5/6 cortical neurons with longer and more sparse apical dendrites (Larkum et al. (2009); see Figure 3.6 a). The differential positioning of the neurons along the radial axis (Figure 3.6 b; distance of soma to pia - superficial: 377.49 μm $\pm$ 28.84, deep: 162.92 μm $\pm$ 24.74 , Mann Whitney: U = 0.0, p = 0.003) together with their different dendritic arbors situated the bulk of superficial and deep vH^{PFC} overall dendritic length at varying distances from the pia (Figure 3.6 c, Repeated measures within and between subjects ANOVA: Interaction between cell-type and distance from pia $F_{(19,209)}$ = 5.3, $p < 0.001$, n = 7 (superficial), 6 (deep) for all measures in this figure). The distribution of basal and apical dendrites was then analysed separately for neurons in both layers and was aligned to the distance of their somas from pia (i.e. the first count of dendritic length for each cell, that closest to the soma, is plotted according to the distance of that cell's soma from pia along the x-axis; Figure 3.6 d). From this summary graph I could see that, on average, apical dendrites from cells in both layers terminate at the same height along the radial hippocampal axis, although the overlap in quantity of apical dendritic branches from the two populations is low in more superficial layers due to the sparse branching of deep cell apical dendrites.

When comparing mean basal dendritic length as a function of distance from soma between deep and superficial layer cells, no difference was apparent (Figure 3.7 a; Repeated measures within and between subjects ANOVA with Greenhouse-Geisser correction for sphericity: $F_{(3.34,36.71)}$ = 7.70, p = 0.179). This was in contrast to mean dendritic apical dendrite length, which was higher in superficial layer cells (Figure 3.7 b; Repeated measures within and between subjects ANOVA: $F_{(38,385)}$ = 1.55, p = 0.027), pointing at higher levels of branching within the apical

dendritic tree of superficial vH^{PFC} cells. A qualitative investigation of overall dendritic branching points with increasing distance from soma is shown in Figure 3.7 c. Interestingly, although the distribution of branching appears different across the two layers, the overall count of branch points (grouping basal and apical dendrites) was not different between superficial and deep cells (superficial: 28.29 $\pm$ 4.29 , deep: 23.67 $\pm$ 3.16; Mann Whitney: U = 15.5, p = 0.473).

To further understand the observed differences in apical dendrite morphology, I measured the distance from the soma to the nexus, the point at which the main apical dendrite bifurcates, as well as the total length of the longest dendritic process. Deep vH^{PFC} apical dendrites branched over twice as far from the soma (Figure 3.7 d; superficial: 186.63 μm $\pm$ 34.49, deep: 460.76 μm $\pm$ 86.97, Mann Whitney: U = 38.5, p = 0.015) and were longer than those from superficial vH^{PFC} cells (superficial: 474.69 μm $\pm$ 66.80, deep: 692.93 μm $\pm$ 58.20, Mann Whitney: U = 35.5, p = 0.045). Cumulative count and length of dendritic processes in each centrifugal order did not differ between superficial and deep cells (3.7 e; count - *left*: Repeated measures within and between subjects ANOVA with Greenhouse-Geisser correction for sphericity: $F_{(5.053,55.694)}$ = 0.262, p = 0.934 and and length - *right*: Repeated measures within and between subjects ANOVA with Greenhouse-Geisser correction for sphericity: $F_{(4.715,51.868)}$ = 0.610, p = 0.683).

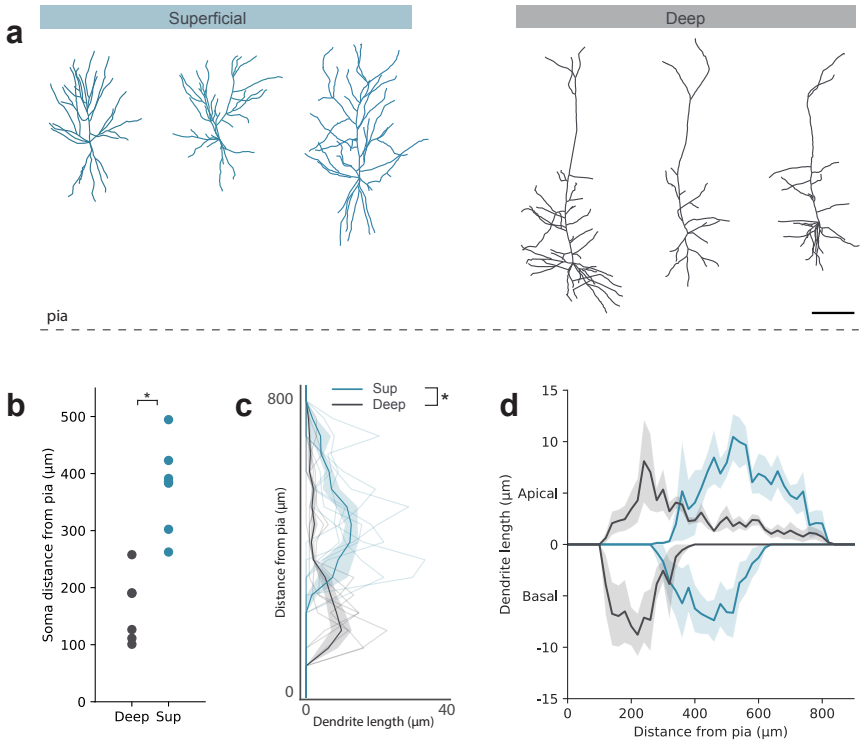

Figure 3.6: Morphological characterisation of superficial and deep PFC-projectors (**a**) Example reconstructions of superficial and deep PFC-projecting hippocampal neurons. Scale bar = 100 μm, dotted line represents pia (**b**) Distance of cell somas relative to pia. (**c**) Average dendrite length as a function of distance from pia. Note that the peak for superficial cells is shifted further from the pia. (**d**) As in (c), but split into apical (above 0) and basal (below 0) dendritic length.

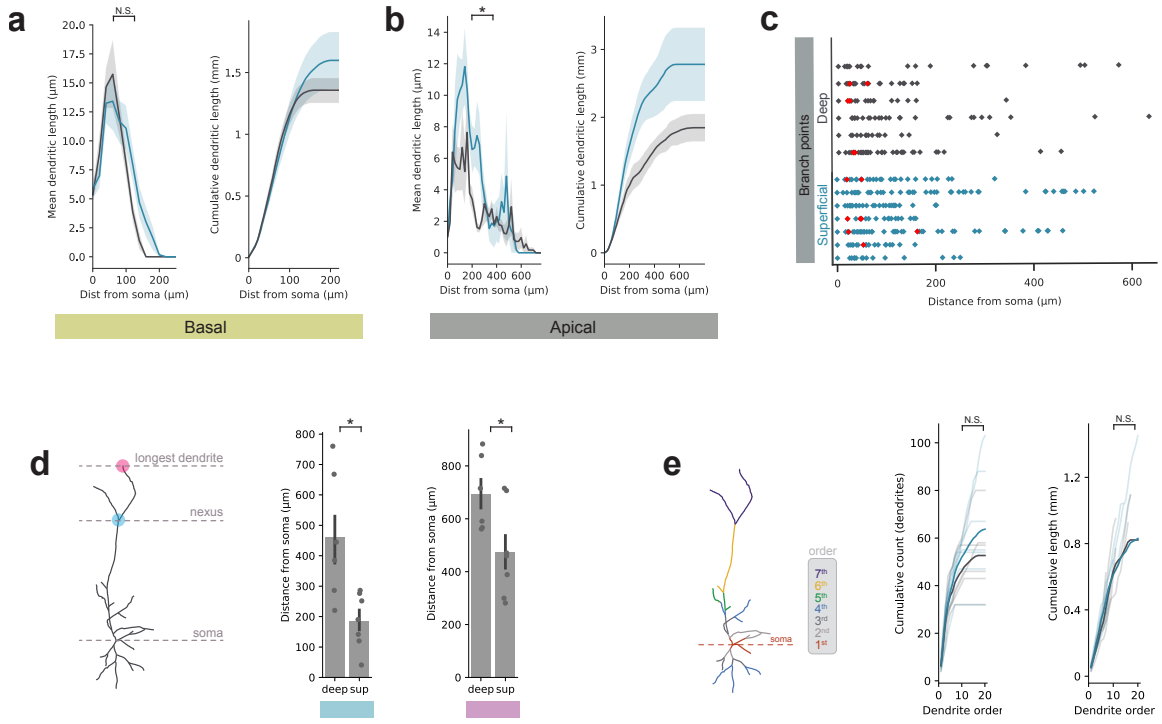

Figure 3.7: Sholl analysis of dendritic arborisations in superficial and deep vH^{PFC} cells (**a**) *Left*: Sholl analysis of basal dendritic length with increasing distance from the soma for superficial and deep neurons. *Right*: As on left but for cumulative length. (**b**) As in (a) but for apical dendrites. Note overall greater amount of apical dendritic length in superficial cells. (**c**) Distribution of branch points with increasing distance from the soma. Red points indicate two branch points in the same 1μm bin. (**d**) Schematic illustrating further characterisation of the apical dendrite: the nexus (base of the tuft where the apical dendrite splits) and distance to the dendrite tip farthest away from the soma. Distance from nexus (*middle*) and longest dendrite (*right*) to soma. (**e**) Schematic illustrating branching order in a sample deep layer pyramidal neuron. Quantification of cumulative number (*middle*) and cumulative length (*right*) of dendrites at each centrifugal dendritic order.

Differences within the vH^{PFC} population are not recapitulated when comparing vH^{PFC} to vH^{NAc}

To ascertain whether the observed differences between PFC-projectors in the deep and superficial layers could be observed by comparing any two projection populations, we pooled data from all PFC-projectors and compared it to data obtained from NAc-projecting cells.

In response to incremental current injections (-20 to 160 pA in 20 pA increments), vH^{NAc} cells responded similarly to superficial vH^{PFC} cells, which both differed from the more excitable deep vH^{PFC} cells. Overall, the higher excitability of deep layer cells dominated the average excitability of the PFC-projection population, such that the general vH^{PFC} population was more excitable than the vH^{NAc} population (Repeated measures within and between subjects ANOVA with Greenhouse-Geisser correction for sphericity: $F_{(1.309,66.762)} = 4.270$, $p = 0.033$; Figure 3.8 c). However, when measuring input resistance and burstiness (Figure 3.8 d and e), differences between the vH^{PFC} and vH^{NAc} populations were not apparent. Pooling superficial and deep vH^{PFC} cell data and treating it as one population (vH^{PFC}) and comparing it to vH^{NAc} cells showed no differences in input resistance (vH^{NAc}: 194.34 MΩ $\pm$ 30.06, vH^{PFC}: 200.30 MΩ $\pm$ 13.34; Mann Whitney, U = 361, $p = 0.18$, n = 18 and 47, respectively) or in the proportion of burst-firing cells (vH^{NAc}: 27.78% $\pm$ 10.86, vH^{PFC}: 27.78% $\pm$ 7.57; Mann Whitney, U = 648, $p = 0.99$, n = 18 and 36, respectively), despite differences being present within the vH^{PFC} population. As reported above, within the PFC-projecting population, input resistance was higher for deep vH^{PFC} neurons compared to cells in the superficial layer (deep: 229.95 $\pm$ 21.47, n = 25 and superficial: 166.61 $\pm$ 11.48, n = 22. Mann Whitney: U = 176, $p = 0.018$) as was the proportion of burst firing cells (deep: 45 % $\pm$ 11.41, n = 20 and superficial: 6.25 % $\pm$ 6.25, n = 16. Mann Whitney: U = 222, $p = 0.012$). Burst firing was visually inspected and classified as an action potential doublet (or in some instances, triplet) at the start of a stimulus train (see Figure 3.8

b) in contrast to regularly spaced out spikes throughout the stimulus duration.

In the cells I recorded from, any observed burst consistently occurred within the first three action potentials. To measure burstiness more quantitatively, I compared the observed first interspike interval (ISI) i.e. the time between peaks of the first and second action potentials, to the expected first ISI for a regular firing cell. The expected regular-spiking ISI was calculated by dividing the stimulus time by the number of spikes in the trace (giving an ISI value representative of the spikes in the given trace being equally spaced out). The dotted grey lines in Figures 3.8 f and g represent a perfectly regular-spiking cell.

Firstly, I asked whether the expected ISI and / or cell type (vH^{NAc}, vH^{PFC}, vH^{PFC} sup or vH^{PFC} deep) were significant predictors of the observed ISI by fitting a linear model to the data. The expected ISI values were robust predictors of the observed ISI when comparing both NAc to PFC-projectors and superficial to deep PFC-projectors (PFC/NAc: t = 18.08, p = 0.0 and Sup/Deep: t = 15.20, p = 0.0, by linear regression). However, cell type was only a significant predictor of the observed ISI when comparing superficial and deep PFC-projectors but not PFC- and NAc-projectors (PFC/NAc: t = -0.005, p = 0.996 and Sup/Deep: t = 4.40, p = 0.0). These findings suggest that there is no gain in statistical strength of the model by adding the cell-type parameter when comparing NAc- to PFC-projectors (Figure 3.8 f), confirming their similarity in bursting behaviour, whereas the opposite is true when comparing superficial and deep vH^{PFC} cells (Figure 3.8 g). This highlights both the difference between superficial and deep vH^{PFC} burstiness and the importance of treating the PFC projection as two separate populations to capture the full variance of the data. Statistically, separating the PFC projection population into its constituent layers better accounts for variance in the data. This is shown by a lower BIC score associated to a 'full' linear model that includes cell type i.e. superficial and deep as a parameter as opposed to a 'reduced' linear model that fits all pooled vH^{PFC} data (full model BIC: -423.4, reduced model BIC: -410.0). For the data

shown in Figure 3.8 f however, a reduced model (that ignores vH^{NAc} and vH^{PFC} labels) performed better than a full model (full model BIC: -475.3, reduced model BIC: -480.9), suggesting that differentiating overall vH^{PFC} from vH^{NAc} cells does not add value to the model. This suggests that differences in electrophysiological properties may not be inherent to every comparison between projection populations.

A subset of vH^{NAc} of cells (n = 4 vH^{NAc} cells) were filled with Alexa 594 dye (mixed into the internal solution) during recordings, and subsequently imaged using a 2-photon microscope mounted onto the electrophysiology rig to later reconstruct their morphology. As shown in Figure 3.8 h-i, NAc-projecting cells were highly branched and in contrast to the differences observed within the PFC-projecting population, the overall spread of dendritic length as a function of distance from pia was not different from that of PFC-projectors (Repeated measures within and between subjects ANOVA with Greenhouse-Geisser correction for sphericity: $F_{(3.718,55.776)} = 0.538$, $p = 0.696$). Again here, the differences in morphology between superficial and deep PFC-projecting cells would have been overlooked if the projection were treated as one group and it would be on average, morphologically indistinguishable from the vH^{NAc} projection.

Overall, these data show that when pooled, the PFC-projecting population as a whole may be seen as a homogeneous population, indiscernible from the NAc-targeting neurons in vH for some measures. When the two layers in the PFC-projection are looked at separately, differences in firing properties and morphology become apparent, adding support to the hypothesis that they may indeed be part of two distinct circuits.

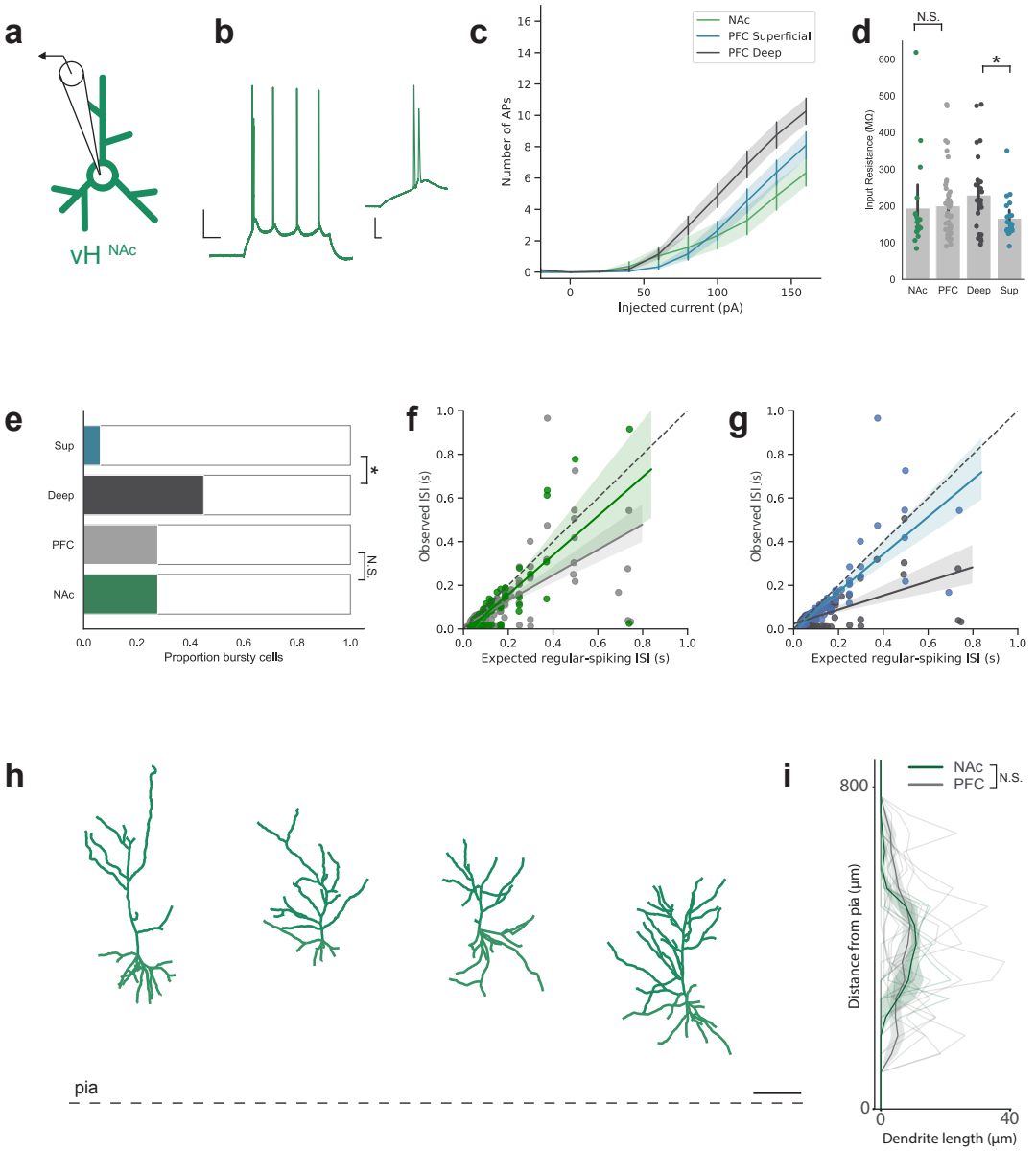

Figure 3.8: Electrophysiological and morphological characterisation of NAc-projectors (**a**) Schematic of experimental setup. Retrobead injections in NAc allowed for visually guided recordings from vH^{NAc} neurons. (**b**) Sample voltage trace in response to 140 pA current injection. Note initial burst in zoom on right. (**c**) Average number of action potentials in response to increasing current injections. Note very similar distribution of vH^{NAc} and superficial vH^{PFC} cells. (**d**) Input resistance calculated from voltage deflection in response to a 20 pA current injection. (**e**) Proportion of cells showing bursts like the sample trace in (b). Traces were visually inspected for bursting behaviour. (**f**) Observed first ISI plotted against the expected first ISI of a regular-spiking cell firing the same number of action potentials. Grey dotted line represents a linear relationship between observed and expected ISI i.e. a regular-spiking cell. (**g**) Same as (f) but for superficial and deep vH^{PFC}. (**h**) Example reconstructions of NAc-projecting hippocampal neurons. Scale bar = 100 μm, dotted line represents pia. (**i**) Profile of dendritic length as a function of distance from pia for vH^{PFC} and vH^{NAc} cells. Note very similar distribution.

3.3 Discussion

In this chapter, I have shown that the neuronal projection from ventral hippocampus to PFC is composed of two distinct populations of cells, situated in the superficial and deep layers of the CA1 / subiculum border. The cells in these two layers are genetically, physiologically and morphologically different from each other and follow gradients in firing properties and gene expression along the radial axis, in line with those previously identified (Kim and Spruston, 2012; Cembrowski and Spruston, 2019; Lee et al., 2014c; Soltesz and Losonczy, 2018). Here, I will discuss the functional implications of the anatomical segregation of this projection population along the radial hippocampal axis, the unique genetic makeup of the two layers and the implications of the electrophysiological characteristics of cells in each layer.

PFC-projecting cells in vH are split into two layers along the radial axis

The segregation of PFC-projecting neurons into two layers in vH has implications for the functional role of the vH-PFC pathway. Cells in the superficial and deep layers of the radial axis have been associated with supporting different behaviours and facilitating parallel processing of information (Soltesz and Losonczy, 2018; Slomianka et al., 2011; Valero et al., 2015; Pi et al., 2020; Gauthier and Tank, 2018; Geiller et al., 2017b). For example, cells in the superficial layer are involved more prominently in sharp wave ripple (SWR) oscillations, which are crucial for memory encoding, while deep cells are not engaged in these events (Valero et al., 2015). In contrast, deep but not superficial layer hippocampal cells have been shown to be involved in place field formation and flexible remapping of place fields during spatial navigation (Mizuseki et al., 2011; Geiller et al., 2017a; Danielson et al., 2016). Although the idea of parallel streams of information being processed by different projection populations in the hippocampus has been suggested before (Ciocchi et al.,

2015; Jimenez et al., 2018; Cembrowski et al., 2018a), it has not been previously observed or suggested to exist within a single projection population. It would be of interest to investigate whether these different roles associated with general, non-projection specific superficial and deep layer cells map onto PFC-projecting superficial and deep neurons.

The anatomical separation confining PFC-projecting neurons to opposite poles of the radial axis accentuates their differences in terms of physiological properties (more bursting activity and higher excitability in deep layer cells and larger sag component in superficial cells), which are usually represented as a gradient along the radial axis (Cembrowski and Spruston, 2019; Kim and Spruston, 2012; Soltesz and Losonczy, 2018). By representing the two extremes of the existing gradients, as opposed to other projection populations like NAc-projecting cells that are organised into a single layer and occupy a more intermediate position along the radial axis (Figure 3.2; Kim and Spruston (2012); Wee and MacAskill (2020)), differences within the PFC-projecting population become more stark. As shown in this chapter, the disparities in properties seen between deep and superficial vH^{PFC} neurons were not apparent when comparing the vH^{PFC} projection as a whole to the vH^{NAc} projection. Although PFC-projecting neurons are unique in their anatomical layered distribution, we cannot exclude the possibility that other (if not all) other projection populations in vH are composites of subgroups as well. However, no other vH projection populations investigated in the lab (to basolateral amygdala and lateral hypothalamus) showed equivalent spatial segregation. Thus, it may prove more difficult to identify differences in properties amongst cells in other projection populations with no clear anatomical border separating potential subgroups. Populations targeting other brain areas may also utilise the established and well-characterised gradients along the vH axes (Greene and Totterdell, 1997; Graves et al., 2012; Jarsky et al., 2008; Kim and Spruston, 2012; Cembrowski and Spruston, 2019), but due to the lack of spatial segregation within the populations, differences may not be as stark. Thus, the anatomical separation of the vH-PFC pathway

into a superficial and a deep layer along the radial axis of the hippocampus may be a unique feature facilitating the use of existing heterogeneity to provide a functional dichotomy within the projection.

The positioning of PFC-projecting neurons at the extreme poles of the radial axis also has an effect on the area covered by their dendritic trees, such that the bulk of their basal and apical dendrites follow different distributions (Figure 3.6; Bannister and Larkman (1995)). Tied together with the differential distribution of incoming axons from diverse brain areas in the CA1 / subiculum area coming in via different tracts and occupying distinct laminae (Masurkar et al., 2017; Pi et al., 2020; Wouterlood et al., 1990; Li et al., 2017; Soltesz and Losonczy, 2018), it provides a basis for differential input / output wiring of deep and superficial vH^{PFC} neurons (Slomianka et al., 2011). Different connectivity across layers in the hippocampus may help to explain why superficial and deep pyramidal cells have been shown to have different levels of involvement in specific neural events, as described above (Valero et al., 2015; Pi et al., 2020; Soltesz and Losonczy, 2018). Specifically, differential connectivity onto the superficial and deep layers of the PFC-projecting population may provide insight into how this pathway can support multiple behavioural roles.

Another observation in support of different circuit modules being represented by cells in the superficial and deep layers is the level of complexity in their morphology (Figures 3.6 and 3.7). From our experiments we found that cells in the superficial layer of the vH^{PFC} population have a higher total apical dendritic length, with a higher level of branching than cells in the deep layer (Figure 3.7). The more complex dendritic arborisation of superficial layer vH^{PFC} neurons, which has been previously observed in dorsal hippocampus in non-projection specified neurons (Li et al., 2017), suggests that inputs onto PFC-projecting neurons in the two layers may be integrated differently. While a highly branched dendritic tree may allow for parallel integration of multiple inputs, longer and more sparse dendritic processes like

those seen in deep vH^{PFC} neurons may lend themselves to serial integration of less numerous inputs (Beierlein, 2014). Several studies have shown that apical dendritic branches independently act as active integration compartments, and suggest that branch-specific plasticity changes are a form of information storage (Harnett et al., 2012, 2013; Losonczy et al., 2008). Furthermore, strong dendritic spikes, which aid in retention time of stored information, are less common in branches further away from the soma (Losonczy et al., 2008). Cells in the deep layer, which I observed to have sparse but longer main apical dendrites, branching further from the soma than their superficial counterparts (Figure 3.7) may thus store different modalities of information or resort to different mechanisms than superficial layer cells to integrate distal inputs. Furthermore, differences in bursting activity (Figure 3.5), with deep layer cells presenting more bursting activity may point at different modalities of broadcasting information, where bursts may be utilised to rapidly transfer salient information as opposed to regular spiking cells in the superficial layer.

Cells in the superficial and deep layers have different transcriptomic profiles

As highlighted by the RNA sequencing experiments in this chapter, cells in the superficial and deep layers of the vH-PFC projection have different transcriptomic signatures (Figure 3.3). Finding specific enrichment of genes in the two layers, in particular *Calbindin1* in the superficial population, is an extremely valuable characteristic that can be exploited to target and investigate the role of genetically identified cells within a circuit by combining genetic and viral approaches (Figure 3.4). In dorsal hippocampus as well as other cortical areas, *Calbindin1* has also been shown to be enriched in superficial layer pyramidal cells (Valero et al., 2015; Leone et al., 2008; Pi et al., 2020). Furthermore, superficial and deep layers characterised by the presence and absence of *Calbindin1* expression respectively, have been shown to have different properties and connectivity (Slomianka et al., 2011; Valero et al., 2015; Soltesz and Losonczy, 2018; Pi et al., 2020; Lee et al., 2014c).

Differential gene expression across all hippocampal axes has been reported and shown to have effects on morphology, physiology and connectivity of cells due to levels of transcripts encoding elements such as transcription factors or ion channels (Cembrowski et al., 2016b,a). For example, the effects of such genetic specificity within the hippocampus can be seen in the cannabinoid pathway, which acts through CBR1 receptors (present only in superficial pyramidal cells) and modulates behaviour by controlling Ih dendritic current (larger in superficial cells; Figure 3.5, Maroso et al. (2016)). Specifically, cells expressing *Calbindin1* in the hippocampus have been shown to have distinct innervation patterns, receiving preferential input from entorhinal cortex, and are involved in specific behaviours which are not attributed to *Calbindin1*-negative deep layer cells such as approach behaviour and olfactory learning (Li et al., 2017; Pi et al., 2020; Lee et al., 2014c). These findings support the idea that superficial layer, *Calbindin1*-positive PFC-projecting cells may carry out different functions to deep layer, *Calbindin1*-negative cells in this projection.

Furthermore, developmentally related neurons are selectively interconnected in the hippocampus, such that neurons born during different developmental periods are organised into parallel connectivity channels (Deguchi et al., 2011). Interestingly, pyramidal cells of the superficial layer arise around 2 to 3 days after those in the deep layer (Soltesz and Losonczy, 2018), suggesting that cells in the two layers of the vH-PFC projection may be embedded in different circuitry and connectivity patterns. Thus, the differences in gene expression and developmental time stamps specific to each layer further support the hypothesis that heterogeneity within the PFC-projection population and its subclassification into layers may point at two parallel circuits from vH to PFC.

Chapter 4

Mapping afferent and local inhibitory connectivity of PFC-projecting vH cells

4.1 Introduction

In the previous chapter I described two distinct populations of neurons in ventral hippocampus that project to prefrontal cortex. This raises interesting questions such as: do they form completely distinct circuits, carry out unique computations and functions, or convey different information from the hippocampus to PFC? I was particularly interested in the possibility that these two populations may be connected differentially within the hippocampal circuit, and receive unique local and long range synaptic input. If this were true it would suggest that they formed two distinct circuits with unique functions.

In the CA1 / subiculum region of the hippocampus there have been numerous reports of graded or biased afferent inputs onto hippocampal neurons defined

either by their different positioning along the hippocampal axes or by their projection target, which in turn affect their functional roles (Witter et al., 2000; O'Mara et al., 2001; Nakamura et al., 2013; Oliva et al., 2016; Soltesz and Losonczy, 2018; Wee and MacAskill, 2020). For example, inputs from hippocampal areas CA2 and CA3 and the adjacent entorhinal cortex onto CA1 pyramidal cells show biased patterns of connectivity. Entorhinal inputs have been shown to preferentially target superficial layer pyramidal neurons in more distal (closer to subiculum) portions of CA1 and deep layer cells more proximally, while CA2 terminals more strongly recruit deep layer cells in CA1 (Li et al., 2017; Masurkar et al., 2017; Kohara et al., 2014; Nasrallah et al., 2019; Fernández-Ruiz et al., 2017). Furthermore, CA3 has been shown to preferentially target superficial layer cells (Li et al., 2017; Soltesz and Losonczy, 2018). More specific investigations have observed gradients along the proximo-distal axis, such that distal CA3 pyramidal cells send terminals to deep CA1 layers and proximal CA3 cells preferentially innervate intermediate and superficial layers distally (Ishizuka et al., 1990; Fernández-Ruiz et al., 2017). Extrahippocampal inputs from medial septum and the diagonal band of Broca (DBB) also target hippocampal pyramidal cells and interneurons in a lamina-specific manner, preferentially innervating both interneurons and excitatory cells in the deep layer stratum oriens, which in turn interferes with patterns of entorhinal input (Gulyás et al., 1990; Leão et al., 2012; Müller and Remy, 2018). Recent experiments have shown that afferent connectivity also varies on the basis of the projection target of hippocampal neurons such that for example, nucleus reuniens input targets cells projecting to NAc and lateral hypothalamus but specifically avoids PFC-projecting cells (Wee and MacAskill, 2020).

However, these functional circuit mapping studies mainly focus on the dorsal hippocampus and therefore how afferent input into ventral hippocampus is organised along the different axes and onto different projection populations is not yet fully understood. This is compounded by the fact that afferent input into ventral hippocampus is diverse, arising from areas such as the amygdala, thalamus, basal

forebrain, as well as classical areas like CA3 and entorhinal cortex (Prasad and Chudasama, 2013; Pi et al., 2020; Fanselow and Dong, 2010; Strange et al., 2014; Wee and MacAskill, 2020). Each of these areas is thought to confer distinct information to the hippocampus, and so the specific targeting of these afferents represents an ideal means of supporting unique computations amongst distinct populations of neurons in vH.

As described in the previous chapter, cells projecting to PFC are segregated along the radial axis of the ventral hippocampus. Therefore, how afferent input onto cells in the two layers of this projection may differ may be based both on their spatial location and projection target. The interplay of projection target and radial axis gradients in input is not known, and is key to understanding this circuit and specifically, how vH output onto PFC is determined and controlled by upstream structures. Overall, investigating whether there are biased afferent input patterns onto the superficial and deep layer PFC-projecting cells in vH will aid in understanding their roles within the vH-PFC pathway and may also shed light on how afferent input could affect other vH parallel projections.

Neurons within the CA1 / subiculum area in the vH, while at most only very sparsely interconnected with direct excitatory connections, are known to engage in robust local inhibitory circuits (Korotkova et al., 2010; Lee et al., 2014c; Mukherjee et al., 2019). This suggests that an additional mechanism of control of the two PFC-projecting layers in vH may be specific connectivity with local interneurons. Interestingly, differences in the inhibitory microcircuitry involving superficial and deep CA1 / subiculum area pyramidal cells have been observed (Lee et al., 2014c). These findings point towards preferential targeting of PV-positive interneurons by cells in the superficial hippocampal layer and a higher inhibitory drive of PV-positive interneurons onto pyramidal cells in the deep layer (Lee et al., 2014c). PV interneurons are also preferentially activated by and in turn target different neurons differently, based on their projection target (Lee et al., 2014c). Thus, local inhibitory

connections may affect hippocampal output from the two PFC-projecting layers in a different manner.

Overall, in this chapter my aim is to investigate the structural and functional afferent and local connectivity of hippocampal projection neurons that target PFC. Given that the vH-PFC projection is organised into two layers, I am interested in studying whether there are any differences in their afferent input. Understanding afferent input onto and local circuitry affecting cells in the superficial and deep layers of the vH-PFC projection will help in clarifying how vH output onto PFC is controlled. By combining viral tracing and optogenetically driven circuit mapping methods, in this chapter I will investigate the afferent input onto deep and superficial vH^{PFC} cells as well as the local interaction of cells in these layers with inhibitory interneurons.

4.2 Results

Utilising TRIO to map candidate afferent areas

Having identified a layered, parallel output distribution of vH^{PFC} cells, I next wondered whether the inputs onto cells in the deep and superficial layers of the PFC-projecting population in vH were different and specific to each layer. To select candidate brain regions providing afferent input onto vH^{PFC} cells in both layers, I implemented the tracing technique TRIO (tracing the relationship between input and output; Schwarz et al. (2015)). A retrograde virus expressing Cre was injected into PFC, such that axon terminals would take up the construct, which was transported back to the cell bodies sending out these axons in vH. During the same surgery, an AAV expressing Cre-dependent rabies helper G-protein and avian receptor TVA (TVA-G; tagged with EGFP) was injected into the ventral hippocampus (see Figure 4.1 a). Cre-positive neurons in vH (those projecting to PFC) would therefore be equipped for the expression of both the TVA receptor and G-protein. After allowing for 2 weeks of transport and expression, pseudotyped rabies coated with the TVA ligand EnvA (Wickersham et al., 2007) was injected into the vH, infecting only those cells expressing the TVA receptor (i.e. vH^{PFC} cells). Due to co-expression of G-protein in these cells, which is necessary for transsynaptic spread of rabies, the mCherry-tagged rabies virus could only 'jump' one synapse upstream from vH^{PFC} neurons, but not from vH cells projecting elsewhere. This allowed us to ask the question of what brain areas target ventral hippocampal cells that project to PFC (Figure 4.1 a).

Cells from which the transsynaptic spread begins are called 'starter cells' and can be seen in white, co-labelled with mCherry-tagged rabies and EGFP-tagged G-protein in Figure 4.1 b, marked with arrowheads. From these starter cells, rabies spreads transsynaptically one synapse upstream, infecting neurons providing

input onto the starter cells (seen in magenta in Figure 4.1 b, *right*, and in white in Figure 4.1 c and d). After allowing one week for rabies-mediated transsynaptic spread and expression, we collected sagittal slices from three brains to search for mCherry-labelled (i.e. rabies-infected) cells in candidate brain regions. We consistently observed mCherry-labelled cells intra-hippocampally in CA3 and medial entorhinal cortex (mENT) and extra-hippocampally in diagonal band of Broca (DBB) and anterior thalamus (ATh) (Figure 4.1 c and d). Overall, these experiments show that TRIO can be used successfully to unbiasedly trace back one synapse from cells of interest in order to understand the input and output patterns of projection neurons - in this case of PFC-projecting neurons in vH. Furthermore, these data describe the connectivity of the vH^{PFC} population as a whole and provide the basis for data-driven enquiry into differential targeting by these areas of superficial and deep vH^{PFC} cells.

To show that transsynaptic spread for input labeling by pseudotyped, G-deleted rabies infection required the presence of both Cre and TVA-G, control experiments were performed in parallel by Ryan W S Wee in the MacAskill lab where injections of either Cre, TVA-G, or both Cre and TVA-G were excluded (Figure 4.2). Neither of the three control experimental conditions resulted in transsynaptic spread to long-range inputs (Figure 4.2 e), confirming that both Cre and TVA-G are necessary for transsynaptic spread from starter cells. Co-expression of TVA-G and rabies led to a minimal amount of mCherry-labelled cells (expressing rabies) locally in the hippocampus (Figure 4.2 a, b, e), suggesting that there may be a very low level of background TVA expression in the absence of Cre. However, the absence of mCherry-positive cells beyond the injection site in this control condition suggests that G-protein was not expressed and thus supports the necessity of both Cre and TVA-G for successful transsynaptic spread.

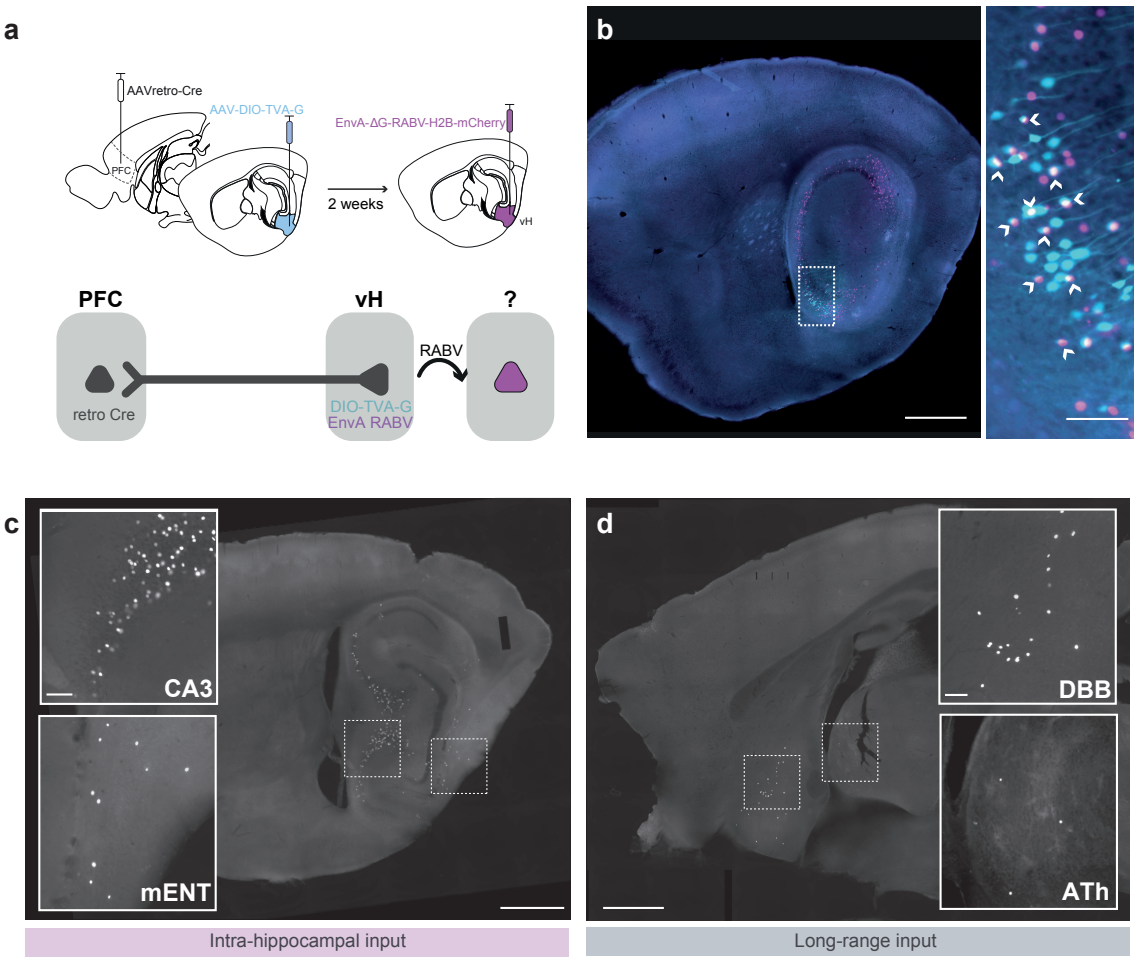

Figure 4.1: Utilisation of TRIO to identify afferent inputs onto vH^{PFC} cells
(a) Schematic of TRIO injection strategy. AAVretro-CAG-Cre was injected in PFC, and an AAV expressing rabies helper proteins was injected into vH to limit subsequent rabies infection to hippocampal PFC-projecting neurons. 2 weeks later, EnvA pseudotyped rabies was injected in vH to label presynaptic neurons that synapse onto PFC-projecting hippocampal neurons with nuclear-localised mCherry. **(b)** Injection site in a sagittal section showing TVA and G-protein expressing hippocampal neurons (cyan), and rabies-infected, mCherry-labelled neurons (magenta). (*Right*) Zoom in to white dotted box. Co-labelled neurons represent starter cells (arrowheads). **(c)** Sagittal section showing insets of rabies-labelled cells in intrahippocampal input regions CA3 and mENT. **(d)** Sagittal section showing insets of rabies-labelled cells in extrahippocampal input regions DBB and ATh. All scale bars = 1mm (overview panels), 100 μm (inset panels).

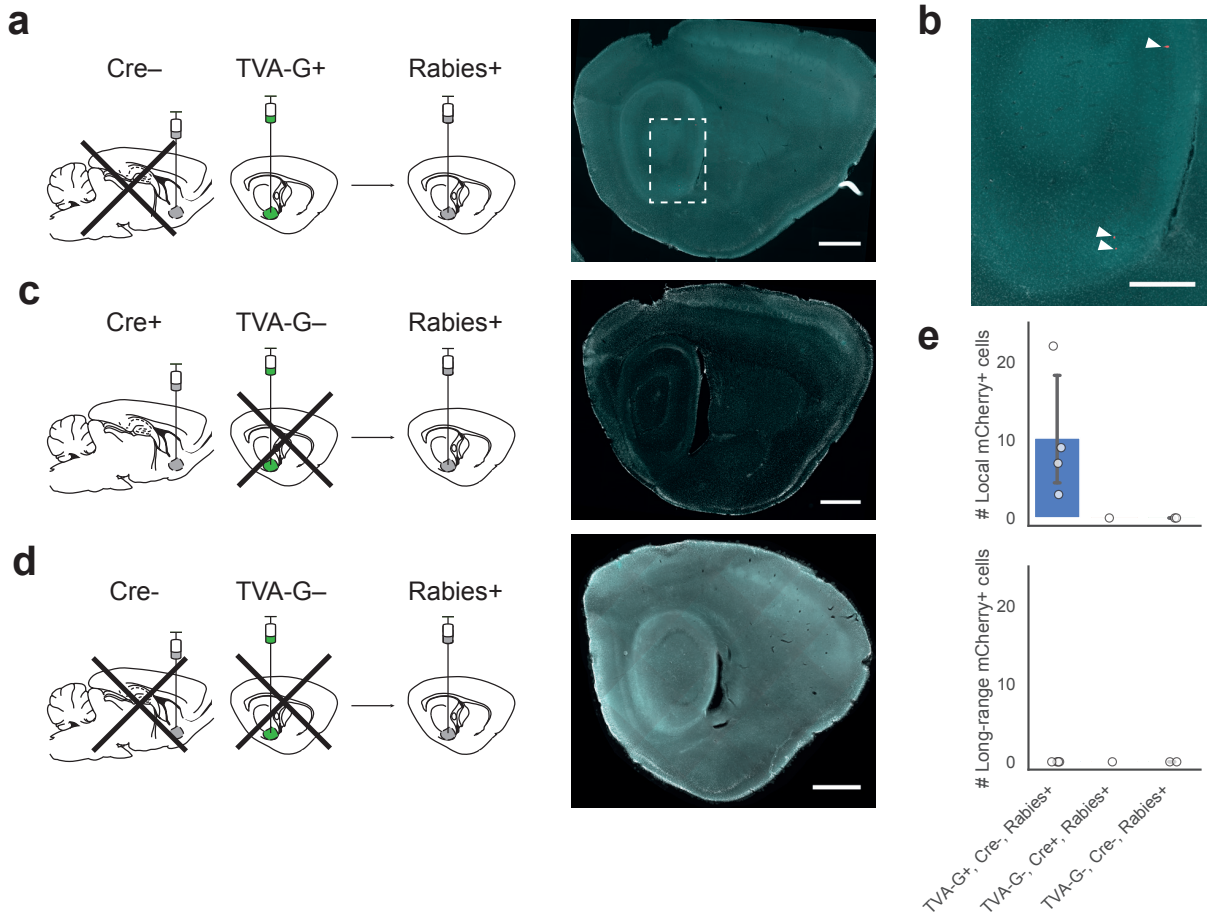

Figure 4.2: Experimental controls for TRIO protocol
(a, c, d) Schematics for control surgeries for TRIO. Example images of sagittal sections containing the hippocampus are shown on the right for each condition. **(a, b)** Controls with injection of the single-construct TVA-G virus into vH without AAV2-retro-Cre injection in the output side. mCherry-tagged rabies virus was injected 2 weeks later (n = 4 brains). **(a)** Right: Sagittal brain section from a representative experiment without Cre injection. **(b)** Zoom-in image of boxed region in (a). Arrowheads indicate sparse mCherry+ rabies-labelled cells, likely due to Cre-independent expression of TVA-G and subsequent rabies infection of starter cells. **(c, d)** No TVA-G (c, n = 1 brain) and no TVA-G and Cre (d, n = 2 brains) controls. No mCherry+ cells were detected in (c) and (d). **(e)** Quantification of mCherry+ labelled inputs in control conditions. All leaky mCherry+ cells were detected locally within the hippocampal formation, surrounding the injection site, and none were detected in long-range input regions. Bar plots indicate mean ± SEM. Scale bars = 1 mm (a,c,d, Right), 500 μm (b, zoomed-in image). All control data shown in this figure was gathered by Ryan W S Wee at the same time as I gathered data for Figure 4.1 and is published in Wee and MacAskill (2020).

To verify the anatomical findings elucidated with TRIO suggesting that CA3, mENT, DBB and ATh send input onto vH^{PFC} cells functionally, I implemented CRACM (channelrhodopsin 2 (ChR2)-assisted circuit mapping) (Petreanu et al., 2007) to test the responses of vH^{PFC} cells in each layer to stimulation of axons originating from the areas singled out from the TRIO data. The setup for these experiments is explained in Figure 4.3. Firstly, an anterogradely transported ChR2-expressing vector was injected into the brain area of interest - contralateral CA3 (cCA3) for this example (Figure 4.3 a). In the same surgery, retrograde beads conjugated with Alexa 555 dye were injected into PFC, in order to later visualise vH^{PFC} cell bodies in hippocampal slices during recordings. Two weeks were allowed for expression of ChR2 and retrograde transport of the fluorescent beads before collecting acute hippocampal slices for electrophysiological experiments. As an example of the experimental setup, in Figure 4.3 b axons coming in from cCA3 are shown in cyan and cells projecting to PFC are shown in magenta. Sample retrobead-labelled superficial and deep layer cells are marked with arrowheads (top and bottom, respectively). The experimental protocol for investigating connectivity using CRACM is summarised in Figure 4.3 c.

In the same slice, pairs of superficial and deep vH^{PFC} cells were recorded from while stimulating incoming e.g. cCA3 ChR2-positive axons with brief pulses of blue light of incremental duration (0.2, 0.5, 1, 2 and 5 ms; blue circle over axons beside recorded pyramidal cells). A pair of cells was taken to be a superficial and a deep vH^{PFC} layer cell at the same depth from the slice surface and in the same column within subiculum i.e. at the same approximate proximo-distal position along the hippocampal slice. Voltage traces in response to light stimulation were recorded in current-clamp mode, as shown in Figure 4.3 d. Voltage response amplitudes within pairs of superficial and deep recorded neurons were compared to obtain a deep:superficial ratio as a measure of connectivity bias. In order to ensure that the recorded responses were a result of mono-synaptic input (i.e. direct input from the ChR2-positive stimulated axons) only traces for which the excitatory

post-synaptic potential (EPSP) response was initiated within the 10 ms following light pulse stimulation were included. The peak of the response used to calculate the response amplitude was taken as the maximum point within the 20 ms following stimulation (only for traces where EPSP responses were initiated within 10 ms of light stimulation). However, owing to the variable kinetics and jittery nature of vesicle release underlying ChR2-elicited EPSPs (Petreanu et al., 2009), this method of restricting the response time window did not capture the true maxima of some traces, where slow rise times resulted in EPSP peaks in response to mono-synaptic input over 20 ms past onset of light stimulation. Where this method (taking the peak value of the mono-synaptically elicited EPSP response within 20 ms) did not represent the true relationship of superficial and deep layer responses, I will also report the separate statistics for the response peaks measured within a time window of 30 ms post light stimulation. In summary, the criteria for mono-synaptic connectivity was taken as the EPSP onset within 10 ms of the light stimulus. The response amplitude was calculated from the EPSP peak within a 20 ms time window following stimulation. More representative statistics of response amplitudes will be shown additionally where appropriate, allowing a time window of 30 ms for calculating the EPSP peak.

Using this set-up, we followed up on the top four candidate regions shown in Figure 4.1 (based on proportion of rabies-positive cells) identified with TRIO and investigated their inputs onto superficial and deep PFC-projecting cells in vH.

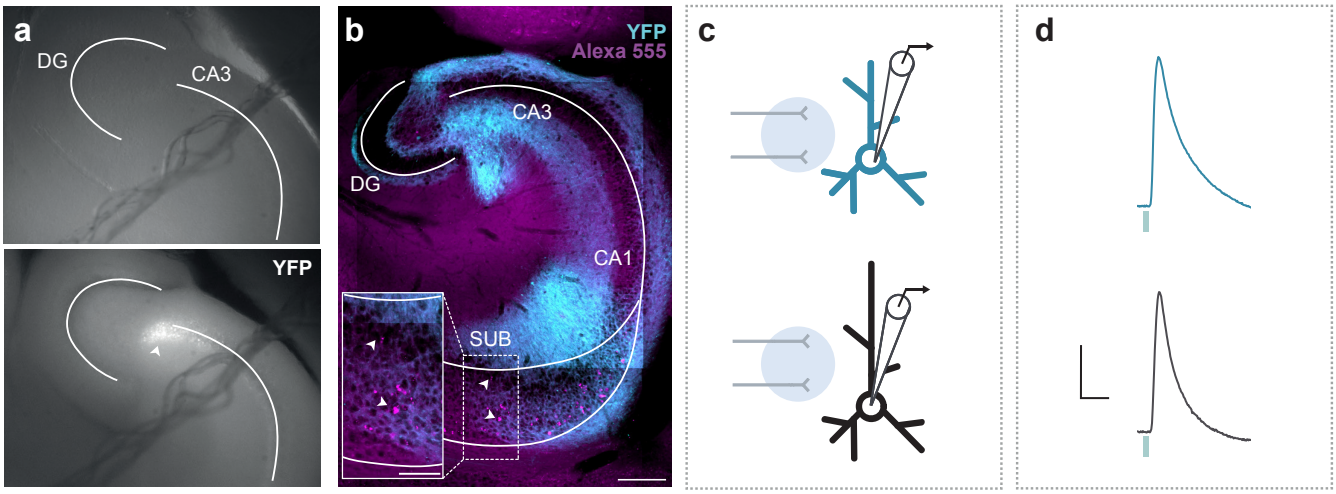

Figure 4.3: Set up for CRACM experiments to test input onto vH^{PFC} cells
(a) *Top*: Brightfield image of acute ventral hippocampal slice ipsilateral to CA3 ChR2-YFP injection. *Bottom*: Fluorescence image of the same slice, showing ChR2-YFP labelling in CA3 (arrowhead). In the same mouse, a retrograde tracer was injected in PFC, to visualise PFC-projecting cells in vH (contralateral to CA3 injection). **(b)** Transverse hippocampal slice from contralateral hemisphere to the injection shown in (a). ChR2-positive axons coming in from the contralateral CA3 shown in cyan. In magenta are Alexa 555-conjugated retrobead-labelled cells of the PFC-projecting population. Arrowheads pointing at superficial (top) and deep (bottom) cells. Scale bar = 200 μm, inset = 100 μm. **(c)** Schematic of experimental setup for patch-clamp experiments to compare relative input from a given brain area to superficial and deep vH^{PFC} cells. In blue, a superficial cell is being recorded from in current-clamp mode while stimulating incoming ChR2-positive axons (in grey) with pulses of blue light (blue halo over axons). In black, the same for a deep cell in the same slice. **(d)** Example voltage traces from a pair of superficial (blue) and deep (black) vH^{PFC} cells in response to stimulation of cCA3 axons with a 5 ms blue light pulse. These cells were recorded from the same slice and the axons stimulated in the same area. Scale bar = 20 ms and 5 mV.

CA3 inputs equally target superficial and deep vH^{PFC} cells

Using the setup explained in detail above, we first studied the effect of contralateral CA3 (cCA3) axonal stimulation on superficial and deep vH^{PFC} cells. ChR2-positive axons from the contralateral CA3 were stimulated with brief pulses of light (5 ms for the example trace in Figure 4.4 b) while recording from PFC-projecting neurons in both layers. The CA3 injection was carried out contralaterally to avoid both viral leak into CA1 ipsilateral to recordings and direct cell body stimulation of ipsilateral CA3 neurons.

As shown in the example trace in Figure 4.4 b, stimulation of cCA3 axons resulted in equivalent depolarisation in deep (black) and superficial (blue) PFC-projecting cell pairs. The order in which superficial and deep cells in a pair were recorded from was counterbalanced to account for rundown i.e. activity in cells and/or afferent terminals diminishing over the length of the recording session due to temporary depletion of vesicles, or any form of short-term plasticity resulting from repeated stimulation. Ratios of excitatory post-synaptic potential (EPSP) amplitudes between cells in each layer were calculated in a pairwise fashion, by normalising the voltage response in the superficial cell in a given pair to that of its deep counterpart. Summarised in Figure 4.4 c, there was no significant difference in the response amplitudes between layers, resulting in a ratio of 1.06 ± 0.35 (Wilcoxon paired, V = 28, p = 1, n = 10 pairs). On the right, the histogram summarises the frequency of observed ratios amongst the 10 pairs recorded. Contralateral Schaffer collaterals were stimulated in the stratum radiatum with five increasing light durations to capture any possible floor and ceiling effects and better understand the connectivity between CA3 and PFC-projecting neurons in the CA1 / subiculum border area. In Figure 4.4 d, the mean voltage response is shown for each increasing light pulse for superficial and deep cells. The mean amplitudes at each light pulse duration are summarised in Figure 4.4 e (top) and the raw amplitude data for the individual pairs is summarised in Figure 4.4 e (bottom). All PFC-projecting

cells recorded received input from cCA3, regardless of their anatomical distribution, summarised as a lack of difference in proportion of connected cells between the deep and superficial layers (Figure 4.4 f; Fisher's exact test: odds ratio = 0, p = 1). Connected cells were taken as cells in which synaptic responses exceeded the amplitude of the standard deviation of the baseline by 6 fold. Overall, we found that optical stimulation of cCA3 axons did not result in biased connectivity onto or depolarisation of vH^{PFC} cells in a layer-specific manner.

In addition to optical stimulation, we wanted to test the effect of electrical stimulation of ipsilateral CA3 afferents on vH^{PFC} cells. Similar to the optical stimulation ramping protocol, we stimulated ipsilateral Schaffer collaterals by placing a stimulating electrode in the stratum radiatum between CA3 and CA1, the area of passage for Schaffer collaterals, and delivered a train of increasing current pulses from 0.2 to 2 mA, while recording from pairs of superficial and deep layer vH^{PFC} cells (Figure 4.4 g). All data shown is for responses to 0.5 mA stimulation, as this current pulse most reliably produced subthreshold post-synaptic responses in both layers. Increasing current pulses above 0.5 mA elicited action potentials, hindering analysis of relative connectivity from subthreshold responses. I recapitulated the data obtained with optogenetic stimulation, seeing no difference in EPSP amplitude between layers, with a deep:superficial response ratio of 2.19 $\pm$ 0.96 (Figure 4.4 h and i; Wilcoxon paired: V = 33, p = 0.63, n = 10 pairs). From these two experiments we concluded that CA3 input to PFC-projecting cells in ventral hippocampus is not preferentially biased towards cells in the superficial or deep layers, suggesting that hippocampally processed information is relayed equally onto both PFC-projecting cell subpopulations.

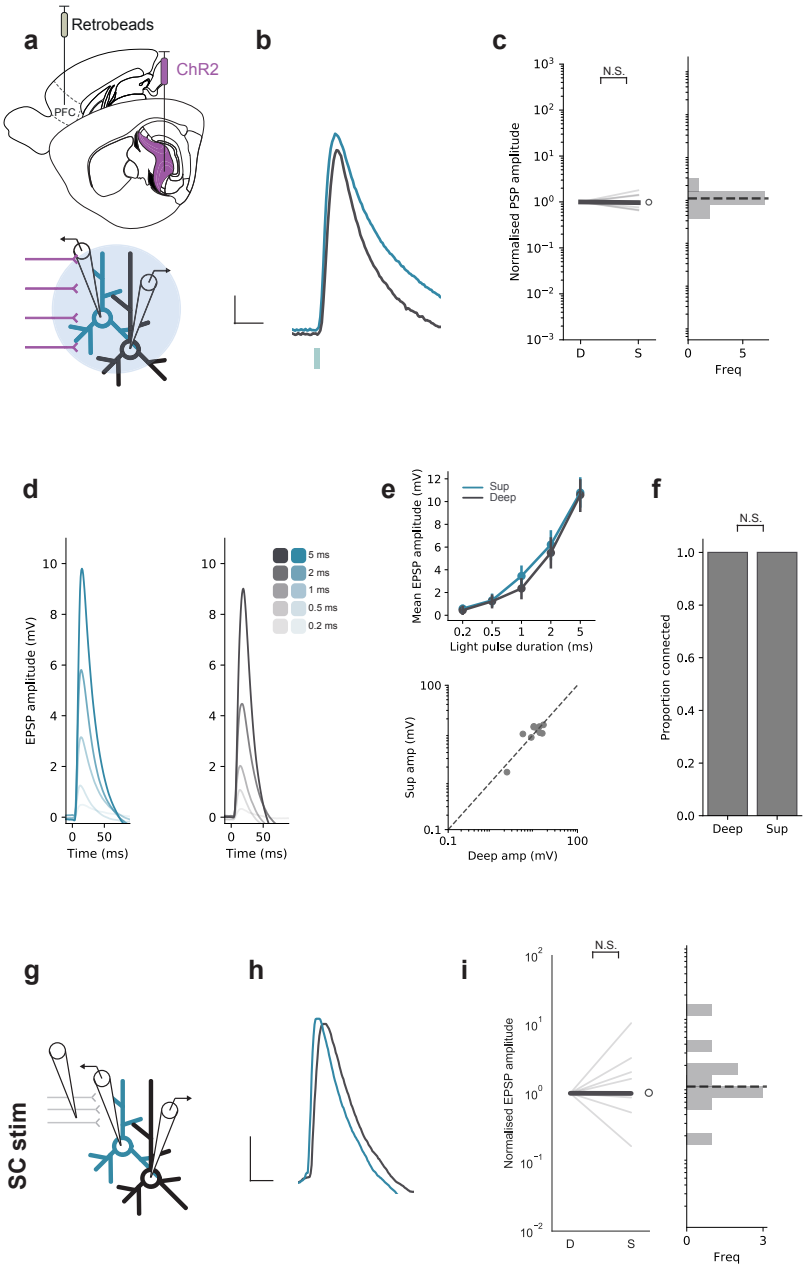

Figure 4.4: CA3 input is equal onto superficial and deep vH^{PFC} cells
(a) Schematic showing experimental setup. ChR2 injected into cCA3 and retrobeads into PFC. Input-specific connectivity was assessed using paired recordings of superficial (blue) and deep (black) vH^{PFC} neurons in acute slices. **(b)** Light-evoked responses in an example pair of superficial and deep vH^{PFC} cells. Scale bar = 20 ms and 2 mV. Blue tick represents light stimulus. **(c)** Ratios of deep:superficial neuron EPSPs. Data normalised to EPSP amplitude in deep cells. Values above 1 mean input is biased to superficial neurons, low values towards deep layer neurons. Dark line marks median. Note log scale. Histogram on right summarises frequency of ratio observations. Dotted line marks 1. **(d)** Mean light-evoked voltage responses to increasing light pulse duration in superficial and deep vH^{PFC} cells. **(e)** *(Top)* Mean light-evoked responses shown in (d). *(Bottom)* Amplitudes of individual pairs in response to 5 ms light stimulation. **(f)** Proportion of recorded cells receiving input from cCA3. **(g-i)** As for (a-c) with electrical stimulation of ipsilateral Schaffer collaterals. Wilcoxon paired test implemented for panels c, e and i. Fisher's exact test implemented for panel f.

Medial entorhinal cortex input is biased towards superficial vH^{PFC} cells

I next investigated any potential bias in the input from medial entorhinal cortex. Lateral and medial entorhinal cortex have been shown to have biased connectivity onto superficial and deep cells along the proximo-distal axis in a non-projection specific manner (Masurkar et al., 2017). In the dorsal hippocampus, medial entorhinal cortex input has been shown by different groups to both preferentially target cells in the deep layer proximally (closer to CA2, Masurkar et al. (2017)) and to equally target both layers (Li et al., 2017), while lateral entorhinal cortex input has been shown to be biased towards superficial layer cells distally (close to subiculum; Li et al. (2017)). However, it is unknown if biases exist regarding entorhinal input in ventral hippocampus and onto PFC-projecting cells specifically. Using CRACM, I addressed this question.

From the obtained TRIO data, medial entorhinal cortex (mEnt) was found to provide input onto vH^{PFC} cells. To test any connectivity biases of mEnt input across the two layers of the vH^{PFC} population, incoming mEnt ChR2-positive axons in the field of view were stimulated with brief pulses of blue (470 nm) light while recording from pairs of superficial and deep vH^{PFC} cells (Figure 4.5 a). As shown in the example voltage traces in Figure 4.5 b, input from medial entorhinal cortex was biased towards depolarising superficial vH^{PFC} cells, with a deep:superficial ratio of 26.87 $\pm$ 40.97 in response to 5 ms light stimulation (Wilcoxon paired: V = 27, p = 0.03, n = 7 pairs). In all recorded pairs, superficial cells responded with larger depolarisation than deep layer vH^{PFC} cells to entorhinal axon stimulation. Mean amplitude responses to increasing duration of stimulating light pulses are summarised in Figures 4.5 d and e. At shorter light pulse durations of 2 ms and 1 ms, superficial cell layer responses were also significantly higher than in deep cells (Wilcoxon paired: V = 28, p = 0.02, n = 7 pairs and V = 27, p = 0.03, n = 7 pairs, respectively). The proportion of connected cells in each layer was similar,

suggesting that a difference in overall number of connected cells was not the driver of biased input onto superficial cells (Fisher's exact test: odds ratio = 0, $p = 1$).

I next sought to confirm this finding with electrical stimulation of temporoammonic (TA) fibres coming into the CA1 / subiculum area directly from entorhinal cortex. We placed a stimulation electrode in the stratum lacunosum moleculare (SLM) at the point of entry of TA axons into subiculum and applied current pulses ranging from 0.2 to 2 mA while recording pairs of superficial and deep vH^{PFC} cells (Figure 4.5 g). As in the previous figure, all recordings shown for this setup are responses to 0.5 mA stimulation. I consistently observed a bias towards superficial layer cell depolarisation within pairs of recorded cells, resulting in a deep:superficial ratio of 6.17 $\pm$ 2.56 (Figure 4.5 h and i; Wilcoxon paired: V = 21, $p = 0.049$, n = 14 pairs). Together, these findings suggest that medial entorhinal cortex input to vH^{PFC} neurons is biased towards cells in the superficial layer.

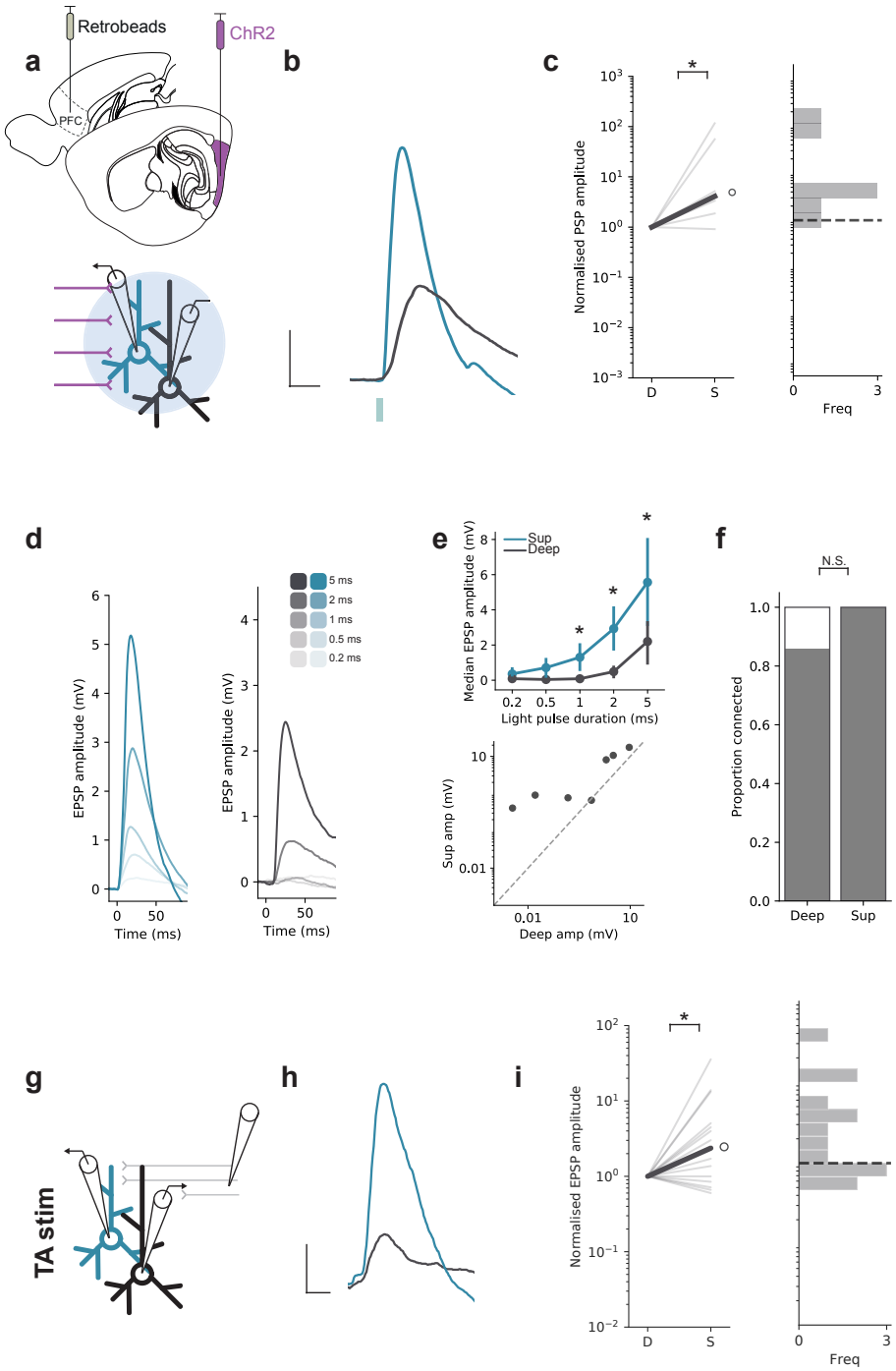

Figure 4.5: Entorhinal cortex input is biased onto superficial vH^{PFC} cells
(a) Schematic of experimental setup. ChR2 was injected into medial entorhinal cortex (mEnt) and retrobeads into PFC. Input-specific connectivity was assessed using paired recordings of superficial and deep vH^{PFC} neurons in acute slices. **(b)** Light-evoked responses in an example pair of superficial (blue) and deep (black) layer vH^{PFC} in response to afferent mEnt input. Scale bar = 20 ms and 2 mV. Blue tick represents light stimulus. **(c)** Ratios of deep:superficial neuron EPSPs. Data normalised to EPSP amplitude in deep cells. Values above 1 show biased input to superficial neurons, low values towards deep layer neurons. Dark line marks median. Note log scale. Histogram on right summarises frequency of ratio observations. **(d)** Mean light-evoked voltage responses to increasing light pulse durations in superficial and deep cells. **(e)** **(e)** *(Top)* Mean light-evoked responses shown in (d). *(Bottom)* Amplitudes of individual pairs in response to 5 ms light stimulation. **(f)** Proportion of recorded cells receiving mEnt input. **(g-i)** As for (a-c) with electrical stimulation of TA fibres. Statistical tests implemented as in Figure 4.4.

Anterior thalamus and diagonal band of Broca inputs are biased towards deep vH^{PFC} cells

The extra-hippocampal brain areas where we found most rabies-positive cells in the TRIO experiments were anterior thalamus (ATh) and the diagonal band of Broca (DBB) (Figure 4.1). As before, to functionally test these inputs onto deep and superficial layer vH^{PFC} cells, I expressed ChR2 in the areas of interest and optogenetically stimulated axon terminals within the hippocampus originating from ATh and DBB. Retrobeads injected in PFC allowed for visually guided recording from superficial and deep vH^{PFC} cells during stimulation of afferent axons.

In Figure 4.6 b, example voltage traces of a recorded pair in response to 5 ms light stimulation of ATh afferent axons show the larger EPSP evoked in the deep layer cell. This trend was consistently apparent across pairs of cells, with a median deep:superficial ratio of 0.07 $\pm$ 69.37 although it did not reach statistical significance (Wilcoxon paired: V = 10, p = 0.08, n = 10 pairs). Note that the median of the data has been chosen here as a representative description due to an outlier skewing the mean, although all data points were included in the statistical analysis, evidenced by the large standard error of the median ratio value. The mean EPSP amplitudes in response to all light pulse durations for an example superficial and deep cell pair is summarised in Figure 4.6 d. An example pair of cells was used in Figure 4.6 d instead of plotting the mean amplitude responses for all recorded cell pairs to provide a representative example of the emerging trend unskewed by the outlier. The median responses for all light pulse durations are shown in Figure 4.6 e (top) and raw amplitude data is shown in the bottom panel of Figure 4.6 e. The number of connected cells did not differ significantly between layers (Fisher's exact test: odds ratio = 0.12, p = 0.06), but trended towards higher connectivity amongst deep layer vH^{PFC} cells (Figure 4.6 f). Importantly, the true peak values for some traces did not fall within 20 ms of light stimulation. Expanding the time window to measure the EPSP peak and calculate the amplitude resulted in a median median

deep:superficial ratio of 0.1 $\pm$ 53.05, significantly biased towards deep layer cells (Wilcoxon paired: V = 12, p = 0.03, n = 12 pairs). This data suggests that additional experiments studying the ATh-subicular projection onto vH^{PFC} cells with more robust responses (the experiments shown here found very low response amplitudes) may elucidate the nature of this connection further, perhaps confirming the bias onto deep layer vH^{PFC} cells.

The second extra-hippocampal brain area with the highest number of rabies-positive cells seen with TRIO was the diagonal band of Broca. As with ATh, I wanted to investigate the relative input of this projection onto vH^{PFC} cells in both the superficial and deep layers. By injecting a ChR2-expressing construct in DBB I was able to optogenetically stimulate axons originating from DBB within hippocampal slices while recording from pairs of vH^{PFC} cells (Figure 4.7 a).

Stimulation of DBB axons with brief pulses of blue light trended towards larger depolarisation in deep layer vH^{PFC} cells than in their superficial pairs (Figure 4.7 b and c) in response to 5 ms light stimulation resulting in a deep:superficial EPSP amplitude ratio of 1.24 $\pm$ 2.54 (Wilcoxon paired: V = 0.057, n = 13 pairs). At a light duration of 2 ms, deep layer cell responses to DBB stimulation were significantly larger to those recorded in the superficial vH^{PFC} ;ayer (Wilcoxon paired: V = 14, p = 0.03, n = 13 pairs). Mean amplitudes in response to increasing light pulse duration are summarised in Figure 4.7 d and e (top) and raw amplitude data for all pairs in response to 2 ms light stimulation are shown in Figure 4.7 e (bottom). The proportion of connected cells recorded from did not differ across layers (Fisher's exact test: odds ratio = inf, p = 0.2, n = 13 pairs). Overall, these experiments show that DBB input is biased towards deep layer vH^{PFC} cells when stimulated with 2 ms, but not 5 ms, of blue light. Interestingly, as with ATh input, expanding the response time window to calculate the EPSP peak to 30 ms renders EPSP pair amplitudes in response to 5 ms light stimulation significantly different, with a deep:superficial ratio of 1.38 $\pm$ 0.92 (Wilcoxon paired: V = 24, p = 0.04, n = 13 pairs).

In summary, by implementing CRACM to investigate the input from upstream areas onto vH^{PFC} cells, I have shown that while CA3 equally targets superficial and deep layer cells, medial entorhinal cortex favours superficial vH^{PFC} cells and both extra-hippocampal areas ATh and DBB trend towards providing more input onto deep vH^{PFC} neurons. When expanding the response time window to calculate EPSP peaks to 30 ms (owing to slow EPSP rise times in response to ChR2-evoked vesicle release), both ATh and DBB input is biased towards deep layer vH^{PFC} cells. These findings point at a possible split of cortical input targeting superficial layer cells and subcortical input favouring deep layer PFC-projecting neurons. Furthermore, they point at two potential routes of differential control of vH output onto PFC.

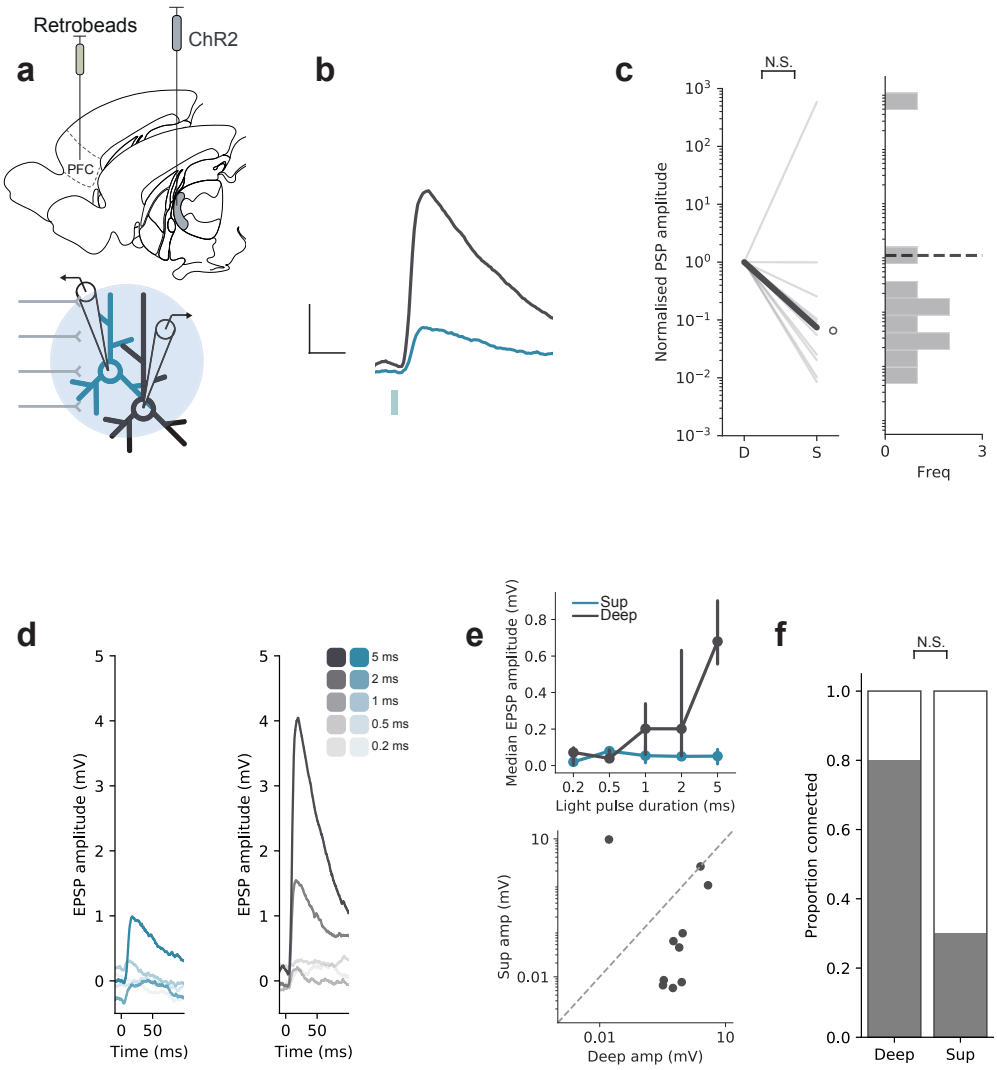

Figure 4.6: ATh input onto onto deep and superficial vH^{PFC} cells
(a) Schematic showing experimental setup. ChR2 injected into ATh and retrobeads into PFC. 2 weeks later input-specific connectivity was assessed using paired recordings of superficial and deep vH^{PFC} neurons in acute slices. **(b)** Light-evoked responses in an example pair of superficial (blue) and deep (black) layer PFC-projecting hippocampal neurons in response to afferent ATh input. Scale bar = 20 ms and 0.5 mV. Blue tick represents the light stimulus. **(c)** Ratios of deep:superficial neuron EPSPs. Data normalised to EPSP amplitude in deep cells. Values above 1 mean input is biased to superficial neurons, low values towards deep layer neurons. Dark line marks median. Note log scale. Histogram on right summarises frequency of ratio observations. **(d)** Mean light-evoked voltage responses to increasing light pulse durations (0.2 ms to 5 ms) in example superficial and deep cells. **(e)** *(Top)* Median light-evoked responses shown in (d). Note that the median has been chosen to plot data here due to presence of an outlier skewing the data, seen in (c). *(Bottom)* Amplitudes of individual pairs in response to 5 ms light stimulation. Graph summarising median light-evoked responses shown in (d). **(f)** Proportion of cells receiving input from ATh out of all cells recorded. Wilcoxon paired test implemented for panels c and e. Fisher's exact test implemented for panel f.

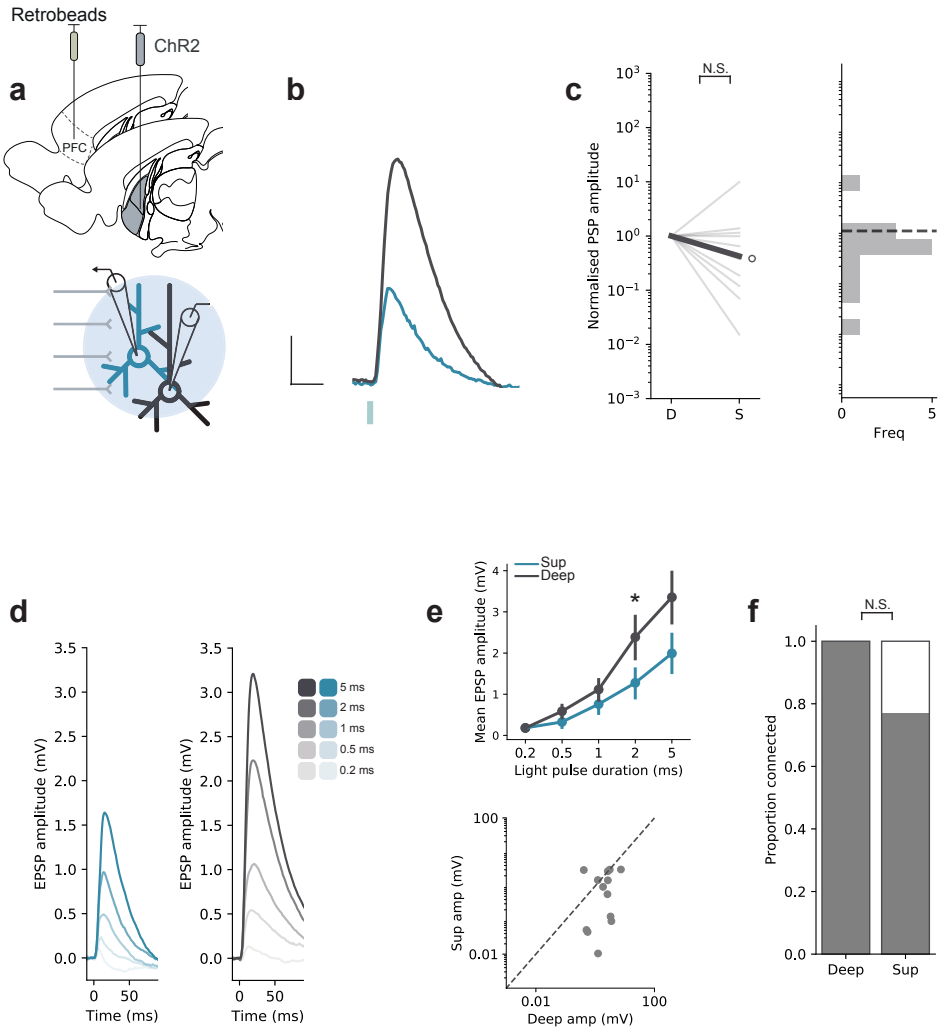

Figure 4.7: DBB input is biased onto deep vH^{PFC} cells

(a) Schematic showing experimental setup. ChR2 injected into DBB and retrobeads into PFC. 2 weeks later input-specific connectivity was assessed using paired recordings of superficial and deep vH^{PFC} neurons in acute slices. **(b)** Light-evoked responses in an example pair of superficial (blue) and deep (black) layer PFC-projecting hippocampal neurons in response to afferent DBB input. Scale bar = 20 ms and 2 mV. Blue tick represents the light stimulus. **(c)** Ratios of deep:superficial neuron EPSPs. Data normalised to EPSP amplitude in deep cells. Values above 1 mean input is biased to superficial neurons, low values towards deep layer neurons. Note log scale. Histogram on right summarises frequency of ratio observations. **(d)** Mean light-evoked voltage responses to increasing light pulse durations (0.2 ms to 5 ms) in superficial and deep cells. **(e)** *(Top)* Mean light-evoked responses shown in (d). *(Bottom)* Amplitudes of individual pairs in response to 2 ms light stimulation. Graph summarising median light-evoked responses shown in (d). **(f)** Proportion of cells receiving input from DBB out of all cells recorded Statistical tests implemented as in Figure 4.6.

Local inhibitory connectivity: interneurons provide equal input onto superficial and deep vH^{PFC} cells

Having seen differences in local and long-range inputs onto cells in the different layers of the vH-PFC projection, I hypothesised that there may be biases or layer-specific patterns in local connectivity with interneurons as well. It has been previously shown in a non-projection specific manner that cells along the superficial-deep axis in both dorsal and ventral hippocampus interact differently with local parvalbumin-positive (PV+) interneurons. Specifically, superficial layer cells provide larger input onto PV+ interneurons than neighbouring deep cells, and these interneurons go on to preferentially target cells in the deep layer resulting in an overall inhibitory bias onto deep layer cells (Lee et al., 2014c). Moreover, Lee et al. (2014c) showed that projection-specificity played a role in interneuron connectivity, with PFC-projecting cells in deep hippocampal layers providing most input onto PV+ interneurons in comparison with amygdala and entorhinal cortex projectors, and amygdala-projectors subsequently receiving most of the inhibition. These data suggest that both position along the radial axis and projection-specificity may influence interaction with local interneurons.

To address the question of whether superficial and deep PFC-projecting cells are differentially targeted by local PV+ interneurons, I used a PV-Cre mouse line, in which Cre is expressed under the control of the parvalbumin locus. Cre-dependent ChR2 was injected into vH, such that PV+ (Cre-expressing) interneurons would express ChR2 under the control of Cre. Fluorescent retrobeads were injected into PFC to visualise PFC-projecting neurons in vH (Figure 4.8 a). Blue light pulses of 5 ms duration were used to stimulate ChR2-positive PV+ interneurons in the CA1 / subiculum area while recording post-synaptic responses in pairs of superficial and deep vH^{PFC} cells (Figure 4.8 b).

In contrast to the non-projection specific inhibitory bias onto deep layer cells mentioned above (Lee et al., 2014c), I did not observe a difference in light-evoked inhibitory post-synaptic current (IPSC) amplitudes amongst pairs of superficial and deep PFC-projecting cells. Inhibitory input from PV+ interneurons was equivalent onto both superficial and deep layer vH^{PFC} cells (Figure 4.8 e; Wilcoxon Paired: V = 57, p = 0.38, n = 17 pairs). This suggests that the common projection target may override radial axis inhibitory connectivity gradients in the case of the PFC projection population.

I next sought out to investigate whether recording exclusively non-PFC projecting cells would replicate previously published findings on projection non-specific biased inhibition onto deep layer cells. In order to address this question, I used the same setup described above (ChR2-expressing PV+ interneurons in vH and retrobead labelled vH^{PFC} cells). I recorded from cells in the superficial and deep layers that were not labelled with retrobeads, to avoid PFC-projectors, while optogenetically stimulating local PV+ interneurons with brief 5 ms pulses of blue light (Figure 4.9 b). In accordance with previously published findings, I saw that inhibition was biased towards deep layer (non-PFC projecting) neurons (Figure 4.9 c-e; Wilcoxon paired: V = 10, p = 0.042, n = 11 pairs), suggesting that differential targeting of cells in both layers by PV+ interneurons may be specific to non-PFC projecting populations.

Overall, with these experiments I have shown that within the PFC-projecting population, inhibitory input from local PV+ interneurons is equivalently spread across cells in the superficial and deep layers. However, this is not the case for non-PFC projecting neurons, where inhibitory input is greater onto cells in the deep layer. These findings highlight the complexity of hippocampal pyramidal cell heterogeneity and all the factors that are involved in determining the characteristics and circuit participation of a particular neuron. In this case, the common prefrontal target structure seems to override the existing gradient in inhibition dependent on

radial axis position to dictate equivalent local inhibitory connectivity between layers for PFC-projecting cells.

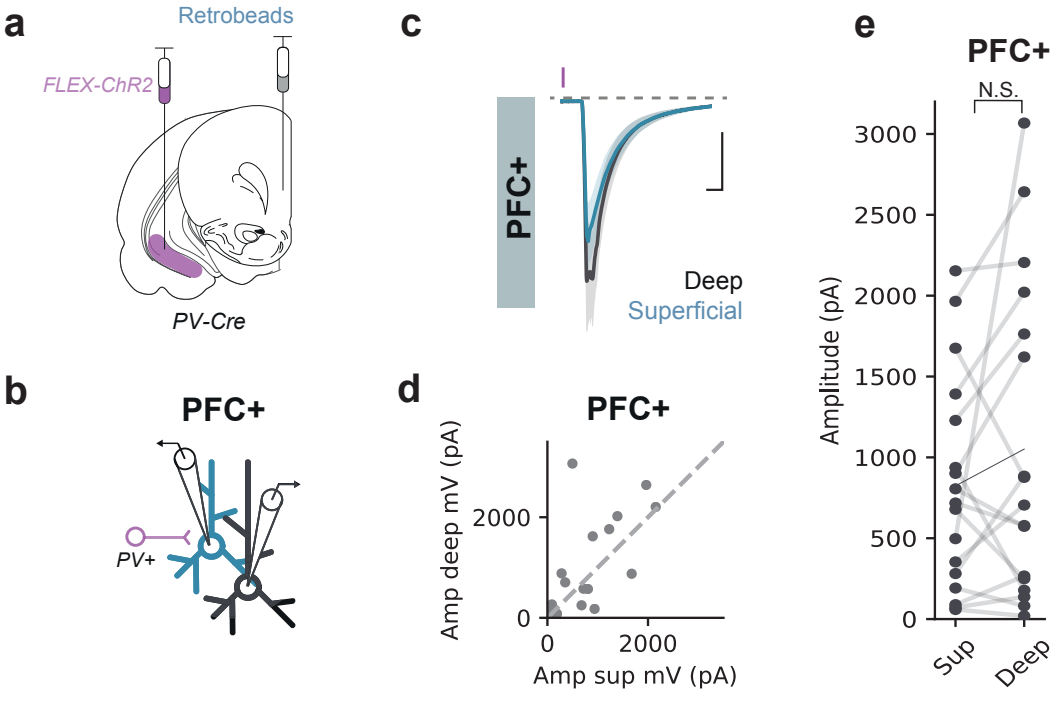

Figure 4.8: Interneuron input is equal onto superficial and deep vH^{PFC} cells
(a) Schematic showing injections carried out for experimental setup. Cre-dependent (FLEX) ChR2 was injected into vH and fluorescent retrobeads were injected into PFC. All experiments were carried out in PV-Cre mice. **(b)** Schematic of experimental protocol. PV+ ChR2-expressing interneurons (magenta) in vH slices were optogenetically stimulated while paired voltage-clamp recordings were carried out in deep (black) and superficial (blue) vH^{PFC} neurons. **(c)** Examples of light-evoked IPSCs in superficial and deep vH^{PFC} cells. Note that IPSCs are plotted as inward currents as recordings were carried out in high chloride internal. Purple tick represents light stimulus. Scale bars = 20 ms and 500 pA. **(d)** Summary of inhibitory connectivity. IPSC amplitudes in deep and superficial cells plotted against each other show a lack of layer-specific bias in inhibition. **(e)** Summary of IPSC amplitudes for all recorded pairs.

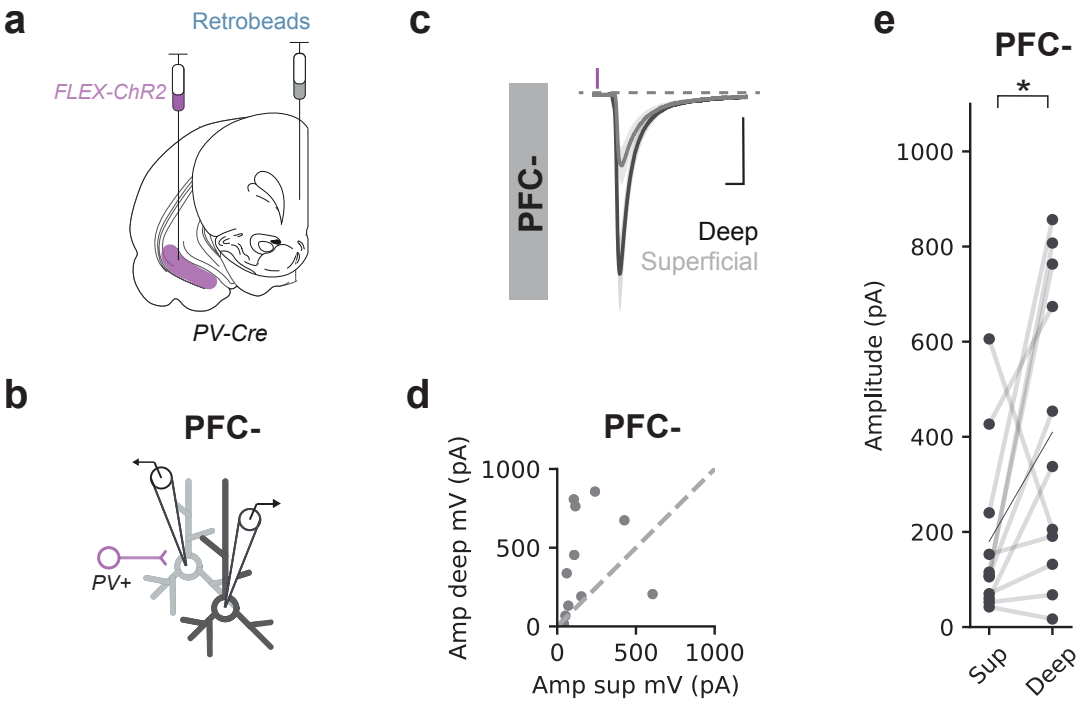

Figure 4.9: Interneuron input is biased onto deep non-projection specific cells
(a) Schematic showing injections carried out for experimental setup. Cre-dependent (FLEX) ChR2 was injected into vH while fluorescent retrobeads were injected into PFC. All experiments were carried out in PV-Cre mice. **(b)** Schematic of experimental protocol. PV-positive ChR2-expressing interneurons (magenta) in vH slices were optogenetically stimulated while paired voltage-clamp recordings were carried out in deep (black) and superficial (blue) non-vH^{PFC} neurons. **(c)** Examples of light-evoked IPSCs in superficial and deep non-vH^{PFC} cells. Scale bars = 20 ms and 200 pA. **(d)** Summary of inhibitory connectivity. IPSC amplitudes in deep and superficial cells plotted against each other showing a bias towards deep cell connectivity. **(e)** Summary of IPSC amplitudes for all recorded pairs.

Local inhibitory connectivity: superficial and deep vH^{PFC} cells provide equal input onto local interneurons

Having seen that both layers in the PFC projection receive equivalent amounts of inhibition from local PV+ interneurons, I wanted to know whether vH^{PFC} neurons in both layers provide input onto neighbouring interneurons to the same extent. I hypothesised that if the two layers act as a push-pull circuit, such that when one is active the activity in the other layer is dampened, they should contact interneurons to the same extent in order to engage in lateral inhibition. To address this question, it was necessary to stimulate cells in either layer separately whilst recording EPSC responses from neighbouring interneurons.

In order to isolate optogenetic stimulation to cell bodies in one layer at a time, I combined somatic ChR2 (SoCoChR2) with a focused beam of light. Retrograde Cre was injected into PFC, such that PFC-projectors in vH would express Cre. Cre-dependent somatic coChR2 and Dlx-mRuby (which fluorescently labels interneurons with mRuby via interneuron specific promoter Dlx-driven expression) were co-injected into vH. This resulted in SoCoChR2-positive PFC-projecting neurons and fluorescently labelled interneurons in vH (Figure 4.10 a, *top*). Firstly, I characterised the SoCoChR2 construct to ensure that it could be implemented to elicit action potentials (APs) in PFC-projecting cells. This would allow for the subsequent study of the post-synaptic effects on interneurons. Figure 4.10 a (*bottom*) shows an example of two SoCoChR2-positive vH^{PFC} neurons in vH, one of which is being recorded from for characterisation. I shone a focused beam of light for 5 ms straight onto SoCoChR2-positive cell somas as well as 50 and 100 μm directly superficial (towards stratum lacunosum moleculare) and deep (towards the pia) of the somas to test for spatial resolution (Figure 4.10 b).

I found that combining the focused light beam with soma-targeted So-

CoChR2 expression allowed for high spatial resolution, such that APs in SoCoChR2-positive vH^{PFC} cells were only elicited when the light beam was directed at the soma, but not beyond a 50 μm distance in either direction along the radial axis (Figure 4.10 c). Furthermore, SoCoChR2 cells fired APs when they were stimulated at the soma as opposed to controls (Wilcoxon paired: V = 28, p = 0.01, n = 7 cells). Controls were taken as the average of any activity occurring during the 100 ms prior to light stimulation in the same cell. This characterisation shows that SoCoChR2 can be used successfully to selectively activate single neurons in specific layers. Given that moving the light beam by a distance of 50 μm from the soma was sufficient to avoid eliciting an AP in SoCoChR2-positive cells and that cells in a superficial-deep recorded pair were generally 150 - 200 μm apart, this protocol proved suitable to address the influence of vH^{PFC} cells in both layers on local interneurons.

Having characterised the SoCoChR2 construct and tested its efficacy in our preparation, I went on to record from interneurons (visualised by Dlx mRuby labelling) while stimulating PFC-projecting cells in both layers as schematised in Figure 4.10 d. Below the schematic is an example current trace recorded in an interneuron while stimulating a deep vH^{PFC} with brief 5 ms pulses of blue light. Of the interneurons receiving input from pairs of PFC-projectors (i.e. connected vH^{PFC}-interneuron pairs), I did not observe a difference in response amplitude to stimulation of cells in the deep or superficial layers (Figure 4.10 e; Mann Whitney: U = 8, p = 0.42, n = 5 connected pairs). Furthermore, the percentage of connected superficial and deep vH^{PFC}-interneuron pairs was equivalent (Figure 4.10 f; Fisher's exact test: odds ratio = 0.95, p = 1.0, n = 19 (sup) and n = 18 (deep)). These findings suggest that, contrary to data from non-projection specific cells (Lee et al., 2014c), PFC-projecting cells in both layers equally contact local interneurons.

Overall, I observed that cells in the PFC-projection population both layers receive and provide equivalent input from and onto neighbouring interneurons, re-

gardless of their position along the radial axis. This was in contrast to cells along the radial axis that do not project to PFC, where cells in the deep layer received larger amounts of input from interneurons than those in the superficial layer. Together, these findings suggest that the two sub-populations of the PFC projection laterally inhibit each other, characteristic of a push-pull circuit.

The summarised circuit findings of this chapter are depicted in Figure 4.11. Here, I highlight the chapter's main findings towards the understanding of the ventral hippocampus to PFC circuitry. In summary, PFC-projecting cells in the superficial layer receive biased input from entorhinal cortex and Schaffer collaterals providing input from CA3 equally contact PFC-projecting neurons in the deep and superficial layers. Deep vH^{PFC} cells receive biased input from both subcortical areas anterior thalamus and diagonal brand of Broca. Within the ventral hippocampus, PFC-projecting cells in both layers receive and also provide equivalent input onto surrounding interneurons, potentially engaging in lateral inhibition such that e.g. superficial vH^{PFC} activity may dampen deep layer vH^{PFC} activity and vice versa. On a larger scale, activity in entorhinal cortex or in anterior thalamus may bias hippocampal output to PFC by silencing the least active layer in the PFC-projecting population.

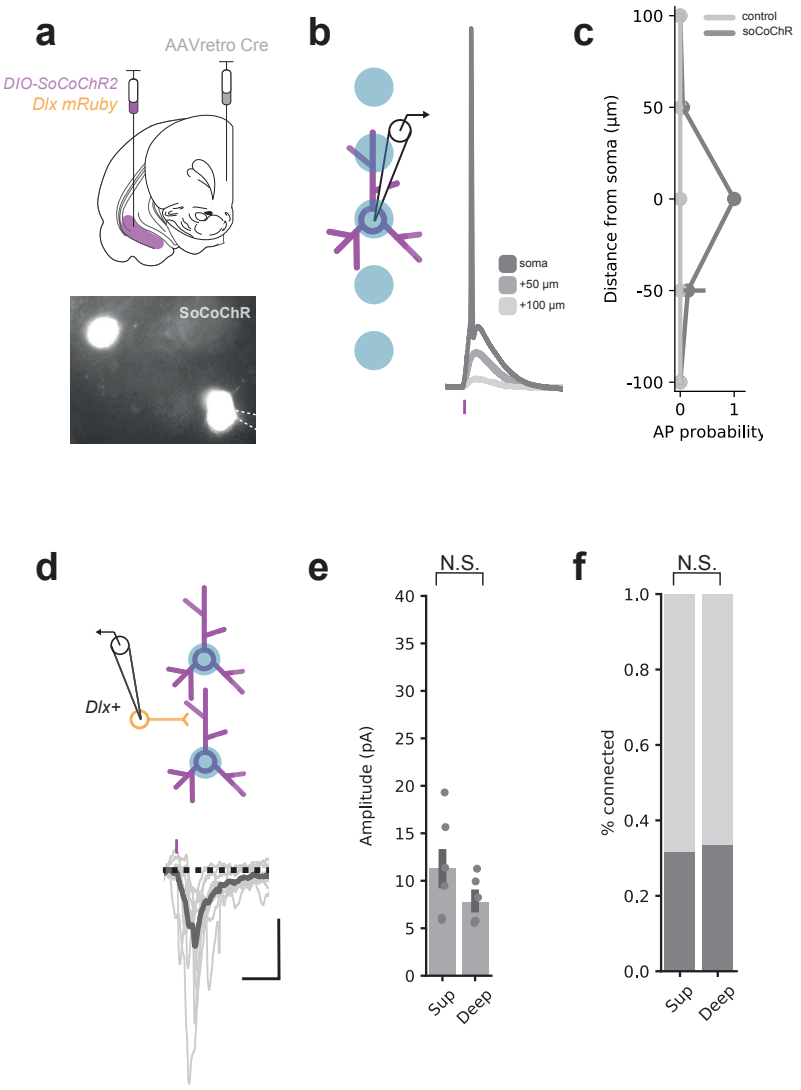

Figure 4.10: Superficial and deep vH^{PFC} cells provide equal input onto local interneurons **(a)** Strategy to investigate superficial and deep vH neuron connectivity onto local interneurons. Retrogradely transported Cre was injected into PFC and Cre-dependent somatic ChR2 (DIO-SoCoChR2) together with Dlx mRuby were injected into vH. Below, an example image of two SoCoChR2-positive cells in an acute vH slice. Note recording pipette on bottom cell for characterisation shown in (b). **(b)** Focused blue light allows activation of neurons expressing soCoChR2 with high spatial resolution. Scale bar = 10 mV, 20 ms. **(c)** Summary graph showing the probability of eliciting an AP in SoCoChR2-positive cells by shining brief 5 ms pulses of blue light at varying distances from the soma. Controls were taken as activity recorded during the 100 ms prior to stimulation in SoCoChR2-positive cells. **(d)** Schematic of experimental setup to investigate input from superficial and deep vH^{PFC} onto local interneurons (Dlx+). Below, raw and average traces of EPSCs in an interneuron in response to optogenetic stimulation of a deep vH^{PFC} cell. Scale bars = 20 ms and 10 pA. **(e)** Amplitude of EPSCs recorded from Dlx+ interneurons in response to superficial and deep layer vH^{PFC} cell stimulation. Note there is no difference in response amplitudes. **(f)** Probability of connectivity is not different across layers.

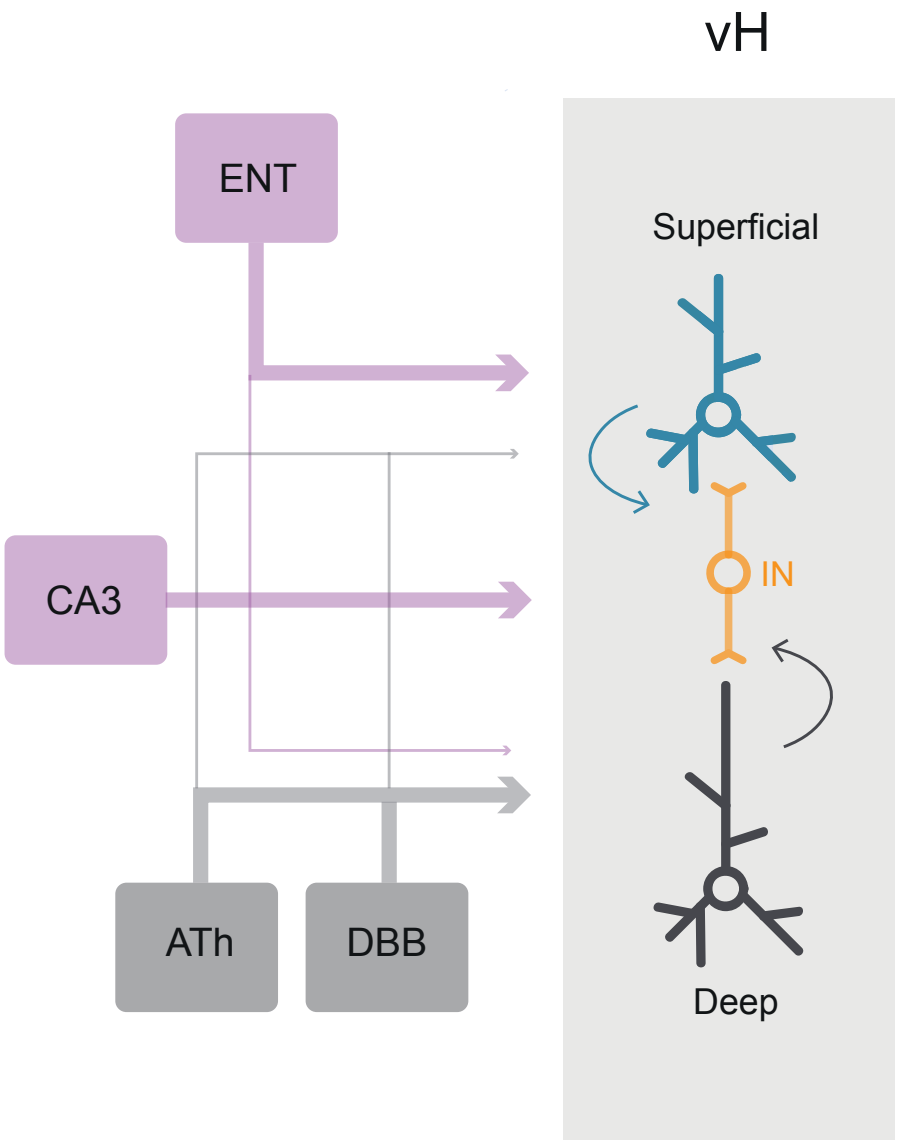

Figure 4.11: Summary schematic of circuit
In this summary schematic, the main circuit findings from Chapter 4 are highlighted. In pink (top left), intra-hippocampal inputs to superficial and deep layer PFC-projecting cells. While medial entorhinal cortex (ENT) inputs are biased towards superficial cells, CA3 inputs equally target both layers. In grey (bottom left), long-range inputs to hippocampal PFC-projecting cells from the anterior thalamus (ATh) and the diagonal band of Broca (DBB) bias towards cells in the deep layer. The thickness of the lines represents connection strength. Within the ventral hippocampus, superficial and deep vH^{PFC} cells equally target interneurons (IN), and are both inhibited equivalently by local interneurons.

4.3 Discussion

In this Chapter I have described the approach for an unbiased mapping of afferent regions providing input to the ventral hippocampal PFC-projecting population. Using TRIO I identified four main regions contacting vH^{PFC} cells and followed up on these anatomical findings to test them functionally by implementing CRACM. I optogenetically stimulated incoming axons from CA3, entorhinal cortex, anterior thalamus (ATh) and the diagonal band of Broca (DBB) while recording from vH^{PFC} projection neurons in the deep and superficial layers. The recordings showed that while CA3 provided equivalent input onto cells in the superficial and deep layers of the projection, entorhinal cortex input was biased towards superficial cells. Furthermore, input from subcortical areas ATh and DBB trended towards having biased input onto neurons in the deep vH^{PFC} layer.

A striking feature of the CRACM data was the split in the targeting bias between cortical and subcortical afferent areas, pointing at a possible top-down and bottom-up control of superficial and deep layer vH^{PFC} cells, respectively (Rajasethupathy et al., 2015; Anderson et al., 2016; Szőnyi et al., 2019). This suggests that the information being processed by superficial and deep layer vH^{PFC} cells may be fundamentally different. This data is consistent with previous studies, where superficial layer hippocampal cells receive more cortically processed multimodal sensory information from entorhinal cortex (Valero and de la Prida, 2018; Li et al., 2017) and deep cells are recipients of sub-cortical sensory and motor information (Müller and Remy, 2018). In contrast to these biased afferent inputs, hippocampal input from CA3 was equivalent onto vH^{PFC} cells in both layers (Figure 4.4).

In addition to the direct entorhinal cortex to CA1 / subiculum temporoammonic pathway, entorhinal input can also reach CA1 and subiculum pyramidal cells via the indirect perforant path involving DG and CA3. Together with our observations, this suggests that in contrast to raw, entorhinal information arriving pref-

erentially into PFC-projecting cells in the superficial layer (Figure 4.5), entorhinal input processed by DG and CA3 arrives equally onto superficial and deep layer cells (Figure 4.4). Thus, the comparator function often associated with the hippocampus (Vinogradova, 2001; Kumaran and Maguire, 2007) may be mainly occurring in the superficial layer, which receives both the direct and the hippocampally processed entorhinal information.

Hippocampally processed information from CA3 and CA2 has been previously shown to differentially target deep and superficial pyramidal cells in the CA1 / subiculum area (Ishizuka et al., 1990; Deguchi et al., 2011; Kohara et al., 2014; Soltesz and Losonczy, 2018; Valero and de la Prida, 2018; Fernández-Ruiz et al., 2017). In contrast to these findings in non-projection specific neurons and as discussed above, we saw that the two layers of PFC-projecting cells were equally innervated by CA3. (Figure 4.4). These data suggest that in this case, the equivalent input onto superficial and deep layer vH cells may be dictated by the common projection target, PFC, rather than by their anatomical position along the radial axis. Thus, unlike preferential CA3 targeting of superficial layer non-projection specific cells in this area (Soltesz and Losonczy, 2018), our findings suggest that specifically PFC-projecting deep layer cells may carry out an important function that requires CA3 input. However, we could not differentiate between proximal and distal CA3 stimulation in our experiments, and doing so in future investigations may bring out more detail in the circuitry. Although CA2 inputs have been shown to preferentially target both excitatory and inhibitory deep layer CA1 cells (Kohara et al., 2014; Nasrallah et al., 2019), we did not pursue this line of enquiry due to difficulty in targeting CA2 cells without specific mouse lines and viral strategies, unavailable to us.

Interestingly, it has been shown that the preferential targeting of deep layer interneurons by CA2 axons that in turn inhibit deep layer pyramidal cells normalises the increased excitatory drive onto the deep layer pyramidal cells to match CA2 in-

put onto the superficial layer, when inhibition is active (Nasrallah et al., 2019). It would be interesting to follow up on the CA2 - CA1 projection specifically onto PFC-projectors in the future, to elucidate whether the common projection target of cells in both layers would modulate these connectivity biases. As with CA3 input, it may be the case that existing or previously observed gradients of input and output may map differently onto specific projection populations in vH. Studying the connectivity of the layers within the PFC-projection population independently and comparing this data to non-projection specific hippocampal neurons has aided in understanding the distinct properties of the vH-PFC projection. Furthermore, it has highlighted the importance of taking the vast heterogeneity of hippocampal pyramidal neurons into account and suggests that projection target and defined connectivity gradients may covary in multiple and unique ways.

Studies in dorsal hippocampus have shown gradients of lateral (LEC) and medial (MEC) entorhinal cortical input onto cells along the proximo-distal and superficial-deep axes of the hippocampus, where LEC preferentially targets superficial cells more distally and MEC targets deep cells proximally (Hargreaves et al., 2005; Masurkar et al., 2017; Li et al., 2017). However, from our TRIO data, we traced substantial inputs onto vH^{PFC} cells predominantly back to medial entorhinal cortex (MEC) (Figure 4.1) and thus focused our functional investigations on input from MEC. Our finding that MEC preferentially targets superficial layer cells within the PFC-projection (Figure 4.5) stands in contrast to non-projection specific preferential targeting of deep layer cells (albeit only in very proximal CA1) (Masurkar et al., 2017). This discrepancy may be due to differences in dorsal and ventral hippocampal circuitry or due to the positioning of PFC-projecting cells, which are located in more distal CA1 / proximal subiculum. Although no specific differences of topographical targeting of CA1 and subiculum by medial and lateral entorhinal axons have been observed along the dorsoventral hippocampal axis (Bienkowski et al., 2018), we cannot exclude that this may depend on projection target.

From our CRACM data, we also found that input from the basal forebrain structure of the diagonal band of Broca (DBB; which is often referred to interchangeably in conjunction with medial septum as one structure MSDB; Müller and Remy (2018); Leão et al. (2015)) is biased towards the deep cell layer (Figure 4.7). Septal / diagonal band input is classically involved in attention and learning and can control the excitability of hippocampal neurons (Fuhrmann et al., 2015; Müller and Remy, 2018). Specifically, input onto ventral hippocampal pyramidal cells has been implicated in fear learning and extinction (Lovett-Barron et al., 2014; Knox and Keller, 2016; Staib et al., 2018). The medial septum and diagonal band of Broca provide glutamatergic, cholinergic and GABAergic input onto hippocampal pyramidal cells and these distinct transmitters mediate different effects and target different groups of cells (Huh et al., 2010; Müller and Remy, 2018). The synergistic action of these neurotransmitters has also been shown to regulate plasticity in CA1 (Park and Spruston, 2012). However, it remains unclear whether the observed connectivity bias is led by a specific neurotransmitter and future work to understand the relative targeting of each of these neurotransmitter systems on PFC-projecting cells in both layers may reveal differences.

Strikingly, consistent with afferent inputs driving the differential activity of each layer, MSDB input has been shown to preferentially target interneurons in deep hippocampal layers that subsequently inhibit the apical dendritic tuft of pyramidal cells, where prominent entorhinal inputs arrive (Lovett-Barron et al., 2014). Via this MSDB-triggered feedforward inhibition of distal apical dendrites, entorhinal cortex input to CA1 is inhibited, reducing sensory interference and facilitating fear learning. This circuit mechanism may be implemented as an aid in the switch from activity in the superficial to the deep layer of the PFC projection and suggests that MSDB input onto deep layer cells and entorhinal input onto superficial cells may be mutually exclusive. However, this inhibitory influence is mediated by cholinergic activity and our circuit mapping experiments were not carried out in the presence of any pharmacological agents to isolate cholinergic, GABAergic or glutamatergic

transmission. It would be of interest to test the nature of MSDB input onto deep pyramidal cells by recording in cholinergic receptor blockers to ascertain whether the same input that drives deep vH^{PFC} activity concomitantly dampens entorhinal cortex input onto superficial layer vH^{PFC} cells.

TRIO labelling also identified input located in the anterior thalamus (Figure 4.1). This region includes nuclei such as the anteroventral nucleus and the PVT (Tsanov and O'Mara, 2015; Hsu and Price, 2009). In line with previous findings showing that anterior thalamic nuclei sparsely innervate the subicular area, connectivity was weak overall (Figure 4.6; Shibata (1993)). However, connectivity trended towards a bias onto PFC-projecting cells in the deep layer (Figure 4.6). The diverse nuclei in the anterior thalamus are together thought to be involved in the modulation of alertness, learning and memory processes and its interaction with the hippocampus is thought to be crucial for these processes (Child and Benarroch, 2013; Jankowski et al., 2013; Tsanov and O'Mara, 2015). Interestingly, the observation that PFC-projecting cells in the superficial layer receive minimal anterior thalamic input is consistent with the idea of cells in this layer hosting more stable representations while those held in deep layer cells are more flexible (Danielson et al., 2016). Contrary to the notion that the nucleus reuniens of the thalamus acts as a node between ventral hippocampus and PFC and may form a closed loop between these structures (Varela et al., 2014; Vertes, 2015), we did not find cells in nucleus reuniens with the TRIO analysis. Interestingly, consistent with these findings, it has been recently shown that nucleus reuniens terminals preferentially target hippocampal cells with subcortical projection targets and specifically avoid vH^{PFC} cells (Wee and MacAskill, 2020).

Interestingly, both DBB and ATh inputs contain theta-modulated cells and are thought to aid in theta oscillation generation in the hippocampus (Müller and Remy, 2018; Child and Benarroch, 2013; Buzsáki, 2002). In CA1, deep layer pyramidal cells (non-projection specific) have been shown to be theta modulated

(Mizuseki et al., 2011; Fernández-Ruiz et al., 2017). The hippocampus in turn synchronises at theta with the prefrontal cortex and this synchronisation (which is supported by excitatory input onto PFC) has been shown to correlate with anxiety-like avoidance behaviour (Adhikari et al., 2010; Padilla-Coreano et al., 2019). In addition, ventral CA1 deep layer cells have recently been shown to promote avoidance behaviour (Pi et al., 2020). Together with preferential DBB and ATh input onto deep layer PFC-projecting cells and previous observations of theta-modulated cells in deep hippocampal layers, these findings suggest that deep vH^{PFC} cells may also be theta modulated and thus, involved in avoidance behaviour. Overall, these concepts add further support to the notion that vH^{PFC} cells in the deep and superficial layers may be involved in different aspects of behaviour and more specifically, that deep layer vH^{PFC} cells may support avoidance behaviour.

In addition to drawing the conclusions that the investigated afferent inputs are biased to preferentially targeting superficial or deep vH^{PFC} cells, it cannot be excluded that alternative mechanisms may be involved. For instance, differences in postsynaptic responses in superficial and deep PFC-projecting cells following entorhinal cortex axon stimulation may also result from higher recurrent excitatory connectivity amongst superficial layer cells. A higher recurrent connectivity amongst e.g. superficial layer cells would lead to a greater, amplified post-synaptic potential relative to that in deep layer cells in response to equivalent targeting of both cell layers. Although no notable difference in recurrent connectivity has been found in the subiculum between e.g. bursting and non-bursting pyramidal cells (Böhm et al., 2015), differences may emerge in a laminar fashion, between superficial and deep vH^{PFC} cells.

Having presented the conclusions drawn from the CRACM data studying afferent inputs from cortical and subcortical areas onto vH^{PFC} cells, an experimental caveat must be discussed. For all CRACM experiments, recorded vH pyramidal cells were held at the putative reversal potential for chloride (-70 mV), with the aim

to isolate excitatory potentials in response to afferent stimulation. This was done as ChR2 expression in afferent axons was expressed under the control of the pan-neuronal synapsin (hSyn) promoter, which includes both excitatory and inhibitory long range inputs. However, the exact reversal potential for chloride was not calculated for each individual cell. Experiments were carried out under the assumption that intra- and extracellular recording solution ion concentrations were identical across recordings. Thus, by holding recorded cells at -70 mV, it is probable that for some cells, both excitatory and inhibitory light-evoked potentials were included in the recordings. As an example, in the sample response traces following entorhinal cortex axon stimulation shown in Figure 4.5 b, response kinetics for the deep vH^{PFC} cell (black trace) are slower than for the superficial vH^{PFC} cell (blue trace), suggesting that inhibitory input may be dampening the excitatory response and thus, that excitatory responses were not adequately isolated by holding the cell at -70 mV. Furthermore, different proportions of open channels at -70 mV in different cells would affect input resistance and consequently response kinetics as well, with an increased number of open channels increasing membrane conductance and thus leading to a decrease in input resistance. A decrease in input resistance would in turn dampen post-synaptic potential amplitudes, requiring a larger current influx to depolarise the cellular membrane. Pharmacological blockade of inhibitory inputs with gabazine (a GABA A receptor antagonist) could be used in future experiments to more robustly isolate excitatory post-synaptic potentials, circumventing this limitation of the current CRACM setup. Nevertheless, the current set-up in current-clamp mode with current injected into cells to keep them at a membrane potential roughly around -70 mV allows for a bigger picture of what the overall effect of stimulating incoming axons from a given brain area is. Contrary to excitatory post-synaptic current (EPSC) recordings in voltage-clamp mode (holding at - 70 mV and 0 mV to record excitation and inhibition, respectively), the set-up shown here may provide a more realistic read-out of the effects of e.g. thalamic or entorhinal inputs on vH^{PFC} cell activity.

Furthermore, it must be noted that differences in time response window to calculate EPSP response amplitudes resulted in variable statistical interpretations of the CRACM data (Figure 4.6 and 4.7). ChR2-elicited vesicle release is not dependent on the firing of an action potential pre-synaptically and so, vesicle release may be more graded than it would be in response to an all-or-nothing event, introducing jitter and variable lag into the vesicle release process and subsequently producing variable post-synaptic responses. For instance, during CRACM experiments, it has been shown that higher stimulating light intensity results in larger response amplitudes and also shorter response onsets (Petreanu et al., 2009). Additionally, a different amount of synapses from e.g. ATh axons onto cells in the different subicular layers of the PFC projection may have influenced both the response amplitude and onset time. So a slow onset of response must not necessarily mean that the response is di-synaptic, but may instead be a consequence of the number of synapses and the light intensity. A third reason for a difference in response kinetics between cells in the two layers may be the cellular location of the stimulated synapses. For smaller superficial layer cells, inputs may occur closer to the soma than for larger deep layer cells, such that the peak of the post-synaptic response would be dampened and slowed in time more for deep layer cells due to passive cable properties of the longer main apical dendrite (Figure 3.7 d). In the future, conducting these CRACM experiments in voltage-clamp mode in the presence of TTX (tetrodotoxin, a Na^+ channel blocker) and 4-AP (4-aminopyridine, a K^+ channel blocker) in the recording solution would block action potentials in the slice, ensuring that any post-synaptic current responses are exclusively light-evoked.

Following these CRACM investigations informed by TRIO labelling experiments, I next focused on investigating how superficial and deep PFC-projecting cells interact with local circuitry. Local excitatory connectivity within ventral hippocampal regions is very low, highlighted by the low degree of collateral axonal terminals (Böhm et al., 2015; Naber and Witter, 1998; Kim and Spruston, 2012; Lee et al., 2020), so I decided to focus on inhibitory local connections. Previous studies

have shown dramatic differences in the targeting of deep and superficial layer non-projection specific cells by PV+ interneurons (Lee et al., 2014c). The reported increased inhibition onto deep layer cells is at least in part supported by greater drive of local PV+ interneurons by cells in the superficial layers. To test whether such biased laminar inhibitory connectivity existed within the PFC projection, I compared inhibitory connections in PFC-projecting and in non PFC-projecting cells of the deep and superficial layers (Figure 4.8 and 4.9). Contrary to increased inhibition onto deep layer non-PFC projecting pyramidal cells (Figure 4.9; Lee et al. (2014c)), superficial and deep vH^{PFC} neurons provided equivalent input onto local interneurons and were equally targeted by neighbouring PV+ interneurons (Figure 4.8 and 4.10). Together, these experiments suggest that the bidirectional targeting of cells in both layers with local interneurons may support their engagement in lateral inhibition. Thus, the effects of biased afferent inputs onto the two layers reported in this chapter may be exacerbated in both directions by lateral inhibition of the less active cell layer - in turn limiting the output onto PFC to one layer at a time.

Interestingly, although non-projection specific superficial layer cells have been shown to contact PV+ interneurons to a larger extent than deep layer cells, deep layer cells projecting to PFC specifically have been shown to connect very strongly onto PV+ interneurons in comparison to deep layer cells with subcortical projection targets (Lee et al., 2014c). However, deep PFC-projecting cells receive much weaker PV+ input in return than other projection populations in deep CA1 layers (Lee et al., 2014c). Thus, this PFC-projection population specific deep layer enhancement in interneuron drive may lead to a match in superficial and deep PFC-projecting drive onto local interneurons and explain the finding that PFC projectors in both layers to engage equivalently with local interneurons (Figure 4.10). As with equivalent CA3 input onto cells in both layers, the common prefrontal projection target of cells in both the superficial and deep layers may in this instance override the previously seen radial differences in inhibitory circuit engagement (Lee et al., 2014c). Examples of interneurons preferentially targeting projection-specific pyra-

midal cells have been observed across the brain (McGarry and Carter, 2016; Courtin et al., 2014; Gittis et al., 2010; Varga et al., 2010; Lu et al., 2017; Marek et al., 2018a; Lee et al., 2014a,c), suggesting that GABAergic microcircuits differentially participate in distinct information processing streams dependent on pyramidal cell projection target.

In fact, there is increasing evidence that cell populations identified by their different downstream projection targets receive different streams of information and form unique local circuits with both neighbouring pyramidal cells and interneurons (Kampa et al., 2006; Anderson et al., 2010; Krook-Magnuson et al., 2012; Morishima and Kawaguchi, 2006; Anastasiades et al., 2018a,b). Interestingly, projection target specificity does not always determine the wiring of cells in certain cortical layers by itself but rather in combination with their anatomical positioning (Anderson et al., 2010; Wee and MacAskill, 2020). Thus, it is possible that different types of interneurons in different brain areas may follow specific rules, targeting pyramidal cells based on projection target in some instances and following gradients of connectivity regardless of projection target identity in others. Consistent with this idea, our data suggests that connectivity of vH^{PFC} projecting neurons is defined by both projection population identity and spatial location. PFC-projecting cells across the two layers follow previously established gradients in e.g. subcortical input (Figures 4.6 and 4.7) but differ from the norm with regards to CA3 afferent input (Figure 4.4) and inhibitory connectivity (Figures 4.8, 4.9 and 4.10).

Overall, the data presented in this chapter provides insight into the highly specific connectivity that cells in the superficial and deep layer of the PFC-projection population are embedded in. I hypothesise that the distinct circuit blueprints of the superficial and deep vH^{PFC} layers underlie parallel pathways of hippocampal input onto PFC which may have divergent effects on PFC circuitry and ultimately, on behaviour.

Chapter 5

Hippocampal input to PFC forms a long-range push-pull circuit

5.1 Introduction

Multiple studies have demonstrated strong afferent input into PFC from vH. More specifically, it has been shown that this input targets the infralimbic (IL), prelimbic (PL) and medial orbital regions of PFC (Thierry et al., 2000; Padilla-Coreano et al., 2016; Liu and Carter, 2018). In Chapter 3 I described two distinct populations of PFC-projecting neurons in vH, situated in the superficial and deep layers of the CA1 / subiculum area. However, it is unknown whether these two layers of PFC-projecting cells in vH send axons to the same prefrontal areas in a uniform manner or whether there is a distinction in their anatomical targets, which could provide the substrate for differential function. For example, vH input onto infralimbic PFC has been shown to mediate relapse of extinguished fear, while prelimbic PFC plays a role in fear extinction (Marek et al., 2018a,b). During the learning of fear and extinction, infralimbic and prelimbic PFC show opposing contributions to behaviour, where the former is required to form new associations while the latter

provides previously formed associations (Mukherjee and Caroni, 2018). Thus, differential targeting of e.g. IL and PL PFC may underlie functional differences of the two layers in the projection.

In addition to potential anatomical specificity of the two layers in the projection forming output pathways to distinct PFC domains, activity in the two populations of vH^{PFC} cells may have different effects on PFC circuitry. Interestingly, the ventral hippocampus is able to both activate and inhibit PFC circuitry dependent on task demands (Jadhav et al., 2016; Adhikari et al., 2011; Tang et al., 2017). For example, during sharp wave ripples (SWRs), hippocampal input excites PFC neurons involved in representing the current spatial representation held in the hippocampus, while PFC cells supporting unrelated representations to the task at hand are inhibited (Jadhav et al., 2016). In addition, hippocampal modulation of PFC SWRs changes during awake (where PFC neurons are both excited and inhibited) and sleep states (where PFC neurons are predominantly excited), reflective of different phases of memory encoding (Tang et al., 2017).

Excitatory vH input onto PFC has also been recorded during representation of anxiogenic environments and anxiety-like behaviour and is crucial for the decision to explore potentially threatening locations (Adhikari et al., 2010, 2011; Padilla-Coreano et al., 2019; Lee et al., 2019a; Parfitt et al., 2017). Exploration of open (potentially threatening) and closed (safe) arms of the elevated plus maze (EPM) is widely used to measure rodent exploratory and anxiety-like avoidance behaviour. Activation of PFC circuitry drives avoidance of the open arms, while inactivation has an anxiolytic effect and promotes open arm exploration (Adhikari et al., 2010; Padilla-Coreano et al., 2016; Parfitt et al., 2017). Furthermore, ventral hippocampal input facilitates PFC representations of anxiety-related information, which can be interrupted by blocking the recruitment of disinhibitory prefrontal circuitry (Adhikari et al., 2011; Lee et al., 2019a). Although many advances have been made in understanding vH-PFC circuitry and the role of this pathway in behaviour,

it remains unclear what synaptic and circuit mechanisms may underlie its dual excitatory and inhibitory role (Jadhav et al., 2016; Adhikari et al., 2011; Tierney et al., 2004; Marek et al., 2018a). In this chapter, I hypothesise that this role may be fulfilled by cells in the different layers of vH engaging with different components of circuitry in PFC. This differential connectivity would allow each subcircuit (layer) to be recruited at different points during behaviour.

In line with this hypothesis, the breadth of hippocampal influence over PFC is thought to arise through flexible recruitment of both excitatory and local inhibitory circuitry (Lee et al., 2019a; Spellman et al., 2015; Kjaerby et al., 2016; Marek et al., 2018a; Phillips et al., 2019; Shin and Jadhav, 2016). Activating excitatory neurons in PFC results in increased anxiety-like and avoidance behaviour (Padilla-Coreano et al., 2019; Berg et al., 2019) while activating inhibitory interneurons depends on the interneuron subtype involved (Marek et al., 2018a; Sun et al., 2020; Abbas et al., 2018; Lee et al., 2019a). The two main types of interneurons found in cortex are fast-spiking (PV-positive) and non fast-spiking (SOM and VIP-positive) (Rudy et al., 2011; Tremblay et al., 2016).

For example, recruitment of VIP-expressing interneurons is implicated in mediating avoidance behaviour (Lee et al., 2019a) while vH input onto PV-positive interneurons supports social behaviour and fear relapse (Marek et al., 2018a; Sun et al., 2020), and input onto SOM-positive interneurons is involved in working memory and spatial encoding (Abbas et al., 2018). Ventral hippocampal input onto excitatory pyramidal cells in PFC also shows connectivity patterns, preferentially targeting specific neuronal populations dependent on projection target, cortical layer and prefrontal area. For example, vH terminals have been shown to preferentially target cortico-cortical projection neurons in cortical layer 5, but equally target amygdala-projecting neurons in layers 2 and 3 (Liu and Carter, 2018). Here, I hypothesised that cells in the superficial and deep vH layers might connect differentially with excitatory and inhibitory cells in PFC and thus, the dichotomy of

inhibitory and excitatory function of the vH-PFC projection may be split across the two layers of the projection.

Overall, I have two hypotheses for the potential role of the two vH-PFC subpopulations within the circuit. First, axon terminals could target different anatomical locations within the same structure (PFC) (Cheriyan et al., 2016; Vertes, 2015; Li et al., 2017; Yun et al., 2018; Wang et al., 2016), or second, they could target different cell types with opposing roles within the same anatomical locations (MacAskill et al., 2012; Lee et al., 2014a; Yang et al., 2018a; McGarry and Carter, 2017). If either of these hypotheses hold true, the two layers of vH may exert unique effects on PFC circuitry, and differentially influence behaviour. Investigating the specific targeting of PFC areas and cell types by cells in the superficial and deep vH layers is key to understanding their unique influence on the PFC circuit. However, how these hypotheses may map onto superficial and deep vH^{PFC} cells is currently unknown and will be investigated throughout this chapter.

In this chapter, I first investigated ventral hippocampal input onto different cell types in PFC. Using a combination of circuit tracing and electrophysiological techniques, I explored the distribution of vH terminals in PFC originating from either superficial or deep layers and their synaptic contacts within PFC. I found that the two populations seemed to exert a distinct influence on PFC via differential recruitment of excitatory and inhibitory neurons such that one layer was biased towards excitation of PFC circuitry and the other towards inhibition. Thus, I hypothesised that the two layers may have different roles in controlling PFC activity during behaviour. To investigate this potential dichotomy of function, I used *in vivo* optogenetics to begin to explore their unique contributions to exploratory behaviour, using a well characterised test of approach-avoidance conflict and anxiety-like behaviour - the elevated plus maze.

5.2 Results

Tracing hippocampal axon terminals in PFC

In order to understand the effects of ventral hippocampal input onto PFC, it was necessary to firstly study the anatomical distribution of superficial and deep layer hippocampal terminals within PFC. To trace the hippocampal axons contacting PFC, I used the anterograde tracer smFP ('spaghetti monster' fluorescent protein). The strategy to bias labeling towards superficial and deep layer vH axons was as follows: for superficial layer (*Calbindin1*-positive) axons, the *Calbindin1*-Cre mouse line was used in combination with Cre-dependent smFP injections in vH. For deep layer (*Calbindin1*-negative) axons, *CaMKii*-Cre was injected into the vH of WT or non-transgenic *Calbindin1-Cre* littermates in combination with Cre-dependent smFP (strategy named CaMKii smFP for clarity in Figure 5.2). I first set out to determine whether this tactic would successfully separate the superficial (*Calbindin1* enriched) and deep (biased towards by using *CaMKii*-dependent constructs) PFC-projecting layers in vH.

In short, Cre-dependent smFP plus or minus *CaMKii*-Cre were injected into the vH of *Calbindin1*-Cre (or Cre-negative littermate) mice and 2 weeks were allowed for expression (see Figure 5.1). Following the 2 week period, transverse hippocampal slices were stained for the Flag tag expressed by the smFP construct and a secondary antibody conjugated to fluorescent Alexa 555 dye was used to capture smFP labelling. The slices were then imaged with a fluorescence microscope to visualise vH cell bodies expressing Cre- or *CaMKii*-dependent smFP (thus labelled with the Alexa 555 signal). As shown from example sections in Figure 5.1 b and the summary fluorescence plot profile in Figure 5.1 c (n = 4 injections), in mice injected with Cre-dependent smFP, fluorescent cell bodies were mainly located in the superficial layer. Conversely, *CaMKii*-smFP positive cells were found

preferentially in the deep layer. Overall, these results suggest that this combination of Cre-dependent construct and the *CaMKii*-dependent strategy (co-injecting *CaMKii*-Cre) can be used successfully to target superficial and deep vH^{PFC} cells respectively for anterograde tracing of their axons and subsequent visualisation in PFC. It is important to note that the expression of smFP in the *CaMKii*-dependent strategy will label all vH pyramidal cells including superficial layer cells, not only deep layer cells. However, this strategy biases towards deep layer cells (Figure 5.1) due to their larger proportion overall.

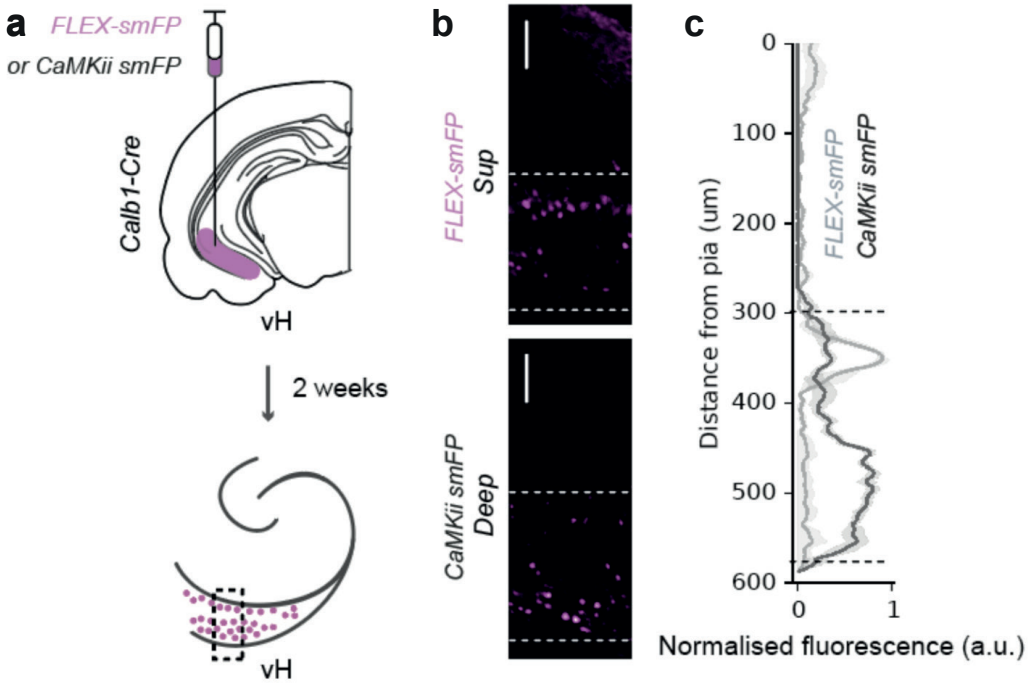

Figure 5.1: Labelling superficial and deep vH^{PFC} cells to visualise axons in PFC
(a) Strategy to express anterograde Cre or *CaMKii*-dependent tracer (smFP) in each layer of vH in *Calb1*-Cre mice. **(b)** Distribution of labelled cells in the two conditions. Note preferential expression of FLEX-smFP in superficial (top) and *CaMKii*-smFP in deep (bottom) layers. Scale bar = 100 μm. **(c)** Summary fluorescence profile of n = 4 injections. Note peak in the superficial layer for FLEX-smFP and a peak in the deep layer for *CaMKii*-smFP.

Having characterised the labelling strategy, coronal sections of PFC were imaged from mice injected with Cre- or *CaMKii*-dependent smFP, as described above, to visualise axonal terminals originating from either of the two vH layers. In Figure 5.2 b, two example PFC slices are shown containing axons originating from the deep (*CaMKii*-smFP) and superficial (FLEX-smFP) vH layers. Qualitatively, the distribution of Cre-dependent and *CaMKii*-dependent smFP expression was very similar. I asked whether the overall distribution of axons within different parts of PFC would differ across experimental conditions. Of the total fluorescence captured in PFC, I calculated the proportion of it within the infralimbic (IL), prelimbic (PL) and medial orbitofrontal (ORBm) areas of PFC (Figure 5.2 c) for *Calbindin1* and *CaMKii*-positive axons. The fluorescence (normalised to total fluorescence in a given PFC slice) within the three areas did not differ between the deep (*CaMKii*-smFP) and superficial (FLEX-smFP) axon labelling conditions (Mann Whitney U; IL: U = 10, $p = 0.69$; PL: U = 4, $p = 0.34$; ORBm: U = 8, $p = 1$) and was found predominantly in IL PFC, followed by PL and ORBm.

Following from the observation that both *Calbindin1* and *CaMKii*-positive axons equally target IL, PL and ORBm, I asked whether there was a distinct distribution of axonal terminals along the different brain axes within PFC. The fluorescence for each condition was quantified along the anteroposterior (AP), mediolateral (ML) and dorsoventral axes (DV) to identify any potential differences in the coverage of axons originating from the superficial or deep vH layers. The fluorescence at increasing distance from bregma, the midline or the pia (for the AP, ML and DV axes, respectively) was normalised to the total fluorescence along the given axis. As with quantification within IL, PL and ORBm, I did not find a difference in distribution of *Calbindin1* and *CaMKii*-positive axons along the three brain axes (Figure 5.2 d - f).

Overall, these data suggest that ventral hippocampal projection neurons in both layers send axons to the same prefrontal areas, with a higher proportion of ter-

minals within IL PFC and cover virtually equal locations with no difference in their occupancy or patterning along the three studied brain axes. These results support early tracing studies that found equal density of vH axonal distribution across cortical layers and areas (Jay and Witter, 1991) as well as more recent findings that show a higher proportion of vH terminals in IL PFC (Liu and Carter, 2018). Importantly however, no differences were apparent between labelling conditions, suggesting that deep and superficial vH layers may not exploit differential innervation of PFC areas as a mechanism for distinct functional output.

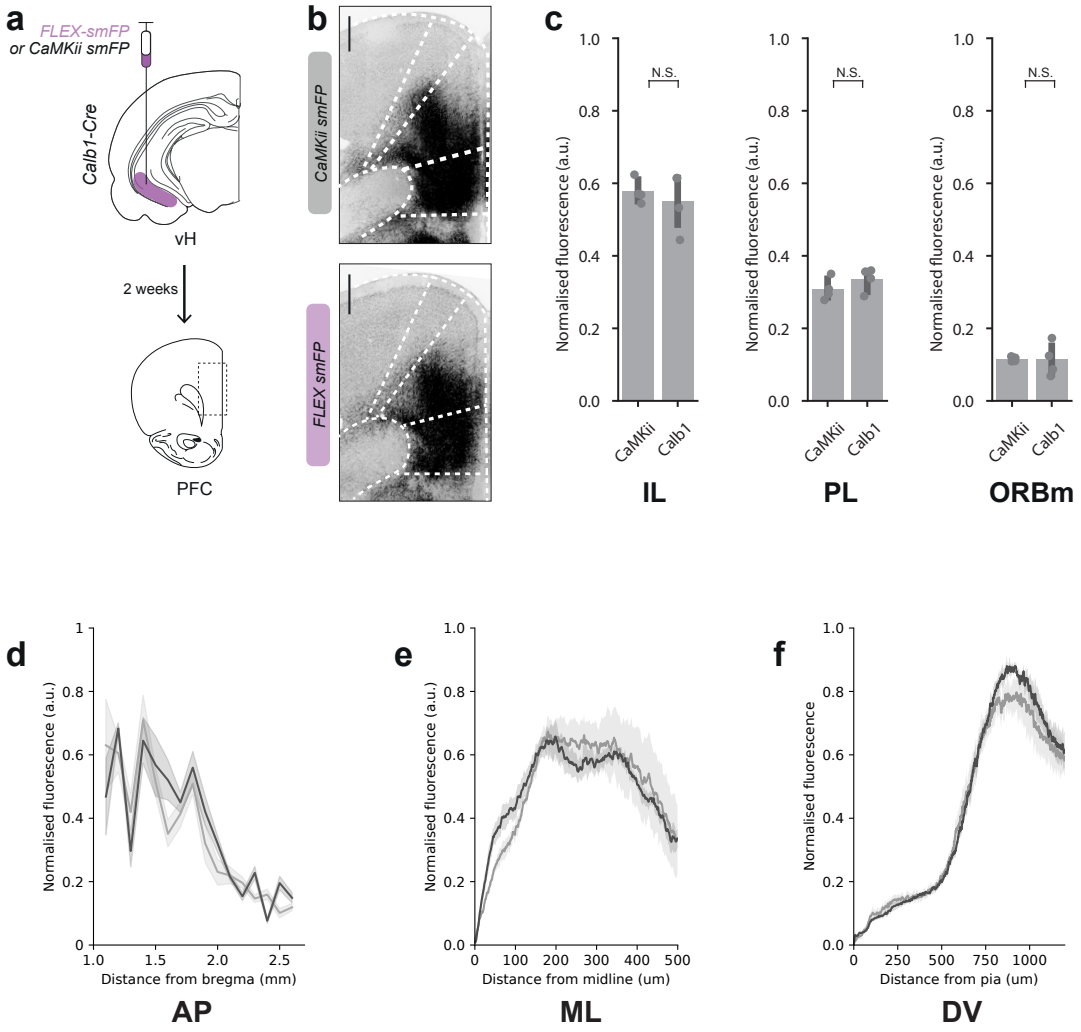

Figure 5.2: Tracing axons in PFC originating from deep and superficial vH layers
(a) Strategy to label axons from superficial and deep layers. Cre or *CaMKii*-dependent anterograde tracer smFP was injected into the vH of *Calbindin1*-Cre mice. 2 weeks were allowed for expression and transport. **(b)** Example images of axons in PFC from deep (top) and superficial (bottom) layers in vH. Scale bars = 100 μm. **(c)** Quantification of axon fluorescence intensity in IL, PL and ORBm regions of PFC. Fluorescence per area was normalised to overall fluorescence in the slice. Note similar distribution of fluorescence. **(d)** Normalised fluorescence of superficial and deep vH axons in PFC along the anteroposterior (AP) axis. Note similar fluorescence for both *Calb1*$^+$ and *CaMKii*$^+$ axons. **(e)** Normalised fluorescence of axons in PFC along the mediolateral (ML) axis. Note similar fluorescence for both *Calb1*$^+$ and *CaMKii*$^+$ axons. **(f)** Normalised fluorescence of axons in PFC along the dorsoventral (DV) axis. Fluorescence peaks are similar for both conditions, around the PL/IL border.

Anatomical evidence for distinct innervation of excitatory and inhibitory neurons in PFC: a rabies tracing approach

Having observed equal axonal patterning originating from both superficial and deep vH neurons in PFC, I next asked whether the axonal terminals were perhaps targeting different types of neurons within the same areas of PFC. I firstly tested this hypothesis anatomically by implementing a rabies tracing approach with the aim to quantify contacts onto both pyramidal cells and interneurons from axons in each vH layer. The viral strategy implemented to trace the hippocampal layer identity of inputs to pyramidal neurons and interneurons in PFC is outlined in Figure 5.3 a and b.

A mixture of fluorescently tagged CTXβ and Cre-dependent rabies helper proteins (TVA-G) was injected into the PFC of either *VGAT-Cre* or wild-type mice (which were co-injected with AAV2/1-CaMKii-Cre). This resulted in expression of the helper proteins in interneurons and pyramidal cells, for the *VGAT-Cre* or wild-type mice co-injected with AAV2/1-CaMKii-Cre in PFC, respectively. CTXβ was taken up by axon terminals and retrogradely transported to PFC-projecting cell bodies, allowing for visualisation of the overall PFC-projecting population in vH (Figure 5.3 c and d, *cyan*). Following two weeks of helper protein expression and CTXβ transport, EnvA pseudotyped mCherry-tagged rabies was injected into PFC to allow for specific retrograde transsynaptic tracing of hippocampal afferent inputs via either *VGAT+* or *CaMKii+* prefrontal neurons. In either condition, *VGAT+* or *CaMKii+* neurons expressed helper proteins, allowing for the retrograde rabies transsynaptic 'jump' one synapse upstream to vH. One week of rabies-mediated expression was allowed, following which horizontal hippocampal sections were taken for visualization of rabies and CTXβ positive cell bodies in vH (Figure 5.3 c and d).

Next, I manually counted rabies-positive and CTXβ-positive cells in each hippocampal layer, averaging every injection across 3 slices spanning $\sim$300 μm along the DV axis. The co-injection of CTXβ in PFC allowed for visualising the two cell layers in hippocampus as well as for controlling for variability in location of rabies-positive cells due to a misplaced PFC injection. Quantitatively, the proportion of total CTXβ-positive cells in the superficial and deep components did not differ between *VGAT+* and *CaMKii+* experiments (Figure 5.3 e, *left*; Mann Whitney: U = 4, p = 0.3, n = 4 injections per condition), suggesting an equivalent distribution of CTXβ and hence an equivalent spread of neurons in the superficial and deep layers in both conditions, as expected.

Analysis of rabies-labelling revealed that, in experiments where retrograde rabies tracing from PFC was initiated via excitatory pyramidal cells (*CaMKii+* scenario), rabies-positive cells were mostly restricted to the deep layer (Figure 5.3 c and e). On the contrary, when tracing was initiated via inhibitory interneurons in PFC (*VGAT+* scenario), rabies labelling was more evenly spread across the two layers and was proportionately higher than *CaMKii*-targeting rabies-positive cells in the superficial layer (Figure 5.3 d and e).

The proportion of rabies-positive cells in each layer was obtained by dividing the number of rabies-positive cells in e.g. the superficial layer (plotted in Figure 5.3 e) by the amount of all rabies-positive cells in the slice. The proportion of rabies labelling in the superficial layer was higher in *VGAT-Cre* mice than in the *CaMKii-Cre* condition, whereas I saw a marked absence of hippocampal rabies-positive cells projecting to excitatory PFC neurons in the superficial layer in the *CaMKii-Cre* condition (Figure 5.3 e; Mann Whitney: U = 16, p = 0.03, n = 4 injections per condition). Together, these findings suggest that hippocampal PFC-projecting neurons from the deep layer target both inhibitory and excitatory neurons in PFC, with a higher proportion of cells contacting excitatory neurons while cells in the superficial layer preferentially target inhibitory interneurons in PFC.

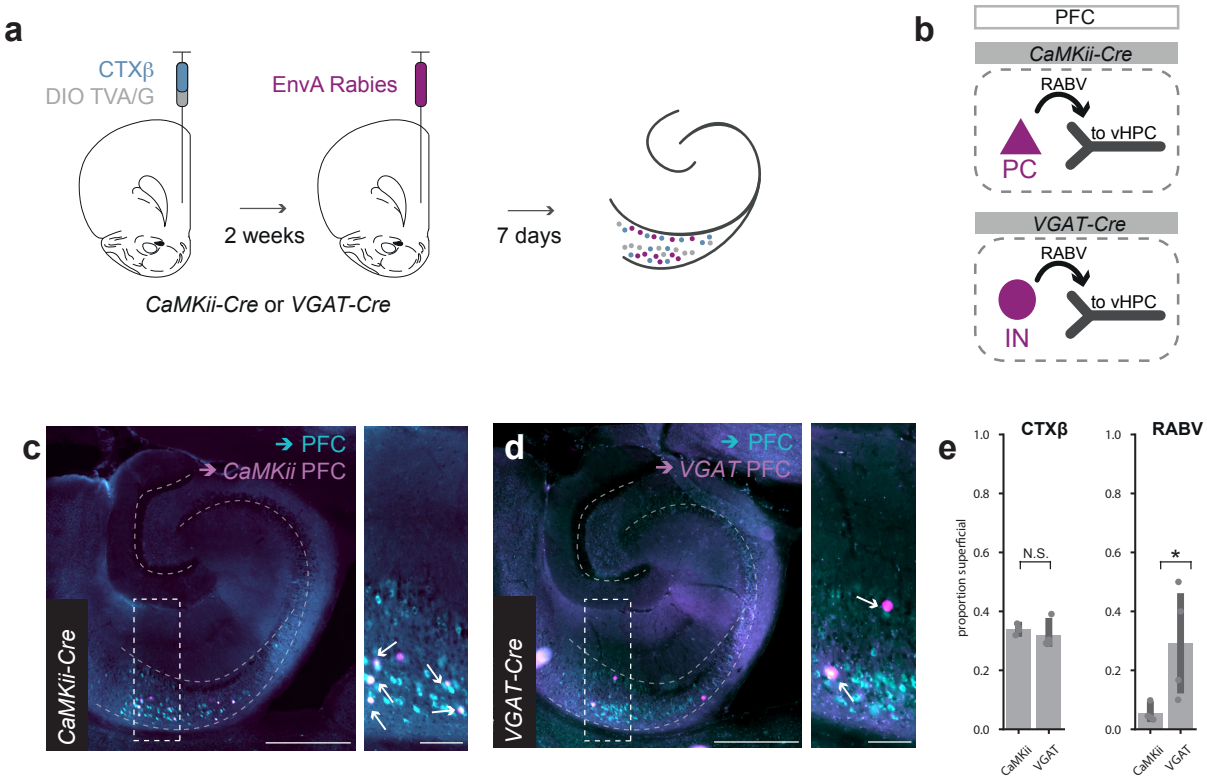

Figure 5.3: Differential targeting of pyramidal cells and interneurons by superficial and deep vH^{PFC} cells

(a) Strategy to label hippocampal neurons projecting to inhibitory and excitatory neurons in PFC. **(b)** Schematic of experimental design to trace hippocampal cells projecting to prefrontal pyramidal cells (top) and interneurons (bottom) from PFC. **(c)** Transverse slice of hippocampus labelled with CTXβ (cyan) and rabies (magenta) after tracing from excitatory neurons in PFC. On right, zoom of boxed region. Arrowheads point at cells co-labelled with CTXβ and rabies. Note the restriction of rabies labelling from excitatory neurons to the deep layer. Scale bars = 500 μm (left) and 100 μm (right). **(d)** Transverse slice of hippocampus labelled with CTXβ (cyan) and rabies (magenta) after tracing from inhibitory interneurons in PFC. Scale bars = 500 μm (left) and 100 μm (right). **(e)** Proportion of CTXβ-positive neurons (left) and rabies-positive neurons (right) in the superficial layer. Note equivalent distribution of CTXβ labelling across both conditions, but a marked absence of rabies-positive neurons projecting to excitatory PFC neurons in the superficial layer.

Analysis of the rabies tracing findings described above was based on visually assigning rabies-positive cells to the superficial or deep layers, guided by CTXβ labelling of the entire PFC-projecting population. In order to obtain an unbiased, more automated analysis of this data, I implemented the same approach used for clustering cell coordinates into components presented in Figure 3.2. As described previously, all labelled PFC-projecting cells (CTXβ-positive) and rabies-positive cells were first manually counted to obtain coordinates. Whilst saving the cell coordinates, CTXβ and rabies-positive cells were labelled with different markers for later identification. The coordinates were clustered using a Gaussian Mixture Model and the best fit for number of components was chosen using Bayesian Information Criterion (Figure 5.4 a). Data was gathered from 5 slices per injection site, and 4 injection sites were used per condition.

Consistent with results seen in Chapter 3, the mean number of components that best fit the distribution of PFC-projecting (CTXβ-positive) cells in vH was 2, selected by the lowest BIC score, with no difference between *VGAT* and *CaMKii* tracing conditions (Figure 5.4 b; Fisher's exact test: Odds ratio = 0.0, p = 1, n = 4 injections). After all cells (rabies-positive and CTXβ-positive cells) were jointly clustered using the GMM, I revealed the coordinates of rabies-positive cells and superimposed them onto the clustering output, as seen in red in Figure 5.4 a (BIC panel on right). This analysis allowed for assigning rabies-positive cells to each layer or component in such a way that both the separation of the CTXβ-positive cells into two components and the subsequent assignment of the rabies-positive cells to either layer (component) were carried out automatically and without bias. The analysis of this data is summarised in Figure 5.4 c. To recapitulate the analysis shown in Figure 5.3 from manually assigned rabies-positive cells, I calculated the proportion of cells in each layer from the data obtained by GMM clustering. The proportion of CTXβ or rabies-positive cells was calculated as a fraction of the total amount of cells with that label and compared across conditions (*CaMKii* - tracing via excitatory cells and *VGAT* - tracing via interneurons). As expected, the proportion of CTXβ-positive

cells in each layer i.e. the proportion of PFC-projecting neurons in each layer did not differ between conditions (Figure 5.4 c; Superficial - Mann Whitney: U = 12, p = 0.312 and Deep - Mann Whitney: U = 4, p = 0.312, n = 4 injections). This control unbiasedly confirms the observation in Figure 5.3 that there is no underlying difference in the distribution of the PFC-projecting population between experimental conditions.

In contrast to the equivalent distribution of CTXβ-labelled cells and in line with the results obtained through manual scoring, the distribution of rabies-positive cells across superficial and deep layers was different between conditions (Figure 5.4 c, light grey). In the superficial layer of vH, there was a higher proportion of rabies-positive cells traced via *VGAT*+ interneurons in PFC compared to rabies-positive cells traced via *CaMKii*+ excitatory cells (Figure 5.4 c; Mann Whitney: U = 16, p = 0.03, n = 4 injections, 9/26 rabies-positive cells in superficial layer traced from *VGAT*+ cells and 11/105 rabies-positive cells in superficial layer traced from *CaMKii*+ cells). In the deep PFC-projecting layer this trend was inverted, with more rabies-positive cells traced back from excitatory *CaMKii*-positive pyramidal cells in PFC than from interneurons (Figure 5.4 c; Mann Whitney: U = 0, p = 0.03, n = 4 injections, 85/105 rabies-positive cells traced from *CaMKii*+ excitatory cells and 16/26 rabies-positive cells traced from *VGAT*+ cells). These findings are schematised in Figure 5.4 d for ease of data visualisation. Overall, this data shows that rabies tracing via prefrontal pyramidal cells results in rabies-positive cells mostly restricted to the deep hippocampal layer, while tracing via prefrontal interneurons results in labelling across both layers. However, we saw significantly more rabies-positive cells in the superficial layer when tracing inputs to PFC via interneurons than via excitatory neurons, suggesting that although rabies-labelled cells were found in both layers when tracing via interneurons, overall the superficial layer is biased towards contacting interneurons while the deep layer is biased towards contacting pyramidal cells (Figure 5.4 c and d).

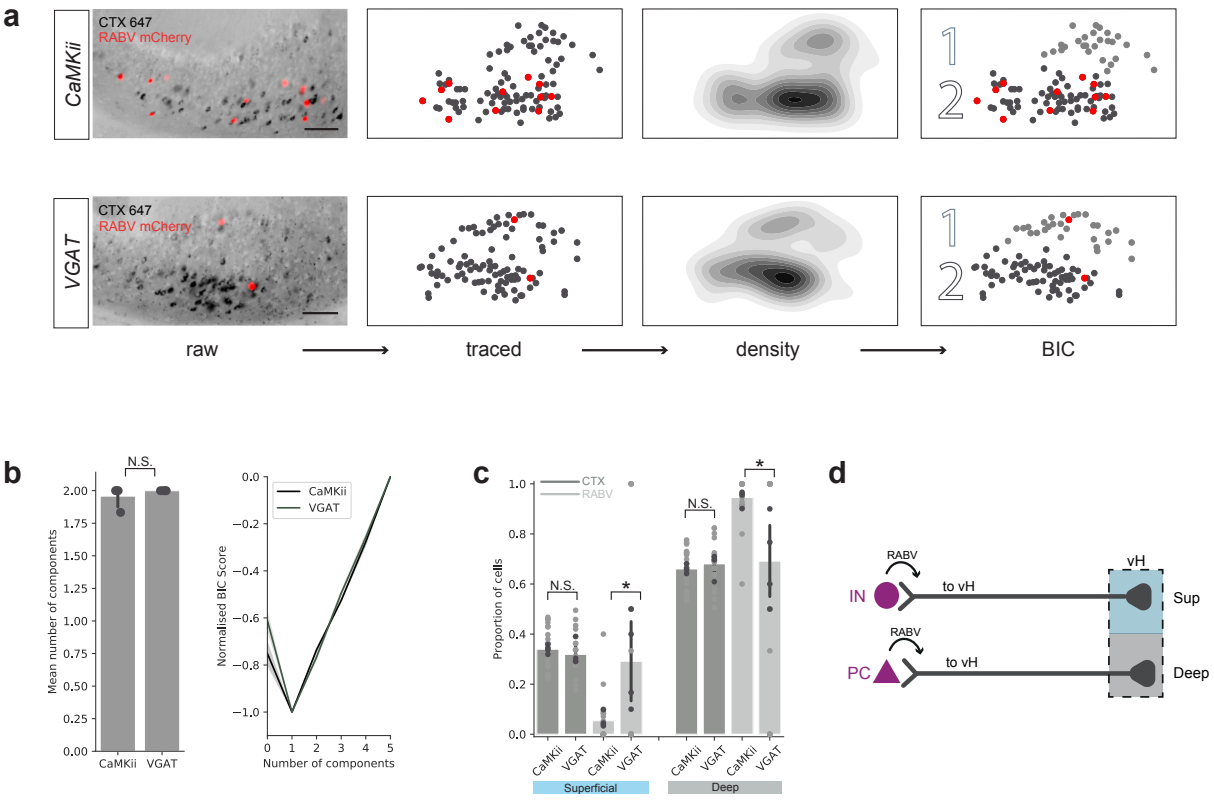

Figure 5.4: Unbiased clustering of rabies positive cells traced from PFC PCs and INs **(a)** Example images of the CA1/subiculum border with rabies (red) and CTXβ (black) positive cells. Note that no red cells are present in the superficial layer in the *CaMKii-Cre* example, while they are evenly spread in *VGAT-Cre* mice (below). Labelled neurons were clustered using a GMM and the best fit was chosen using Bayesian Information Criterion (BIC). See Methods 2.3.4 for detail. **(b)** Left: Mean number of components (i.e. cell layers) the CTXβ-labelled cells were clustered into. Right: Normalised BIC scores for 1 to 6 components. For normalisation between 0 and -1, the maximum value was subtracted from the data, which was then divided by the new minimum. The lowest BIC score represents the best fit of component number (2). Note no difference in best fit of components for the *VGAT-Cre* and *CaMKii-Cre* scenarios. **(c)** Proportion of cells labelled with CTXβ or rabies in the superficial and deep components (layers) respectively, in the *VGAT-Cre* and *CaMKii-Cre* scenarios. Dark grey circles show average proportion per injection, light grey circles show raw data from averaged slices per injection. Note the different spread of rabies (RABV)-positive cells in the superficial and deep layers across conditions. **(d)** Summary schematic of viral strategy and outcome. In *VGAT-Cre* animals (top), rabies jumped one synapse from interneurons (IN) and in the *CaMKii-Cre* scenario (bottom), hippocampal inputs were traced from pyramidal cells (PC). Note that rabies-positive cells contacting interneurons were found in the superficial to a larger extent than when tracing via PCs. The converse is true for rabies-positive cells contacting PCs, of which a greater proportion were seen in the deep layer.

Characterisation of viral strategy to stimulate superficial and deep layer vH^{PFC} axons in PFC

To functionally confirm the distinct anatomical targeting of interneurons and pyramidal cells described above, I used CRACM of input from superficial and deep layer vH cells onto layer V PFC pyramidal cells, where the highest concentration of axonal terminals was found (Figure 5.2 e). In order to carry out these experiments it was necessary to independently stimulate deep and superficial vH layer axons coming into PFC. To test whether I could bias the expression of ChR2 to select for superficial or deep cells, I injected Cre-dependent (DIO ChR2) or *CaMKii*-dependent ChR2 into vH respectively, and CTXβ into PFC of *Calb1-Cre* mice (Figure 5.5 a). Co-localisation of these two markers in vH cells (DIO-ChR2 and CTXβ for superficial layer cells and *CaMKii*-dependent ChR2 and CTXβ for deep layer cells) would identify ChR2-positive PFC-projecting neurons, as shown in Figure 5.5 b. Although *CaMKii* is a generic marker for excitatory pyramidal cells, the higher proportion of cells in the deep layer of the vH-PFC projection (roughly 70% of the PFC-projecting population is in the deep layer: Figure 3.2 h and Figure 5.4 c) was the reasoning behind using a *CaMKii*-dependent ChR2 construct to preferentially recruit deep vH^{PFC} cells.

Co-labelled cells per slice were counted for both conditions to obtain a proportion ChR2-positive cells in each vH^{PFC} layer. The proportion of Cre-dependent and *CaMKii*-dependent ChR2-positive vH^{PFC} cells in the superficial layer is summarised in Figure 5.5 c. Double positive cells were preferentially located in the superficial layer in brains injected with Cre-dependent ChR2 (i.e. ChR2 expressing in *Calb1*+ cells), while *CaMKii*-ChR2 and CTXβ double positive cells were preferentially biased away from the superficial layer (Mann Whitney: U = 24, p = 0.014, n = 4 slices (DIO ChR2), 6 slices (*CaMKii* Chr2)). These data suggest that DIO-ChR2 is preferentially expressed in superficial layer vH^{PFC} cells in *Calb1*-Cre mice, while *CaMKii*-ChR2 is predominantly expressed in deep layer vH^{PFC} cells.

The reason for non-binary targeting of superficial and deep layer cells is two-fold. Firstly, although the expression of *Calb1* is enriched in the superficial layer and can be used as a superficial layer marker (see Chapter 3), some cells in the deep layer also express *Calb1* to a lesser extent and will thus express ChR2 when DIO-ChR2 is injected into *Calb1-Cre* mice. Secondly, as discussed above, by using *CaMKii*-dependent ChR2, ChR2 is expressed in all *CaMKii*-expressing vH pyramidal cells (both superficial and deep layer pyramidal cells), but biased towards the deep layer due to its more numerous cell population. Despite these considerations, overall, these findings provide support for the implementation of this viral strategy in CRACM experiments, with DIO-ChR2 being expressed mainly in the superficial vH^{PFC} cell layer, and *CaMKii*-ChR2 expression being more predominant in the deep vH^{PFC} cell layer (Figure 5.5).

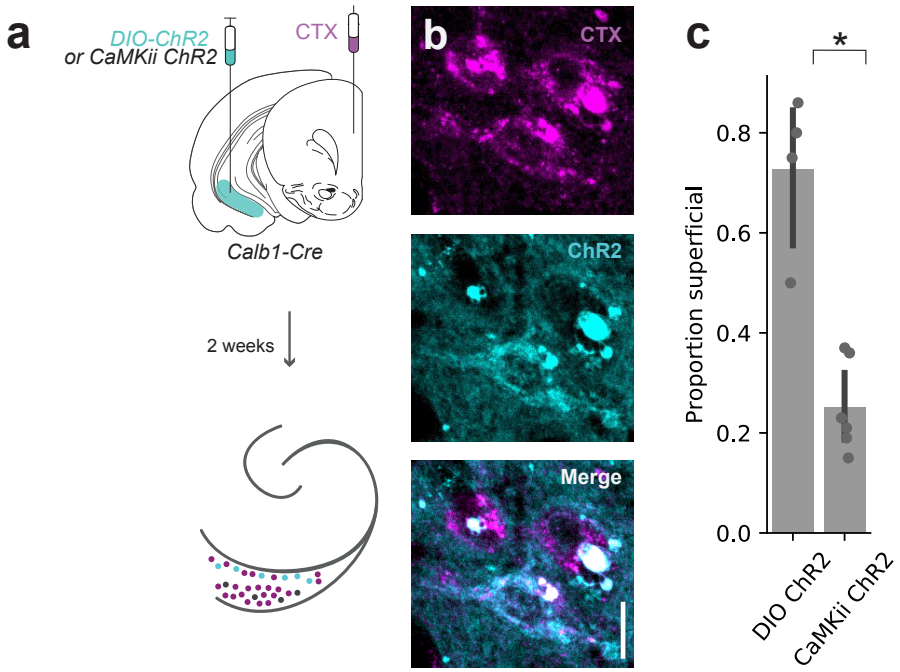

Figure 5.5: Characterisation of viral strategy for studying superficial and deep layer vH input to PFC
(a) Schematic summarising the injections carried out to study vH input to PFC. DIO-ChR2 or *CaMKii*-ChR2 was injected into the vH of *Calb1-Cre* mice, and CTXβ was injected into PFC to label PFC-projecting vH neurons. 2 weeks were allowed for ChR2 expression and retrograde transport of CTXβ. **(b)** Example images of CTXβ+ neurons (that project to PFC) positive for ChR2. Scale bar = 20 μm. **(c)** Proportion of ChR2 and CTXβ double positive neurons in the superficial vH layer for each condition. Note that the two conditions preferentially label either the superficial or deep layer.

Hippocampal cells in the superficial and deep vH layers exert different excitatory and inhibitory drives on PFC

Following the characterisation of the viral strategy, CRACM was implemented to investigate the effects of hippocampal input from each layer in the projection on PFC circuitry. DIO- or *CaMKii*-ChR2 were injected into vH to express ChR2 in superficial and deep layer vH cells respectively. After 2 weeks of expression and anterograde transport, acute coronal PFC slices were collected for recordings (Figure 5.6 a). The vH injection sites for the brains recorded from for both of these constructs are presented in Figure 5.6 b and c.

Voltage-clamp recordings were taken from layer V pyramidal neurons in PFC while optogenetically stimulating incoming vH axons from either vH layer (Figure 5.6 d). PFC pyramidal cells were held at -70 mV and 0 mV to isolate excitatory and inhibitory currents, respectively. At -70 mV the cell sits at the reversal potential for chloride ions and thus, excitatory AMPA-mediated currents can be isolated. At a holding potential of 0 mV the cell is at the reversal potential for AMPA receptors and thus inhibitory currents can be isolated, revealing any feedforward inhibition present. APV, an NMDA receptor antagonist, was added to the bath in order to isolate inhibitory currents when recording at 0 mV, as NMDA receptors may otherwise be active at this potential and contribute excitatory currents to the recording. Excitation:inhibition (E/I) ratios were calculated on a cell by cell basis by normalising the inhibitory to the excitatory responses. In Figure 5.6 e, example traces of excitatory (-70 mV) and inhibitory (0 mV) postsynaptic currents in PFC pyramidal cells are shown in response to optogenetic stimulation of superficial (Calb1) and deep (CaMKii) hippocampal axons. The inhibitory responses (upward traces) are normalised to the excitatory (downward) deflections, showing that *Calb1*-positive axon stimulation drove more feedforward inhibition onto PFC pyramidal cells compared to deep layer stimulation. In contrast, deep layer axonal stimulation drove more excitation. Figure 5.6 f shows the amplitude of excitatory responses recorded

at -70mV plotted against amplitudes of inhibitory responses recorded at 0mV in the same cells. The dotted line represents a linear relationship between the two, if responses at -70mV and 0mV were equal. In line with the anatomical data shown previously suggesting that proportionally, cells in the superficial layer contact more interneurons than they do pyramidal cells, stimulation of *Calb1*-positive axons produced larger inhibitory than excitatory responses in PFC pyramidal cells. This is shown by the majority of the data points in the top Calb1 panel in Figure 5.6 f falling above the dotted line. Conversely, for postsynaptic responses recorded in PFC in response to stimulation of *CaMKii*-positive axons (bottom CaMKii panel in Figure 5.6 f) more data points fell on or below the dotted line, suggesting that stimulation of deep layer axons exerts both inhibitory and excitatory drive on PFC, with a bias towards excitation. This data is summarised in the form of E/I ratios in Figure 5.6 g, highlighting the differential output of the two vH^{PFC} layers and their effects on PFC pyramidal cell activity (Mann Whitney: U = 51, p = 0.017, n = 12 *Calb1*, 18 *CaMKii)*.

In Figure 5.6, the example traces shown and ratios plotted correspond to postsynaptic responses to 5 ms light pulse axonal stimulation. This pulse duration was chosen as representative of the data as it summarises the overall findings. Additionally, 5 ms stimulation resulted in EPSC responses in pyramidal cells with amplitudes large enough to be capable of firing an action potential (when recording in current-clamp conditions). This was taken as a proxy that nearby interneurons contacted by hippocampal axons would also fire action potentials and thus be recruited for feedforward inhibition of pyramidal cells, allowing for reliable calculation of E/I ratios. However, a variety of other light pulse durations was used to record responses over a wider range. Mean response amplitudes in PFC pyramidal cells to increasing light pulse duration at -70 mV and 0 mV are shown in Figure 5.7. The inhibitory currents recorded in response to *Calb1*-positive axon stimulation were overall larger than the excitatory currents recorded at -70 mV, with the largest difference occurring at 5 ms light pulse duration, as described in

the previous figure (Repeated measures within and between subjects ANOVA with Greenhouse-Geisser: $F_{(1.545,32.453)} = 4.089$, $p = 0.035$). In contrast, when stimulating *CaMKii*-positive axons with increasing light pulse duration, no difference was apparent between the response amplitudes recorded at 0 mV and -70 mV (Repeated measures within and between subjects ANOVA with Greenhouse-Geisser, $F_{(1.249,39.968)} = 1.012$, $p = 0.339$). However, the E/I ratio on a cell by cell basis shown in Figure 5.6 g points at the excitatory bias of postsynaptic responses driven by *CaMKii*-positive axon stimulation and is a more reliable measure of relative excitatory and inhibitory currents than mean amplitude of response across cells. Thus together, these experiments show that stimulation of *Calbindin1*-positive (superficial layer) axons exerts a predominantly inhibitory drive on layer V PFC pyramidal cells, while stimulation of *CaMKii*-positive (deep layer) axons provides robust excitation as well as feed-forward inhibition, to a lesser extent.

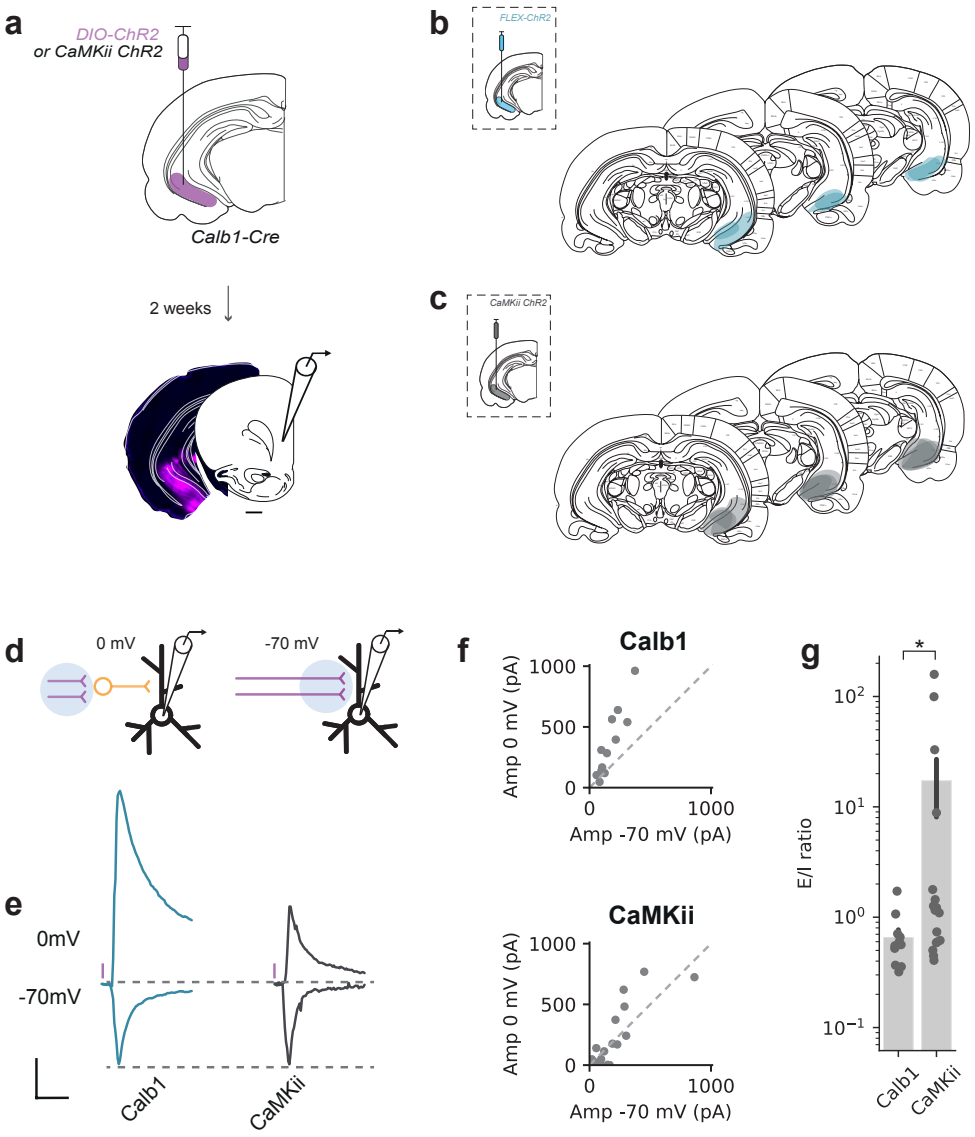

Figure 5.6: Effects of *Calb1*- and *CaMKii*-specific input to PFC
(a) Strategy to record E/I ratio in PFC in response to input from each layer in vH. AAV containing either FLEX-ChR2 (to express in *Calb1*+ superficial neurons) or *CaMKii*-ChR2 (to bias expression to deep layer neurons) was injected into vH of *Calbindin1-Cre* mice. Two weeks later voltage clamp recordings were carried out in PFC layer V neurons in acute slices in the presence of the NMDA antagonist APV. **(b)** Schematic summarising the injection site coordinates in vH carried out to study inputs onto PFC from *Calb1*+ neurons (top), and *CaMKii*+ neurons (bottom). All injections were carried out in *Calbindin1-Cre* mice and were histologically confirmed (n = 6 injections for each condition). **(d)** Brief blue light pulses allowed input specific excitatory and feedforward inhibitory postsynaptic currents to be recorded by holding neurons at -70 mV and 0 mV, respectively. **(e)** Responses to superficial (blue) or deep (black) hippocampal inputs at -70 mV (EPSCs) and 0 mV (IPSCs) in layer V PFC neurons. Purple tick indicates light pulse. Scale bar = 20 ms and 0.5 (fold response of amplitude at -70 mV, which is normalized to 1). **(f)** Summary of recordings described in (e). Amplitude of IPSC recorded at 0 mV plotted against EPSC amplitude recorded at -70 mV. **(g)** Summary of E/I ratios. Note log scale.

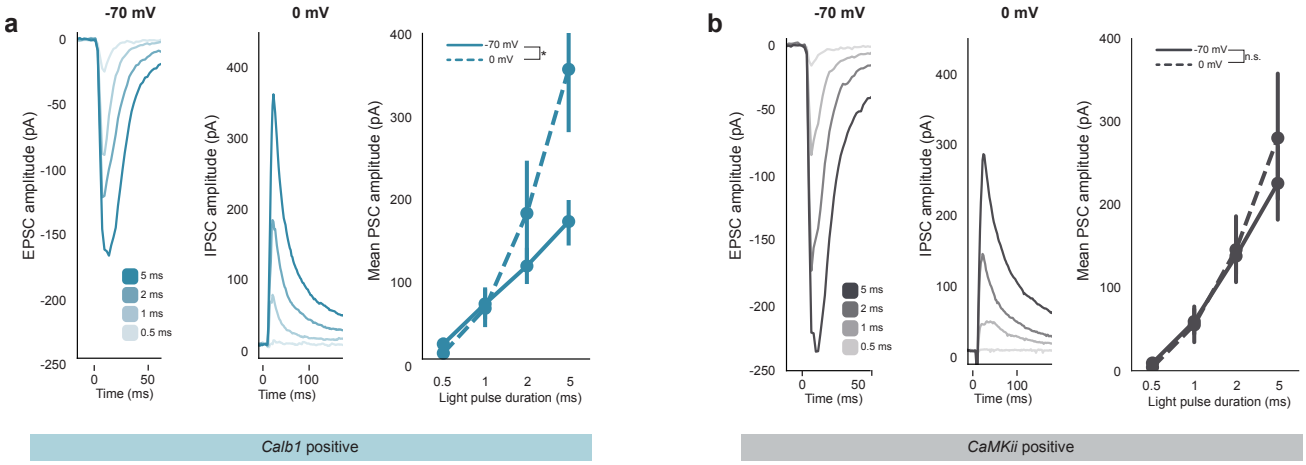

Figure 5.7: Characterising *Calb1* and *CaMKii*-specific input to PFC
(a) Mean EPSC (left) and IPSC (centre) amplitudes recorded in pyramidal cells in PFC in response to increasing duration of light pulse stimulation of hippocampal *Calb1*-positive axons. Summarised on right, mean response amplitudes for EPSCs and IPSCs with increasing light pulse duration recorded at -70 mV and 0mV, respectively. **(b)** As for (a), but here stimulating ventral hippocampal *CaMKii*-positive axons. Note that while the response curves in (a) diverge, excitatory and inhibitory responses to *CaMKii*-positive axon stimulation are more similar.

Characterising interneurons in PFC

Following from the finding that superficial and deep hippocampal axon stimulation in PFC had differential inhibitory and excitatory drives onto PFC pyramidal cells, I wanted to carry out a more in-depth investigation into the underlying mechanism. The strategy was to record responses to input from the two layers of vH onto pairs of pyramidal cells and identified interneurons in PFC directly. In order to add mechanistic detail to the differential effects of superficial and deep layer vH input on PFC circuitry, I grouped recorded interneurons into two sub-classes based on their firing properties. Interneurons can be classified into two general subgroups: soma-targeting fast-spiking interneurons, and dendrite-targeting non-fast-spiking interneurons, based on their intrinsic properties and the expression of peptides such as parvalbumin and somatostatin, respectively (Rudy et al., 2011; Tremblay et al., 2016). In this section, I will describe how interneurons were characterised post-hoc from voltage trace recordings in response to current injections.

Both hyperpolarising and depolarising current steps were injected into interneurons during whole-cell recordings to obtain subthreshold and spike-related electrophysiological features, respectively. From voltage traces in response to hyperpolarising current steps I calculated the decay time constant tau (τ) - a measure of how quickly the cell membrane charges - which is used to characterise interneurons (Marlin and Carter, 2014). To extract tau, exponentials were fit to the traces from their initial decrease in voltage to the end of the stimulus, and τ was calculated off the exponential curves as the time elapsed until the exponential had decreased to 1 / e $\approx$ 36.8 % of its original voltage value. From action potential traces in response to depolarising current steps, I measured the action potential (AP) half width (width of AP at half amplitude; Figure 5.8 a). Qualitatively, fast spiking interneurons showed faster tau as well as shorter AP half width (Figure 5.8 a).

By plotting tau against AP half width, I observed the relationship between

these two measures and compared the observations against published figures in order to cluster interneurons into fast spiking and non-fast spiking sub-classes ((Marlin and Carter, 2014; Kawaguchi, 1993); Figure 5.8 a). Cells with $\tau < 25$ ms and an AP half width < 1.2 ms were classified as fast spiking and the remaining cells were classified as non-fast spiking (Figure 5.8 b).

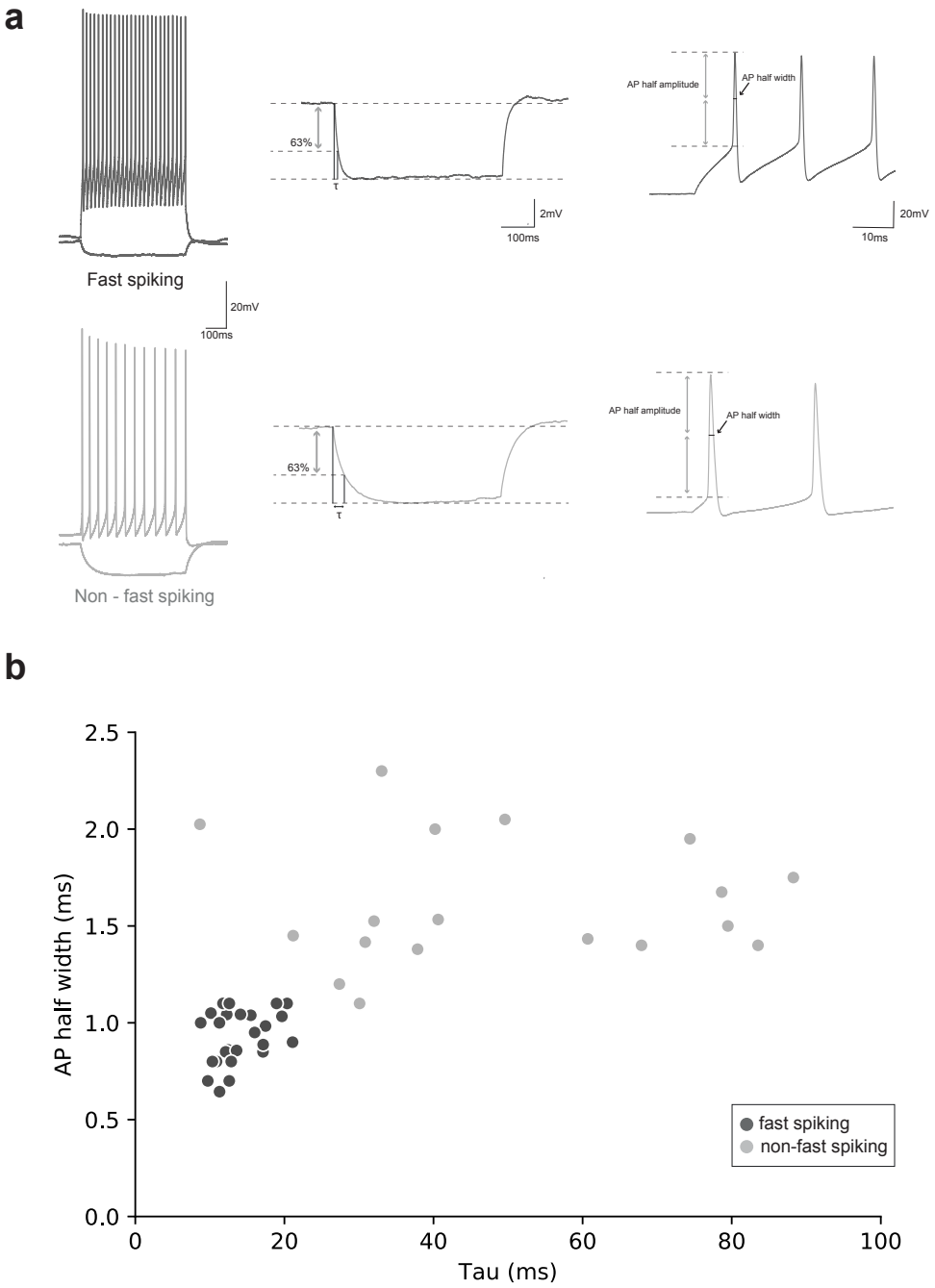

Figure 5.8: Characterisation of IN types recorded in PFC
(a) Example current clamp recording from DLX+ interneuron in PFC classified as a fast-spiking interneuron. *Top*: Left, example responses to positive and negative current steps in a fast-spiking interneuron. Middle and Right, details of currents showing tau, half amplitude and half width of action potentials. Note fast tau and AP half width. Below, as above but for an interneuron classified as non-fast-spiking. Note slower tau and bigger AP half width. Scale bars = 100 ms and 20 mV; 100 ms and 2mV and 10ms and 20mV. **(b)** Clustering of DLX+ interneurons into fast-spiking and non-fast-spiking based on action potential half width and tau. Classifications are used in Figure 5.9.

Differential innervation of interneuron types in PFC by superficial and deep vH^{PFC} terminals

Having established a characterisation protocol for prefrontal interneurons, I went on to record responses to vH input from pyramidal cells and specific interneuron types. This allowed for a comparative investigation of the direct effect of vH axonal stimulation on inhibitory and excitatory PFC circuitry rather than an inferred observation of inhibitory drive via feed-forward inhibition onto pyramidal cells.

As above, either anterograde Cre-dependent or *CaMKii*-dependent ChR2 was injected into the vH of *Calb1-Cre* mice. An additional injection of DLX mRuby was made into PFC to label inhibitory interneurons (Figure 5.9 a). With this construct, the fluorescent marker mRuby is expressed under the control of the interneuron specific DLX promoter, thus allowing for targeted whole-cell recordings from labelled inhibitory interneurons (Dimidschstein et al., 2016). After allowing 2 weeks for expression and transport, pairs of pyramidal cells and neighbouring interneurons (identified by mRuby labelling) were recorded in acute PFC slices while stimulating incoming vH axons (Figure 5.9 b). Figure 5.9 c shows an example DLX+, mRuby expressing interneuron in PFC during a recording.

Similar to the CRACM setup to study E/I ratios above, input form ventral hippocampal axons onto pyramidal cells and interneurons was recorded in voltage-clamp mode to obtain post-synaptic current (PSC) responses. However, interneurons were patched in current-clamp internal solution (see Table 2.6) in order to first characterise the interneuron type with current steps (Figure 5.9 d). Once the current step stimulation had been carried out for post-hoc characterisation of the interneuron, the recording was switched to voltage-clamp mode in order to record current traces in response to optogenetic axon stimulation. Due to the significantly smaller size of interneurons in comparison to pyramidal cells, space clamp problems present

as less of an issue, and current-clamp internal can be used in voltage-clamp mode to obtain PSC recordings. Examples of fast and non-fast spiking interneuron types recorded from in PFC can be seen in Figure 5.9 d. These current-clamp voltage traces show recordings in response to negative (-30 pA; downward deflection) and positive (+150 pA; action potentials) current injections for a fast-spiking (FS; dark grey) and a non-fast spiking (non FS; light grey) interneuron.

Postsynaptic current amplitudes in pyramidal cells and interneurons in response to superficial (Figure 5.9 e, top; Calb1) and deep (Figure 5.9 e, bottom; CaMKii) layer axon stimulation are summarised in the scatter plots in Figure 5.9 e. Each point on the scatter plots represents one pyramidal cell (PC) / interneuron (IN) pair (dark grey - FS IN/PC pair; light grey - non FS IN/PC pair). Note that in Figure 5.9 e only dark grey points representing FS IN / PC pairs lie above the dotted line in the bottom panel (CaMKii), while in the top panel (Calb1) the spread is more even. This data suggests that superficial layer axon stimulation (Calb1) produced similarly sized responses in both interneuron classes investigated, while deep layer axonal stimulation preferentially targeted FS interneurons. This result is summarised as pyramidal cell to interneuron amplitude ratios in Figure 5.9 f and g showing that in fact, input from superficial layer cells innervated both FS and non-FS interneurons in PFC to the same extent (Figure 5.9 f; Mann Whitney: U = 84, $p = 0.77$, n = 12 pairs (FS), 13 pairs (non-FS)) and deep layer vH input was biased away from non-FS interneurons (Figure 5.9 g; Mann Whitney: U = 59, $p = 0.026$, n = 14 pairs (FS), 5 pairs (non-FS)), providing robust input onto both pyramidal cells and neighbouring fast-spiking interneurons.

Overall, these results show broader recruitment of interneuron cell types in PFC by superficial vH axons, which contact both FS and non-FS interneurons, while deep layer vH axons recruit only FS interneurons to a similar extent than they do pyramidal cells. The overall inhibitory bias of superficial vH input onto PFC observed in Figure 5.6 may thus be explained by a more widespread recruitment of

both dendrite- and soma-targeting inhibitory circuits within PFC.

The circuit findings discussed in this chapter are brought together with data from Chapter 4 in Figure 5.10. Following on from differential input onto hippocampal projection neurons in the two layers and local inhibitory circuitry described in Chapter 4, the data presented in the current chapter describes the downstream targets of superficial and deep layer vH projections in PFC. In summary, superficial cells preferentially provide inhibition onto PFC, targeting both FS and non-FS interneurons. Deep vH^{PFC} cells provide more direct excitation by robustly targeting pyramidal cells and FS, but not non-FS interneurons.

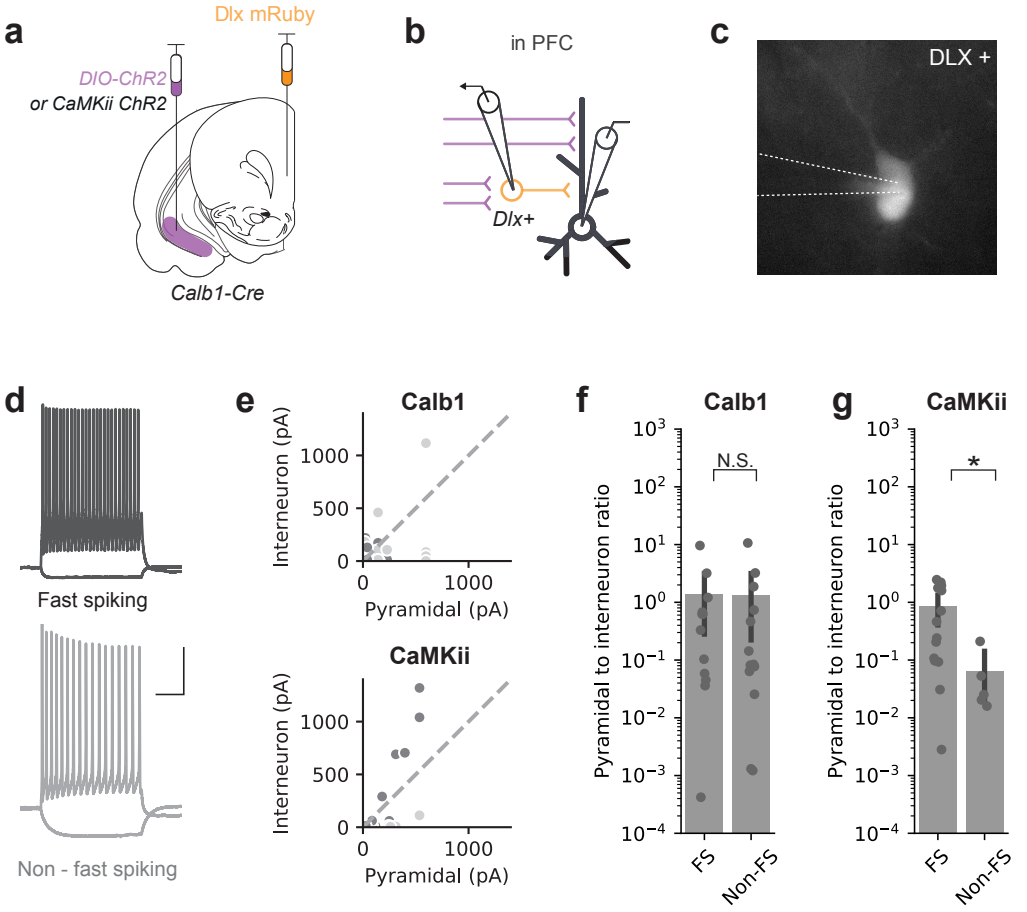

Figure 5.9: *Calb1* and *CaMKii*-positive hippocampal axons differentially contact fast-spiking and non-fast spiking INs in PFC
(a) Schematic of viral strategy for the experiment. In *Calb1*-Cre mice, either Cre-dependent of CaMKii-dependent anterograde ChR2 was injected into vH. DLX mRuby was injected into the PFC of the same mice, to label interneurons (INs). **(b)** Strategy to record from INs and pyramidal cells (PCs) in PFC. Axons coming in from the *Calb1*-enriched superficial layer or from *CaMKii*-positive cells were stimulated with light whilst recording from pairs of INs (orange) and PCs (black) to obtain a relative measure of input onto INs versus PCs. **(c)** Example image of a DLX mRuby+ cell in PFC being patched for recording. **(d)** Example current clamp recordings from fast-spiking (FS - black) and non-fast-spiking (Non-FS - grey) INs in PFC. Scale bar = 100 ms and 30 mV. **(e)** EPSC amplitude in INs plotted against response amplitude in PCs upon stimulating *Calb1* (top) or *CaMKii*-positive hippocampal axons. Black dots indicate that the IN in the pair was fast-spiking, grey dots that it was non-fast spiking. **(f)** Summary of PC to IN amplitude ratio in response to *Calb1*-axons stimulation. Input from superficial layer axons innervates both FS and non-FS interneurons to the same extent. **(g)** As for (f) but stimulating *CaMKii*-axons. Deep layer input is biased away from non-FS interneurons.

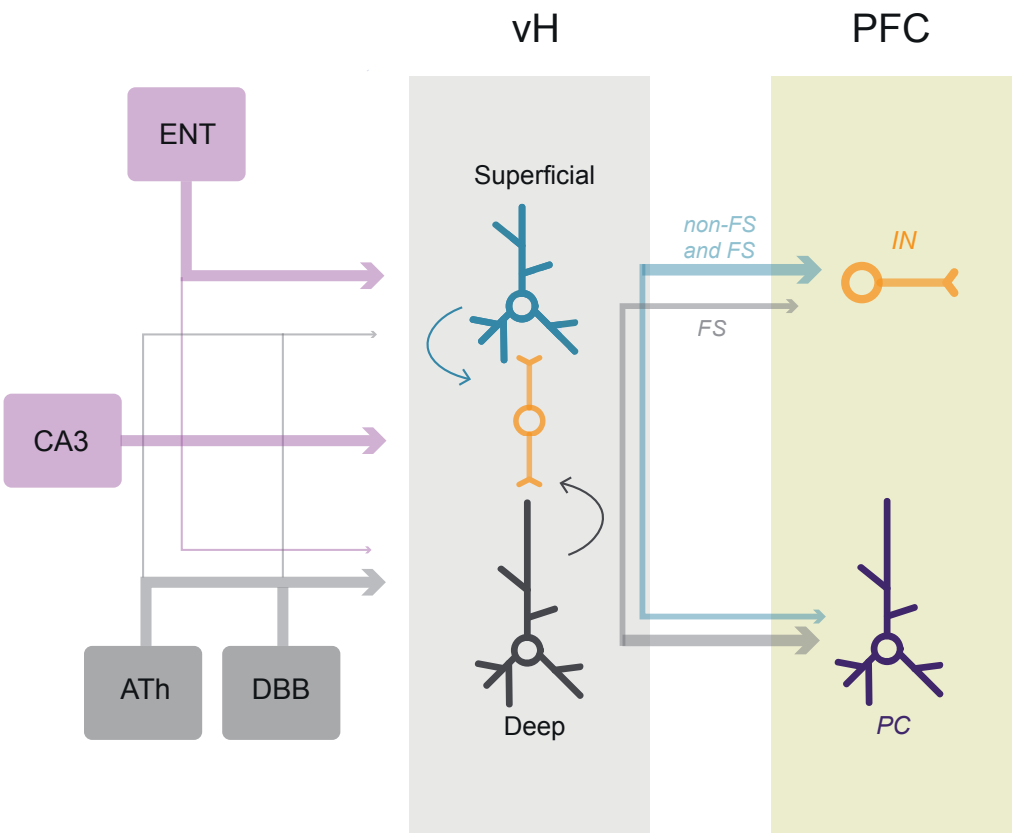

Figure 5.10: Updated summary schematic of circuit
In magenta (top left), intra-hippocampal inputs to superficial and deep layer vH^{PFC} cells. Entorhinal cortex (ENT) inputs are biased towards superficial cells and CA3 inputs equally target both layers. In grey (bottom left), long-range inputs onto vH^{PFC} cells from the anterior thalamus (ATh) and the diagonal band of Broca (DBB) are biased towards cells in the deep layer. The thickness of the lines represents connection strength. Within the vH (grey box) interneurons (orange) target and are targeted by both superficial (blue) and deep (black) PFC-projecting cells. Superficial cells preferentially provide inhibition onto cortical neurons by recruiting both fast-spiking (FS) and non-fast-spiking (non-FS) interneurons in PFC while deep cells preferentially target pyramidal cells and FS interneurons.

Superficial and deep vH^{PFC} subpopulations bidirectionally influence exploratory behaviour

The differences observed in PFC pyramidal cell and interneuron responses to superficial and deep layer vH^{PFC} terminal stimulation prompted the hypothesis that the two layers may be differentially involved in vH-PFC associated behaviour. The ventral hippocampus-prefrontal cortex pathway is strongly implicated in exploration of the elevated plus maze (EPM) and anxiety-related behavioural measures (Parfitt et al., 2017; Padilla-Coreano et al., 2016; Adhikari et al., 2010). PFC cells receiving vH input have strong anxiety-related firing patterns and their activity tracks the decision to enter the potentially threatening open arms of the maze (Adhikari et al., 2011; Padilla-Coreano et al., 2016; Ciocchi et al., 2015). The differential inhibitory and excitatory circuit connectivity of the two identified layers within the vH-PFC projection suggests that they may be differentially active during behaviour and are poised to drive different aspects of exploration within the EPM.

To address this question, I designed an experiment to test the effects of optogenetically activating axon terminals in PFC originating from either the superficial or the deep vH layer during EPM exploration. In *Calbindin-Cre* mice, either *CaMKii*-dependent or Cre-dependent (DIO) ChR2 was injected into vH to bias towards recruitment of deep and superficial layer terminals, respectively, as described above. Non-light responsive CaMKii-GFP was used as a control for injections and light delivery during behaviour. Animals were also fitted unilaterally with an optical fibre implant over PFC to illuminate the axon terminals for stimulation during EPM exploration (Figure 5.11 a). During testing, mice were placed in the centre of the EPM and allowed to explore for a total of 9 minutes, split into three 3-minute epochs. The first and last epochs were not coupled with blue light stimulation ('off') and the middle 3 minute epoch consisted of free exploration coupled with blue light stimulation at 20Hz ('on'). In line with published data, light stimulation during the 'on' epoch was only delivered when the mice entered the central choice point in the

EPM and explored the open arms (Jimenez et al., 2018; Lee et al., 2019a). While the mice explored the open arms, the light was kept on constantly, flashing at 20 Hz, until they returned to the closed arms (Figure 5.11 b).

Stimulation of superficial layer vH axon terminals in PFC during the middle 3 minute epoch promoted the exploration of the open arms compared to GFP-expressing controls (Figure 5.11 c). This is shown as percentage change in exploration (time spent) of the open arm relative to controls. In contrast, stimulation of deep layer vH axon terminals in PFC reduced exploration of the open arms relative to GFP controls (2-way repeated measures ANOVA: Interaction between group and epoch, $F_{(4,56)} = 4.36$, $p = 0.018$, n = 15 (GFP), n = 8 (Sup), n = 8 (Deep)). Figure 5.11 d shows a summary of the stimulation-induced alteration to open arm exploration in both conditions relative to controls (Welch t-test with Holm-Sidak correction: GFP-Sup: $t(23) = 3.78$, $p = 0.004$; GFP-Deep: $t(23) = 2.48$, $p = 0.026$).

Overall, these findings suggest that in line with their differential targeting of PFC circuitry, superficial and deep layer neurons within the vH-PFC projection provide bidirectional hippocampal control of PFC during open arm exploration. Specifically, superficial layer activity results in increased open arm exploration while activity in the deep layer promotes anxiety-like avoidance behaviour. Thus, activity in the vH-PFC pathway supports opposite behaviours during conflict-based approach-avoidance tasks via its two subpopulations.

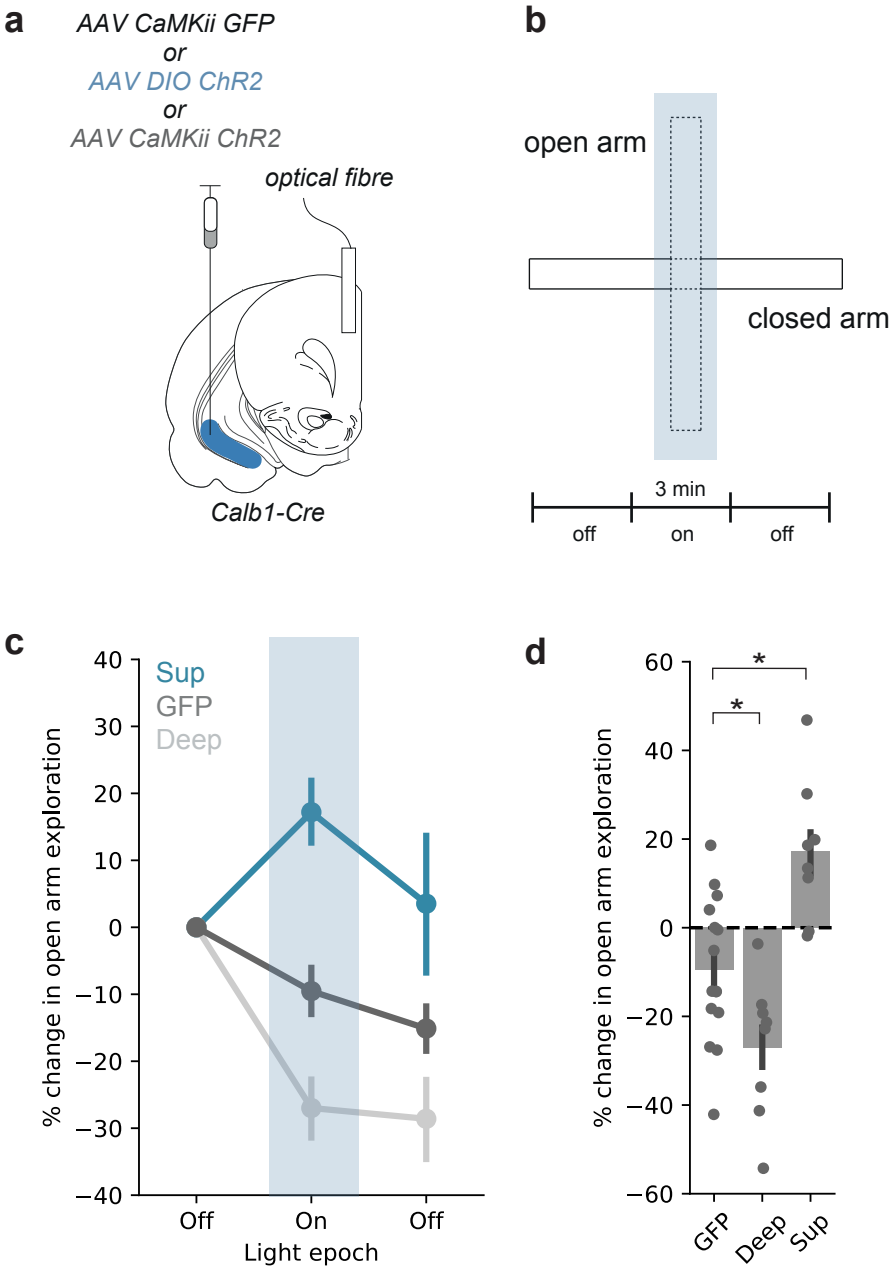

Figure 5.11: Superficial and deep vH^{PFC} axon stimulation during EPM exploration drives opposing behaviours

(a) Strategy for *in vivo* optogenetic manipulation of vH axons from each layer in PFC. Cre- or *CaMKii*-dependent Chr2 (or *CaMKii*-dependent GFP for controls) was injected into vH, and an optic fibre implanted above PFC. **(b)** Experimental design: after a 3 min baseline, for a second 3 min epoch 20 Hz light was delivered via the optical fiber when the mouse entered the centre point of the maze, and continued until return to the closed arms. Mice then remained in the maze for a third post stimulation 3 min epoch. **(c)** Change in open arm exploration due to stimulation of superficial, deep or control axons in PFC. Stimulation dramatically altered exploration with superficial axon stimulation increasing and deep axon stimulation decreasing open arm exploration relative to controls. **(d)** Summary of stimulation-induced alteration to open arm exploration.

5.3 Discussion

In this Chapter, I have shown the differential recruitment of prefrontal circuitry by the two layers of the vH-PFC projection. Following the observation that hippocampal axons originating from both layers innervated equivalent prefrontal areas along all three brain axes (Figure 5.2), I investigated what cell types were contacted by these axons in PFC. Combining Cre-dependent rabies tracing and transgenic mouse lines, I traced vH inputs onto interneurons and pyramidal cells in PFC and found that cells in the superficial vH^{PFC} layer made more synaptic contacts onto interneurons than their deep counterparts, which in turn made more synaptic contacts with excitatory pyramidal cells (Figures 5.3 and 5.4). These anatomical findings were confirmed functionally using CRACM to show that superficial layer cells provide a larger inhibitory drive onto PFC, while deep layer cells provide stronger direct excitation onto PFC pyramidal cells (Figure 5.6). More specifically, axons from the two layers contacted different classes of interneurons in PFC to varying extents, with *CaMKii*-positive (deep layer) axons targeting exclusively soma-targeting fast-spiking interneurons and *Calb1*-positive (superficial layer) axons targeting both fast and non-fast spiking interneurons (Figure 5.9). Together, these findings suggest that superficial layer vH cells exert a preferentially inhibitory drive onto PFC pyramidal cells via broader direct recruitment of interneurons as opposed to preferentially pyramidal cell recruiting deep layer vH cells.

However, the rabies-mediated anatomical investigation of vH synaptic contacts onto excitatory and inhibitory cells in PFC (Figure 5.3) may lend itself to an alternative conclusion. Although the low overall number of rabies-labelled cells in vH traced via interneurons may be due to low expression of Cre-recombinase in the cortex of the *VGAT*-Cre transgenic line (Vong et al., 2011), it cannot be excluded that vH cells (especially superficial layer cells) projecting to PFC simply contact interneurons very sparsely. Furthermore, the functional verification of the anatomical data (Figure 5.6) may also be interpreted within this framework. Increased

inhibitory drive onto PFC pyramidal cells by superficial layer vH cells (Figure 5.6) could result from the preferential recruitment of feedback inhibition, such that prefrontal pyramidal cells contacted by superficial cells in turn recruit local interneurons to dampen their own activity rather than via direct recruitment of interneurons. Some hints of a feedback inhibitory mechanism may be found in Figure 5.7, where inhibitory post-synaptic current amplitudes increase more quickly with incremental light pulse duration in response to *Calb1*-positive than with increasing duration of *CaMKii*-positive axon stimulation. This observation suggests that local, recurrent feedback inhibition mediated by vH-recruited PFC pyramidal cells may drive the observed E/I ratios. Nevertheless, extensive data investigating direct contacts by vH axons onto prefrontal interneurons (Figure 5.9) suggests that the driving mechanisms behind the observed E/I ratios (Figure 5.6) may be varied and involve at least in part, direct recruitment of prefrontal interneurons.

Behaviourally, during EPM exploration I observed that superficial layer axon stimulation drove increased exploration of the open arms, while stimulation of deep layer axons increased avoidance behaviour such that mice spent more time in the closed arms compared to controls (Figure 5.11). Together, these observations provide a more complete circuit understanding and mechanistic insight into how the vH engages the PFC in a push-pull circuit to bidirectionally modulate PFC activity and exploratory behaviour.

Throughout the next few pages, I will firstly discuss the implications and mechanistic utility of the differential inhibitory and excitatory drive onto PFC exerted by superficial and deep layer vH^{PFC} cells and its link to their opposing roles during exploratory behaviour. Following from this, I will discuss the relevance of targeting different types of interneurons in PFC. Lastly, I will discuss what the differential involvement of the two vH-PFC cell layers during exploratory behaviour may clarify regarding how cellular heterogeneity in the hippocampus is used to support multiple functions via the same circuitry. I will focus on how the experiments

presented in this chapter may help explain some conflicting findings regarding the role of the vH-PFC projection in behaviour.

Superficial and deep layer vH^{PFC} inputs have differential effects on PFC circuitry

In this chapter I have shown that the superficial and deep layers of the vH have different downstream effects on PFC circuitry. This observation poises the vH-PFC circuit to have unique effects during behaviour, given that the different layers of the projection preferentially excite or inhibit prefrontal pyramidal cells (Figure 5.6). The role of the hippocampus being both excitatory and inhibitory fits well with observations of alternating inhibitory and excitatory hippocampal input onto PFC dependent on task demands (Jadhav et al., 2016; Shin and Jadhav, 2016). For example, inhibiting vH during learned fear recall results in increased PFC activity (Sotres-Bayon et al., 2012) - suggesting an inhibitory role - while inhibiting vH during approach-avoidance conflict in the elevated plus maze (EPM) results in decreased PFC activity (Padilla-Coreano et al., 2016) - suggesting an excitatory role. In particular, different levels of activity in PFC are differentially associated with anxiety-like and threat behaviour.

Increased activity in PFC has been shown to correlate with increased anxiety-like behaviour during elevated plus maze exploration (Bi et al., 2013; Canetta et al., 2016; Berg et al., 2019). On the contrary, PFC lesions resulting in reduced prefrontal activity are accompanied by a reduction in anxiety-like behaviour during EPM exploration (Deacon et al., 2003; Shah and Treit, 2003, 2004; Berg et al., 2019). In line with these effects on behaviour of increased and decreased prefrontal activity, modulating vH input onto PFC has also been shown to bidirectionally influence exploratory EPM behaviour. In fact, increased activity in the vH-PFC pathway occurs during exploration of anxiogenic environments (Adhikari

et al., 2010, 2011; Ciocchi et al., 2015; Padilla-Coreano et al., 2016, 2019) and a reduction in excitatory vH drive onto PFC disrupts anxiety-like behaviour during EPM exploration (Padilla-Coreano et al., 2016). In contrast, vH inhibitory influence on PFC has been shown to gate (prevent) the expression of fear following extinction via feedforward inhibition of prefrontal projection neurons (Sotres-Bayon et al., 2012). In line with this role, a reduction in vH-PFC activity when vH input is mostly inhibitory onto PFC (thus leading to increased excitatory drive on PFC) increases fear expression in previously extinguished rats, suggesting that inhibitory influence onto PFC may indeed reduce anxiety-like and threat behaviour (Sotres-Bayon et al., 2012). Thus, increased and decreased vH-driven PFC activity has opposite effects on anxiety-like behaviour, with the former leading to increased avoidance and the latter promoting exploration and reducing fear expression. From our findings, deep and superficial layer vH^{PFC} cells exert a predominantly excitatory and inhibitory drive on PFC , respectively (Figure 5.6). Together, these findings led me to hypothesise that activity in the deep vH^{PFC} layer may correlate with increased avoidance during EPM exploration, and that activity in the superficial vH^{PFC} layer may have the opposite effect, promoting open arm exploration via an anxiolytic effect of PFC inhibition.

Overall, the characterisation of the vH-PFC pathway presented in this chapter suggests that the relative excitatory and inhibitory effects of deep and superficial layer vH^{PFC} activity respectively bias exploratory behaviour. However, to confirm this assumption, *in vivo* calcium imaging of prefrontal interneurons and pyramidal cells may be necessary in future to show that the observed differences in superficial and deep vH-PFC circuitry underlie the opposite behavioural outcomes observed during *in vivo* axonal stimulation.

Superficial and deep layer vH terminals differentially target fast spiking and non-fast spiking interneurons in PFC

It has been shown that different interneuron classes in PFC, which are targeted by vH terminals, mediate different aspects of behaviour (Cummings and Clem, 2020; Abbas et al., 2018; Marek et al., 2018a; Muñoz et al., 2017). Fast-spiking PV+ interneurons mainly target pyramidal cell bodies and inhibit prefrontal output, while non fast-spiking SOM+ interneurons target pyramidal cell dendrites, interfering with dendritic integration of afferent inputs, and can also mediate prefrontal disinhibition by silencing PV+ interneurons (Marek et al., 2018a; Cummings and Clem, 2020; Xu et al., 2019; McGarry and Carter, 2016; Yavorska and Wehr, 2016). Furthermore, a different subclass of non-fast spiking interneurons that express vasoactive intestinal polypeptide (VIP) mediates both feed-forward inhibition and disinhibition in cortex by contacting pyramidal neurons and inhibiting both PV+ and SOM+ interneurons (Garcia-Junco-Clemente et al., 2017; Muñoz et al., 2017; Lee et al., 2013).

In order to further understand the specific targeting of cells in PFC by superficial and deep layer vH axons, I studied their relative input onto different classes of interneurons *in vitro* (Figure 5.9) and found that cells in both layers of the vH-PFC projection differentially recruited interneuron classes. Specifically, I saw that the enhanced inhibitory drive from superficial layer vH cells seen in Figure 5.6 onto PFC pyramidal cells was mediated by superficial vH axons contacting both soma-targeting (fast-spiking) and dendrite-targeting (non fast-spiking) interneurons. Cells in the deep layer preferentially contacted fast-spiking interneurons, with minimal input onto non-fast spiking interneurons (Figure 5.9). This suggests that in contrast to cells in the deep vH^{PFC} layer, which seem to exclusively target fast-spiking soma-targeting interneurons, superficial layer cells may interfere with both integration of inputs via feedforward dendritic inhibition as well as with the firing of action potentials in prefrontal pyramidal cells via feedforward somatic inhibition (Kvitsiani

et al., 2013).

There are many roles associated with non-fast spiking SOM+ interneurons which both conflict and align with our finding that superficial layer activation (and thus recruitment of non-fast spiking interneurons; Figure 5.9) leads to a reduction in avoidance behaviour. In contradiction to our findings, activation of SOM+ interneurons specifically in PFC has been shown to induce freezing and avoidance during fear conditioning, potentially via the inhibition of PV+ interneurons and resulting cortical disinhibition (Cummings and Clem, 2020; Xu et al., 2019). However, it is important to note that these SOM-specific effects are only seen in previously fear-conditioned, but not in naive mice, suggesting that SOM+ output is learning dependent (Khan et al., 2018). Thus, their targeting by superficial layer axons may reflect the ability of this layer in the vH-PFC projection to utilise learned associations to guide behaviour. The avoidance or fear-promoting effect of SOM+ interneuron activation reported by these studies is mediated by a disinhibition of cortical output. However, I observed an overall bias towards inhibitory input onto prefrontal pyramidal cells in response to superficial layer axon stimulation *in vitro* (Figure 5.6), suggesting that different mechanisms may be at play here. Thus, as discussed above, it would be of interest to record PFC pyramidal cell population activity *in vivo* during vH superficial layer terminal stimulation in order to clarify whether the inhibitory drive observed *in vitro* is recapitulated during exploratory behaviour and may explain the behavioural observations presented in this chapter.

SOM+ interneurons have also been shown to be recruited by vH terminals to mediate spatial memory (Abbas et al., 2018), to display opposing activity patterns during whisking behaviour dependent on the cortical layer they occupy (Muñoz et al., 2017) and to support sociosexual behaviour in female mice (Nakajima et al., 2014) suggesting that they can adopt different roles and functions dependent on location and task demands. In line with the results showing that superficial layer stimulation drives a reduction in avoidance behaviour (Figure 5.11), acute inhibi-

tion of SOM+ interneuron activity in cortex has been shown to increase anxiety-like behaviour (Soumier and Sibille, 2014). Thus, perhaps different mechanisms may be implemented by SOM+ interneurons to increase or decrease overall PFC activity dependent on behavioural context. Overall, SOM+ interneuron activity has been associated with a vast variety of behaviours and further investigation to understand whether superficial layer vH axonal stimulation recruits them for a feed-forward inhibitory or specific disinhibitory purpose may aid in clarifying their role during EPM exploration. Our data suggests that vH might recruit SOM+ interneurons at the decision point of avoidance or exploration of EPM open arms to reduce prefrontal activity via feed-forward inhibition and thus anxiety-like behaviour, promoting exploration.

Fast-spiking PV+ interneurons have also been studied in the context of a variety of behaviours from avoidance and fear expression to reward seeking behaviour and adaptation to rule shifting (Kvitsiani et al., 2013; Courtin et al., 2014; Cho et al., 2020; Lee et al., 2014b). My results show that while both the superficial and deep vH layers contact PV+ interneurons in PFC, deep layer vH cells provide inhibition onto PFC almost exclusively via PV+ interneurons (Figure 5.9). As for non-fast-spiking interneurons, from the data presented in this chapter I cannot conclude whether superficial and deep layer vH terminals recruit fast-spiking PV+ interneurons into similar circuit motifs. Further investigation and *in vivo* recordings of PFC activity during vH deep and superficial layer stimulation may aid in clarifying these outstanding questions. However, from the available literature, some hypotheses can be drawn.

Interestingly, ablation of NMDA receptors from and thus silencing of PV+ interneurons in the hippocampus has been shown to disrupt hippocampal theta oscillations (Korotkova et al., 2010). Additionally, in contrast to the classical role of PV+ interneurons in promoting gamma frequency oscillations (Buzsáki and Wang, 2012; Cardin et al., 2009; Ferguson and Gao, 2018), it has recently been shown

that PV+ interneurons preferentially promote synchronisation of spikes at theta frequencies in PFC as well (Jang et al., 2020). Thus, prefrontal PV+ interneuron activity may support theta synchrony in the vH-PFC pathway and hence mediate anxiety-like avoidance behaviour (Adhikari et al., 2010; Padilla-Coreano et al., 2016). Perhaps, distinct interneuron subtypes have frequency-selective roles within the vH-PFC pathway. Thus, a possible mechanism underlying deep layer vH^{PFC} terminal stimulation-induced avoidance behaviour may be the specific recruitment of PV+ prefrontal interneurons (Figure 5.9) which in turn increase theta-synchrony between vH and PFC, leading to increased avoidance behaviour (Adhikari et al., 2010; Padilla-Coreano et al., 2019). In line with this hypothesis, prefrontal PV+ interneuron recruitment by vH terminals has been shown to counter fear extinction and promote fear relapse such that *in vivo* silencing of vH terminals reduced fear behaviour.

Overall, these findings suggest that the preferential recruitment of PV+ interneurons in PFC by deep layer vH axons may facilitate the increase in avoidance behaviour seen during optogenetic activation of deep layer axons (Figure 5.11) possibly in part by increasing theta synchrony between vH and PFC. Importantly, distinct behaviours may result from the engagement of different PV+ to SOM+ interneuron ratios at different time points, and the same class of interneuron may have opposing roles for different behaviours (Xu et al., 2019; Kvitsiani et al., 2013; Khan et al., 2018; Cho et al., 2020).

In addition to classic PV+ and SOM+ interneurons there is another class of interneurons that is less studied but has received a lot of recent interest. Soma-targeting non-fast spiking vasoactive intestinal polypeptide (VIP) positive interneurons in PFC, which are classically involved in disinhibition (Pi et al., 2013), have also been shown to be targeted by ventral hippocampal terminals (Lee et al., 2019a). vH input onto prefrontal VIP+ interneurons leads to disinhibition of pyramidal cells, increasing overall vH-PFC synchrony and promoting avoidance behaviour during

EPM exploration (Lee et al., 2019a). In accordance with their facilitatory role in vH-driven avoidance behaviour, prefrontal VIP+ interneuron inhibition leads to a dampening of vH excitatory drive on PFC and an increase in open arm exploration (Lee et al., 2019a). Furthermore, activity in VIP+ interneurons has been shown to suppress SOM+ interneurons (Pi et al., 2013). Although our data does not allow for robust discrimination of these interneuron types, it would be of interest to determine whether the vH terminals targeting VIP+ interneurons in PFC originate primarily from deep-layer cells (deep layer cells target non-fast spiking interneurons to a small extent; Figure 5.9). Not only would this align with our behavioural data, but it would additionally be a mechanism for suppressing SOM+ interneurons, further reducing superficial layer influence on PFC by counteracting their drive of non-fast spiking (potentially SOM+) interneurons. Thus, deep-layer vH cells targeting VIP+ interneurons in PFC could be a potential mechanism to reinforce the push-pull nature of the vH-PFC circuit. In summary, the disinhibition of prefrontal pyramidal cells via VIP+ interneurons, the vH-PFC synchronisation and the control of cortical gain via PV+ interneurons (Lee et al., 2019a; Kvitsiani et al., 2013; Atallah et al., 2012) may underlie part of the function of deep layer vH input to PFC during EPM exploration. Conversely, superficial layer terminals may avoid VIP+ interneurons and instead modulate the inputs and outputs of a subset of pyramidal PFC cells, modulating vH-PFC in a task-specific manner and shutting down prefrontal anxiogenic representations via SOM+ and PV+ mediated inhibition of specific projection populations (Abbas et al., 2018; Xu et al., 2019; Courtin et al., 2014; Marek et al., 2018a).

Superficial and deep layer vH input onto PFC drives opposite behaviours during EPM exploration

To test the hypothesis discussed above that the superficial and deep layer vH^{PFC} subpopulations may bidirectionally modulate anxiety-like behaviour during EPM exploration, we stimulated axon terminals in PFC originating from each layer sep-

arately during an EPM exploration task. We found that, in line with our hypothesis, stimulation of superficial layer vH axons promoted exploration of the open arms, while deep layer axonal stimulation promoted the opposite behaviour, such that mice avoided the open arms and spent more time in the safer, closed arms (Figure 5.11). Although activity in the vH-PFC projection is associated with increased avoidance behaviour (Adhikari et al., 2010; Padilla-Coreano et al., 2016), our observation was that activity in a subset of the vH-PFC projection (the superficial layer) leads to reduced avoidance behaviour. This suggests that it is not only through inactivation of the vH-PFC pathway that anxiety-like behaviours are reduced as was previously thought (Padilla-Coreano et al., 2016; Jimenez et al., 2018), but rather that there are inhibitory and excitatory subcircuits within the vH-PFC pathway that independently exert control over the decision to explore or avoid threatening parts of the environment.

Overall, my findings support the idea that in addition to a strong excitatory vH input onto PFC that promotes avoidance behaviour (Padilla-Coreano et al., 2019), there is a separate vH input that promotes approach, that comes from the superficial layer. There is support for this idea from studies examining the overall activity of the superficial vH (non-projection specific) neurons. Activation of non-projection specific superficial, *Calbindin1*-positive ventral CA1 neurons has been shown to mediate approach behaviour while activating deep layer *Calbindin1*-negative cells promotes avoidance behaviour (Pi et al., 2020). The fact that stimulation of *Calbindin1*+ cells has been seen to promote approach behaviour despite making up a large proportion of the PFC projection suggests that the vH^{PFC} projection population not only actively mediates avoidance behaviour as previously thought, but in line with our findings (Figure 5.11), also plays an active role in mediating approach behaviour.

The presence of two vH-PFC subcircuits may also help explain the difficulty in producing a gain-of-function manipulation for the vH-PFC projection. Recent

work has focused on studying the physiological and behavioural effects of vH terminal activation in PFC with light stimulation oscillating at theta frequency (8 Hz) versus pulses of light (Padilla-Coreano et al., 2019), as theta synchrony between vH and PFC is known to increase in anxiogenic environments and promote avoidance of open arms (Adhikari et al., 2010; Padilla-Coreano et al., 2016). In line with previous studies, the 8Hz oscillatory stimulation protocol implemented by Padilla-Coreano et al. (2019) led to avoidance behaviour during EPM exploration. However, it produced postsynaptic response amplitudes in prefrontal pyramidal cells unlikely to elicit action potentials. Thus, this protocol is likely to fail in engaging feedforward inhibition due to a lack of vH-driven action potential firing in interneurons. This scenario would align with deep-layer vH^{PFC} terminal stimulation, which is biased towards exciting PFC circuitry and drives avoidance *in vivo* (Figures 5.6 and 5.11).

Interestingly, deep layer hippocampal neurons have been shown to be theta-modulated (de la Prida, 2020) and from our CRACM data, receive preferential input from theta modulated regions like anterior thalamus and medial septum/DBB (Figures 4.6 and 4.7). As discussed above, deep layer cells preferentially recruit PV+ interneurons in PFC (Figure 5.9) and PV+ interneurons in PFC have been shown to promote spike synchronisation at theta frequency (Jang et al., 2020). Together, these findings add support to the notion that deep layer cells may indeed recruit PV+ interneurons during theta synchrony to drive avoidance behaviour. Overall, it seems that the behavioural data presented here is supported by and complements experiments carried out in other labs but also adds detail and complexity to the vH-PFC pathway by highlighting its previously overlooked segregation into two layers. It would be of interest to investigate the effects of superficial and deep layer vH axonal stimulation in PFC at different frequencies and oscillations to discern whether both layers synchronise with PFC at theta or whether this property is unique to the deep vH layer.

In summary, the results presented in this chapter suggest that the two sub-

populations within the vH-PFC pathway form a push-pull circuit where superficial vH neurons inhibit PFC circuitry via broad recruitment of local interneurons and promote exploration, while deep layer neurons activate PFC via more robust direct recruitment of pyramidal neurons and promote avoidance behaviour.

Caveats and limitations - prefrontal heterogeneity

Although the finding that vH control over PFC circuitry is segregated across two subpopulations adds to the mechanistic understanding of the vH-PFC pathway, there are aspects of prefrontal heterogeneity beyond the scope of this thesis that could be investigated.

Different areas of PFC, namely IL and PL PFC have been associated with mediating fear extinction and fear conditioning, respectively (Marek et al., 2018a,b; Milad and Quirk, 2002; Sierra-Mercado et al., 2011; Mukherjee and Caroni, 2018). Silencing the vH impairs both extinction and expression of fear (Sierra-Mercado et al., 2011), suggesting that the two layers of the hippocampal-PFC projection may be differentially involved in the expression of conditioned and extinguished fear as well. Although we did not observe differential targeting of IL and PL by axons from both layers of the vH-PFC projection (Figure 5.2), recent reports looking more closely at vH axonal distribution in PFC have observed differential innervation of layers II/III and V by vH terminals in IL and PL (Liu and Carter, 2018). Thus, I cannot dismiss the possibility that more specific analysis may reveal differences in laminar and cellular targets of vH terminals from the two layers. Prefrontal pyramidal cells with distinct dowsntream targets are known to occupy specific cell layers. Thus, it is possible that superficial and deep vH^{PFC} terminals may differentially target prefrontal projection populations with distinct long-range and/or local connectivity. For example vH input onto IL PFC has been shown to selectively inhibit amygdala-projecting and to preferentially excite cortico-cortical projecting pyramidal cells in both IL and PL (Marek et al., 2018a; Liu and Carter, 2018). However,

the lack of vH axonal terminals observed by Liu and Carter (2018) in layer II/III of PL PFC suggests that superficial-layer residing amygdala-projecting cells are only recruited by vH terminals in IL, but not PL PFC (Gabbott et al., 2005). More in depth analysis of axonal terminals from the two vH layers in PFC combined with CRACM onto projection-identified prefrontal pyramidal cells may aid in clarifying yet unidentified differences in post-synaptic targeting.

In addition to the potential heterogeneity in projection target of prefrontal pyramidal cells recruited by vH afferents, the interneurons targeted by vH axons originating from superficial and deep layers may also engage in different local circuits or target distinct downstream areas. Namely, specific interneuron classes have been shown to silence neighbouring pyramidal cells based on their projection targets (Lee et al., 2014a,c; Lu et al., 2017; Marek et al., 2018a; Gittis et al., 2010). Furthermore prefrontal PV+ interneurons have been shown to directly project to NAc to promote avoidance behaviour (Lee et al., 2014b) and it is possible that different long-range projecting inhibitory interneurons are targeted by superficial and deep vH^{PFC} cells. Thus, superficial and deep vH input onto both prefrontal excitatory pyramidal cells and inhibitory interneurons may be wired in accordance with their downstream targets and effect their opposite behavioural roles during EPM exploration via excitation or feed-forward inhibition of distinct prefrontal projection populations. Projection-defined circuit investigation in PFC will be necessary to determine the downstream brain areas involved in bringing about vH^{PFC}-driven behaviour during EPM exploration.

Chapter 6

General Conclusions

6.1 Summary

Throughout this thesis, I have presented experiments that highlight the unique characteristics of the ventral hippocampus to prefrontal cortex pathway. My interest in this pathway stems from its implication in a wide variety of affective disorders, as well as the lack of clarity on the microcircuitry linking the two brain structures - particularly in relation to the ventral hippocampus and its pyramidal cells, which project onto the PFC. Initially, the questions this thesis set out to answer were: what are the characteristics of PFC-projecting pyramidal cells in vH and what local and long-range connectivity are they involved in? Whilst pursuing this line of research, I observed that the projection consisted of two distinct cell layers, with different transcriptomic profiles, anatomical positions within the vH, electrophysiological and morphological properties (Chapter 3). Because of these observations, the central question of the thesis expanded to: what is the functional and behavioural purpose of having two separate layers within the ventral hippocampal PFC-projecting population and how does this fit with what is currently known about this pathway? Throughout Chapters 4 and 5 I addressed these questions. In Chapter 4, I studied

the afferent inputs onto PFC-projecting vH cells and their local connectivity with interneurons. I found that cells in the superficial layer of the vH-PFC projection are preferentially modulated by entorhinal cortical inputs, while deep layer cells receive subcortical inputs from anterior thalamic and diagonal band of Broca regions. In Chapter 5, I studied the separate influence of superficial and deep layer terminal stimulation on PFC circuitry *in vitro* and *in vivo*, during exploratory behaviour on the elevated plus maze. These experiments led to the conclusions that the two separate layers within the vH-PFC projection are utilised to bidirectionally modulate PFC activity with superficial layer stimulation providing predominantly feedforward inhibition onto PFC and deep layer stimulation resulting in a robust excitatory drive. Behaviourally, activation of the two layers had opposite effects on the decision to explore anxiogenic environments, with superficial layer stimulation leading to increased exploration of the open arms in the EPM and deep layer stimulation resulting in increased anxiety-like avoidance behaviour. Throughout this discussion, I will comment on the implications of these findings and what they may clarify regarding the role of cellular heterogeneity within brain circuits.

6.2 Discussion

There is much literature describing the heterogeneity of hippocampal pyramidal cells (Witter et al., 1990; Tannenholz et al., 2014; Strange et al., 2014; Fanselow and Dong, 2010; Soltesz and Losonczy, 2018; Cembrowski et al., 2018b; Thompson et al., 2008; Cembrowski and Spruston, 2019). However, it is unknown what features of heterogeneity are most important within brain circuits or which impinge on behavioural roles associated with a given population of cells. For example, there are different potential roles associated with superficial and deep layer cells in the hippocampus (Valero et al., 2015; Slomianka et al., 2011; Li et al., 2017; Soltesz and Losonczy, 2018) as well as a growing body of research focusing on characterising the connectivity, cellular characteristics and behavioural function of projection-specific neurons (Wee and MacAskill, 2020; Kim and Spruston, 2012;

Xu et al., 2016; Jimenez et al., 2018; Phillips et al., 2019; Padilla-Coreano et al., 2019; Ciocchi et al., 2015). However, it is not well understood how different levels of heterogeneity covary and uniquely inform circuit function.

Overall, my aim with this thesis was to shed light on the heterogeneity within the vH^{PFC} projection population and its functional consequences. Especially, I was interested in investigating how projection-specific characteristics and the lamina-specific properties of cells in the different superficial and deep hippocampal layers segregated across the two PFC-projection subpopulations. Due to the anatomical distribution of this particular pathway, both of these properties covary in vH^{PFC} cells in a unique fashion. Studying the covariance of different properties along the hippocampal axes and across different projection populations may help in understanding a more general pattern of how heterogeneity may be used to confer different functions within other brain areas. In fact, it is argued that the heterogeneity seen within hippocampal cell types is likely to be a general feature of the mammalian brain (Cembrowski and Spruston, 2019). Thus, I believe that the vH-PFC pathway may serve as a useful model to study the impingement of cellular heterogeneity on circuit function.

There are a plethora of functions associated with the vH-PFC projection, as well as many studies describing properties that are characteristic of cells along the superficial - deep (radial) axis of the hippocampus. The latter have led to hypotheses about parallel streams of information processing from the hippocampal formation (Slomianka et al., 2011; Soltesz and Losonczy, 2018). In the following sections, I will discuss the published data and general consensus on both vH-PFC function and parallel processing from hippocampus as an emergent property of hippocampal heterogeneity. I will interpret possible overarching functions of the superficial and deep vH PFC-projecting subpopulations and how these may coexist during behaviour. Throughout the discussion, I will highlight how the data gathered for this thesis may fit into the current models of vH-PFC function and lastly, comment on

the possible roles of vH-PFC heterogeneity in disease.

6.2.1 Heterogeneity of vH^{PFC} neurons along the radial axis

In recent years, the idea that heterogeneity within cell types in the hippocampus may be widespread has taken precedence over the view that cells in a particular region must adhere to a common blueprint. Heterogeneity within cell types has been well-documented across the multiple hippocampal axes (Dong et al., 2009; Slomianka et al., 2011; Graves et al., 2012; Soltesz and Losonczy, 2018; Cembrowski et al., 2016a, 2018b,a; Bienkowski et al., 2018; Cembrowski and Spruston, 2019). For example, cells along the proximo-distal axis of CA1 have been found to be regular firing, involved in path integration (inner representation of cumulated locomotion used to estimate current position) and be more spatially tuned proximally, while cells located more distally exhibit more burst firing, are less spatially tuned and are involved in encoding local landmarks (Knierim et al., 2014; Graves et al., 2012; Jarsky et al., 2008; Henriksen et al., 2010). Interstingly, path integration and landmark-based navigation are also segregated along the radial axis onto superficial and deep layer cells, respectively in covariance with burst firing activity similar to the proximo-distal axis (Fattahi et al., 2018). Cells along the radial axis have also been shown to have different afferent connectivity and differ in electrophysiological properties such as Ih-current and burst-firing (Masurkar et al., 2017; Soltesz and Losonczy, 2018; Jarsky et al., 2008). Thus, heterogeneity along the radial axis may aid in supporting the variety of functions associated with the hippocampus from spatial and non-spatial to emotional and time representations (O'Keefe and Dostrovsky, 1971; MacDonald et al., 2011; Aronov et al., 2017; Jimenez et al., 2018; Ciocchi et al., 2015; Valero and de la Prida, 2018).

The idea that distinct hippocampal domains may underlie distinct types of behaviour is widely accepted, especially owing to observations of segregated input and output streams (Risold and Swanson, 1996; Witter et al., 2000; Tannenholz

et al., 2014). For example, the dorsal hippocampus receives and sends projections to the retrosplenial cortex, which supports its role in spatial navigation and ventral hippocampal cells receive inputs and project to areas involved in emotional and fear behaviour such as the amygdala (Tannenholz et al., 2014; Pikkarainen et al., 1999). Consistent with the segregation of function across hippocampal domains being supported by distinct inputs, I found that superficial and deep PFC-projecting neurons preferentially receive cortical and subcortical inputs, respectively, despite sharing a common target structure (Chapter 4). What is striking about vH^{PFC} cells is that their anatomical segregation into opposite poles of the radial axis (and absence in the intermediate layers) makes the usually graded nature of hippocampal heterogeneity (Cembrowski and Menon, 2018) along the radial axis very stark within this population of cells. This perhaps makes it easier to characterise subgroups within the pathway than for other projection populations that occupy more intermediate regions along axes and don't segregate anatomically, existing rather in a mosaic-like form amongst other neurons. For example, the segregation of vH^{PFC} cells to the superficial and deep layers allowed for targeted, visually-guided recordings that revealed unique electrophysiological and morphological properties of each layer (Chapter 3). Furthermore, we were able to manually separate the two layers for RNA sequencing to elucidate their differential transcriptomic profiles (Figure 3.3). As argued by Cembrowski and Spruston (2019), using anatomical hippocampal axes as a framework makes it easier to register observed heterogeneity along a given hippocampal axis against other published findings, aiding to form a more complete working model of the functional implications of hippocampal heterogeneity.

The data presented in this thesis adds a new dimension to the vH-PFC projection, by considering its previously uninvestigated laminar organisation along the radial axis. Previously, cells in the superficial layer of the hippocampus have been shown to differ to those in deeper layers on many accounts, leading to the formulation of several hypotheses about unique functions of superficial and deep pyramidal

cells. The data in this thesis supports the idea that these properties may also be segregated within the vH-PFC projection.

The emergence of separate layers along the radial axis becomes more apparent towards distal CA1 and subiculum, where the hippocampal cell layer expands from a tight 2 to 3 cell-thick layer throughout the cornu ammonis regions to a less dense 5 to 8 cell-thick layer spanning over 100 μm in width (O'Mara et al., 2001; Andersen et al., 2006; Kim and Spruston, 2012). Cells in the deep layer are born at a developmentally earlier time point than superficial layer cells, they have longer apical dendrites, more complex basal dendritic trees, are more likely to be burst-firing cells, have less of an Ih current component (i.e. less depolarising sag) in response to hyperpolarising current injections and lack the expression of Calbindin and zinc (Soltesz and Losonczy, 2018; Mizuseki et al., 2011; Maroso et al., 2016; Cembrowski and Spruston, 2019; Baimbridge et al., 1991; Slomianka et al., 2011; Sørensen et al., 1995). This is consistent with my data of vH-PFC cells, where I saw longer principal apical dendrites in deep layer cells (Figure 3.7), which fired more bursts than their superficial counterparts and presented with a lower Ih component (Figure 3.5). Cells in the superficial pole of the radial axis are born at a later developmental time point, present a larger Ih current component, express cannabinoid receptors, Calbindin and zinc, and are less coupled by gap junctions than deep cells (Britanova et al., 2008; Ishihara and Fukuda, 2016; Slomianka et al., 2011; Celio, 1990; Valero et al., 2015; Mercer et al., 2006; Geiller et al., 2017b). My data suggests that there is a previously overlooked population of superficial cells in the vH-PFC projection, that fits with this description.

Interestingly, the connectivity data presented in Chapter 4 shows some similarities in superficial and deep connectivity with that of published differences in neocortical superficial and deep layers. For instance, cells in the deeper layer in the CA1 / subiculum area both receive (Figure 4.6) and project (Ishizuka, 2001) to anterior thalamus while cells in the superficial layer preferentially receive (Figure

4.5; Masurkar et al. (2017) and project (Honda and Ishizuka, 2015) to cortical areas. In neocortex, superficial layer cells are also biased towards cortico-cortical communication and away from subcortical communication, which is carried out by cells in deeper layers (Akers and Killackey, 1978; Kawaguchi, 2017; Slomianka et al., 2011). This suggests that there may be common organising principles in both vH and cortex, and that the heterogeneity observed along the radial axis in hippocampus may perhaps support similar roles across other layered brain structures.

Hippocampal superficial and deep pyramidal cells have also been shown to differ in their engagement with local inhibitory circuitry. As discussed in Chapter 4, superficial pyramidal cells have been seen to provide more excitation onto local PV+ interneurons that in turn inhibit deep cells to a larger extent (Lee et al., 2014c). Especially interesting in this context is the observation that within the PFC-projecting population (and in contrast to non-PFC projecting neurons) layer-specific inhibitory biases did not emerge (Figures 4.8 and 4.9). As discussed in previous chapters, this suggests that cellular and circuit characteristics may covary along the hippocampal axes in unique ways dependent on projection-target specificity, where on occasion the common projection target of cells may override existing property gradients and when appropriate, the local heterogeneity will be adopted regardless of projection target.

Functionally, superficial and deep layer pyramidal cells in the CA1 / subiculum area are associated to a varying extent with specific events. For example, during sharp-wave-ripples (SWR; oscillations crucial for memory encoding) superficial cells are engaged, while deep cells are mostly inhibited (Valero et al., 2015). Temporally precise interactions between hippocampal excitatory pyramidal cells and local interneurons supports ripple generation (Stark et al., 2014) and thus, it is highly probable that layer-specific patterns of inhibition may influence the role played by neurons in each layer in such events. Furthermore, cells in the two layers are used differently during associative learning, where superficial but not deep layer cells

have been shown to be required for learning in an olfactory task (Li et al., 2017), suggesting that cells in both layers may be involved in different aspects of learning. In spatial navigation tasks, it has been observed that superficial CA1 cells use different mechanisms to deep CA1 cells to infer spatial position, resulting in the encoding of a more global position representation in superficial cells, while cells in the deep layer integrate sensory information on an object-specific basis (Fattahi et al., 2018). Additionally, during spatial navigation, cells in the superficial layer have been shown to form fewer place fields (Mizuseki et al., 2011; Geiller et al., 2017b) and represent salient features in the environment less flexibly than their deep counterparts (Danielson et al., 2016). Place maps encoded in deep pyramidal cells remap to a greater degree when cues in the environment are altered than superficial place maps in the same environment (Danielson et al., 2016). My data suggests that these properties may also be split within the vH-PFC projection. For instance, the higher bursting activity observed in deep layer neurons (Figure 3.5) makes them better subjects to undergo synaptic plasticity and may underlie their flexibility during behaviour compared to superficial cells creating more rigid representations. This example of radial variation in the stability of representations further points in the direction that the hippocampus may utilise heterogeneity to convey distinct types of information - stable maps in superficial layers and flexible, up-to-date representations of relevant, task-related information in deep layers. In other words, it is possible that superficial cells may encode the 'rule' of the task at hand, while deep layer cells may more flexibly and constantly update information relevant to the task at hand dependent on e.g. emotional state or changes in the environment. Such flexible updating of task-relevant features may in turn inform of changes in contingencies to update the 'rule'. This concept has been explored, showing that there are rigid and plastic cell-types in the hippocampus that encode memories in different ways, albeit it was not tested in a laminar and projection specific manner but rather based on firing properties (Grosmark and Buzsáki, 2016).

In summary, it is interesting to think about the two PFC-projecting vH cell

layers within such a framework. Specifically for the vH-PFC pathway, it may be that cortical information provides input to superficial layer cells, which in turn relay more rigid and rule-like representations of a given task to PFC to inform decision-making, while subcortical, flexible, salience and emotionally-modulated activity provides input onto deep layer cells, which in turn can fine-tune how PFC follows a given rule. With this in mind it is interesting to note that the role of vH-PFC circuitry has classically been investigated using SWRs and theta synchrony as a means of inferring connectivity. Studies focused on SWRs (thought to mainly occur in the superficial layers) (Valero et al., 2015) are focused on a role in predictive decision making behaviour (Tang et al., 2017; Joo and Frank, 2018), while studies focused on theta oscillations (thought to mainly occur in the deep layers) (de la Prida, 2020) focus on a role in avoidance behaviour (Padilla-Coreano et al., 2019; Adhikari et al., 2010). Furthermore, the vH-PFC pathway has been associated with opposing roles during the expression and extinction of fear (Marek et al., 2018a; Sotres-Bayon et al., 2012). This suggests that the conflicting roles of the vH-PFC projection may be encoded by the different layers identified in the pathway. The vH-PFC projection may thus be a prime example of how broad heterogeneity within cell types may be an efficient way of driving functional diversity in a circuit, carrying out multiple and distinct computations via the 'same' circuitry.

6.2.2 Heterogeneity of vH^{PFC} neurons might explain contrasting roles during avoidance behaviour

Functionally, vH-PFC pathway activity has been associated with increased anxiety-like and avoidance behaviour. Theta synchrony between vH and PFC has been shown to increase in anxiogenic environments such as the EPM, especially when the animal is exploring the closed (relatively safer) arms (Adhikari et al., 2010) and is thought to be key to driving avoidance of the open arms (Padilla-Coreano et al., 2019). It has been suggested that excitatory vH input to PFC transmits anxiety-related information during exploratory behaviour, such that PFC neurons receiving

vH input host an anxiety representation or representation of an anxiogenic environment (Adhikari et al., 2011; Ciocchi et al., 2015; Lee et al., 2019a) which in turn leads to avoidant behaviour. Consistent with these findings, the experiments presented in Chapter 5 show that excitatory drive in a subset (the deep layer) of the vH-PFC projection increases avoidance of the open arms during EPM exploration. This was not true for stimulation of superficial layer axons, which reduced avoidance behaviour. Thus, if both superficial and deep layer vH cells drive anxiogenic representations in PFC, it would be difficult to explain how increasing superficial layer activity would reduce avoidance behaviour (Figure 5.11).

One way to look at this conundrum would be to consider that superficial and deep layer input may be taking on different roles with regards to information transfer to PFC. In fact, while excitatory vH input onto PFC and vH-PFC theta synchrony have been shown to inhibit exploratory behaviour, overall vH-driven task-related activity in PFC during EPM exploration (thought to encode open arm representations and thus promote avoidance) is negatively correlated with anxiety-like behaviour (Adhikari et al., 2011). This suggests that the increase observed in superficial layer vH^{PFC} cell activity upon open arm entry (Sánchez-Bellot and MacAskill, 2019) may represent this non-anxiety correlated task-related activity. Thus, superficial and deep layer input to PFC may drive different representations. Alternatively, this vH-driven non-anxiety correlated activity during EPM exploration could point at a role for increased superficial layer input in reducing avoidance by silencing deep-layer driven representations of anxiogenic environments like the open arms. Hence, the separation of functions across the two layers of the projection may explain previously conflicting observations. Overall, my data suggests that theta-synchrony related avoidance may be mediated by deep layer cells while feedforward inhibition onto PFC and specific task-related activity negatively correlated with anxiety-behaviour are driven by superficial layer cells to reduce avoidance behaviour.

While I only investigated anxiety-like behaviour directly in this thesis, the

vH-PFC circuit is also associated with fear behaviour, in particular with both the inhibition and the expression of fear extinction (Sotres-Bayon et al., 2012; Marek et al., 2018a). Similar to bidirectional modulation of exploratory behaviour observed in Chapter 5, inhibitory drive in the vH-PFC pathway has been associated with the blockade of fear extinction (Marek et al., 2018a), while excitatory drive onto PFC has been implicated in extinction of fear memories (Peters et al., 2010). Interestingly, inhibitory drive onto distinct prefrontal regions has opposite effects on the expression of extinguished fear (Sotres-Bayon et al., 2012; Marek et al., 2018a). Thus, it seems that the balance of excitatory and inhibitory influence of vH onto specific areas of PFC determines the direction of extinction. This suggests that the expression of conditioned fear and fear extinction might present another scenario in which segregation of roles across the two vH PFC-projecting layers may explain contradicting duties carried out by the apparent same circuitry. It has been shown that silencing of the vH-PFC pathway impairs extinction of fear (Hugues and Garcia, 2007) and that this impairment is mediated by an increase in PFC firing due to lower recruitment of interneurons (Sotres-Bayon et al., 2012). Together, these findings suggest that one role of vH input to PFC is to suppress conditioned responses to previously fear-inducing stimuli (i.e. drive fear extinction) via recruitment of feed-forward inhibition. In contradiction to these findings, Marek et al. (2018a) show that recruitment of prefrontal interneurons prevents fear extinction, leading to a relapse of fear expression. Our data suggests that these two roles may be carried out by the two different layers of vH-PFC neurons recruiting different interneuron subtypes to varying extents, in turn leading to either approach or avoidance of previously fear-inducing environments.

Interestingly, in addition to direct lesions of vH and PFC, lesions to input areas such as the medial septum and DBB, which preferentially drive deep vH^{PFC} cells (Figure 4.7), also impair fear extinction (Kjelstrup et al., 2002; Tronson et al., 2009; Knox and Keller, 2016). One interpretation of these findings is that decreased deep layer activity would result in lower overall excitatory drive into PFC - asso-

ciated with fear relapse (Peters et al., 2010; Milad and Quirk, 2002). However, in Chapter 4, I found that superficial and deep layer PFC-projecting cells engage in strong lateral inhibition. Therefore reduced activation of deep layer vH^{PFC} cells may also lead to a compensatory increased activity in the superficial vH^{PFC} layer. In Chapter 5 I show that this would result in more feedforward inhibition onto PFC. This increase in feedforward inhibition has been shown to be crucial to impair fear extinction (Marek et al., 2018a), providing a separate or complementary interpretation of septal and DBB lesion findings. Thus, the targeting of different interneuron populations or differentially exciting prefrontal circuitry may go beyond mediating anxiety behaviour as it is apparent that behavioural contradictions occur in fear behaviour as well. It will be interesting to investigate if this is the case in future work.

Overall, it is clear that the vH-PFC pathway is involved in seemingly opposing roles during both anxiety-like avoidance and fear behaviour, and that the recruitment of distinct PFC circuitry may underlie these differences. Further understanding of the recruitment of interneurons and projection-specific pyramidal cells in PFC may provide a basis from which to explain discrepancies and circuit-wide implications of e.g. lesions to regions sending afferents to vH. It may also aid in clarifying the anatomical routing of information throughout the vH-PFC pathway during different behaviours. Interestingly, our findings are not in opposition of either of the hitherto explored roles for the vH-PFC projection, but rather provide a mechanism to explain the apparent dual role of the vH-PFC pathway. By segregating the projection into two layers it becomes apparent that the many ascribed functions to the pathway may be spread across its two components, which may be recruited in a task-dependent manner.

6.2.3 vH-PFC heterogeneity and disease

Understanding the different afferent and efferent connectivity of the superficial and deep vH^{PFC} subpopulations allows for the proposition of new hypotheses regarding their involvement in separate circuits and functions. One such hypothesis is that cells in the two layers of the PFC projection population may be differentially affected in models of disease, and in particular in mental illness. Heterogeneity in hippocampal involvement in disease has been studied in other neurological disorders like Alzheimers disease, where disease progression is thought to differentially affect principal cells dependent on their positioning along the hippocampal axes (Masurkar, 2018).

As discussed in Chapter 4, the chronic stress model of depression causes a decrease in excitation at entorhinal to hippocampal TA - CA1 synapses, which can be reversed by chronic antidepressant SSRI treatment to rescue normal behaviour (Kallarackal et al., 2013; Cai et al., 2013). From our data, we see that entorhinal input is biased towards cells in the superficial PFC-projecting layer. Thus, I hypothesised that in a depression model, reduced excitability at TA - CA1 synapses may affect superficial vH^{PFC} output to a greater extent than that of deep vH^{PFC} cells. In fact, ongoing experiments in the lab discussed in the following section have shown that the excitability of superficial layer vH^{PFC} cells is selectively affected following juvenile social isolation (an animal model of depressive behaviour), while deep layer excitability remains unchanged with respect to group-housed controls. Reduced activity in one layer may lead to increased activity in the other, due to reduced lateral inhibition and so it is easy to imagine how relatively small changes in some aspects of circuit activity may affect the overall output of vH cells onto PFC.

The more detailed picture of the circuitry now also allows us to see that deep vH^{PFC} cells, which preferentially drive excitation of PFC pyramidal cells and subsequent avoidance behaviour receive more input from DBB and ATh than their

superficial counterparts. Both the ATh and the medial septum / DBB areas act as pacemakers for the production of hippocampal theta rhythm (Vertes and Kocsis, 1997; Child and Benarroch, 2013; Jankowski et al., 2013; Müller and Remy, 2018). Interestingly, hippocampal theta oscillations are sensitive to serotonergic modulation (Sörman et al., 2011), suggesting that pharmacological intervention - with for example, widely used antidepressant SSRI (selective serotonin reuptake inhibitor) drugs - may modulate both physiological and pathological processes associated with hippocampal theta oscillations. This is an example of how the same treatment may affect activity in the two layers in different ways by affecting their respective afferent connections. Whats more, in-depth knowledge of the vH-PFC circuitry opens further access routes for modulation of prefrontal activity. For example, entorhinal cortex activation may silence PFC, providing anxiolysis while DBB and ATh stimulation may increase theta synchrony between vH and PFC and thus anxiety-like behaviours (Bi et al., 2013; Padilla-Coreano et al., 2019).

Importantly, dysregulation in theta synchrony between hippocampus and PFC is a hallmark of a variety of psychiatric disorders (Sigurdsson et al., 2010; Godsil et al., 2013; Sigurdsson and Duvarci, 2016). Furthermore, disruption in the balance of excitation and inhibition in PFC is closely associated with the transition to mental illness (Gao and Penzes, 2015) and alterations in vH input to PFC are thought to be key for this disruption (Mukherjee et al., 2019; Sigurdsson et al., 2010). Together with the findings presented in this thesis highlighting the differential recruitment of prefrontal circuitry by vH cells in both layers, it seems plausible to hypothesise that superficial and deep vH^{PFC} cells may be uniquely affected in different models of affective disorders and may mediate different associated symptoms. Better understanding of the vH-PFC circuitry may thus help in getting to the root of how one circuit can give rise to many circuitopathies with varying degrees of overlapping symptomatology and how these may be individually addressed.

Synthesis

Overall, the findings presented in this thesis suggest that for the vH-PFC pathway, hippocampal superficial and deep layer-specific characteristics are utilised by the same projection population. This in turn leads to a differential implication in behaviour for cells in the two layers of the projection. In relation to the current knowledge on hippocampal heterogeneity, the data presented in this thesis favours the argument of a parallel processing of information in hippocampus underlying distinct cognitive functions. The utilisation of the existing heterogeneity by the vH-PFC projection population in turn provides a mechanistic basis for multifaceted nature of hippocampal-prefrontal communication in health and disease. The vH-PFC projection may be an example of a more general circuit motif implemented throughout the hippocampus and perhaps other brain structures (Cembrowski and Spruston, 2019).

6.3 Outlook and future experiments

Understanding the circuitry linking ventral hippocampus and PFC in more depth opens up many possibilities to better investigate the role of this pathway in behaviour, both in health and in disease. Although the findings presented in this thesis add a wealth of information to the current knowledge of the vH-PFC circuitry, many questions remain unanswered. In future experiments, I would like to investigate the projection-specificity of pyramidal cells in PFC contacted by axons from superficial and deep vH^{PFC} neurons. These experiments would shed light on the downstream circuitry involved in bringing about the behavioural differences driven by the two vH layers.

Pertaining to circuitry and with the aim to obtain cleaner, less confounded results I would plan to repeat the *in vivo* optogenetic experiments as well as the *in vitro* E/I ratio and interneuron targeting experiments shown in Chapter 5 with a 'Cre-OFF' virus (in *Calb1-Cre* mice) to isolate deep layer cells. A 'Cre-OFF' virus will not be expressed in Cre-recombinase positive cells i.e. *Calb1*-positive cells in the *Calb1-Cre* mouse line. Currently in the lab we are running CRACM experiments using an in-house built Cre-OFF construct: AAV1-EF1α-CreOFF-loxFAS-ChR2(H134R)-EGFP. In this construct, the Cre-OFF FAS vector design uses a ChR2-EGFP transgene flanked by FAS sites such that in the presence of Cre the transgene is excised and thus is not expressed. Alternatively, in Cre-negative cells, the transgene will be expressed. This approach would allow for a cleaner recruitment of deep layer cells on the basis of the absence of *Calbindin1* (Pi et al., 2020), and thus Cre, rather than biasing towards the deep layer population by implementing *CaMKii* promoter dependent viral constructs. These experiments are currently underway and are showing promising results, similar but cleaner than those obtained with the *CaMKii*-dependent approach.

A secondary future outlook and budding sideline of this project is to study

the characteristics of the vH-PFC projection in the context of an affective disorder model. In particular, I have chosen to look at the role of the vH-PFC pathway in a rodent model of early life stress leading to depressive-like symptoms - juvenile social isolation. Juvenile social isolation is often termed chronic social isolation due to the extended timeline of 8 weeks of single housing conditions in comparison to acute social isolation, which ranges from hours to two weeks in isolation. Chronic social isolation is a known risk for depressive illness and is associated with impairments in hippocampal as well as prefrontal function, with reductions in attentional control and memory consolidation and is accompanied by anxiety- and anhedonia-like symptoms (Ibi et al., 2008; Lander et al., 2017; Liston et al., 2009; Wallace et al., 2009; Chang et al., 2015). Importantly, isolation-rearing has been shown to alter activity patterns in prefrontal circuitry during social interaction (Minami et al., 2017). Interestingly, bidirectional changes in excitatory synaptic drive onto PFC pyramidal neurons have been shown to signal susceptibility or resilience to stress such that synaptic strengthening correlates with susceptibility and synaptic weakening correlates with resilience to stress (Wang et al., 2014). Although there is consensus that both the hippocampus and the PFC (and the vH-PFC pathway specifically) are heavily implicated in psychopathological behaviours (Campbell and Macqueen, 2004; Covington et al., 2010; Godsil et al., 2013; Izumi and Zorumski, 2014; Li et al., 2015; Jett et al., 2015; Garcia-Garcia et al., 2017), there is still much debate regarding the underlying circuit mechanisms that bring about the symptomatology of affective disorders and those that underlie remission of symptoms (Cai et al., 2013; Fuchikami et al., 2015; Carreno et al., 2015; Zanos et al., 2016; Yang et al., 2018b; Yun et al., 2018; Hare et al., 2019; Van Dyke et al., 2019). It is known that exposure to chronic stress or to psychostimulant drugs can alter the intrinsic excitability of and the input-specific connectivity of neurons in brain areas implicated in affective behaviour (Cooper et al., 2003; Kallarackal et al., 2013; MacAskill et al., 2014). Therefore, I am interested in investigating the effects of social isolation at this level within the vH-PFC pathway.

To address this question, I have begun looking at the effects of chronic social isolation (8 weeks isolation post-weaning) on the intrinsic excitability of superficial and deep vH^{PFC} neurons. By recording responses in pyramidal cells of the superficial and deep vH^{PFC} layers to current injections, I have observed that in response to equivalent current steps, superficial vH^{PFC} neurons in isolation-reared mice were overall less excitable than group-housed controls. In contrast, excitability in the deep layer cells remained the same in isolation-reared and group-housed mice. These preliminary findings suggest that activity in the superficial layer cells of the vH-PFC projection may be specifically dampened by chronic social isolation. Thus, vH output onto PFC may differ in socially isolated mice leading to an alteration in e.g. exploratory behaviour in anxiogenic environments. Interestingly, it has been shown recently that chronic exposure to stress in rodents leads to a decrease in regular-spiking and an increase in burst-firing activity in the ventral subiculum (Lee et al., 2019b). From our findings, cells in the deep layer of the vH-PFC projection are more burst firing than those in the superficial layer, which are predominantly regular firing (Figure 3.5). Thus, our preliminary results showing a reduction in superficial layer excitability may consequently result in an increase in bursting activity in the subiculum as a compensatory mechanism. It will be interesting to study the wider implications of juvenile social isolation on the vH-PFC circuit as well as exploring whether there may be a node of malfunction in the pathway in affective disorders, or whether there is a more complex, widespread circuitopathy (Spellman and Liston, 2020).

References

Abbas, A. I.; Sundiang, M. J. M.; Henoch, B.; Morton, M. P.; Bolkan, S. S.; Park, A. J.; Harris, A. Z.; Kellendonk, C., and Gordon, J. A. Somatostatin Interneurons Facilitate Hippocampal-Prefrontal Synchrony and Prefrontal Spatial Encoding. *Neuron*, 100(4):926–939.e3, November 2018.

Adhikari, A.; Topiwala, M. A., and Gordon, J. A. Synchronized activity between the ventral hippocampus and the medial prefrontal cortex during anxiety. *Neuron*, 65(2):257–269, January 2010.

Adhikari, A.; Topiwala, M. A., and Gordon, J. A. Single units in the medial prefrontal cortex with anxiety-related firing patterns are preferentially influenced by ventral hippocampal activity. *Neuron*, 71(5):898–910, September 2011.

Adhikari, A.; Lerner, T. N.; Finkelstein, J.; Pak, S.; Jennings, J. H.; Davidson, T. J.; Ferenczi, E.; Gunaydin, L. A.; Mirzabekov, J. J.; Ye, L.; Kim, S.-Y.; Lei, A., and Deisseroth, K. Basomedial amygdala mediates top-down control of anxiety and fear. *Nature*, 527(7577):179–185, November 2015.

Aggleton, J. P. A description of the amygdalo-hippocampal interconnections in the macaque monkey. *Experimental brain research*, 64(3):515–526, 1986.

Aggleton, J. P. and Brown, M. W. Episodic memory, amnesia, and the hippocampal-anterior thalamic axis. *The Behavioral and brain sciences*, 22(3):425–44– discussion 444–89, June 1999.

Aggleton, J. P. and Christiansen, K. The subiculum: the heart of the extended hippocampal system. *Progress in brain research*, 219:65–82, 2015.

Agster, K. L. and Burwell, R. D. Hippocampal and subicular efferents and afferents of the perirhinal, postrhinal, and entorhinal cortices of the rat. *Behavioural brain research*, 254:50–64, October 2013.

Akers, R. M. and Killackey, H. P. Organization of corticocortical connections in the parietal cortex of the rat. *The Journal of comparative neurology*, 181(3):513–537, October 1978.

Amaral, D. G. and Cowan, W. M. Subcortical afferents to the hippocampal formation in the monkey. *The Journal of comparative neurology*, 189(4):573–591, February 1980.

Amaral, D. G. and Witter, M. P. The three-dimensional organization of the hippocampal formation: a review of anatomical data. *Neuroscience*, 31(3):571–591, 1989.

Amaral, D. G.; Dolorfo, C., and Alvarez-Royo, P. Organization of CA1 projections to the subiculum: a PHA-L analysis in the rat. *Hippocampus*, 1(4):415–435, October 1991.

Amat, J.; Baratta, M. V.; Paul, E.; Bland, S. T.; Watkins, L. R., and Maier, S. F. Medial prefrontal cortex determines how stressor controllability affects behavior and dorsal raphe nucleus. *Nature neuroscience*, 8(3):365–371, March 2005.

Anastasiades, P. G.; Boada, C., and Carter, A. G. Cell-Type-Specific D1 Dopamine Receptor Modulation of Projection Neurons and Interneurons in the Prefrontal Cortex. *Cerebral cortex (New York, N.Y. : 1991)*, December 2018a.

Anastasiades, P. G.; Marlin, J. J., and Carter, A. G. Cell-Type Specificity of Callosally Evoked Excitation and Feedforward Inhibition in the Prefrontal Cortex. *Cell reports*, 22(3):679–692, January 2018b.

Andersen, P.; Morris, R.; Amaral, D.; Bliss, T., and O'Keefe, J. *The Hippocampus Book*. Oxford Neuroscience Series. Oxford University Press, 2006.

Anderson, C. T.; Sheets, P. L.; Kiritani, T., and Shepherd, G. M. G. Sublayer-specific microcircuits of corticospinal and corticostriatal neurons in motor cortex. *Nature neuroscience*, 13(6):739–744, June 2010.

Anderson, J. S.; Carandini, M., and Ferster, D. Orientation tuning of input conductance, excitation, and inhibition in cat primary visual cortex. *Journal of neurophysiology*, 84(2):909–926, August 2000.

Anderson, M. C.; Bunce, J. G., and Barbas, H. Prefrontal-hippocampal pathways underlying inhibitory control over memory. *Neurobiology of learning and memory*, 134 Pt A:145–161, October 2016.

Aronov, D.; Nevers, R., and Tank, D. W. Mapping of a non-spatial dimension by the hippocampal-entorhinal circuit. *Nature*, 543(7647):719–722, March 2017.

Artinian, J. and Lacaille, J.-C. Disinhibition in learning and memory circuits: New vistas for somatostatin interneurons and long-term synaptic plasticity. *Brain research bulletin*, 141:20–26, July 2018.

Atallah, B. V.; Bruns, W.; Carandini, M., and Scanziani, M. Parvalbumin-expressing interneurons linearly transform cortical responses to visual stimuli. *Neuron*, 73(1):159–170, January 2012.

Bagot, R. C.; Parise, E. M.; Peña, C. J.; Zhang, H.-X.; Maze, I.; Chaudhury, D.; Persaud, B.; Cachope, R.; Bolaños-Guzmán, C. A.; Cheer, J.; Deisseroth, K.; Han, M.-H., and Nestler, E. J. Ventral hippocampal afferents to the nucleus accumbens regulate susceptibility to depression. *Nature Communications*, 6:7062, May 2015.

Baimbridge, K. G.; Peet, M. J.; McLennan, H., and Church, J. Bursting response to current-evoked depolarization in rat CA1 pyramidal neurons is correlated with

lucifer yellow dye coupling but not with the presence of calbindin-D28k. *Synapse (New York, N.Y.)*, 7(4):269–277, April 1991.

Bannerman, D. M.; Deacon, R. M. J.; Offen, S.; Friswell, J.; Grubb, M., and Rawlins, J. N. P. Double dissociation of function within the hippocampus: spatial memory and hyponeophagia. *Behavioral neuroscience*, 116(5):884–901, October 2002.

Bannerman, D. M.; Grubb, M.; Deacon, R. M. J.; Yee, B. K.; Feldon, J., and Rawlins, J. N. P. Ventral hippocampal lesions affect anxiety but not spatial learning. *Behavioural brain research*, 139(1-2):197–213, February 2003.

Bannerman, D. M.; Rawlins, J. N. P.; McHugh, S. B.; Deacon, R. M. J.; Yee, B. K.; Bast, T.; Zhang, W.-N.; Pothuizen, H. H. J., and Feldon, J. Regional dissociations within the hippocampus–memory and anxiety. *Neuroscience and biobehavioral reviews*, 28(3):273–283, May 2004.

Bannister, N. J. and Larkman, A. U. Dendritic morphology of CA1 pyramidal neurones from the rat hippocampus: I. Branching patterns. *The Journal of comparative neurology*, 360(1):150–160, September 1995.

Barbas, H. and Blatt, G. J. Topographically specific hippocampal projections target functionally distinct prefrontal areas in the rhesus monkey. *Hippocampus*, 5(6): 511–533, 1995.

Barry, C. and Burgess, N. Neural mechanisms of self-location. *Current biology : CB*, 24(8):R330–9, April 2014.

Beer, Z.; Vavra, P.; Atucha, E.; Rentzing, K.; Heinze, H.-J., and Sauvage, M. M. The memory for time and space differentially engages the proximal and distal parts of the hippocampal subfields CA1 and CA3. *PLoS biology*, 16(8):e2006100, August 2018.

Beierlein, M. Chapter 17 - Cable Properties and Information Processing in Dendrites. In Byrne, J. H.; Heidelberger, R., and Waxham, M. N., editors, *From*

Molecules to Networks (Third Edition), pages 509–529. Academic Press, Boston, 2014.

Belforte, J. E.; Zsiros, V.; Sklar, E. R.; Jiang, Z.; Yu, G.; Li, Y.; Quinlan, E. M., and Nakazawa, K. Postnatal NMDA receptor ablation in corticolimbic interneurons confers schizophrenia-like phenotypes. *Nature neuroscience*, 13(1):76–83, January 2010.

Belzung, C. and Griebel, G. Measuring normal and pathological anxiety-like behaviour in mice: a review. *Behavioural brain research*, 125(1-2):141–149, November 2001.

Benchenane, K.; Peyrache, A.; Khamassi, M.; Tierney, P. L.; Gioanni, Y.; Battaglia, F. P., and Wiener, S. I. Coherent theta oscillations and reorganization of spike timing in the hippocampal- prefrontal network upon learning. *Neuron*, 66(6): 921–936, June 2010.

Berg, L.; Eckardt, J., and Masseck, O. A. Enhanced activity of pyramidal neurons in the infralimbic cortex drives anxiety behavior. *PloS one*, 14(1):e0210949, 2019.

Bertram, E. H. and Zhang, D. X. Thalamic excitation of hippocampal CA1 neurons: a comparison with the effects of CA3 stimulation. *Neuroscience*, 92(1):15–26, 1999.

Best, P. J.; White, A. M., and Minai, A. Spatial processing in the brain: the activity of hippocampal place cells. *Annual review of neuroscience*, 24:459–486, 2001.

Beyeler, A.; Namburi, P.; Glober, G. F.; Simonnet, C.; Calhoon, G. G.; Conyers, G. F.; Luck, R.; Wildes, C. P., and Tye, K. M. Divergent Routing of Positive and Negative Information from the Amygdala during Memory Retrieval. *Neuron*, 90 (2):348–361, April 2016.

Bi, L.-L.; Wang, J.; Luo, Z.-Y.; Chen, S.-P.; Geng, F.; Chen, Y.-h.; Li, S.-J.; Yuan, C.-h.; Lin, S., and Gao, T.-M. Enhanced excitability in the infralimbic cortex

produces anxiety-like behaviors. *Neuropharmacology*, 72:148–156, September 2013.

Bicks, L. K.; Koike, H.; Akbarian, S., and Morishita, H. Prefrontal Cortex and Social Cognition in Mouse and Man. *Frontiers in psychology*, 6:1805, 2015.

Bienkowski, M. S.; Bowman, I.; Song, M. Y.; Gou, L.; Ard, T.; Cotter, K.; Zhu, M.; Benavidez, N. L.; Yamashita, S.; Abu-Jaber, J.; Azam, S.; Lo, D.; Foster, N. N.; Hintiryan, H., and Dong, H.-W. Integration of gene expression and brain-wide connectivity reveals the multiscale organization of mouse hippocampal networks. *Nature neuroscience*, 21(11):1628–1643, November 2018.

Bischofberger, J.; Engel, D.; Li, L.; Geiger, J. R. P., and Jonas, P. Patch-clamp recording from mossy fiber terminals in hippocampal slices. *Nature protocols*, 1 (4):2075–2081, 2006.

Blanchard, R. J. and Blanchard, D. C. An ethoexperimental analysis of defense, fear, and anxiety. *Otago conference series*, (1):124–133, 1990.

Böhm, C.; Peng, Y.; Maier, N.; Winterer, J.; Poulet, J. F. A.; Geiger, J. R. P., and Schmitz, D. Functional Diversity of Subicular Principal Cells during Hippocampal Ripples. *The Journal of neuroscience : the official journal of the Society for Neuroscience*, 35(40):13608–13618, October 2015.

Brady, A. M.; Saul, R. D., and Wiest, M. K. Selective deficits in spatial working memory in the neonatal ventral hippocampal lesion rat model of schizophrenia. *Neuropharmacology*, 59(7-8):605–611, December 2010.

Britanova, O.; de Juan Romero, C.; Cheung, A.; Kwan, K. Y.; Schwark, M.; Gyorgy, A.; Vogel, T.; Akopov, S.; Mitkovski, M.; Agoston, D.; Sestan, N.; Molnár, Z., and Tarabykin, V. Satb2 is a postmitotic determinant for upper-layer neuron specification in the neocortex. *Neuron*, 57(3):378–392, February 2008.

Broadbent, N. J.; Squire, L. R., and Clark, R. E. Spatial memory, recognition

memory, and the hippocampus. *Proceedings of the National Academy of Sciences of the United States of America*, 101(40):14515–14520, October 2004.

Brumberg, J. C.; Nowak, L. G., and McCormick, D. A. Ionic mechanisms underlying repetitive high-frequency burst firing in supragranular cortical neurons. *The Journal of neuroscience : the official journal of the Society for Neuroscience*, 20 (13):4829–4843, July 2000.

Buzsáki, G. Theta oscillations in the hippocampus. *Neuron*, 33(3):325–340, January 2002.

Buzsáki, G. and Wang, X.-J. Mechanisms of gamma oscillations. *Annual review of neuroscience*, 35(1):203–225, 2012.

Cai, X.; Kallarackal, A. J.; Kvarta, M. D.; Goluskin, S.; Gaylor, K.; Bailey, A. M.; Lee, H.-K.; Huganir, R. L., and Thompson, S. M. Local potentiation of excitatory synapses by serotonin and its alteration in rodent models of depression. *Nature Neuroscience*, 16(4):464–472, March 2013.

Calhoon, Gwendolyn G, and Tye, Kay M, . Resolving the neural circuits of anxiety. *Nature Neuroscience*, 18(10):1394–1404, October 2015.

Campbell, S. and Macqueen, G. The role of the hippocampus in the pathophysiology of major depression. *Journal of psychiatry & neuroscience : JPN*, 29(6): 417–426, November 2004.

Canetta, S.; Bolkan, S.; Padilla-Coreano, N.; Song, L. J.; Sahn, R.; Harrison, N. L.; Gordon, J. A.; Brown, A., and Kellendonk, C. Maternal immune activation leads to selective functional deficits in offspring parvalbumin interneurons. *Molecular Psychiatry*, 21(7):956–968, July 2016.

Canteras, N. S. and Swanson, L. W. Projections of the ventral subiculum to the amygdala, septum, and hypothalamus: a PHAL anterograde tract-tracing study in the rat. *The Journal of comparative neurology*, 324(2):180–194, October 1992.

Cardin, J. A.; Carlén, M.; Meletis, K.; Knoblich, U.; Zhang, F.; Deisseroth, K.; Tsai, L.-H., and Moore, C. I. Driving fast-spiking cells induces gamma rhythm and controls sensory responses. *Nature*, 459(7247):663–667, June 2009.

Carr, D. B. and Sesack, S. R. Hippocampal afferents to the rat prefrontal cortex: synaptic targets and relation to dopamine terminals. *The Journal of comparative neurology*, 369(1):1–15, May 1996.

Carreno, F. R.; Donegan, J. J.; Boley, A. M.; Shah, A.; DeGuzman, M.; Frazer, A., and Lodge, D. J. Activation of a ventral hippocampus–medial prefrontal cortex pathway is both necessary and sufficient for an antidepressant response to ketamine. *Molecular Psychiatry*, 21(9):1298–1308, December 2015.

Carter, A. G. and Sabatini, B. L. State-dependent calcium signaling in dendritic spines of striatal medium spiny neurons. *Neuron*, 44(3):483–493, October 2004.

Celio, M. R. Calbindin D-28k and parvalbumin in the rat nervous system. *Neuroscience*, 35(2):375–475, 1990.

Cembrowski, M.; Phillips, M.; DiLisio, S. F.; Shields, B.; Winnubst, J.; Chandrashekar, J.; Bas, E., and Spruston, N. Dissociable Structural and Functional Hippocampal Outputs via Distinct Subiculum Cell Classes. *Cell*, 173(5):1280–1292, April 2018a.

Cembrowski, M. S. and Menon, V. Continuous Variation within Cell Types of the Nervous System. *Trends in neurosciences*, 41(6):337–348, June 2018.

Cembrowski, M. S. and Spruston, N. Heterogeneity within classical cell types is the rule: lessons from hippocampal pyramidal neurons. *Nature reviews. Neuroscience*, 20(4):193–204, April 2019.

Cembrowski, M. S.; Bachman, J. L.; Wang, L.; Sugino, K.; Shields, B. C., and Spruston, N. Spatial Gene-Expression Gradients Underlie Prominent Heterogeneity of CA1 Pyramidal Neurons. *Neuron*, 89(2):351–368, January 2016a.

Cembrowski, M. S.; Wang, L.; Sugino, K.; Shields, B. C., and Spruston, N. Hipposeq: a comprehensive RNA-seq database of gene expression in hippocampal principal neurons. *eLife*, 5:e14997, April 2016b.

Cembrowski, M. S.; Wang, L.; Lemire, A. L.; Copeland, M.; DiLisio, S. F.; Clements, J., and Spruston, N. The subiculum is a patchwork of discrete subregions. *eLife*, 7:65, October 2018b.

Cenquizca, L. A. and Swanson, L. W. Spatial organization of direct hippocampal field CA1 axonal projections to the rest of the cerebral cortex. *Brain research reviews*, 56(1):1–26, November 2007.

Cetin, A.; Komai, S.; Eliava, M.; Seeburg, P. H., and Osten, P. Stereotaxic gene delivery in the rodent brain. *Nature Protocols*, 1(6):3166–3173, January 2007.

Chang, C.-H.; Hsiao, Y.-H.; Chen, Y.-W.; Yu, Y.-J., and Gean, P.-W. Social isolation-induced increase in NMDA receptors in the hippocampus exacerbates emotional dysregulation in mice. *Hippocampus*, 25(4):474–485, April 2015.

Cheriyan, J.; Kaushik, M. K.; Ferreira, A. N., and Sheets, P. L. Specific Targeting of the Basolateral Amygdala to Projectionally Defined Pyramidal Neurons in Prelimbic and Infralimbic Cortex. *eNeuro*, 3(2):ENEURO.0002–16.2016, March 2016.

Child, N. D. and Benarroch, E. E. Anterior nucleus of the thalamus: functional organization and clinical implications. *Neurology*, 81(21):1869–1876, November 2013.

Cho, K. K. A.; Davidson, T. J.; Bouvier, G.; Marshall, J. D.; Schnitzer, M. J., and Sohal, V. S. Cross-hemispheric gamma synchrony between prefrontal parvalbumin interneurons supports behavioral adaptation during rule shift learning. *Nature Neuroscience*, 23(7):892–902, July 2020.

Ciocchi, S.; Passecker, J.; Malagon-Vina, H.; Mikus, N., and Klausberger, T. Brain

computation. Selective information routing by ventral hippocampal CA1 projection neurons. *Science (New York, N.Y.)*, 348(6234):560–563, May 2015.

Conte, W. L.; Kamishina, H., and Reep, R. L. The efficacy of the fluorescent conjugates of cholera toxin subunit B for multiple retrograde tract tracing in the central nervous system. *Brain structure & function*, 213(4-5):367–373, September 2009.

Cooper, D. C.; Moore, S. J.; Staff, N. P., and Spruston, N. Psychostimulant-induced plasticity of intrinsic neuronal excitability in ventral subiculum. *The Journal of neuroscience : the official journal of the Society for Neuroscience*, 23(30):9937–9946, October 2003.

Courtin, J.; Chaudun, F.; Rozeske, R. R.; Karalis, N.; Gonzalez-Campo, C.; Wurtz, H.; Abdi, A.; Baufreton, J.; Bienvenu, T. C. M., and Herry, C. Prefrontal parvalbumin interneurons shape neuronal activity to drive fear expression. *Nature*, 505 (7481):92–96, January 2014.

Covington, H. E.; Lobo, M. K.; Maze, I.; Vialou, V.; Hyman, J. M.; Zaman, S.; LaPlant, Q.; Mouzon, E.; Ghose, S.; Tamminga, C. A.; Neve, R. L.; Deisseroth, K., and Nestler, E. J. Antidepressant effect of optogenetic stimulation of the medial prefrontal cortex. *The Journal of neuroscience : the official journal of the Society for Neuroscience*, 30(48):16082–16090, December 2010.

Croxson, P. L.; Johansen-Berg, H.; Behrens, T. E. J.; Robson, M. D.; Pinsk, M. A.; Gross, C. G.; Richter, W.; Richter, M. C.; Kastner, S., and Rushworth, M. F. S. Quantitative investigation of connections of the prefrontal cortex in the human and macaque using probabilistic diffusion tractography. *The Journal of neuroscience : the official journal of the Society for Neuroscience*, 25(39):8854–8866, September 2005.

Cullinan, W. E.; Herman, J. P., and Watson, S. J. Ventral subicular interaction with the hypothalamic paraventricular nucleus: evidence for a relay in the bed nucleus of the stria terminalis. *The Journal of comparative neurology*, 332(1):1–20, June 1993.

Cummings, K. A. and Clem, R. L. Prefrontal somatostatin interneurons encode fear memory. *Nature Neuroscience*, 23(1):61–74, January 2020.

Damasio, H.; Grabowski, T.; Frank, R.; Galaburda, A. M., and Damasio, A. R. The return of Phineas Gage: clues about the brain from the skull of a famous patient. *Science (New York, N.Y.)*, 264(5162):1102–1105, May 1994.

Danielson, N. B.; Zaremba, J. D.; Kaifosh, P.; Bowler, J.; Ladow, M., and Losonczy, A. Sublayer-Specific Coding Dynamics during Spatial Navigation and Learning in Hippocampal Area CA1. *Neuron*, 91(3):652–665, August 2016.

Davidson, R. J. Anxiety and affective style: role of prefrontal cortex and amygdala. *Biological Psychiatry*, 51(1):68–80, January 2002.

de la Prida, L. M. Potential factors influencing replay across CA1 during sharp-wave ripples. *Philosophical transactions of the Royal Society of London. Series B, Biological sciences*, 375(1799):20190236, May 2020.

Deacon, R. M. J.; Penny, C., and Rawlins, J. N. P. Effects of medial prefrontal cortex cytotoxic lesions in mice. *Behavioural brain research*, 139(1-2):139–155, February 2003.

Dedovic, K.; Duchesne, A.; Andrews, J.; Engert, V., and Pruessner, J. C. The brain and the stress axis: the neural correlates of cortisol regulation in response to stress. *NeuroImage*, 47(3):864–871, September 2009.

Dégenètais, E.; Thierry, A.-M.; Glowinski, J., and Gioanni, Y. Synaptic influence of hippocampus on pyramidal cells of the rat prefrontal cortex: an in vivo intracellular recording study. *Cerebral cortex (New York, N.Y. : 1991)*, 13(7):782–792, July 2003.

Deguchi, Y.; Donato, F.; Galimberti, I.; Cabuy, E., and Caroni, P. Temporally matched subpopulations of selectively interconnected principal neurons in the hippocampus. *Nature neuroscience*, 14(4):495–504, April 2011.

DeVito, J. L. Subcortical projections to the hippocampal formation in squirrel monkey (Saimira sciureus). *Brain research bulletin*, 5(3):285–289, May 1980.

DeVito, L. M. and Eichenbaum, H. Distinct contributions of the hippocampus and medial prefrontal cortex to the "what-where-when" components of episodic-like memory in mice. *Behavioural brain research*, 215(2):318–325, December 2010.

Ding, S.-L.; Yao, Z.; Hirokawa, K. E.; Nguyen, T. N.; Graybuck, L. T.; Fong, O.; Bohn, P.; Ngo, K.; Smith, K. A.; Koch, C.; Phillips, J. W.; Lein, E. S.; Harris, J. A.; Tasic, B., and Zeng, H. Distinct Transcriptomic Cell Types and Neural Circuits of the Subiculum and Prosubiculum along the Dorsal-Ventral Axis. *Cell reports*, 31(7):107648, May 2020.

Dolleman-Van Der Weel, M. J. and Witter, M. P. Projections from the nucleus reuniens thalami to the entorhinal cortex, hippocampal field CA1, and the subiculum in the rat arise from different populations of neurons. *The Journal of comparative neurology*, 364(4):637–650, January 1996.

Dolleman-Van der Weel, M. J.; Lopes da Silva, F. H., and Witter, M. P. Nucleus reuniens thalami modulates activity in hippocampal field CA1 through excitatory and inhibitory mechanisms. *The Journal of neuroscience : the official journal of the Society for Neuroscience*, 17(14):5640–5650, July 1997.

Donato, F.; Chowdhury, A.; Lahr, M., and Caroni, P. Early- and late-born parvalbumin basket cell subpopulations exhibiting distinct regulation and roles in learning. *Neuron*, 85(4):770–786, February 2015.

Dong, H.-W.; Swanson, L. W.; Chen, L.; Fanselow, M. S., and Toga, A. W. Genomic-anatomic evidence for distinct functional domains in hippocampal field CA1. *Proceedings of the National Academy of Sciences of the United States of America*, 106(28):11794–11799, July 2009.

Dougherty, K. A.; Islam, T., and Johnston, D. Intrinsic excitability of CA1 pyramidal neurones from the rat dorsal and ventral hippocampus. *The Journal of physiology*, 590(22):5707–5722, November 2012.

Duval, E. R.; Javanbakht, A., and Liberzon, I. Neural circuits in anxiety and stress disorders: a focused review. *Therapeutics and clinical risk management*, 11: 115–126, 2015.

Eichenbaum, H. and Fortin, N. J. Bridging the gap between brain and behavior: cognitive and neural mechanisms of episodic memory. *Journal of the experimental analysis of behavior*, 84(3):619–629, November 2005.

Eichenbaum, H. and Robitsek, R. J. Olfactory memory: a bridge between humans and animals in models of cognitive aging. *Annals of the New York Academy of Sciences*, 1170:658–663, July 2009.

Euston, D. R.; Gruber, A. J., and McNaughton, B. L. The role of medial prefrontal cortex in memory and decision making. *Neuron*, 76(6):1057–1070, December 2012.

Fanselow, M. S. and Dong, H.-W. Are the dorsal and ventral hippocampus functionally distinct structures? *Neuron*, 65(1):7–19, January 2010.

Fattahi, M.; Sharif, F.; Geiller, T., and Royer, S. Differential Representation of Landmark and Self-Motion Information along the CA1 Radial Axis: Self-Motion Generated Place Fields Shift toward Landmarks during Septal Inactivation. *The Journal of neuroscience : the official journal of the Society for Neuroscience*, 38 (30):6766–6778, July 2018.

Felix-Ortiz, A. C.; Burgos-Robles, A.; Bhagat, N. D.; Leppla, C. A., and Tye, K. M. Bidirectional modulation of anxiety-related and social behaviors by amygdala projections to the medial prefrontal cortex. *Neuroscience*, 321:197–209, May 2016.

Felix-Ortiz, A. C.; Beyeler, A.; Seo, C.; Leppla, C. A.; Wildes, C. P., and Tye, K. M. BLA to vHPC inputs modulate anxiety-related behaviors. *Neuron*, 79(4): 658–664, August 2013.

Ferguson, B. R. and Gao, W.-J. PV Interneurons: Critical Regulators of E/I Balance for Prefrontal Cortex-Dependent Behavior and Psychiatric Disorders. *Frontiers in Neural Circuits*, 12:37, 2018.

Fernández-Ruiz, A.; Oliva, A.; Nagy, G. A.; Maurer, A. P.; Berenyi, A., and Buzsáki, G. Entorhinal-CA3 Dual-Input Control of Spike Timing in the Hippocampus by Theta-Gamma Coupling. *Neuron*, 93(5):1213–1226.e5, March 2017.

Floresco, S. B.; Seamans, J. K., and Phillips, A. G. Selective roles for hippocampal, prefrontal cortical, and ventral striatal circuits in radial-arm maze tasks with or without a delay. *The Journal of neuroscience : the official journal of the Society for Neuroscience*, 17(5):1880–1890, March 1997.

Fuchikami, M.; Thomas, A.; Liu, R.; Wohleb, E. S.; Land, B. B.; DiLeone, R. J.; Aghajanian, G. K., and Duman, R. S. Optogenetic stimulation of infralimbic PFC reproduces ketamine's rapid and sustained antidepressant actions. *Proceedings of the National Academy of Sciences*, 112(26):8106–8111, June 2015.

Fuhrmann, F.; Justus, D.; Sosulina, L.; Kaneko, H.; Beutel, T.; Friedrichs, D.; Schoch, S.; Schwarz, M. K.; Fuhrmann, M., and Remy, S. Locomotion, Theta Oscillations, and the Speed-Correlated Firing of Hippocampal Neurons Are Controlled by a Medial Septal Glutamatergic Circuit. *Neuron*, 86(5):1253–1264, June 2015.

Fuster, J. M. The prefrontal cortex–an update: time is of the essence. *Neuron*, 30 (2):319–333, May 2001.

Fuster, J. and Barbas, H. *Encyclopedia of Neuroscience*. Academic Press, Oxford, 2009.

Gabbott, P. L. A.; Warner, T. A.; Jays, P. R. L.; Salway, P., and Busby, S. J. Prefrontal cortex in the rat: projections to subcortical autonomic, motor, and limbic centers. *The Journal of comparative neurology*, 492(2):145–177, November 2005.

Gao, R. and Penzes, P. Common mechanisms of excitatory and inhibitory imbalance in schizophrenia and autism spectrum disorders. *Current molecular medicine*, 15 (2):146–167, 2015.

Garcia-Garcia, A. L.; Meng, Q.; Canetta, S.; Gardier, A. M.; Guiard, B. P.; Kellendonk, C.; Dranovsky, A., and Leonardo, E. D. Serotonin Signaling through Prefrontal Cortex 5-HT1A Receptors during Adolescence Can Determine Baseline Mood-Related Behaviors. *Cell reports*, 18(5):1144–1156, January 2017.

Garcia-Junco-Clemente, P.; Ikrar, T.; Tring, E.; Xu, X.; Ringach, D. L., and Trachtenberg, J. T. An inhibitory pull-push circuit in frontal cortex. *Nature Neuroscience*, 20(3):389–392, March 2017.

Gauthier, J. L. and Tank, D. W. A Dedicated Population for Reward Coding in the Hippocampus. *Neuron*, 99(1):179–193.e7, July 2018.

Gaykema, R. P.; van der Kuil, J.; Hersh, L. B., and Luiten, P. G. Patterns of direct projections from the hippocampus to the medial septum-diagonal band complex: anterograde tracing with Phaseolus vulgaris leucoagglutinin combined with immunohistochemistry of choline acetyltransferase. *Neuroscience*, 43(2-3):349–360, 1991.

Geiller, T.; Fattahi, M.; Choi, J.-S., and Royer, S. Place cells are more strongly tied to landmarks in deep than in superficial CA1. *Nature communications*, 8:14531, February 2017a.

Geiller, T.; Royer, S., and Choi, J.-S. Segregated Cell Populations Enable Distinct Parallel Encoding within the Radial Axis of the CA1 Pyramidal Layer. *Experimental neurobiology*, 26(1):1–10, February 2017b.

Gergues, M. M.; Han, K. J.; Choi, H. S.; Brown, B.; Clausing, K. J.; Turner, V. S.; Vainchtein, I. D.; Molofsky, A. V., and Kheirbek, M. A. Circuit and molecular architecture of a ventral hippocampal network. *Nature Neuroscience*, 65(11): 7–1452, September 2020.

Gittis, A. H.; Nelson, A. B.; Thwin, M. T.; Palop, J. J., and Kreitzer, A. C. Distinct roles of GABAergic interneurons in the regulation of striatal output pathways. *The Journal of neuroscience : the official journal of the Society for Neuroscience*, 30(6):2223–2234, February 2010.

Godsil, B. P.; Kiss, J. P.; Spedding, M., and Jay, T. M. The hippocampal-prefrontal pathway: the weak link in psychiatric disorders? *European neuropsychopharmacology : the journal of the European College of Neuropsychopharmacology*, 23 (10):1165–1181, October 2013.

Goto, Y. and Grace, A. A. Dopaminergic modulation of limbic and cortical drive of nucleus accumbens in goal-directed behavior. *Nature neuroscience*, 8(6):805–812, June 2005.

Goto, Y. and Grace, A. A. Dopamine modulation of hippocampal-prefrontal cortical interaction drives memory-guided behavior. *Cerebral cortex (New York, N.Y. : 1991)*, 18(6):1407–1414, June 2008.

Graeff, F. G. Neuroanatomy and neurotransmitter regulation of defensive behaviors and related emotions in mammals. *Brazilian journal of medical and biological research = Revista brasileira de pesquisas medicas e biologicas*, 27(4):811–829, April 1994.

Graves, A. R.; Moore, S. J.; Bloss, E. B.; Mensh, B. D.; Kath, W. L., and Spruston, N. Hippocampal pyramidal neurons comprise two distinct cell types that are countermodulated by metabotropic receptors. *Neuron*, 76(4):776–789, November 2012.

Greene, J. R. and Mason, A. Neuronal diversity in the subiculum: correlations with the effects of somatostatin on intrinsic properties and on GABA-mediated IPSPs in vitro. *Journal of neurophysiology*, 76(3):1657–1666, September 1996.

Greene, J. R. and Totterdell, S. Morphology and distribution of electrophysiologically defined classes of pyramidal and nonpyramidal neurons in rat ventral

subiculum in vitro. *The Journal of comparative neurology*, 380(3):395–408, April 1997.

Grosmark, A. D. and Buzsáki, G. Diversity in neural firing dynamics supports both rigid and learned hippocampal sequences. *Science (New York, N.Y.)*, 351(6280): 1440–1443, March 2016.

Gruber, A. J.; Calhoon, G. G.; Shusterman, I.; Schoenbaum, G.; Roesch, M. R., and O'Donnell, P. More is less: a disinhibited prefrontal cortex impairs cognitive flexibility. *The Journal of neuroscience : the official journal of the Society for Neuroscience*, 30(50):17102–17110, December 2010.

Gulyás, A. I.; Görcs, T. J., and Freund, T. F. Innervation of different peptide-containing neurons in the hippocampus by GABAergic septal afferents. *Neuroscience*, 37(1):31–44, 1990.

Hafting, T.; Fyhn, M.; Molden, S.; Moser, M.-B., and Moser, E. I. Microstructure of a spatial map in the entorhinal cortex. *Nature*, 436(7052):801–806, August 2005.

Hare, B. D.; Shinohara, R.; Liu, R. J.; Pothula, S.; DiLeone, R. J., and Duman, R. S. Optogenetic stimulation of medial prefrontal cortex Drd1 neurons produces rapid and long-lasting antidepressant effects. *Nature Communications*, 10(1):223–12, January 2019.

Hargreaves, E. L.; Rao, G.; Lee, I., and Knierim, J. J. Major dissociation between medial and lateral entorhinal input to dorsal hippocampus. *Science (New York, N.Y.)*, 308(5729):1792–1794, June 2005.

Harnett, M. T.; Makara, J. K.; Spruston, N.; Kath, W. L., and Magee, J. C. Synaptic amplification by dendritic spines enhances input cooperativity. *Nature*, 491 (7425):599–602, October 2012.

Harnett, M. T.; Xu, N.-L.; Magee, J. C., and Williams, S. R. Potassium Channels

Control the Interaction between Active Dendritic Integration Compartments in Layer 5 Cortical Pyramidal Neurons. *Neuron*, 79(3):516–529, August 2013.

Harris, E.; Witter, M. P.; Weinstein, G., and Stewart, M. Intrinsic connectivity of the rat subiculum: I. Dendritic morphology and patterns of axonal arborization by pyramidal neurons. *The Journal of comparative neurology*, 435(4):490–505, 2001.

Harris, K. D.; Hochgerner, H.; Skene, N. G.; Magno, L.; Katona, L.; Bengtsson Gonzales, C.; Somogyi, P.; Kessaris, N.; Linnarsson, S., and Hjerling-Leffler, J. Classes and continua of hippocampal CA1 inhibitory neurons revealed by single-cell transcriptomics. *PLoS biology*, 16(6):e2006387, June 2018.

Harrison, P. J. The hippocampus in schizophrenia: a review of the neuropathological evidence and its pathophysiological implications. *Psychopharmacology*, 174 (1):151–162, June 2004.

Hartley, T.; Lever, C.; Burgess, N., and O'Keefe, J. Space in the brain: how the hippocampal formation supports spatial cognition. *Philosophical transactions of the Royal Society of London. Series B, Biological sciences*, 369(1635):20120510, February 2014.

Henke, P. G. Hippocampal pathway to the amygdala and stress ulcer development. *Brain research bulletin*, 25(5):691–695, November 1990.

Henriksen, E. J.; Colgin, L. L.; Barnes, C. A.; Witter, M. P.; Moser, M.-B., and Moser, E. I. Spatial representation along the proximodistal axis of CA1. *Neuron*, 68(1):127–137, October 2010.

Herkenham, M. The connections of the nucleus reuniens thalami: evidence for a direct thalamo-hippocampal pathway in the rat. *The Journal of comparative neurology*, 177(4):589–610, February 1978.

Herman, J. P.; Ostrander, M. M.; Mueller, N. K., and Figueiredo, H. Limbic system mechanisms of stress regulation: hypothalamo-pituitary-adrenocortical

axis. *Progress in neuro-psychopharmacology & biological psychiatry*, 29(8): 1201–1213, December 2005.

Hobin, J. A.; Ji, J., and Maren, S. Ventral hippocampal muscimol disrupts context-specific fear memory retrieval after extinction in rats. *Hippocampus*, 16(2):174–182, 2006.

Hok, V.; Save, E.; Lenck-Santini, P. P., and Poucet, B. Coding for spatial goals in the prelimbic/infralimbic area of the rat frontal cortex. *Proceedings of the National Academy of Sciences of the United States of America*, 102(12):4602–4607, March 2005.

Holland, F. H.; Ganguly, P.; Potter, D. N.; Chartoff, E. H., and Brenhouse, H. C. Early life stress disrupts social behavior and prefrontal cortex parvalbumin interneurons at an earlier time-point in females than in males. *Neuroscience letters*, 566:131–136, April 2014.

Honda, Y. and Ishizuka, N. Topographic distribution of cortical projection cells in the rat subiculum. *Neuroscience research*, 92:1–20, March 2015.

Hoover, W. B. and Vertes, R. P. Anatomical analysis of afferent projections to the medial prefrontal cortex in the rat. *Brain structure & function*, 212(2):149–179, September 2007.

Hsu, D. T. and Price, J. L. Paraventricular thalamic nucleus: subcortical connections and innervation by serotonin, orexin, and corticotropin-releasing hormone in macaque monkeys. *Journal of Comparative Neurology*, 512(6):825–848, February 2009.

Huang, Z. J. and Paul, A. The diversity of GABAergic neurons and neural communication elements. *Nature reviews. Neuroscience*, 20(9):563–572, September 2019.

Hugues, S. and Garcia, R. Reorganization of learning-associated prefrontal synap-

tic plasticity between the recall of recent and remote fear extinction memory. *Learning & memory (Cold Spring Harbor, N.Y.)*, 14(8):520–524, August 2007.

Huh, C. Y. L.; Goutagny, R., and Williams, S. Glutamatergic neurons of the mouse medial septum and diagonal band of Broca synaptically drive hippocampal pyramidal cells: relevance for hippocampal theta rhythm. *The Journal of neuroscience : the official journal of the Society for Neuroscience*, 30(47):15951–15961, November 2010.

Hunsaker, M. R.; Fieldsted, P. M.; Rosenberg, J. S., and Kesner, R. P. Dissociating the roles of dorsal and ventral CA1 for the temporal processing of spatial locations, visual objects, and odors. *Behavioral neuroscience*, 122(3):643–650, June 2008.

Hunt, D. L.; Linaro, D.; Si, B.; Romani, S., and Spruston, N. A novel pyramidal cell type promotes sharp-wave synchronization in the hippocampus. *Nature Neuroscience*, 21(7):985–995, June 2018.

Ibi, D.; Takuma, K.; Koike, H.; Mizoguchi, H.; Tsuritani, K.; Kuwahara, Y.; Kamei, H.; Nagai, T.; Yoneda, Y.; Nabeshima, T., and Yamada, K. Social isolation rearing-induced impairment of the hippocampal neurogenesis is associated with deficits in spatial memory and emotion-related behaviors in juvenile mice. *Journal of neurochemistry*, 105(3):921–932, May 2008.

Igarashi, K. M.; Ito, H. T.; Moser, E. I., and Moser, M.-B. Functional diversity along the transverse axis of hippocampal area CA1. *FEBS letters*, 588(15):2470–2476, August 2014a.

Igarashi, K. M.; Lu, L.; Colgin, L. L.; Moser, M.-B., and Moser, E. I. Coordination of entorhinal-hippocampal ensemble activity during associative learning. *Nature*, 510(7503):143–147, June 2014b.

Isaacson, J. S. and Scanziani, M. How inhibition shapes cortical activity. *Neuron*, 72(2):231–243, October 2011.

Isaacson, R. L. and Kimble, D. P. Lesions of the limbic system: their effects upon hypotheses and frustration. *Behavioral biology*, 7(6):767–793, December 1972.

Ishihara, Y. and Fukuda, T. Immunohistochemical investigation of the internal structure of the mouse subiculum. *Neuroscience*, 337:242–266, November 2016.

Ishizuka, N. Laminar organization of the pyramidal cell layer of the subiculum in the rat. *The Journal of comparative neurology*, 435(1):89–110, June 2001.

Ishizuka, N.; Weber, J., and Amaral, D. G. Organization of intrahippocampal projections originating from CA3 pyramidal cells in the rat. *The Journal of comparative neurology*, 295(4):580–623, May 1990.

Izumi, Y. and Zorumski, C. F. Metaplastic effects of subanesthetic ketamine on CA1 hippocampal function. *Neuropharmacology*, 86:273–281, November 2014.

Jacobson, L. and Sapolsky, R. The role of the hippocampus in feedback regulation of the hypothalamic-pituitary-adrenocortical axis. *Endocrine reviews*, 12(2):118–134, May 1991.

Jadhav, S. P.; Rothschild, G.; Roumis, D. K., and Frank, L. M. Coordinated Excitation and Inhibition of Prefrontal Ensembles during Awake Hippocampal Sharp-Wave Ripple Events. *Neuron*, 90(1):113–127, April 2016.

Jang, H. J.; Chung, H.; Rowland, J. M.; Richards, B. A.; Kohl, M. M., and Kwag, J. Distinct roles of parvalbumin and somatostatin interneurons in gating the synchronization of spike times in the neocortex. *Science advances*, 6(17):eaay5333, April 2020.

Jankowski, M. M.; Ronnqvist, K. C.; Tsanov, M.; Vann, S. D.; Wright, N. F.; Erichsen, J. T.; Aggleton, J. P., and O'Mara, S. M. The anterior thalamus provides a subcortical circuit supporting memory and spatial navigation. *Frontiers in systems neuroscience*, 7:45, 2013.

Jarsky, T.; Mady, R.; Kennedy, B., and Spruston, N. Distribution of bursting neurons in the CA1 region and the subiculum of the rat hippocampus. *The Journal of comparative neurology*, 506(4):535–547, February 2008.

Jay, T. M. and Witter, M. P. Distribution of hippocampal CA1 and subicular efferents in the prefrontal cortex of the rat studied by means of anterograde transport of Phaseolus vulgaris-leucoagglutinin. *The Journal of comparative neurology*, 313(4):574–586, November 1991.

Jay, T. M.; Burette, F., and Laroche, S. NMDA receptor-dependent long-term potentiation in the hippocampal afferent fibre system to the prefrontal cortex in the rat. *The European journal of neuroscience*, 7(2):247–250, February 1995.

Jay, T. M.; Thierry, A.-M.; Wiklund, L., and Glowinski, J. Excitatory Amino Acid Pathway from the Hippocampus to the Prefrontal Cortex. Contribution of AMPA Receptors in Hippocampo-prefrontal Cortex Transmission. *The European journal of neuroscience*, 4(12):1285–1295, 1992.

Jett, J. D.; Boley, A. M.; Girotti, M.; Shah, A.; Lodge, D. J., and Morilak, D. A. Antidepressant-like cognitive and behavioral effects of acute ketamine administration associated with plasticity in the ventral hippocampus to medial prefrontal cortex pathway. *Psychopharmacology*, 232(17):3123–3133, May 2015.

Jimenez, J. C.; Su, K.; Goldberg, A. R.; Luna, V. M.; Biane, J. S.; Ordek, G.; Zhou, P.; Ong, S. K.; Wright, M. A.; Zweifel, L.; Paninski, L.; Hen, R., and Kheirbek, M. A. Anxiety Cells in a Hippocampal-Hypothalamic Circuit. *Neuron*, 97(3): 670–683.e6, February 2018.

Jimenez, J. C.; Berry, J. E.; Lim, S. C.; Ong, S. K.; Kheirbek, M. A., and Hen, R. Contextual fear memory retrieval by correlated ensembles of ventral CA1 neurons. *Nature Communications*, pages 1–11, July 2020.

Jin, J. and Maren, S. Fear renewal preferentially activates ventral hippocampal neurons projecting to both amygdala and prefrontal cortex in rats. *Scientific reports*, 5:8388, February 2015a.

Jin, J. and Maren, S. Prefrontal-Hippocampal Interactions in Memory and Emotion. *Frontiers in systems neuroscience*, 9:170, 2015b.

Joo, H. R. and Frank, L. M. The hippocampal sharp wave-ripple in memory retrieval for immediate use and consolidation. *Nature Reviews Neuroscience*, 19(12):744–757, December 2018.

Kallarackal, A. J.; Kvarta, M. D.; Cammarata, E.; Jaberi, L.; Cai, X.; Bailey, A. M., and Thompson, S. M. Chronic stress induces a selective decrease in AMPA receptor-mediated synaptic excitation at hippocampal temporoammonic-CA1 synapses. *The Journal of neuroscience : the official journal of the Society for Neuroscience*, 33(40):15669–15674, October 2013.

Kampa, B. M.; Letzkus, J. J., and Stuart, G. J. Cortical feed-forward networks for binding different streams of sensory information. *Nature neuroscience*, 9(12): 1472–1473, December 2006.

Kawaguchi, Y. Groupings of nonpyramidal and pyramidal cells with specific physiological and morphological characteristics in rat frontal cortex. *Journal of neurophysiology*, 69(2):416–431, February 1993.

Kawaguchi, Y. Pyramidal Cell Subtypes and Their Synaptic Connections in Layer 5 of Rat Frontal Cortex. *Cerebral cortex (New York, N.Y. : 1991)*, 27(12):5755–5771, December 2017.

Kennedy, P. J. and Shapiro, M. L. Retrieving memories via internal context requires the hippocampus. *The Journal of neuroscience : the official journal of the Society for Neuroscience*, 24(31):6979–6985, August 2004.

Khan, A. G.; Poort, J.; Chadwick, A.; Blot, A.; Sahani, M.; Mrsic-Flogel, T. D., and Hofer, S. B. Distinct learning-induced changes in stimulus selectivity and interactions of GABAergic interneuron classes in visual cortex. *Nature Neuroscience*, 21(6):851–859, June 2018.

Kim, E. J.; Pellman, B., and Kim, J. J. Stress effects on the hippocampus: a critical review. *Learning & memory (Cold Spring Harbor, N.Y.)*, 22(9):411–416, September 2015.

Kim, J. J. and Fanselow, M. S. Modality-specific retrograde amnesia of fear. *Science (New York, N.Y.)*, 256(5057):675–677, May 1992.

Kim, S.-Y.; Adhikari, A.; Lee, S. Y.; Marshel, J. H.; Kim, C. K.; Mallory, C. S.; Lo, M.; Pak, S.; Mattis, J.; Lim, B. K.; Malenka, R. C.; Warden, M. R.; Neve, R.; Tye, K. M., and Deisseroth, K. Diverging neural pathways assemble a behavioural state from separable features in anxiety. *Nature*, 496(7444):219–223, April 2013.

Kim, T.-K. and Han, P.-L. Functional Connectivity of Basolateral Amygdala Neurons Carrying Orexin Receptors and Melanin-concentrating Hormone Receptors in Regulating Sociability and Mood-related Behaviors. *Experimental neurobiology*, 25(6):307–317, December 2016.

Kim, Y. and Spruston, N. Target-specific output patterns are predicted by the distribution of regular-spiking and bursting pyramidal neurons in the subiculum. *Hippocampus*, 22(4):693–706, April 2012.

Kishi, T.; Tsumori, T.; Yokota, S., and Yasui, Y. Topographical projection from the hippocampal formation to the amygdala: a combined anterograde and retrograde tracing study in the rat. *The Journal of comparative neurology*, 496(3):349–368, May 2006.

Kjaerby, C.; Athilingam, J.; Robinson, S. E.; Iafrati, J., and Sohal, V. S. Serotonin 1B Receptors Regulate Prefrontal Function by Gating Callosal and Hippocampal Inputs. *Cell reports*, 17(11):2882–2890, December 2016.

Kjelstrup, K. B.; Solstad, T.; Brun, V. H.; Hafting, T.; Leutgeb, S.; Witter, M. P.; Moser, E. I., and Moser, M.-B. Finite scale of spatial representation in the hippocampus. *Science (New York, N.Y.)*, 321(5885):140–143, July 2008.

Kjelstrup, K. G.; Tuvnes, F. A.; Steffenach, H.-A.; Murison, R.; Moser, E. I., and Moser, M.-B. Reduced fear expression after lesions of the ventral hippocampus. *Proceedings of the National Academy of Sciences of the United States of America*, 99(16):10825–10830, August 2002.

Knierim, J. J.; Neunuebel, J. P., and Deshmukh, S. S. Functional correlates of the lateral and medial entorhinal cortex: objects, path integration and local-global reference frames. *Philosophical Transactions of the Royal Society of London. Series B, Biological Sciences*, 369(1635):20130369, February 2014.

Knox, D. and Keller, S. M. Cholinergic neuronal lesions in the medial septum and vertical limb of the diagonal bands of Broca induce contextual fear memory generalization and impair acquisition of fear extinction. *Hippocampus*, 26(6): 718–726, June 2016.

Kohara, K.; Pignatelli, M.; Rivest, A. J.; Jung, H.-Y.; Kitamura, T.; Suh, J.; Frank, D.; Kajikawa, K.; Mise, N.; Obata, Y.; Wickersham, I. R., and Tonegawa, S. Cell type-specific genetic and optogenetic tools reveal hippocampal CA2 circuits. *Nature Neuroscience*, 17(2):269–279, February 2014.

Komorowski, R. W.; Garcia, C. G.; Wilson, A.; Hattori, S.; Howard, M. W., and Eichenbaum, H. Ventral hippocampal neurons are shaped by experience to represent behaviorally relevant contexts. *The Journal of neuroscience : the official journal of the Society for Neuroscience*, 33(18):8079–8087, May 2013.

Koppensteiner, P.; Von Itter, R.; Melani, R.; Galvin, C.; Lee, F. S., and Ninan, I. Diminished Fear Extinction in Adolescents Is Associated With an Altered Somatostatin Interneuron-Mediated Inhibition in the Infralimbic Cortex. *Biological Psychiatry*, 86(9):682–692, November 2019.

Korotkova, T.; Fuchs, E. C.; Ponomarenko, A.; von Engelhardt, J., and Monyer, H. NMDA receptor ablation on parvalbumin-positive interneurons impairs hippocampal synchrony, spatial representations, and working memory. *Neuron*, 68 (3):557–569, November 2010.

Krnjević, K. and Ropert, N. Electrophysiological and pharmacological characteristics of facilitation of hippocampal population spikes by stimulation of the medial septum. *Neuroscience*, 7(9):2165–2183, 1982.

Krook-Magnuson, E.; Varga, C.; Lee, S.-H., and Soltesz, I. New dimensions of interneuronal specialization unmasked by principal cell heterogeneity. *Trends in neurosciences*, 35(3):175–184, March 2012.

Kumaran, D. and Maguire, E. A. Which computational mechanisms operate in the hippocampus during novelty detection? *Hippocampus*, 17(9):735–748, 2007.

Kupferschmidt, D. A. and Gordon, J. A. The dynamics of disordered dialogue: Prefrontal, hippocampal and thalamic miscommunication underlying working memory deficits in schizophrenia. *Brain and neuroscience advances*, 2, January 2018.

Kvitsiani, D.; Ranade, S.; Hangya, B.; Taniguchi, H.; Huang, J. Z., and Kepecs, A. Distinct behavioural and network correlates of two interneuron types in prefrontal cortex. *Nature*, 498(7454):363–366, June 2013.

Lagler, M.; Ozdemir, A. T.; Lagoun, S.; Malagon-Vina, H.; Borhegyi, Z.; Hauer, R.; Jelem, A., and Klausberger, T. Divisions of Identified Parvalbumin-Expressing Basket Cells during Working Memory-Guided Decision Making. *Neuron*, 91(6): 1390–1401, September 2016.

Lander, S. S.; Linder-Shacham, D., and Gaisler-Salomon, I. Differential effects of social isolation in adolescent and adult mice on behavior and cortical gene expression. *Behavioural Brain Research*, 316:245–254, January 2017.

Larkum, M. E.; Nevian, T.; Sandler, M.; Polsky, A., and Schiller, J. Synaptic Integration in Tuft Dendrites of Layer 5 Pyramidal Neurons: A New Unifying Principle. *Science*, 325(5941):756–760, August 2009.

Laubach, M.; Amarante, L. M.; Swanson, K., and White, S. R. What, If Anything, Is Rodent Prefrontal Cortex? *eNeuro*, 5(5), September 2018.

Leão, R. N.; Mikulovic, S.; Leão, K. E.; Munguba, H.; Gezelius, H.; Enjin, A.; Patra, K.; Eriksson, A.; Loew, L. M.; Tort, A. B. L., and Kullander, K. OLM interneurons differentially modulate CA3 and entorhinal inputs to hippocampal CA1 neurons. *Nature neuroscience*, 15(11):1524–1530, November 2012.

Leão, R. N.; Targino, Z. H.; Colom, L. V., and Fisahn, A. Interconnection and synchronization of neuronal populations in the mouse medial septum/diagonal band of Broca. *Journal of neurophysiology*, 113(3):971–980, February 2015.

Lee, A. T.; Gee, S. M.; Vogt, D.; Patel, T.; Rubenstein, J. L., and Sohal, V. S. Pyramidal Neurons in Prefrontal Cortex Receive Subtype-Specific Forms of Excitation and Inhibition. *Neuron*, 81(1):61–68, January 2014a.

Lee, A. T.; Vogt, D.; Rubenstein, J. L., and Sohal, V. S. A class of GABAergic neurons in the prefrontal cortex sends long-range projections to the nucleus accumbens and elicits acute avoidance behavior. *The Journal of neuroscience : the official journal of the Society for Neuroscience*, 34(35):11519–11525, August 2014b.

Lee, A. T.; Cunniff, M. M.; See, J. Z.; Wilke, S. A.; Luongo, F. J.; Ellwood, I. T.; Ponnavolu, S., and Sohal, V. S. VIP Interneurons Contribute to Avoidance Behavior by Regulating Information Flow across Hippocampal-Prefrontal Networks. *Neuron*, April 2019a.

Lee, H.; GoodSmith, D., and Knierim, J. J. Parallel processing streams in the hippocampus. *Current opinion in neurobiology*, 64:127–134, June 2020.

Lee, S.-H.; Marchionni, I.; Bezaire, M.; Varga, C.; Danielson, N.; Lovett-Barron, M.; Losonczy, A., and Soltesz, I. Parvalbumin-positive basket cells differentiate among hippocampal pyramidal cells. *Neuron*, 82(5):1129–1144, June 2014c.

Lee, S.; Kruglikov, I.; Huang, Z. J.; Fishell, G., and Rudy, B. A disinhibitory circuit mediates motor integration in the somatosensory cortex. *Nature Neuroscience*, 16(11):1662–1670, November 2013.

Lee, S.; Lee, C.; Woo, C.; Kang, S. J., and Shin, K. S. Chronic social defeat stress-induced enhancement of T-type calcium channels increases burst-firing neurons in the ventral subiculum. *Biochemical and biophysical research communications*, 508(4):1182–1187, January 2019b.

LeGates, T. A.; Kvarta, M. D.; Tooley, J. R.; Francis, T. C.; Lobo, M. K.; Creed, M. C., and Thompson, S. M. Reward behaviour is regulated by the strength of hippocampus-nucleus accumbens synapses. *Nature*, 564(7735):258–262, December 2018.

Lein, E. S.; Hawrylycz, M. J.; Ao, N.; Ayres, M.; Bensinger, A.; Bernard, A.; Boe, A. F.; Boguski, M. S.; Brockway, K. S.; Byrnes, E. J.; Chen, L.; Chen, L.; Chen, T.-M.; Chin, M. C.; Chong, J.; Crook, B. E.; Czaplinska, A.; Dang, C. N.; Datta, S.; Dee, N. R.; Desaki, A. L.; Desta, T.; Diep, E.; Dolbeare, T. A.; Donelan, M. J.; Dong, H.-W.; Dougherty, J. G.; Duncan, B. J.; Ebbert, A. J.; Eichele, G.; Estin, L. K.; Faber, C.; Facer, B. A.; Fields, R.; Fischer, S. R.; Fliss, T. P.; Frensley, C.; Gates, S. N.; Glattfelder, K. J.; Halverson, K. R.; Hart, M. R.; Hohmann, J. G.; Howell, M. P.; Jeung, D. P.; Johnson, R. A.; Karr, P. T.; Kawal, R.; Kidney, J. M.; Knapik, R. H.; Kuan, C. L.; Lake, J. H.; Laramee, A. R.; Larsen, K. D.; Lau, C.; Lemon, T. A.; Liang, A. J.; Liu, Y.; Luong, L. T.; Michaels, J.; Morgan, J. J.; Morgan, R. J.; Mortrud, M. T.; Mosqueda, N. F.; Ng, L. L.; Ng, R.; Orta, G. J.; Overly, C. C.; Pak, T. H.; Parry, S. E.; Pathak, S. D.; Pearson, O. C.; Puchalski, R. B.; Riley, Z. L.; Rockett, H. R.; Rowland, S. A.; Royall, J. J.; Ruiz, M. J.; Sarno, N. R.; Schaffnit, K.; Shapovalova, N. V.; Sivisay, T.; Slaughterbeck, C. R.; Smith, S. C.; Smith, K. A.; Smith, B. I.; Sodt, A. J.; Stewart, N. N.; Stumpf, K.-R.; Sunkin, S. M.; Sutram, M.; Tam, A.; Teemer, C. D.; Thaller, C.; Thompson, C. L.; Varnam, L. R.; Visel, A.; Whitlock, R. M.; Wohnoutka, P. E.; Wolkey, C. K.; Wong, V. Y.; Wood, M.; Yaylaoglu, M. B.; Young, R. C.; Youngstrom, B. L.; Yuan, X. F.; Zhang, B.; Zwingman, T. A., and Jones, A. R. Genome-wide atlas of gene expression in the adult mouse brain. *Nature*, 445(7124):168–176, January 2007.

Lencer, W. I. and Tsai, B. The intracellular voyage of cholera toxin: going retro. *Trends in biochemical sciences*, 28(12):639–645, December 2003.

Leonardo, E. D.; Richardson-Jones, J. W.; Sibille, E.; Kottman, A., and Hen, R. Molecular heterogeneity along the dorsal-ventral axis of the murine hippocampal CA1 field: a microarray analysis of gene expression. *Neuroscience*, 137(1):177–186, 2006.

Leone, D. P.; Srinivasan, K.; Chen, B.; Alcamo, E., and McConnell, S. K. The determination of projection neuron identity in the developing cerebral cortex. *Current opinion in neurobiology*, 18(1):28–35, February 2008.

Li, M.; Long, C., and Yang, L. Hippocampal-prefrontal circuit and disrupted functional connectivity in psychiatric and neurodegenerative disorders. *BioMed research international*, 2015(1):810548–10, 2015.

Li, Y.; Xu, J.; Liu, Y.; Zhu, J.; Liu, N.; Zeng, W.; Huang, N.; Rasch, M. J.; Jiang, H.; Gu, X.; Li, X.; Luo, M.; Li, C.; Teng, J.; Chen, J.; Zeng, S.; Lin, L., and Zhang, X. A distinct entorhinal cortex to hippocampal CA1 direct circuit for olfactory associative learning. *Nature Neuroscience*, 20(4):559–570, April 2017.

Liang, J.; Xu, W.; Hsu, Y.-T.; Yee, A. X.; Chen, L., and Südhof, T. C. Conditional neuroligin-2 knockout in adult medial prefrontal cortex links chronic changes in synaptic inhibition to cognitive impairments. *Molecular psychiatry*, 20(7):850–859, July 2015.

Liston, C.; McEwen, B. S., and Casey, B. J. Psychosocial stress reversibly disrupts prefrontal processing and attentional control. *Proceedings of the National Academy of Sciences of the United States of America*, 106(3):912–917, January 2009.

Liu, P. and Bilkey, D. K. The effect of excitotoxic lesions centered on the hippocampus or perirhinal cortex in object recognition and spatial memory tasks. *Behavioral neuroscience*, 115(1):94–111, February 2001.

Liu, X. and Carter, A. G. Ventral Hippocampal Inputs Preferentially Drive Corticocortical Neurons in the Infralimbic Prefrontal Cortex. *The Journal of neuroscience : the official journal of the Society for Neuroscience*, 38(33):7351–7363, August 2018.

Losonczy, A.; Makara, J. K., and Magee, J. C. Compartmentalized dendritic plasticity and input feature storage in neurons. *Nature*, 452(7186):436–441, March 2008.

Lovett-Barron, M.; Kaifosh, P.; Kheirbek, M. A.; Danielson, N.; Zaremba, J. D.; Reardon, T. R.; Turi, G. F.; Hen, R.; Zemelman, B. V., and Losonczy, A. Dendritic inhibition in the hippocampus supports fear learning. *Science (New York, N.Y.)*, 343(6173):857–863, February 2014.

Lowry, C. A. Functional subsets of serotonergic neurones: implications for control of the hypothalamic-pituitary-adrenal axis. *Journal of neuroendocrinology*, 14 (11):911–923, November 2002.

Lu, J.; Tucciarone, J.; Padilla-Coreano, N.; He, M.; Gordon, J. A., and Huang, Z. J. Selective inhibitory control of pyramidal neuron ensembles and cortical subnetworks by chandelier cells. *Nature Neuroscience*, 20(10):1377–1383, October 2017.

Lüthi, A. and McCormick, D. A. H-current: properties of a neuronal and network pacemaker. *Neuron*, 21(1):9–12, July 1998.

MacAskill, A. F.; Little, J. P.; Cassel, J. M., and Carter, A. G. Subcellular connectivity underlies pathway-specific signaling in the nucleus accumbens. *Nature Neuroscience*, 15(12):1624–1626, November 2012.

MacAskill, A. F.; Cassel, J. M., and Carter, A. G. Cocaine exposure reorganizes cell type- and input-specific connectivity in the nucleus accumbens. *Nature Neuroscience*, 17(9):1198–1207, September 2014.

MacDonald, C. J.; Lepage, K. Q.; Eden, U. T., and Eichenbaum, H. Hippocampal "time cells" bridge the gap in memory for discontiguous events. *Neuron*, 71(4): 737–749, August 2011.

Malik, R.; Dougherty, K. A.; Parikh, K.; Byrne, C., and Johnston, D. Mapping the electrophysiological and morphological properties of CA1 pyramidal neurons along the longitudinal hippocampal axis. *Hippocampus*, 26(3):341–361, March 2016.

Mammarella, I. C.; Lucangeli, D., and Cornoldi, C. Spatial Working Memory and Arithmetic Deficits in Children With Nonverbal Learning Difficulties. *Journal of Learning Disabilities*, 43(5):455–468, November 2009.

Marek, R.; Jin, J.; Goode, T. D.; Giustino, T. F.; Wang, Q.; Acca, G. M.; Holehonnur, R.; Ploski, J. E.; Fitzgerald, P. J.; Lynagh, T.; Lynch, J. W.; Maren, S., and Sah, P. Hippocampus-driven feed-forward inhibition of the prefrontal cortex mediates relapse of extinguished fear. *Nature Neuroscience*, 21(3):384–392, March 2018a.

Marek, R.; Xu, L.; Sullivan, R. K. P., and Sah, P. Excitatory connections between the prelimbic and infralimbic medial prefrontal cortex show a role for the prelimbic cortex in fear extinction. *Nature Neuroscience*, 21(5):654–658, May 2018b.

Maren, S. Neurotoxic or electrolytic lesions of the ventral subiculum produce deficits in the acquisition and expression of Pavlovian fear conditioning in rats. *Behavioral neuroscience*, 113(2):283–290, April 1999.

Maren, S. and Fanselow, M. S. Synaptic plasticity in the basolateral amygdala induced by hippocampal formation stimulation in vivo. *The Journal of neuroscience : the official journal of the Society for Neuroscience*, 15(11):7548–7564, November 1995.

Maren, S. Seeking a spotless mind: extinction, deconsolidation, and erasure of fear memory. *Neuron*, 70(5):830–845, June 2011.

Maren, S.; Phan, K. L., and Liberzon, I. The contextual brain: implications for fear conditioning, extinction and psychopathology. *Nature reviews. Neuroscience*, 14 (6):417–428, June 2013.

Marlin, J. J. and Carter, A. G. GABA-A receptor inhibition of local calcium signaling in spines and dendrites. *The Journal of neuroscience : the official journal of the Society for Neuroscience*, 34(48):15898–15911, November 2014.

Maroso, M.; Szabo, G. G.; Kim, H. K.; Alexander, A.; Bui, A. D.; Lee, S.-H.; Lutz, B., and Soltesz, I. Cannabinoid Control of Learning and Memory through HCN Channels. *Neuron*, 89(5):1059–1073, March 2016.

Masurkar, A. V. Towards a circuit-level understanding of hippocampal CA1 dysfunction in Alzheimer's disease across anatomical axes. *Journal of Alzheimer's disease & Parkinsonism*, 8(1), 2018.

Masurkar, A. V.; Srinivas, K. V.; Brann, D. H.; Warren, R.; Lowes, D. C., and Siegelbaum, S. A. Medial and Lateral Entorhinal Cortex Differentially Excite Deep versus Superficial CA1 Pyramidal Neurons. *Cell reports*, 18(1):148–160, January 2017.

Maurer, A. P.; Vanrhoads, S. R.; Sutherland, G. R.; Lipa, P., and McNaughton, B. L. Self-motion and the origin of differential spatial scaling along the septo-temporal axis of the hippocampus. *Hippocampus*, 15(7):841–852, 2005.

Mayberg, H. S.; Liotti, M.; Brannan, S. K.; McGinnis, S.; Mahurin, R. K.; Jerabek, P. A.; Silva, J. A.; Tekell, J. L.; Martin, C. C.; Lancaster, J. L., and Fox, P. T. Reciprocal limbic-cortical function and negative mood: converging PET findings in depression and normal sadness. *The American journal of psychiatry*, 156(5): 675–682, May 1999.

McDonald, A. J. and Mott, D. D. Functional neuroanatomy of amygdalohippocampal interconnections and their role in learning and memory. *Journal of neuroscience research*, 95(3):797–820, March 2017.

McGarry, L. M. and Carter, A. G. Inhibitory Gating of Basolateral Amygdala Inputs to the Prefrontal Cortex. *The Journal of neuroscience : the official journal of the Society for Neuroscience*, 36(36):9391–9406, September 2016.

McGarry, L. M. and Carter, A. G. Prefrontal Cortex Drives Distinct Projection Neurons in the Basolateral Amygdala. *Cell reports*, 21(6):1426–1433, November 2017.

McGuire, J. T. and Botvinick, M. M. Prefrontal cortex, cognitive control, and the registration of decision costs. *Proceedings of the National Academy of Sciences of the United States of America*, 107(17):7922–7926, April 2010.

McNaughton, N. Fear, anxiety and their disorders: Past, present and future neural theories. *Psychology & Neuroscience*, 4(2):173–181, 2011.

Meira, T.; Leroy, F.; Buss, E. W.; Oliva, A.; Park, J., and Siegelbaum, S. A. A hippocampal circuit linking dorsal CA2 to ventral CA1 critical for social memory dynamics. *Nature Communications*, 9(1):4163, October 2018.

Menendez de la Prida, L.; Suarez, F., and Pozo, M. A. Electrophysiological and morphological diversity of neurons from the rat subicular complex in vitro. *Hippocampus*, 13(6):728–744, 2003.

Mercer, A.; Bannister, A. P., and Thomson, A. M. Electrical coupling between pyramidal cells in adult cortical regions. *Brain cell biology*, 35(1):13–27, February 2006.

Meyer, H. C.; Odriozola, P.; Cohodes, E. M.; Mandell, J. D.; Li, A.; Yang, R.; Hall, B. S.; Haberman, J. T.; Zacharek, S. J.; Liston, C.; Lee, F. S., and Gee, D. G. Ventral hippocampus interacts with prelimbic cortex during inhibition of threat response via learned safety in both mice and humans. *Proceedings of the National Academy of Sciences of the United States of America*, 116(52):26970–26979, December 2019.

Milad, M. R. and Quirk, G. J. Neurons in medial prefrontal cortex signal memory for fear extinction. *Nature*, 420(6911):70–74, November 2002.

Miller, E. K. and Cohen, J. D. An integrative theory of prefrontal cortex function. *Annual review of neuroscience*, 24(1):167–202, 2001.

Minami, C.; Shimizu, T., and Mitani, A. Neural activity in the prelimbic and infralimbic cortices of freely moving rats during social interaction: Effect of isolation rearing. *PloS one*, 12(5):e0176740, 2017.

Mitchell, A. S. and Dalrymple-Alford, J. C. Dissociable memory effects after medial thalamus lesions in the rat. *The European journal of neuroscience*, 22(4): 973–985, August 2005.

Mizuseki, K.; Diba, K.; Pastalkova, E., and Buzsáki, G. Hippocampal CA1 pyramidal cells form functionally distinct sublayers. *Nature neuroscience*, 14(9):1174–1181, August 2011.

Morishima, M. and Kawaguchi, Y. Recurrent connection patterns of corticostriatal pyramidal cells in frontal cortex. *The Journal of neuroscience : the official journal of the Society for Neuroscience*, 26(16):4394–4405, April 2006.

Morris, R. G.; Garrud, P.; Rawlins, J. N., and O'Keefe, J. Place navigation impaired in rats with hippocampal lesions. *Nature*, 297(5868):681–683, June 1982.

Moser, E.; Moser, M. B., and Andersen, P. Spatial learning impairment parallels the magnitude of dorsal hippocampal lesions, but is hardly present following ventral lesions. *Journal of Neuroscience*, 13(9):3916–3925, September 1993.

Moser, M. B. and Moser, E. I. Functional differentiation in the hippocampus. *Hippocampus*, 8(6):608–619, 1998.

Moser, M. B.; Moser, E. I.; Forrest, E.; Andersen, P., and Morris, R. G. Spatial learning with a minislab in the dorsal hippocampus. *Proceedings of the National Academy of Sciences of the United States of America*, 92(21):9697–9701, October 1995.

Mukherjee, A. and Caroni, P. Infralimbic cortex is required for learning alternatives to prelimbic promoted associations through reciprocal connectivity. *Nature communications*, 9(1):2727, July 2018.

Mukherjee, A.; Carvalho, F.; Eliez, S., and Caroni, P. Long-Lasting Rescue of Network and Cognitive Dysfunction in a Genetic Schizophrenia Model. *Cell*, 178(6):1387–1402.e14, September 2019.

Müller, C. and Remy, S. Septo-hippocampal interaction. *Cell and tissue research*, 373(3):565–575, September 2018.

Muñoz, W.; Tremblay, R.; Levenstein, D., and Rudy, B. Layer-specific modulation of neocortical dendritic inhibition during active wakefulness. *Science*, 355(6328): 954–959, March 2017.

Myers-Schulz, B. and Koenigs, M. Functional anatomy of ventromedial prefrontal cortex: implications for mood and anxiety disorders. *Molecular psychiatry*, 17 (2):132–141, February 2012.

Naber, P. A. and Witter, M. P. Subicular efferents are organized mostly as parallel projections: A double-labeling, retrograde-tracing study in the rat. *The Journal of comparative neurology*, 393(3):284–297, April 1998.

Nakajima, M.; Görlich, A., and Heintz, N. Oxytocin modulates female sociosexual behavior through a specific class of prefrontal cortical interneurons. *Cell*, 159(2): 295–305, October 2014.

Nakamura, N. H.; Flasbeck, V.; Maingret, N.; Kitsukawa, T., and Sauvage, M. M. Proximodistal segregation of nonspatial information in CA3: preferential recruitment of a proximal CA3-distal CA1 network in nonspatial recognition memory. *The Journal of neuroscience : the official journal of the Society for Neuroscience*, 33(28):11506–11514, July 2013.

Nakazawa, Y.; Pevzner, A.; Tanaka, K. Z., and Wiltgen, B. J. Memory retrieval

along the proximodistal axis of CA1. *Hippocampus*, 26(9):1140–1148, September 2016.

Namburi, P.; Beyeler, A.; Yorozu, S.; Calhoon, G. G.; Halbert, S. A.; Wichmann, R.; Holden, S. S.; Mertens, K. L.; Anahtar, M.; Felix-Ortiz, A. C.; Wickersham, I. R.; Gray, J. M., and Tye, K. M. A circuit mechanism for differentiating positive and negative associations. *Nature*, 520(7549):675–678, April 2015.

Nasrallah, K.; Therreau, L.; Robert, V.; Huang, A. J. Y.; McHugh, T. J.; Piskorowski, R. A., and Chevaleyre, V. Routing Hippocampal Information Flow through Parvalbumin Interneuron Plasticity in Area CA2. *Cell reports*, 27(1): 86–98.e3, April 2019.

Numan, R. A Prefrontal-Hippocampal Comparator for Goal-Directed Behavior: The Intentional Self and Episodic Memory. *Frontiers in behavioral neuroscience*, 9:323, 2015.

Ohta, K.-I.; Suzuki, S.; Warita, K.; Sumitani, K.; Tenkumo, C.; Ozawa, T.; Ujihara, H.; Kusaka, T., and Miki, T. The effects of early life stress on the excitatory/inhibitory balance of the medial prefrontal cortex. *Behavioural Brain Research*, 379:112306, February 2020.

Okada, K. and Okaichi, H. Functional cooperation between the hippocampal subregions and the medial septum in unreinforced and reinforced spatial memory tasks. *Behavioural brain research*, 209(2):295–304, June 2010.

O'Keefe, J. A review of the hippocampal place cells. *Progress in Neurobiology*, 13 (4):419–439, 1979.

O'Keefe, J. and Dostrovsky, J. The hippocampus as a spatial map. Preliminary evidence from unit activity in the freely-moving rat. *Brain research*, 34(1):171–175, November 1971.

Okuyama, T.; Kitamura, T.; Roy, D. S.; Itohara, S., and Tonegawa, S. Ventral CA1 neurons store social memory. *Science*, 353(6307):1536–1541, September 2016.

Oliva, A.; Fernández-Ruiz, A.; Buzsáki, G., and Berényi, A. Role of Hippocampal CA2 Region in Triggering Sharp-Wave Ripples. *Neuron*, 91(6):1342–1355, September 2016.

O'Mara, S. M.; Commins, S.; Anderson, M., and Gigg, J. The subiculum: a review of form, physiology and function. *Progress in neurobiology*, 64(2):129–155, June 2001.

O'Mara, S. Controlling hippocampal output: the central role of subiculum in hippocampal information processing. *Behavioural brain research*, 174(2):304–312, November 2006.

Ongür, D. and Price, J. L. The organization of networks within the orbital and medial prefrontal cortex of rats, monkeys and humans. *Cerebral cortex (New York, N.Y. : 1991)*, 10(3):206–219, March 2000.

Osakada, F. and Callaway, E. M. Design and generation of recombinant rabies virus vectors. *Nature protocols*, 8(8):1583–1601, August 2013.

Padilla-Coreano, N.; Bolkan, S. S.; Pierce, G. M.; Blackman, D. R.; Hardin, W. D.; Garcia-Garcia, A. L.; Spellman, T. J., and Gordon, J. A. Direct Ventral Hippocampal-Prefrontal Input Is Required for Anxiety-Related Neural Activity and Behavior. *Neuron*, 89(4):857–866, February 2016.

Padilla-Coreano, N.; Canetta, S.; Mikofsky, R. M.; Alway, E.; Passecker, J.; Myroshnychenko, M. V.; Garcia-Garcia, A. L.; Warren, R.; Teboul, E.; Blackman, D. R.; Morton, M. P.; Hupalo, S.; Tye, K. M.; Kellendonk, C.; Kupferschmidt, D. A., and Gordon, J. A. Hippocampal-Prefrontal Theta Transmission Regulates Avoidance Behavior. *Neuron*, 104(3):601–610.e4, November 2019.

Parent, M. A.; Wang, L.; Su, J.; Netoff, T., and Yuan, L.-L. Identification of the hippocampal input to medial prefrontal cortex in vitro. *Cerebral cortex (New York, N.Y. : 1991)*, 20(2):393–403, February 2010.

Parfitt, G. M.; Nguyen, R.; Bang, J. Y.; Aqrabawi, A. J.; Tran, M. M.; Seo, D. K.; Richards, B. A., and Kim, J. C. Bidirectional Control of Anxiety-Related Behaviors in Mice: Role of Inputs Arising from the Ventral Hippocampus to the Lateral Septum and Medial Prefrontal Cortex. *Neuropsychopharmacology : official publication of the American College of Neuropsychopharmacology*, 42(8): 1715–1728, July 2017.

Park, J.-Y. and Spruston, N. Synergistic actions of metabotropic acetylcholine and glutamate receptors on the excitability of hippocampal CA1 pyramidal neurons. *The Journal of neuroscience : the official journal of the Society for Neuroscience*, 32(18):6081–6091, May 2012.

Passolunghi, M. C. and Mammarella, I. C. Spatial and visual working memory ability in children with difficulties in arithmetic word problem solving. *European Journal of Cognitive Psychology*, 22(6):944–963, September 2010.

Pellow, S. and File, S. E. Anxiolytic and anxiogenic drug effects on exploratory activity in an elevated plus-maze: a novel test of anxiety in the rat. *Pharmacology, biochemistry, and behavior*, 24(3):525–529, March 1986.

Pellow, S.; Chopin, P.; File, S. E., and Briley, M. Validation of open:closed arm entries in an elevated plus-maze as a measure of anxiety in the rat. *Journal of neuroscience methods*, 14(3):149–167, August 1985.

Peters, J.; Dieppa-Perea, L. M.; Melendez, L. M., and Quirk, G. J. Induction of fear extinction with hippocampal-infralimbic BDNF. *Science (New York, N.Y.)*, 328 (5983):1288–1290, June 2010.

Petreanu, L.; Huber, D.; Sobczyk, A., and Svoboda, K. Channelrhodopsin-2-assisted circuit mapping of long-range callosal projections. Technical report, Howard Hughes Medical Institute, Janelia Farm Research Campus, 19700 Helix Drive, Ashburn, Virginia 20147, USA., May 2007.

Petreanu, L.; Mao, T.; Sternson, S. M., and Svoboda, K. The subcellular orga-

nization of neocortical excitatory connections. *Nature*, 457(7233):1142–1145, February 2009.

Phillips, M. L.; Robinson, H. A., and Pozzo-Miller, L. Ventral hippocampal projections to the medial prefrontal cortex regulate social memory. *eLife*, 8:679, May 2019.

Phillips, R. G. and LeDoux, J. E. Differential contribution of amygdala and hippocampus to cued and contextual fear conditioning. *Behavioral neuroscience*, 106(2):274–285, April 1992.

Pi, G.; Gao, D.; Wu, D.; Wang, Y.; Lei, H.; Zeng, W.; Gao, Y.; Yu, H.; Xiong, R.; Jiang, T.; Li, S.; Wang, X.; Guo, J.; Zhang, S.; Yin, T.; He, T.; Ke, D.; Li, R.; Li, H.; Liu, G.; Yang, X.; Luo, M.-H.; Zhang, X.; Yang, Y., and Wang, J.-Z. Posterior basolateral amygdala to ventral hippocampal CA1 drives approach behaviour to exert an anxiolytic effect. *Nature communications*, 11(1):183, January 2020.

Pi, H.-J.; Hangya, B.; Kvitsiani, D.; Sanders, J. I.; Huang, Z. J., and Kepecs, A. Cortical interneurons that specialize in disinhibitory control. *Nature*, 503(7477): 521–524, November 2013.

Pikkarainen, M.; Rönkkö, S.; Savander, V.; Insausti, R., and Pitkänen, A. Projections from the lateral, basal, and accessory basal nuclei of the amygdala to the hippocampal formation in rat. *The Journal of comparative neurology*, 403(2): 229–260, January 1999.

Pitkänen, A.; Pikkarainen, M.; Nurminen, N., and Ylinen, A. Reciprocal connections between the amygdala and the hippocampal formation, perirhinal cortex, and postrhinal cortex in rat. A review. *Annals of the New York Academy of Sciences*, 911:369–391, June 2000.

Place, R.; Farovik, A.; Brockmann, M., and Eichenbaum, H. Bidirectional prefrontal-hippocampal interactions support context-guided memory. *Nature Neuroscience*, 19(8):992–994, August 2016.

Prasad, J. A. and Chudasama, Y. Viral tracing identifies parallel disynaptic pathways to the hippocampus. *The Journal of neuroscience : the official journal of the Society for Neuroscience*, 33(19):8494–8503, May 2013.

Quirk, G. J. and Beer, J. S. Prefrontal involvement in the regulation of emotion: convergence of rat and human studies. *Current opinion in neurobiology*, 16(6): 723–727, December 2006.

Rajasethupathy, P.; Sankaran, S.; Marshel, J. H.; Kim, C. K.; Ferenczi, E.; Lee, S. Y.; Berndt, A.; Ramakrishnan, C.; Jaffe, A.; Lo, M.; Liston, C., and Deisseroth, K. Projections from neocortex mediate top-down control of memory retrieval. *Nature*, 526(7575):653–659, October 2015.

Ramanathan, K. R.; Jin, J.; Giustino, T. F.; Payne, M. R., and Maren, S. Prefrontal projections to the thalamic nucleus reuniens mediate fear extinction. *Nature communications*, 9(1):4527, October 2018.

Ramón y Cajal, S. Histologie du système nerveux de l'homme & des vertébrés. 1909.

Ramos, J. M. Long-term spatial memory in rats with hippocampal lesions. *The European journal of neuroscience*, 12(9):3375–3384, September 2000.

Remondes, M. and Schuman, E. M. Role for a cortical input to hippocampal area CA1 in the consolidation of a long-term memory. *Nature*, 431(7009):699–703, October 2004.

Ressler, K. J. and Mayberg, H. S. Targeting abnormal neural circuits in mood and anxiety disorders: from the laboratory to the clinic. *Nature Neuroscience*, 10(9): 1116–1124, September 2007.

Ridderinkhof, K. R.; Ullsperger, M.; Crone, E. A., and Nieuwenhuis, S. The Role of the Medial Frontal Cortex in Cognitive Control. *Science*, 306(5695):443–447, October 2004.

Risold, P. Y. and Swanson, L. W. Structural evidence for functional domains in the rat hippocampus. *Science (New York, N.Y.)*, 272(5267):1484–1486, June 1996.

Roesler, R.; Henriques, J. A. P., and Schwartsmann, G. Gastrin-releasing peptide receptor as a molecular target for psychiatric and neurological disorders. *CNS & neurological disorders drug targets*, 5(2):197–204, April 2006.

Rosene, D. L. and Van Hoesen, G. W. Hippocampal efferents reach widespread areas of cerebral cortex and amygdala in the rhesus monkey. *Science (New York, N.Y.)*, 198(4314):315–317, October 1977.

Rudy, B.; Fishell, G.; Lee, S., and Hjerling-Leffler, J. Three groups of interneurons account for nearly 100% of neocortical GABAergic neurons. *Developmental neurobiology*, 71(1):45–61, January 2011.

Ruediger, S.; Spirig, D.; Donato, F., and Caroni, P. Goal-oriented searching mediated by ventral hippocampus early in trial-and-error learning. *Nature neuroscience*, 15(11):1563–1571, November 2012.

Russo, S. J.; Dietz, D. M.; Dumitriu, D.; Morrison, J. H.; Malenka, R. C., and Nestler, E. J. The addicted synapse: mechanisms of synaptic and structural plasticity in nucleus accumbens. *Trends in neurosciences*, 33(6):267–276, June 2010.

Salzman, C. D. and Fusi, S. Emotion, cognition, and mental state representation in amygdala and prefrontal cortex. *Annual review of neuroscience*, 33:173–202, 2010.

Sánchez-Bellot, C. and MacAskill, A. F. Push-pull regulation of exploratory behavior by two opposing hippocampal to prefrontal cortex pathways. *bioRxiv*, page 2019.12.18.880831, January 2019.

Sapolsky, R. M.; Uno, H.; Rebert, C. S., and Finch, C. E. Hippocampal damage associated with prolonged glucocorticoid exposure in primates. *The Journal of neuroscience : the official journal of the Society for Neuroscience*, 10(9):2897–2902, September 1990.

Schiller, D.; Eichenbaum, H.; Buffalo, E. A.; Davachi, L.; Foster, D. J.; Leutgeb, S., and Ranganath, C. Memory and Space: Towards an Understanding of the Cognitive Map. *The Journal of neuroscience : the official journal of the Society for Neuroscience*, 35(41):13904–13911, October 2015.

Schmidt-Hieber, C.; Toleikyte, G.; Aitchison, L.; Roth, A.; Clark, B. A.; Branco, T., and Häusser, M. Active dendritic integration as a mechanism for robust and precise grid cell firing. *Nature neuroscience*, 20(8):1114–1121, August 2017.

Schoenfeld, T. J.; Kloth, A. D.; Hsueh, B.; Runkle, M. B.; Kane, G. A.; Wang, S. S.-H., and Gould, E. Gap junctions in the ventral hippocampal-medial prefrontal pathway are involved in anxiety regulation. *The Journal of neuroscience : the official journal of the Society for Neuroscience*, 34(47):15679–15688, November 2014.

Schwarz, L. A.; Miyamichi, K.; Gao, X. J.; Beier, K. T.; Weissbourd, B.; DeLoach, K. E.; Ren, J.; Ibanes, S.; Malenka, R. C.; Kremer, E. J., and Luo, L. Viral-genetic tracing of the input-output organization of a central noradrenaline circuit. *Nature*, 524(7563):88–92, August 2015.

Scoville, W. B. and Milner, B. Loss of recent memory after bilateral hippocampal lesions. *Journal of neurology, neurosurgery, and psychiatry*, 20(1):11–21, February 1957.

Scoville, W. B. and Milner, B. *Loss of recent memory after bilateral hippocampal lesions. 1957.*, volume 12 of *Patient H. M.* American Psychiatric Publishing, 2000.

Serrano, M. and Caroni, P. Managing Neuronal Ensembles: Somatostatin Interneuron Subpopulations Shape and Protect Cortical Neuronal Ensembles for Learning. *Neuron*, 102(1):6–8, April 2019.

Shah, A. A. and Treit, D. Excitotoxic lesions of the medial prefrontal cortex attenuate fear responses in the elevated-plus maze, social interaction and shock probe burying tests. *Brain research*, 969(1-2):183–194, April 2003.

Shah, A. A. and Treit, D. Infusions of midazolam into the medial prefrontal cortex produce anxiolytic effects in the elevated plus-maze and shock-probe burying tests. *Brain research*, 996(1):31–40, January 2004.

Shibata, H. Direct projections from the anterior thalamic nuclei to the retrohippocampal region in the rat. *The Journal of comparative neurology*, 337(3):431–445, November 1993.

Shin, J. D. and Jadhav, S. P. Multiple modes of hippocampal-prefrontal interactions in memory-guided behavior. *Current opinion in neurobiology*, 40:161–169, October 2016.

Shrestha, P.; Mousa, A., and Heintz, N. Layer 2/3 pyramidal cells in the medial prefrontal cortex moderate stress induced depressive behaviors. *eLife*, 4, September 2015.

Sierra-Mercado, D.; Padilla-Coreano, N., and Quirk, G. J. Dissociable roles of prelimbic and infralimbic cortices, ventral hippocampus, and basolateral amygdala in the expression and extinction of conditioned fear. *Neuropsychopharmacology : official publication of the American College of Neuropsychopharmacology*, 36 (2):529–538, January 2011.

Sigurdsson, T. and Duvarci, S. Hippocampal-Prefrontal Interactions in Cognition, Behavior and Psychiatric Disease. *Frontiers in systems neuroscience*, 9:257, January 2016.

Sigurdsson, T.; Stark, K. L.; Karayiorgou, M.; Gogos, J. A., and Gordon, J. A. Impaired hippocampal-prefrontal synchrony in a genetic mouse model of schizophrenia. *Nature*, 464(7289):763–767, April 2010.

Simons, J. S. and Spiers, H. J. Prefrontal and medial temporal lobe interactions in long-term memory. *Nature reviews. Neuroscience*, 4(8):637–648, August 2003.

Slomianka, L.; Amrein, I.; Knuesel, I.; Sørensen, J. C., and Wolfer, D. P. Hippocam-

pal pyramidal cells: the reemergence of cortical lamination. *Brain structure & function*, 216(4):301–317, May 2011.

Smith, S. M. and Vale, W. W. The role of the hypothalamic-pituitary-adrenal axis in neuroendocrine responses to stress. *Dialogues in clinical neuroscience*, 8(4): 383–395, 2006.

Smythe, J. W.; Cristie, B. R.; Colom, L. V.; Lawson, V. H., and Bland, B. H. Hippocampal theta field activity and theta-on/theta-off cell discharges are controlled by an ascending hypothalamo-septal pathway. *The Journal of neuroscience : the official journal of the Society for Neuroscience*, 11(7):2241–2248, July 1991.

Sohal, V. S. and Rubenstein, J. L. R. Excitation-inhibition balance as a framework for investigating mechanisms in neuropsychiatric disorders. *Molecular Psychiatry*, 24(9):1248–1257, September 2019.

Soltesz, I. and Losonczy, A. CA1 pyramidal cell diversity enabling parallel information processing in the hippocampus. *Nature Neuroscience*, 21(4):484–493, April 2018.

Sørensen, J. C.; Slomianka, L.; Christensen, J., and Zimmer, J. Zinc-containing telencephalic connections to the rat striatum: a combined Fluoro-Gold tracing and histochemical study. *Experimental brain research*, 105(3):370–382, 1995.

Sörman, E.; Wang, D.; Hajos, M., and Kocsis, B. Control of hippocampal theta rhythm by serotonin: role of 5-HT2c receptors. *Neuropharmacology*, 61(3):489–494, September 2011.

Sotres-Bayon, F.; Sierra-Mercado, D.; Pardilla-Delgado, E., and Quirk, G. J. Gating of Fear in Prelimbic Cortex by Hippocampal and Amygdala Inputs. *Neuron*, 76 (4):804–812, November 2012.

Soumier, A. and Sibille, E. Opposing effects of acute versus chronic blockade of frontal cortex somatostatin-positive inhibitory neurons on behavioral emotional-

ity in mice. *Neuropsychopharmacology : official publication of the American College of Neuropsychopharmacology*, 39(9):2252–2262, August 2014.

Spellman, T. and Liston, C. Toward Circuit Mechanisms of Pathophysiology in Depression. *The American journal of psychiatry*, 177(5):381–390, May 2020.

Spellman, T.; Rigotti, M.; Ahmari, S. E.; Fusi, S.; Gogos, J. A., and Gordon, J. A. Hippocampal–prefrontal input supports spatial encoding in working memory. *Nature*, 522(7556):309–314, June 2015.

Squire, L. R. Memory and the hippocampus: a synthesis from findings with rats, monkeys, and humans. *Psychological review*, 99(2):195–231, April 1992.

Staff, N. P.; Jung, H. Y.; Thiagarajan, T.; Yao, M., and Spruston, N. Resting and active properties of pyramidal neurons in subiculum and CA1 of rat hippocampus. *Journal of neurophysiology*, 84(5):2398–2408, November 2000.

Staib, J. M.; Della Valle, R., and Knox, D. K. Disruption of medial septum and diagonal bands of Broca cholinergic projections to the ventral hippocampus disrupt auditory fear memory. *Neurobiology of learning and memory*, 152:71–79, July 2018.

Stark, E.; Roux, L.; Eichler, R.; Senzai, Y.; Royer, S., and Buzsáki, G. Pyramidal cell-interneuron interactions underlie hippocampal ripple oscillations. *Neuron*, 83(2):467–480, July 2014.

Starkweather, C. K.; Gershman, S. J., and Uchida, N. The Medial Prefrontal Cortex Shapes Dopamine Reward Prediction Errors under State Uncertainty. *Neuron*, 98 (3):616–629.e6, May 2018.

Strange, B. A.; Fletcher, P. C.; Henson, R. N.; Friston, K. J., and Dolan, R. J. Segregating the functions of human hippocampus. *Proceedings of the National Academy of Sciences of the United States of America*, 96(7):4034–4039, March 1999.

Strange, B. A.; Witter, M. P.; Lein, E. S., and Moser, E. I. Functional organization of the hippocampal longitudinal axis. *Nature Reviews Neuroscience*, 15(10):655–669, September 2014.

Stuber, G. D.; Sparta, D. R.; Stamatakis, A. M.; van Leeuwen, W. A.; Hardjoprajitno, J. E.; Cho, S.; Tye, K. M.; Kempadoo, K. A.; Zhang, F.; Deisseroth, K., and Bonci, A. Excitatory transmission from the amygdala to nucleus accumbens facilitates reward seeking. *Nature*, 475(7356):377–380, June 2011.

Sun, Q.; Li, X.; Li, A.; Zhang, J.; Ding, Z.; Gong, H., and Luo, Q. Ventral Hippocampal-Prefrontal Interaction Affects Social Behavior via Parvalbumin Positive Neurons in the Medial Prefrontal Cortex. *iScience*, 23(3):100894, March 2020.

Swanson, L. W. A direct projection from Ammon's horn to prefrontal cortex in the rat. *Brain research*, 217(1):150–154, July 1981.

Szőnyi, A.; Sos, K. E.; Nyilas, R.; Schlingloff, D.; Domonkos, A.; Takács, V. T.; Pósfai, B.; Hegedüs, P.; Priestley, J. B.; Gundlach, A. L.; Gulyás, A. I.; Varga, V.; Losonczy, A.; Freund, T. F., and Nyiri, G. Brainstem nucleus incertus controls contextual memory formation. *Science*, 364(6442):eaaw0445, May 2019.

Tanaka, K. F.; Samuels, B. A., and Hen, R. Serotonin receptor expression along the dorsal-ventral axis of mouse hippocampus. *Philosophical Transactions of the Royal Society of London. Series B, Biological Sciences*, 367(1601):2395–2401, September 2012.

Tang, W.; Shin, J. D.; Frank, L. M., and Jadhav, S. P. Hippocampal-Prefrontal Reactivation during Learning Is Stronger in Awake Compared with Sleep States. *The Journal of neuroscience : the official journal of the Society for Neuroscience*, 37(49):11789–11805, December 2017.

Tannenholz, L.; Jimenez, J. C., and Kheirbek, M. A. Local and regional heterogeneity underlying hippocampal modulation of cognition and mood. *Frontiers in behavioral neuroscience*, 8:147, 2014.

Tavares, R. M.; Mendelsohn, A.; Grossman, Y.; Williams, C. H.; Shapiro, M.; Trope, Y., and Schiller, D. A Map for Social Navigation in the Human Brain. *Neuron*, 87(1):231–243, July 2015.

Thierry, A. M.; Gioanni, Y.; Dégénétais, E., and Glowinski, J. Hippocampo-prefrontal cortex pathway: anatomical and electrophysiological characteristics. *Hippocampus*, 10(4):411–419, 2000.

Thompson, C. L.; Pathak, S. D.; Jeromin, A.; Ng, L. L.; MacPherson, C. R.; Mortrud, M. T.; Cusick, A.; Riley, Z. L.; Sunkin, S. M.; Bernard, A.; Puchalski, R. B.; Gage, F. H.; Jones, A. R.; Bajic, V. B.; Hawrylycz, M. J., and Lein, E. S. Genomic anatomy of the hippocampus. *Neuron*, 60(6):1010–1021, December 2008.

Tierney, P. L.; Dégenètais, E.; Thierry, A.-M.; Glowinski, J., and Gioanni, Y. Influence of the hippocampus on interneurons of the rat prefrontal cortex. *European Journal of Neuroscience*, 20(2):514–524, July 2004.

Tovote, P.; Fadok, J. P., and Lüthi, A. Neuronal circuits for fear and anxiety. *Nature reviews. Neuroscience*, 16(6):317–331, June 2015.

Tremblay, R.; Lee, S., and Rudy, B. GABAergic Interneurons in the Neocortex: From Cellular Properties to Circuits. *Neuron*, 91(2):260–292, July 2016.

Tronson, N. C.; Schrick, C.; Guzman, Y. F.; Huh, K. H.; Srivastava, D. P.; Penzes, P.; Guedea, A. L.; Gao, C., and Radulovic, J. Segregated populations of hippocampal principal CA1 neurons mediating conditioning and extinction of contextual fear. *The Journal of neuroscience : the official journal of the Society for Neuroscience*, 29(11):3387–3394, March 2009.

Trouche, S.; Koren, V.; Doig, N. M.; Ellender, T. J.; El-Gaby, M.; Lopes-Dos-Santos, V.; Reeve, H. M.; Perestenko, P. V.; Garas, F. N.; Magill, P. J.; Sharott, A., and Dupret, D. A Hippocampus-Accumbens Tripartite Neuronal Motif Guides Appetitive Memory in Space. *Cell*, 176(6):1393–1406.e16, March 2019.

Tsanov, M. and O'Mara, S. M. Decoding signal processing in thalamo-hippocampal circuitry: implications for theories of memory and spatial processing. *Brain research*, 1621:368–379, September 2015.

Tsao, A.; Moser, M.-B., and Moser, E. I. Traces of experience in the lateral entorhinal cortex. *Current biology : CB*, 23(5):399–405, March 2013.

Tsao, A.; Sugar, J.; Lu, L.; Wang, C.; Knierim, J. J.; Moser, M.-B., and Moser, E. I. Integrating time from experience in the lateral entorhinal cortex. *Nature*, 561(7721):57–62, September 2018.

Tye, K. M.; Prakash, R.; Kim, S.-Y.; Fenno, L. E.; Grosenick, L.; Zarabi, H.; Thompson, K. R.; Gradinaru, V.; Ramakrishnan, C., and Deisseroth, K. Amygdala circuitry mediating reversible and bidirectional control of anxiety. *Nature*, 471(7338):358–362, March 2011.

Ulrich-Lai, Y. M. and Herman, J. P. Neural regulation of endocrine and autonomic stress responses. *Nature reviews. Neuroscience*, 10(6):397–409, June 2009.

Uno, H.; Tarara, R.; Else, J. G.; Suleman, M. A., and Sapolsky, R. M. Hippocampal damage associated with prolonged and fatal stress in primates. *The Journal of neuroscience : the official journal of the Society for Neuroscience*, 9(5):1705–1711, May 1989.

Valero, M. and de la Prida, L. M. The hippocampus in depth: a sublayer-specific perspective of entorhinal-hippocampal function. *Current opinion in neurobiology*, 52:107–114, October 2018.

Valero, M.; Cid, E.; Averkin, R. G.; Aguilar, J.; Sanchez-Aguilera, A.; Viney, T. J.; Gomez-Dominguez, D.; Bellistri, E., and de la Prida, L. M. Determinants of different deep and superficial CA1 pyramidal cell dynamics during sharp-wave ripples. *Nature Neuroscience*, 18(9):1281–1290, September 2015.

Van Dyke, A. M.; Francis, T. C.; Chen, H.; Bailey, A. M., and Thompson, S. M.

Chronic fluoxetine treatment in vivo enhances excitatory synaptic transmission in the hippocampus. *Neuropharmacology*, 150:38–45, May 2019.

van Groen, T. and Wyss, J. M. Extrinsic projections from area CA1 of the rat hippocampus: olfactory, cortical, subcortical, and bilateral hippocampal formation projections. *The Journal of comparative neurology*, 302(3):515–528, December 1990.

Van Groen, T. and Wyss, J. M. Projections from the anterodorsal and anteroventral nucleus of the thalamus to the limbic cortex in the rat. *The Journal of comparative neurology*, 358(4):584–604, August 1995.

van Groen, T.; Kadish, I., and Michael Wyss, J. Role of the anterodorsal and anteroventral nuclei of the thalamus in spatial memory in the rat. *Behavioural brain research*, 132(1):19–28, April 2002.

van Welie, I.; Remme, M. W. H.; van Hooft, J. A., and Wadman, W. J. Different levels of Ih determine distinct temporal integration in bursting and regular-spiking neurons in rat subiculum. *The Journal of physiology*, 576(Pt 1):203–214, October 2006.

Varela, C.; Kumar, S.; Yang, J. Y., and Wilson, M. A. Anatomical substrates for direct interactions between hippocampus, medial prefrontal cortex, and the thalamic nucleus reuniens. *Brain structure & function*, 219(3):911–929, May 2014.

Varga, C.; Lee, S. Y., and Soltesz, I. Target-selective GABAergic control of entorhinal cortex output. *Nature neuroscience*, 13(7):822–824, July 2010.

Vertes, R. P. and Kocsis, B. Brainstem-diencephalo-septohippocampal systems controlling the theta rhythm of the hippocampus. *Neuroscience*, 81(4):893–926, December 1997.

Vertes, R. P. Differential projections of the infralimbic and prelimbic cortex in the rat. *Synapse (New York, N.Y.)*, 51(1):32–58, January 2004.

Vertes, R. P. Interactions among the medial prefrontal cortex, hippocampus and midline thalamus in emotional and cognitive processing in the rat. *Neuroscience*, 142(1):1–20, September 2006.

Vertes, R. P. Major diencephalic inputs to the hippocampus: supramammillary nucleus and nucleus reuniens. Circuitry and function. *Progress in brain research*, 219:121–144, 2015.

Vertes, R. P.; Hoover, W. B., and Viana Di Prisco, G. Theta rhythm of the hippocampus: subcortical control and functional significance. *Behavioral and cognitive neuroscience reviews*, 3(3):173–200, September 2004.

Vidal-Gonzalez, I.; Vidal-Gonzalez, B.; Rauch, S. L., and Quirk, G. J. Microstimulation reveals opposing influences of prelimbic and infralimbic cortex on the expression of conditioned fear. *Learning & memory (Cold Spring Harbor, N.Y.)*, 13(6):728–733, November 2006.

Vinogradova, O. S. Hippocampus as comparator: role of the two input and two output systems of the hippocampus in selection and registration of information. *Hippocampus*, 11(5):578–598, 2001.

Vong, L.; Ye, C.; Yang, Z.; Choi, B.; Chua, S., and Lowell, B. B. Leptin action on GABAergic neurons prevents obesity and reduces inhibitory tone to POMC neurons. *Neuron*, 71(1):142–154, July 2011.

Walf, A. A. and Frye, C. A. The use of the elevated plus maze as an assay of anxiety-related behavior in rodents. *Nature protocols*, 2(2):322–328, 2007.

Wallace, D. L.; Han, M.-H.; Graham, D. L.; Green, T. A.; Vialou, V.; Iñiguez, S. D.; Cao, J.-L.; Kirk, A.; Chakravarty, S.; Kumar, A.; Krishnan, V.; Neve, R. L.; Cooper, D. C.; Bolaños, C. A.; Barrot, M.; McClung, C. A., and Nestler, E. J. CREB regulation of nucleus accumbens excitability mediates social isolation-induced behavioral deficits. *Nature Neuroscience*, 12(2):200–209, February 2009.

Wang, G.-W. and Cai, J.-X. Disconnection of the hippocampal-prefrontal cortical circuits impairs spatial working memory performance in rats. *Behavioural Brain Research*, 175(2):329–336, December 2006.

Wang, M.; Perova, Z.; Arenkiel, B. R., and Li, B. Synaptic Modifications in the Medial Prefrontal Cortex in Susceptibility and Resilience to Stress. *Journal of Neuroscience*, 34(22):7485–7492, May 2014.

Wang, Q.; Jin, J., and Maren, S. Renewal of extinguished fear activates ventral hippocampal neurons projecting to the prelimbic and infralimbic cortices in rats. *Neurobiology of learning and memory*, 134 Pt A:38–43, October 2016.

Warden, M. R.; Selimbeyoglu, A.; Mirzabekov, J. J.; Lo, M.; Thompson, K. R.; Kim, S.-Y.; Adhikari, A.; Tye, K. M.; Frank, L. M., and Deisseroth, K. A prefrontal cortex-brainstem neuronal projection that controls response to behavioural challenge. *Nature*, 492(7429):428–432, December 2012.

Wee, R. W. S. and MacAskill, A. F. Biased Connectivity of Brain-wide Inputs to Ventral Subiculum Output Neurons. *Cell reports*, 30(11):3644–3654.e6, March 2020.

Wickersham, I. R.; Lyon, D. C.; Barnard, R. J. O.; Mori, T.; Finke, S.; Conzelmann, K.-K.; Young, J. A. T., and Callaway, E. M. Monosynaptic restriction of transsynaptic tracing from single, genetically targeted neurons. *Neuron*, 53(5):639–647, March 2007.

Wikenheiser, A. M.; Marrero-Garcia, Y., and Schoenbaum, G. Suppression of Ventral Hippocampal Output Impairs Integrated Orbitofrontal Encoding of Task Structure. *Neuron*, 95(5):1197–1207.e3, August 2017.

Witter, M. P. Organization of the entorhinal-hippocampal system: a review of current anatomical data. *Hippocampus*, 3 Spec No:33–44, 1993.

Witter, M. P.; Naber, P. A.; van Haeften, T.; Machielsen, W. C.; Rombouts, S. A.; Barkhof, F.; Scheltens, P., and Lopes da Silva, F. H. Cortico-hippocampal com-

munication by way of parallel parahippocampal-subicular pathways. *Hippocampus*, 10(4):398–410, 2000.

Witter, M. P. Connections of the subiculum of the rat: topography in relation to columnar and laminar organization. *Behavioural Brain Research*, 174(2):251–264, November 2006.

Witter, M. P. and Amaral, D. G. *Hippocampal Formation*, pages 635–704. Elsevier Inc., May 2004. ISBN 9780080542614.

Witter, M. P.; Ostendorf, R. H., and Groenewegen, H. J. Heterogeneity in the Dorsal Subiculum of the Rat. Distinct Neuronal Zones Project to Different Cortical and Subcortical Targets. *The European journal of neuroscience*, 2(8):718–725, 1990.

Wouterlood, F. G.; Saldana, E., and Witter, M. P. Projection from the nucleus reuniens thalami to the hippocampal region: light and electron microscopic tracing study in the rat with the anterograde tracer Phaseolus vulgaris-leucoagglutinin. *The Journal of comparative neurology*, 296(2):179–203, June 1990.

Wyss, J. M.; Swanson, L. W., and Cowan, W. M. A study of subcortical afferents to the hippocampal formation in the rat. *Neuroscience*, 4(4):463–476, 1979.

Xia, F.; Richards, B. A.; Tran, M. M.; Josselyn, S. A.; Takehara-Nishiuchi, K., and Frankland, P. W. Parvalbumin-positive interneurons mediate neocortical-hippocampal interactions that are necessary for memory consolidation. *eLife*, 6: 191, September 2017.

Xu, C.; Krabbe, S.; Gründemann, J.; Botta, P.; Fadok, J. P.; Osakada, F.; Saur, D.; Grewe, B. F.; Schnitzer, M. J.; Callaway, E. M., and Lüthi, A. Distinct Hippocampal Pathways Mediate Dissociable Roles of Context in Memory Retrieval. *Cell*, 167(4):961–972.e16, November 2016.

Xu, H.; Liu, L.; Tian, Y.; Wang, J.; Li, J.; Zheng, J.; Zhao, H.; He, M.; Xu, T.-L.; Duan, S., and Xu, H. A Disinhibitory Microcircuit Mediates Conditioned Social Fear in the Prefrontal Cortex. *Neuron*, 102(3):668–682.e5, May 2019.

Yang, H.; de Jong, J. W.; Tak, Y.; Peck, J.; Bateup, H. S., and Lammel, S. Nucleus Accumbens Subnuclei Regulate Motivated Behavior via Direct Inhibition and Disinhibition of VTA Dopamine Subpopulations. *Neuron*, 97(2):434–449.e4, January 2018a.

Yang, Y.; Cui, Y.; Sang, K.; Dong, Y.; Ni, Z.; Ma, S., and Hu, H. Ketamine blocks bursting in the lateral habenula to rapidly relieve depression. *Nature*, 554(7692): 317–322, February 2018b.

Yavorska, I. and Wehr, M. Somatostatin-Expressing Inhibitory Interneurons in Cortical Circuits. *Frontiers in Neural Circuits*, 10(52):76, 2016.

Yun, S.; Reynolds, R. P.; Petrof, I.; White, A.; Rivera, P. D.; Segev, A.; Gibson, A. D.; Suarez, M.; DeSalle, M. J.; Ito, N.; Mukherjee, S.; Richardson, D. R.; Kang, C. E.; Ahrens-Nicklas, R. C.; Soler, I.; Chetkovich, D. M.; Kourrich, S.; Coulter, D. A., and Eisch, A. J. Stimulation of entorhinal cortex-dentate gyrus circuitry is antidepressive. *Nature Medicine*, 24(5):658–666, May 2018.

Zanos, P.; Moaddel, R.; Morris, P. J.; Georgiou, P.; Fischell, J.; Elmer, G. I.; Alkondon, M.; Yuan, P.; Pribut, H. J.; Singh, N. S.; Dossou, K. S. S.; Fang, Y.; Huang, X.-P.; Mayo, C. L.; Wainer, I. W.; Albuquerque, E. X.; Thompson, S. M.; Thomas, C. J.; Zarate Jr, C. A., and Gould, T. D. NMDAR inhibition-independent antidepressant actions of ketamine metabolites. *Nature*, 533(7604): 481–486, May 2016.

Zhang, D. X. and Bertram, E. H. Midline thalamic region: widespread excitatory input to the entorhinal cortex and amygdala. *The Journal of neuroscience : the official journal of the Society for Neuroscience*, 22(8):3277–3284, April 2002.

Zugaro, M. B.; Tabuchi, E.; Fouquier, C.; Berthoz, A., and Wiener, S. I. Active locomotion increases peak firing rates of anterodorsal thalamic head direction cells. *Journal of neurophysiology*, 86(2):692–702, August 2001.